



University of
Reading



Atmospheric Rivers and the Land Surface: Drivers of Extreme Winter Floods Across the UK?

Submitted for the degree of Doctor of Philosophy
School of Archaeology, Geography and Environmental Science

Helen V. M. Griffith
September 2021

Declaration

I confirm that this is my own work and the use of all material from other sources has been properly and fully acknowledged.

Helen Verity McCandlish Griffith

7th September 2021

Table of Contents

<i>Declaration</i>	2
<i>Table of Contents</i>	3
<i>Acknowledgements</i>	7
<i>Abstract</i>	8
<i>List of Figures</i>	9
<i>List of Tables</i>	12
<i>List of Abbreviations</i>	13
<i>Publications and Awards</i>	15
<i>Science Communication</i>	16
2021	16
Carbon Brief Article	16
Interview with BBC Radio Berks	16
Featured in the Times	16
Prevention Web reproduces Carbon Brief Article	16
Engagement with the Departmental social media	16
2020	16
HEPEX Blog	16
2019	16
Environment Agency Placement (6-months).....	16
2018	16
COP CAS Blog.....	16
<i>Chapter 1 – Introduction</i>	18
1.1. Rationale	18
1.2. The Atmospheric River	18
1.3. Research Gaps and Objectives	20
1.4. Thesis Structure	20
<i>Chapter 2 – Literature Review and Research Objectives</i>	23
2.1. Introduction	23
2.2. Water Vapour in the Mid-Latitudes	23
2.2.1. Dominant Processes and Early Work	23
2.2.2. What is an Atmospheric River?.....	25
2.3. Atmospheric River Origin	29
2.3.1. Atmospheric River Moisture Sources.....	29
2.3.2. Atmospheric River Formation Processes	31
2.4. Atmospheric River Impacts	32
2.4.1. Early field campaigns – moving towards an AR definition?.....	32
2.4.2. Impact Across the World	33
2.5. Detecting, Modelling and Forecasting Atmospheric Rivers	39

2.5.1. Field Campaign Development	39
2.5.2. Atmospheric River Detection	40
2.5.3. Atmospheric Rivers and Climate Change.....	43
2.5.4. Forecasting Potential	44
2.6. The Catchment Influence.....	47
2.6.1. Orographic Precipitation	47
2.6.2. The Catchment Control?	48
2.6.3. Combining Meteorology and Hydrology.....	50
2.7. Research Objectives	58
2.7.1. Key Research Gap.....	58
2.7.2. Thesis Aims and Objectives.....	59
<i>Chapter 3 – Study Area, Data and Methods.....</i>	61
3.1. Introduction.....	61
3.2. Research Design.....	61
3.3. Study Area	62
3.3.1. South Western England.....	65
3.3.2. Wales and the English Borders	66
3.3.3. North Western England	69
3.3.4. Scotland	70
3.3.5. Selection of Catchment Descriptors	73
3.4. Reanalysis Data	83
3.4.1. ERA5 Global Reanalysis.....	83
3.4.2. Atmospheric River Detection Method (ARDM)	84
3.5. Hydrological Data	86
3.5.1. Flow Data	86
3.5.2. POT Flood Selection.....	87
3.5.3. Rainfall Data	88
3.6. Additional Methods	88
3.6.1. Statistical Methods	88
3.6.2. Principal Component Analysis.....	89
3.6.3. Random Forest Regression.....	89
<i>Chapter 4 – Atmospheric River Orientation Determines Flood Occurrence.....</i>	91
4.1 Introduction.....	91
4.2. Atmospheric River Orientation Determines Flood Occurrence.....	91
4.2.1. Abstract	91
4.2.2. Introduction.....	92
4.2.3. Study Areas and Data	93
4.2.4. Results and Discussion	95
4.2.5. Conclusions and Future Work	101
4.3. Summary.....	103
<i>Chapter 5 – Verification of Atmospheric River Detection Method.....</i>	104
5.1 Introduction.....	104
5.2. Improving the Detection Algorithm	105
5.2.1. Rationale	105
5.2.2. Algorithm Modifications	106
5.2.3. Application to the Dyfi and Teifi catchments.....	109

5.3. AR Properties According to the Modified Algorithm.....	113
5.3.1. Rationale	113
5.3.2. Data Extraction.....	114
5.3.3. AR Axis	115
5.3.4. AR Width.....	116
5.3.5. AR Cross Sections	121
5.4. Conclusions	125
<i>Chapter 6 – Atmospheric Rivers and the Catchment</i>	<i>127</i>
6.1. Introduction.....	127
6.2. How Important Are ARs across the UK?	128
6.2.1. Rationale	128
6.2.2. AR-Flood Relationships at Orientation and Flux Dominated Catchments.....	132
6.3. Incorporation of Catchment Properties	135
6.3.1. Rationale	135
6.3.2. Refining the Descriptor Dataset	135
6.3.3. Principal Component Analysis – Linking the Descriptors to AR Properties	137
6.3.4. One Dimensional Descriptor Relationships	139
6.3.5. Event Specific Descriptors	142
6.4. Calculating the IVT Threshold from Catchment Properties.....	145
6.5. Conclusions	149
<i>Chapter 7 Bringing it All Together: An AR Impacts Prediction Framework and Discussion of Results.....</i>	<i>151</i>
7.1 Introduction.....	151
7.2. A Proposed AR Prediction Framework.....	151
7.3. Case Study Applications	153
7.3.1. Storm Desmond: 3 rd -8 th December 2015	153
7.3.2. Storms Ciara and Dennis: 8-9 th and 15-16 th February 2020.....	158
7.3.3. Storm Christoph: 19-20 th January 2021	163
7.4. Discussion	165
7.4.1. How important are ARs in flood generation across the UK?.....	165
7.4.2. How important are catchment properties in modulating the most impactful ARs?	168
7.4.3. Can the inclusion of catchment properties help in predicting AR floods?.....	170
7.5. Conclusions	173
<i>Chapter 8 – Conclusions and Further Work.....</i>	<i>174</i>
8.1. Context	174
8.2. Overall Conclusions.....	174
8.2.1. How important are ARs in flood generation across the UK?.....	174
8.2.2. How important are catchment properties in modulating the most impactful ARs?	175
8.2.3. Can the inclusion of catchment properties help in predicting AR floods?.....	176
8.3. Operational Impact	177
8.3.1. Existing Operational Tools.....	177
8.3.2. The Inclusion of Atmospheric Rivers	177
8.4. Intentions for Further Work.....	178
8.4.1. Develop	178
8.4.2. Operationalise	179
8.4.3. Extend	179

8.5. Final Remarks	180
<i>References</i>	<i>181</i>
<i>Appendices</i>	<i>202</i>

Acknowledgements

First to my supervisors – Andrew Wade, David Lavers and Glenn Watts – thank you for your unwavering support in what hasn't been the most straightforward few years! Your advice and enthusiasm have been second to none, and I feel very lucky to have had the opportunity to work with you all.

Secondly to SCENARIO and the Environment Agency, whose financial support has made this work possible. Thank you also to Harriett Orr and the wider Climate Change team at the Environment Agency for being so accommodating during my placement.

To all those who have provided space for me to present and talk about my work – Water@Reading, the Flood Forecasting Centre, EMS and AGU and many more – the opportunity to discuss and develop my ideas is one that I will no longer take for granted.

To the wider ARTMIP community – thank you for taking a chance on a first-year PhD student and being so welcoming during the workshops that followed.

Thank you to all those with whom I had contact during my data collection process – your advice has no doubt improved the quality of this thesis.

Thank you to Rob Williams at YGC for permitting a change of circumstances when I needed it the most. This PhD wouldn't have happened without your support.

Finally – to my family and friends. Thank you for everything.

Abstract

Atmospheric Rivers (ARs) are one of the main mechanisms of water vapour transport outside of the tropics. Defined as a region of strong horizontal water vapour flux typically located just ahead of the cold front of an extratropical cyclone, they can result in large quantities of precipitation when forced upward, for example by mountains or ascent in the Warm Conveyor Belt. Previous work has investigated the relationship between ARs and the strongest winter floods across a series of British river basins over the period 1979-2010, finding that between 40-80% of all landfalling AR events were followed by a subsequent flooding event. Two Welsh catchments ~70 km apart demonstrated the strongest and weakest relationships respectively; a surprising result given the typical width of ARs to be on the order of 1000 km.

This thesis uses newly available high-resolution datasets to link the arrival of large-scale atmospheric features (in the form of ARs) to local hydrological observations. AR orientation in relation to the land-surface is found to be a primary control on AR impact potential. The role of additional catchment properties is quantified, allowing for the first time, a measure of the extent to which the land-surface modulates the impact of the strongest ARs. In combination with a refining of the AR detection tool, it is possible to predict where an AR will be the most impactful based on its orientation and magnitude alone. These results have developed an understanding of the extent to which ARs are responsible for winter flooding events across the UK as well as increasing flood forecasting potential.

List of Figures

Figure 1.1. ARs associated with Storms Ciara and Dennis in February 2020.

Figure 1.2. Thesis Structure and Layout.

Figure 2.1. Schematic of Large-Scale Mid-Latitude Processes

Figure 2.2. Plan and Cross-Sectional View of Atmospheric Rivers, and their Vertical Structure.

Figure 2.3. Atmospheric Rivers, Warm Conveyor Belts, Mid-Latitude Cyclones and Tropical Moisture Exports.

Figure 2.4. ARs and the WCB

Figure 2.5. Global Properties of Atmospheric Rivers.

Figure 2.6. Landfalling Locations of ARs and Global Impacts.

Figure 2.7. Atmospheric Rivers and European Precipitation

Figure 2.8. The Catchment Perceptual Model.

Figure 2.9. Atmospheric Rivers and the Land Surface – What do we know?

Figure 3.1. Extended Study Area.

Figure 3.2. South Western England.

Figure 3.3. Wales and the English Borders.

Figure 3.4. North Western England.

Figure 3.5. Southern Scotland.

Figure 3.6. Northern Scotland.

Figure 3.7. Size and Configuration.

Figure 3.8. Altitude.

Figure 3.9. Slope and Aspect.

Figure 3.10. Attenuation.

Figure 3.11. Climate and Soils.

Figure 3.12. Land Use.

Figure 3.13. Bedrock.

Figure 3.14. Calculation of IVT Threshold.

Figure 4.1. The location of the Dyfi and Teifi catchments in Wales

Figure 4.2. The distribution of IVT orientation and magnitude of POT3 correlated and non-POT3 correlated ARs at the Dyfi catchment

Figure 4.3. The distribution of IVT orientation and magnitude of POT3 correlated and non-POT3 correlated ARs at the Teifi catchment

Figure 4.4. Time series analysis of landfalling IVT, rainfall and flow patterns at the Dyfi and Teifi catchments in response to an AR on the 11th of February 2002.

Figure 4.5. Summary schematic of the conclusions of Chapter 4.

Figure 5.1. Chapter Summary.

Figure 5.2. Mesoscale Frontal Waves and Secondary Limbs.

Figure 5.3. Missing Timestep Modifications.

Figure 5.4. Secondary Limb Modifications.

Figure 5.5. Updated AR Catalogues according to the Modified Algorithm.

Figure 5.6. Distribution Results according to the Modified Algorithm.

Figure 5.7. Atmospheric River Variability.

Figure 5.8. Atmospheric River Landfalling Locations.

Figure 5.9. Atmospheric River Width.

Figure 5.10. Width Variation over Lifetime.

Figure 5.11. AR Width and Additional Properties.

Figure 5.12. Coastal Atmospheric River Cross Section.

Figure 5.13. Inland Atmospheric River Cross Sections.

Figure 6.1. Orientation and Flux Dominated Catchments.

Figure 6.2. Percentage of POT3 floods associated with ARs of duration 9hr +

Figure 6.3. Orientation Dominated Catchments.

Figure 6.4. IVT Thresholds

Figure 6.5. Correlation Matrix of all Catchment Descriptors

Figure 6.6. Final Descriptor Variables.

Figure 6.7. Principal Component Analysis and Loading Plots

Figure 6.8. Score Plot According to IVT Threshold.

Figure 6.9. Catchment Altitude

Figure 6.10. Catchment Geology, Area and BFIHOST

Figure 6.11. AR Duration and AR-Flood Relationship

Figure 6.12. AR Duration and IVT Threshold

Figure 6.13. Initial Flow and IVT Threshold.

Figure 6.14. Multiple Model Builds.

Figure 6.15. Single Model Build (example).

Figure 6.16. Example Trees from the Forest.

Figure 7.1. The Proposed AR Impacts Framework.

Figure 7.2. Storm Desmond.

Figure 7.3. Storm Desmond Impacts.

Figure 7.4. Storms Ciara and Dennis

Figure 7.5. Storm Ciara Impacts.

Figure 7.6. Storm Dennis Impacts.

Figure 7.7. Storm Christoph.

Figure 7.8. Storm Christoph Impacts.

Figure 7.9. Storm Christoph Algorithm Performance.

List of Tables

Table 2.1. Atmospheric River Detection Schemes

Table 3.1. Selection of Catchments for South Western England.

Table 4.1. Matrix of AR Occurrence

Table 5.1. Matching Events According to the Modified Algorithms.

Table 5.2. AR-Flood Percentages according to the Modified Algorithm.

Table 5.3. Distribution Results according to each AR catalogue.

Table 6.1. Catchments with Preferential Subset of ARs.

List of Abbreviations

- ASPBAR** Mean direction of catchment slopes.
- ASPVAR** Variability in catchment slopes, where values near zero suggest considerable variability. A value of one suggests catchment slopes face in one direction.
- ALTBAR** Mean altitude of the catchment.
- ALTMAX** Maximum altitude of the catchment.
- AMAX** Annual Maximum.
- AR** Atmospheric River.
- ARDM** Atmospheric River Detection Method.
- ARO** Atmospheric River Observatory.
- ARTMIP** Atmospheric River Tracking Method Intercomparison Project.
- ASM** Antecedent Soil Moisture.
- BFIHOST** Base Flow Index derived from the HOST Classification.
- BGS** British Geological Survey.
- CALJET** California Landfalling Jets Experiment
- CEH** Centre for Ecology and Hydrology.
- DPLBAR** Mean distance between catchment nodes and outlet. Characterises catchment shape.
- DSPBAR** Mean catchment slope.
- EA** Environment Agency.
- ECMWF** European Centre for Medium-Range Weather Forecasts.
- EFI** Extreme Forecast Index.
- ERA5** ECMWF Reanalysis 5th Generation.
- FARL** Index of Flood Attenuation attributable to reservoirs and lakes.
- FEH** Flood Estimation Handbook.
- GCM** Global Climate Model
- IFS** Integrated Forecasting System
- IHDTM** Integrated Hydrological Digital Terrain Model.
- IVT** Integrated Vapour Transport.
- IWV** Integrated Water Vapour.
- LDP** Longest Drainage Path.
- LLJ** Low Level Jet.

MERRA Modern Era Retrospective-Analysis for Research and Applications.

MFW Mesoscale Frontal Waves.

NRFA National River Flow Archive.

NRW Natural Resources Wales.

PCA Principal Component Analysis.

POT Peaks Over Threshold.

PROPWET Measure of historical catchment wetness.

RFR Random Forest Regression.

SAAR Standard Period (1961-90) average annual rainfall.

SEPA Scottish Environment Protection Agency.

Sf Shape Factor.

SPRHOST Standard Percentage Runoff derived from HOST classification.

TME Tropical Moisture Export.

UK United Kingdom.

URBEXT Extent of urban and suburban land cover.

WCB Warm Conveyor Belt.

Publications and Awards

1. **Griffith, H. V.**, Wade, A. J., Lavers, D. A., & Watts, G. (2020). Atmospheric river orientation determines flood occurrence. *Hydrological Processes*, 34(23), 4547-4555.
2. Rutz, J. J., Shields, C. A., Lora, J. M., Payne, A. E., Guan, B., Ullrich, P., ... (incl. **Griffith. H**) & Viale, M. (2019). The atmospheric river tracking method intercomparison project (ARTMIP): quantifying uncertainties in atmospheric river climatology. *Journal of Geophysical Research: Atmospheres*, 124(24), 13777-13802. (Part of analysis team)
3. “What is Catchment Resilience?” Output from Environment Agency placement – **Griffith H** (August 2019).
4. Environment Agency “Catchment Resilience” Workshop Report (July 2019) – one of the co-authors.
5. Neumann, J. L., Arnal, L., Emerton, R. E., **Griffith, H.**, Hyslop, S., Theofanidi, S., & Cloke, H. L. (2018). Can seasonal hydrological forecasts inform local decisions and actions? A decision-making activity. *Geoscience Communication*, 1(1), 35-57. (Note taker and Facilitator)
6. **‘PhD Researcher of the Year’** awarded by the School of Environmental Science at Reading for work across 2020-21.

Science Communication

2021

Carbon Brief Article

An article written for the Carbon Brief that describes Atmospheric Rivers, their role in winter flooding and how the frequency of Atmospheric Rivers and therefore flooding might change in the future.

<https://www.carbonbrief.org/guest-post-the-role-of-atmospheric-rivers-in-uk-winter-floods>

Interview with BBC Radio Berks

Featured in the Times

Prevention Web reproduces Carbon Brief Article

Engagement with the Departmental social media

2020

HEPEX Blog

A short article regarding the influence of Atmospheric Rivers on Storms Ciara and Dennis and the subsequent widespread flooding that was observed in February 2020.

<https://hepex.inrae.fr/atm-rivers-ciara-dennis/>

2019

Environment Agency Placement (6-months)

Midway through my PhD, I undertook a 6-month placement with the Environment Agency, based within the Climate Change and Resource Efficiency team. Working alongside experienced colleagues, I delivered a project focused on 'Understanding Catchment Resilience' and how this concept may be quantified. Highlights from the placement were the creation of a thorough literature review, the development of an internal workshop (including leading a session and facilitating discussions) and collating the workshop report.

2018

COP CAS Blog

A piece for the Student COP-CAS blog regarding experiences of virtual participation of COP23 within the Walker Institute at Reading.

<http://www.walker.ac.uk/academy/cop-cas/participant-blogs/cop23-reflections-on-my-first-cop/>

Chapter 1 – Introduction

1.1. Rationale

There is strong evidence of change in the UK climate (Watts et al., 2015). Since 2009, the UK has experienced its wettest February, April, June, November and December, in combination with consistently rising mean annual temperatures (Kendon et al., 2021). Storms Ciara and Dennis of February 2020 alone, made headlines not only for their unprecedented rainfall totals, but the widespread flooding that displaced thousands from their homes across England and Wales.

For centuries, a drop in atmospheric pressure has signalled advancing unsettled conditions. The age of satellites and increased technical capability has permitted a steady accumulation of knowledge regarding the meteorological processes behind such observations (Bauer et al., 2015). Synoptic scale, low pressure cyclones travel across oceanic storm tracks, generating the majority of precipitation across the UK during the winter months (Chapter 2, section 2.2; Browning & Harrold, 1970).

Large-scale circulation patterns such as the North-Atlantic Oscillation (NAO), in combination with variations in the position and strength of the “jet stream” (Chapter 2, section 2.2), go some way towards controlling the strength and frequency of winter cyclonic storms affecting the UK. In particular, the storms of February 2020 were likely driven by a combination of extremes of both effects. However, the sheer volume of rainfall generated by the most extreme of these events can be attributed to a coincident ‘tail’ of low-level atmospheric moisture. This feature can now be identified as an ‘atmospheric river’ (AR).

1.2. The Atmospheric River

An AR can be defined as a narrow band of horizontal water vapour flux located just ahead of the cold front of a landfalling cyclone (Chapter 2, section 2.2). The flux is primarily concentrated within the lowest 2 km of the atmosphere which, in combination with moist-neutral stability, results in a region highly susceptible to orographic forcing (Ralph et al., 2005). When a storm makes landfall therefore, accompanied by its AR, the presence of mountainous coastal topography can induce heavy and persistent rainfall.

ARs are associated with some of the most extreme rainfall events across the mid-latitudes (chapter 2, section 2.4), including storms Ciara and Dennis (Fig 1.1; Chapter 7, section 7.3). Across the UK, they have been found to account for between 40 and 80% of the most intense flood events across a series of nine river basins across the historical, 1979-2010, period (Lavers et al., 2012). The strongest and weakest associations, however, were found across two catchments located within western Wales. Existing less than 70 km apart, the Dyfi at Dyfi Bridge and Teifi at Glan Teifi catchments respectively, provided the first evidence that the presence of an AR alone is insufficient to generate the strongest hydrological responses. It is this observation that has driven the development of this thesis.

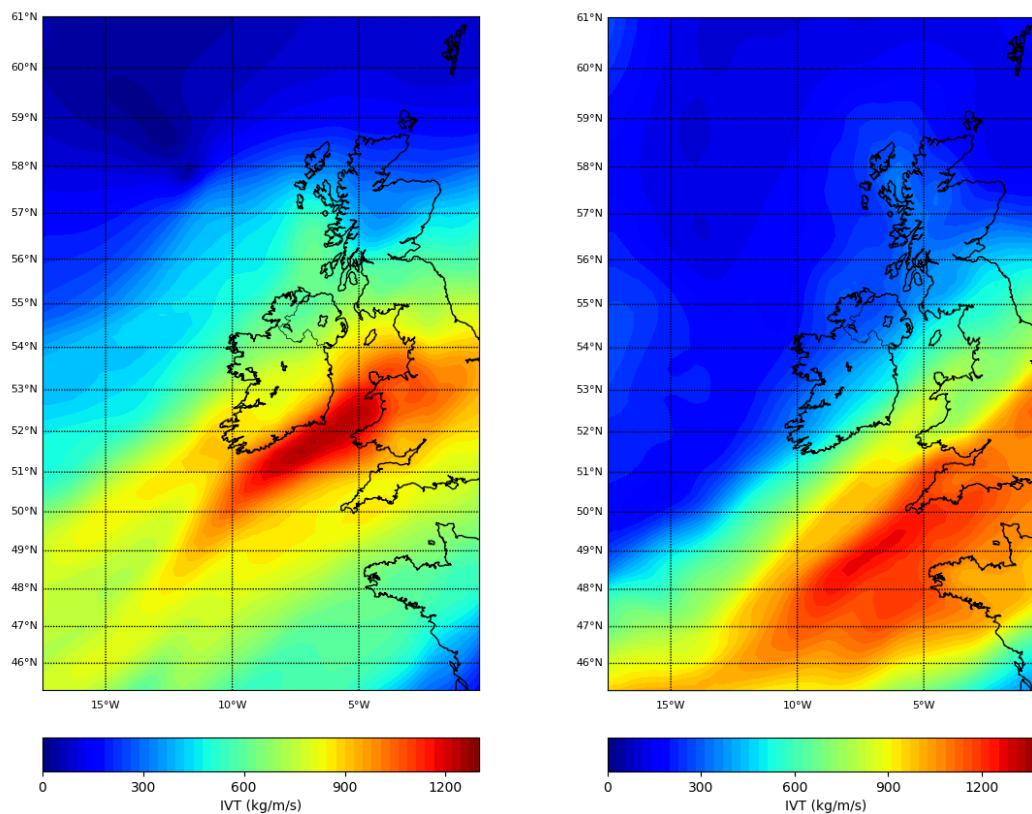


Figure 1.1. Storms Ciara and Dennis. The Integrated Vapour Transport as calculated from ERA5 reanalysis on the 9th of February 2020 0700UTC (left-hand panel; Storm Ciara) and the 16th of February 2020 0200UTC (right-hand panel; Storm Dennis). Where storm Ciara delivered high-intensity, short duration moisture flux to regions of north and western Wales, storm Dennis was centred on parts of south Wales and Cornwall and resulted in more sustained rainfall. Both storms were associated with a ‘tail’ of intense moisture flux, known as an atmospheric river.

1.3. Research Gaps and Objectives

The UK typically experiences between four to five intense AR events each winter, however not all result in impacts on the scale of that observed in February 2020. An AR Categorisation Scale has been recently proposed by Ralph et al. (2019) for US west coast, later extended to European regions by Eiras-Barca et al., (2021). This scale uses a combination of (maximum) overhead moisture flux and duration to infer a category spanning 1 through 5. A category 1 AR is primarily beneficial, providing essential moisture recharge during the winter months, whilst a category 5 AR may be strong and/or persistent enough to present a hazard (Chapter 7, section 7.5).

It is likely however, that the land-surface properties of the landfalling region will play a role in enhancing, or suppressing, the initial ‘risk scales’ as proposed in the scale above. Indeed, a whole suite of meteorological and land-surface properties have been identified as important in controlling the impact potential of landfalling AR (Chapter 2, section 2.6; Ralph et al., 2020, Chapter 5). Within a warming climate, ARs are expected to become stronger and more numerous (Lavers et al., 2013) and thus, understanding how and why the most extreme events occur is essential for adequate preparation and forecasts.

The aim of this thesis, therefore, is to understand the role that land-surface properties play in modulating AR impact. This aim will be addressed via several objectives as outlined below and explored in greater detail towards the end of the following Chapter (Chapter 2, section 2.7).

- 1) How important are ARs in flood generation across the UK?
- 2) To what extent do land-surface and additional catchment properties modulate AR impact?
- 3) Can the inclusion of catchment properties help in predicting AR floods?

1.4. Thesis Structure

The thesis structure is detailed below alongside an illustration of the layout and inter-relationships between the chapters (Fig. 1.2). Chapter 2 provides a review of the literature, exploring the history of ARs and expanding on their structure and origin. The chapter cumulates

in an identification of the research gap and expands on the detailed research objectives as outlined in the previous section. Chapter 3 describes the study areas used in the thesis, alongside an overview of the data and methods applied. This will include the algorithm used to detect ARs in atmospheric datasets and the statistical processes and models developed in later stages of analysis. It aims to exist as a point of reference for the following research chapters.

Chapters 4, 5 and 6 describe the research findings of this thesis. Initially building on the work of Lavers et al. (2012) by invoking newly available high-resolution hydrological and atmospheric datasets, the role of ARs in wintertime flooding at the Dyfi and Teifi catchments is inspected across the historical period. Chapter 5 quantifies the performance of the chosen AR detection scheme in the context of high resolution data and offers several improvements. It also tests numerous underlying assumptions regarding AR properties, ensuring that the most appropriate metrics are extracted.

Chapter 6 further explores the relationship between landfalling ARs and significant wintertime flooding events across a series of 81 study catchments, primarily located within the western half of the UK. In particular, the role of catchment properties is quantified, allowing for the first time an identification of the aspects of a catchment that influence the strongest hydrological response from a landfalling AR.

Chapter 7 combines the findings of the previous chapters of the thesis into an operational style framework. Given the properties of a landfalling AR, is it possible to identify, on the basis of land-surface and catchment level processes, where its impacts will be strongest? This work intends to provide a starting point for the inclusion of atmospheric river consideration into forecasting tools. A critical analysis of the overall results is performed in the context of a discussion section. Finally, chapter 8 synthesises the findings and develops the final conclusions. The thesis ends with suggestions for future work.

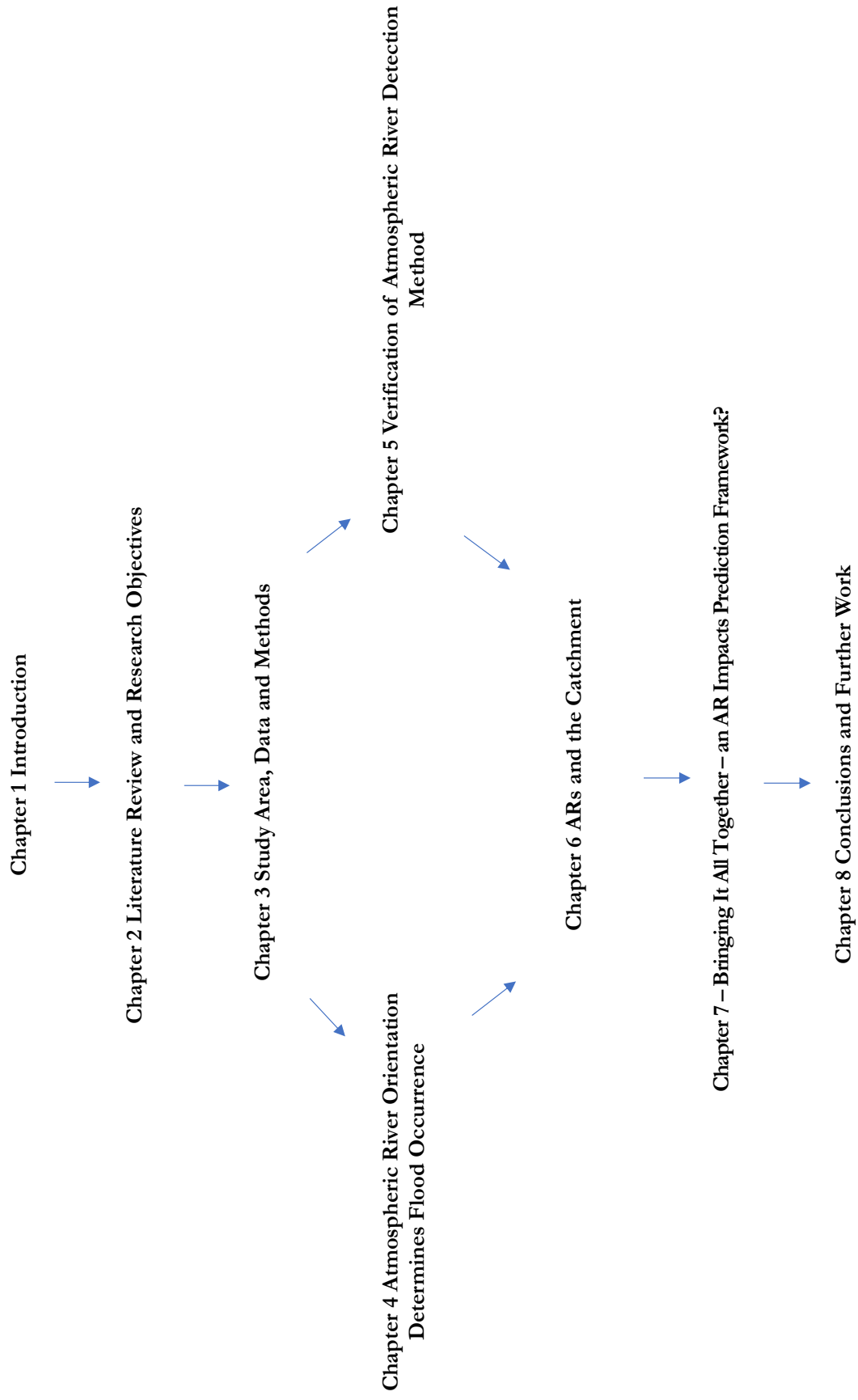


Fig 1.2. Thesis Structure.

Chapter 2 – Literature Review and Research Objectives

2.1. Introduction

The scientific study of atmospheric rivers (ARs) has increased greatly over the last 30 years. In the early 1990s, only a handful of papers published contained the term, however a search towards the end of 2020 identified nearly 600 papers published across the previous 12 months¹, written by scientists from a variety of disciplines, including meteorology, hydrology, engineering, biology and polar science.

An important aspect of the global hydrological cycle, ARs provide an essential source of water resource where they make landfall, as well influencing flood and drought risk to populated coastal areas. The ‘rivers in the sky’ concept has attracted media and public attention, encouraging the involvement of stakeholders across the forecasting and response chain. This collaboration has permitted the development of novel and pioneering field campaigns, moving forward not only understanding of the meteorological processes behind the strongest winter storms, but also the detailed hydrometeorological interactions between such storms and the land surface. From a forecasting perspective, such knowledge is essential.

This chapter provides a review of AR science, with particular focus on catchment impacts. Following this, a gap emerges to develop understanding of AR processes from a hydrological perspective, with the aim of ultimately enhancing our ability to detect, and forecast, the most extreme events.

2.2. Water Vapour in the Mid-Latitudes

2.2.1. Dominant Processes and Early Work

The mid-latitudes describe a turbulent band of the troposphere where the movement of warm, moist air from the tropics and cool, dry air from the poles results in a region of strong baroclinic

¹ Source: Google Scholar search for “atmospheric river”; 14th December 2020.

instability. The presence of large-scale ocean currents and seasonal changes in solar input result in a complex interplay between the air-ocean system that fundamentally drives everyday weather systems at a range of scales.

At ground level, a perturbation in the surface where air masses meet, and the resulting pressure gradient, can result in a local pressure minimum at sea level. Warm, lighter air rises above its cooler, dense counterpart, leading to the development of a frontal system driven by strong anticlockwise winds (or clockwise, in the southern hemisphere). This frontal system is known more commonly as a mid-latitude (or extratropical) cyclone and was first explored by in the early 20th century by Bjerknes (1910) in the development of the ‘Bergen School Cyclone’ or later the ‘Conveyor Belt’ Theory (Fig. 2.1).

Towards higher latitudes, the pressure imbalance is reversed as the cooler polar air is concentrated towards the surface. However, at this height the frictional forces are negligible compared to those at the surface, and therefore the rotational forces of the Earth deflect the winds into strong upper-level flows known more commonly as the Westerlies. This ribbon of high-speed air meanders its way around the globe, shaping what we now know as the jet stream (Fig. 2.1), a key driver of everyday weather patterns.

Aided by the presence of the jet stream, the passage of extratropical cyclones across major oceans are generally confined to a narrow region known as the ‘storm track’. A large proportion (up to 90%) of rainfall in these regions is associated with frontal systems (Catto et al., 2012), and the characteristic comma-shaped frontal pattern that results is a key feature in modern day weather maps, instantly recognisable and a key control on winter precipitation in the UK (Browning & Harrold, 1970a)².

Early studies therefore, attempted to understand the precipitation generating processes at these comma-shaped, frontal systems as they were too small to be adequately detected by the routine synoptic observations of the time (Browning & Harrold, 1970b). The wind, temperature and humidity distribution across typical cold fronts in south east England were analysed via

² <https://www.metoffice.gov.uk/weather/learn-about/weather/types-of-weather/rain/how-much-does-it-rain-in-the-uk>

radarsondes, revealing a marked fall in humidity in regions above 700 mb (around 3km above the surface) without a corresponding fall in temperature and/or wind direction (Miles, 1962).

Subsequently, Browning & Harrold (1970), in their case study of a cold front affecting the UK, found that nearly all precipitation could be traced back to a narrow band of convection just ahead of the cold front. This band was noted to be part of a broader flow (typically 200km wide and 2km deep) that ultimately ascended along the main frontal zone (Browning et al., 1973; Browning & Pardoe, 1973; Fig. 2.2).

This flow can now be identified as the so-called Warm Conveyor Belt (Eckhardt et al., 2004); a tongue of warm, moist air responsible for the majority of latent heat transport across frontal zones. The region containing the convection band has been termed the 'convective boundary layer' and defines a band of anomalously warm moist air bounded on its forward side by a so-called low-level jet (LLJ). This jet acts to transport warm, saturated air along the region just ahead of, and parallel to, the cold front (Fig. 2.2.). When this low-lying flow encounters coastal terrain, orographic uplift of the moist air can result in heavy precipitation (Miglietta & Rotunno, 2005).

2.2.2. What is an Atmospheric River?

The Measurement of Air Pollution by Satellites (MAPS) program by NASA in the early 1990s, inadvertently revealed filaments of global tropospheric water vapour flux, with lengths many times greater than their width., persisting across the mid-latitudes for many days at time. These regions were initially termed 'tropospheric rivers' (Newell et al., 1992), later updated to the term 'atmospheric rivers' (ARs). Noted to exist across most the world's major oceans, the leading 'heads' of the rivers were observed to coincide with precipitating frontal systems, with the 'tails' spanning many thousands of kilometres back across the ocean (Newell & Zhu, 1994).

An understanding of the importance of ARs in the water cycle came through the development of the first quantitative method to identify them in atmospheric data sets (Zhu & Newell, 1998a). They were found to account for almost all the meridional water vapour transport across the mid-latitudes (>90%) at any one time, despite occupying less than 10% of the total longitudinal length. The analysis also confirmed the association of the rivers with cyclonic storm tracks and linked the moisture convergence at their head to rapidly developing cyclones.

It was suspected that possible alignment of the rivers with the LLJ region of cyclones (Browning & Pardoe, 1973) could result in favourable conditions for orographic enhancement if and when the system made landfall. However, limitations in the observational methods at the time meant that processes controlling the extent of such enhancement (namely the water vapour content and horizontal winds) were difficult to measure, alongside legitimate and expected resistance to such novel ideas and concepts. There was some doubt in particular regarding the existence of ARs as a separate phenomenon to the well-known Warm Conveyor Belt.

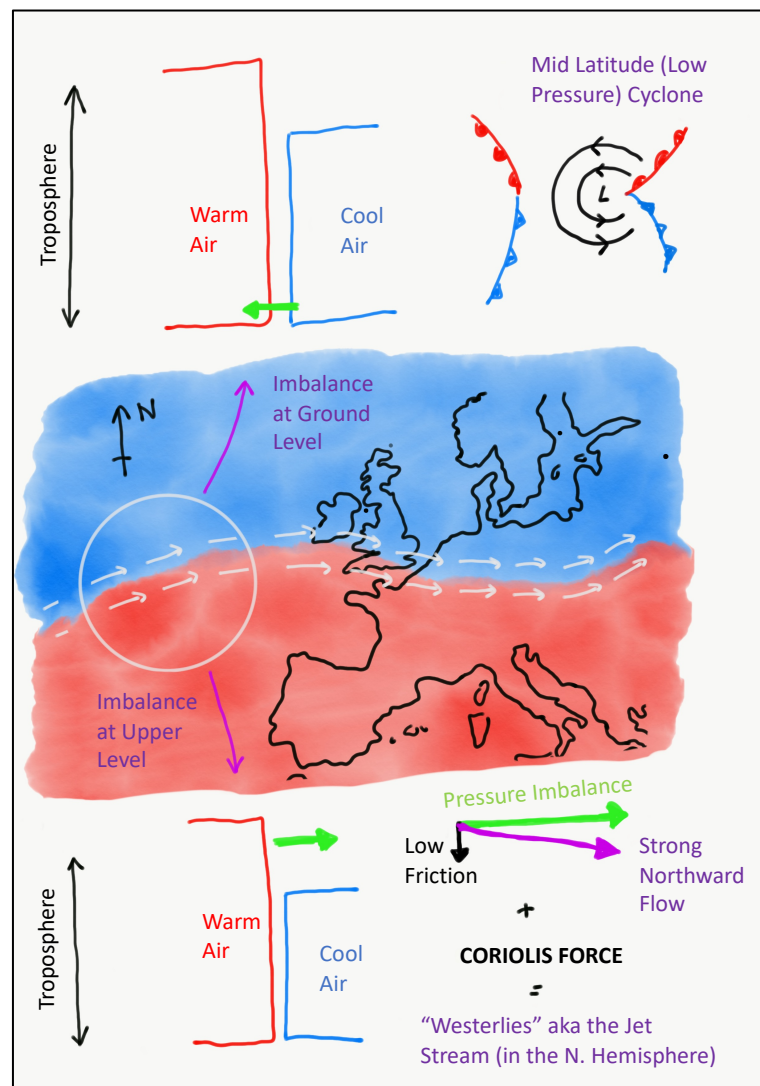


Figure 2.1. Schematic of Large-Scale Mid-Latitude Processes. The meeting of warm tropical air and cool polar air, the latter of which is concentrated towards the surface, results in an upper-level thermal gradient. The resulting winds are shaped into a narrow ribbon of meandering winds toward the top of the troposphere, more commonly known as the jet stream. A perturbation in the surface between the air masses near ground level can result in the formation of a low-pressure system, characterised by anti-clockwise winds (in the northern hemisphere).

The turn of the century brought several key developments that helped address such concerns. The California Landfalling Jets (CALJET) campaign was proposed to probe US west coast winter storms in greater detail than ever before (Ralph et al., 2004), and the number of special sensor microwave/imager (SSM/I) satellites had grown to allow a near global view of water vapour across the oceans. This allowed the first reanalysis (a combination of weather prediction models with real time observation) to be developed at National Centers for Atmospheric Prediction and Atmospheric Research in the USA (NCEP/NCAR; Kalnay et al., 1996).

CALJET (and later PACJET) were developed to study the characteristics of landfalling winter storms along the California coast during the winter of 1997/8 (Ralph et al., 2004; Ralph et al., 2005). Working with the US Air Force, dropsondes were released through mid-latitude cyclones and LLJs to build up a cross sectional view of storm structure that would have been impossible through remote sensing methods alone. It was hoped that the results would lead to a better understanding of the underlying physical processes associated with heavy rains and strong winds brought by winter storms along the US west coast.

A narrow band of strong horizontal water vapour flux just ahead of the cold front of the landfalling cyclones was identified as an AR (Fig. 2.2), primarily concentrated at low altitudes where a combination of strong winds and large water vapour content exist as part of the low-level jet. A layer of moist-neutral stability was identified to extend upwards from the sea surface to well above the altitude of the low-level jet and California's coastal mountains (Ralph et al., 2005) which, in combination with the region of enhanced flux, results in a region highly susceptible to orographic forcing.

This ultimately explains why ARs are important in terms of precipitation; the conditions are aligned for the inducement of heavy rainfall when the warm, moist air is forced to rise during landfall. It also shows how the early studies of Browning & Pardoe (1973) were correct in identifying the LLJ as a key control on precipitation.

With these ideas came a call for clarity on the relationship between ARs and the well-known warm conveyor belt (WCB). To what extent does the presence of an AR depend on the occurrence of mid-latitude cyclone? And how accurate is their description in terms of 'rivers'? Are they indeed responsible for the long-range transport of moisture out of the tropics and across the world's vast oceans, or are there more subtle processes at work? How about intense moisture transports located

within the tropical regions themselves? The following section will attempt to bring these ideas and concepts together.

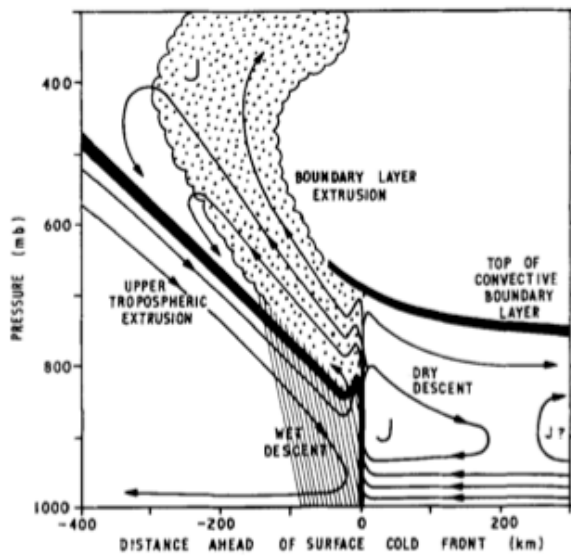


Figure 2.2 The Origin of Precipitation Across UK Cold Fronts. Taken from Browning & Pardoe (1973) we note the location of the Convective Boundary Layer and the embedded Low Level Jet. The broad, moist air flow ascending along the frontal zone can now be recognised as the well-known Warm Conveyor Belt (Eckhardt et al., 2004)

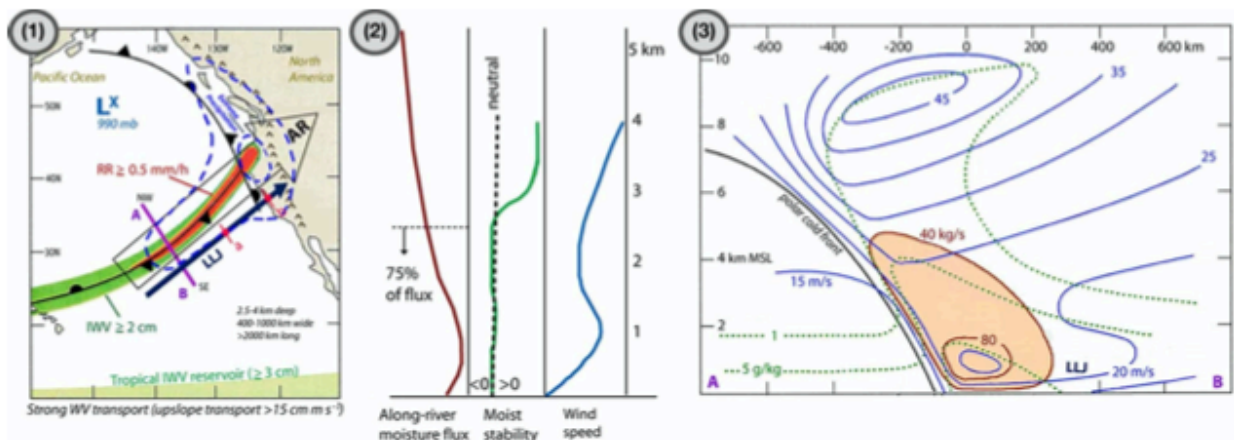


Figure 2.2 Plan and Cross-Sectional View of Atmospheric Rivers, and their Vertical Structure. Taken from Gimeno et al., (2014), this figure provides a schematic overview of the structure of atmospheric rivers including plan and section view as well as the vertical structure of moisture flux, moist static stability and wind speed. In combination these subplots explain the susceptibility of atmospheric rivers to orographic enhancement of precipitation when they impact on elevated terrain.

2.3. Atmospheric River Origin

2.3.1. Atmospheric River Moisture Sources

This section begins with a definition of the key components of the water vapour system at the relevant meso- to synoptic- scales. ARs describe, as previously mentioned, filamentary bands of intense water vapour transport across the mid latitudes, with the Warm Conveyor Belts (WCBs) referring instead to the broad ribbon of ascending warm air within extratropical cyclones (Eckhardt et al., 2004). Previously unmentioned, but important aspects of the global water vapour system, are the Tropical Moisture Exports (TMEs), which describe regions of intense moisture flux out of the tropics towards the subtropics and/or midlatitudes. Whilst the history of the Warm Conveyor Belt can be traced back further than a century (Bjerknes 1910), those of ARs and TMEs are much more recent (Knippertz & Wernli, 2010; Newell et al., 1992). A lack of clear quantitative definitions regarding these concepts is likely responsible for much early confusion within the scientific community about how one is related and/or differs from the other.

A meeting of AR scientists in June 2015 (Dettinger et al., 2015) went some way to producing a combined definition of the relative roles of ARs, WCBs and TMEs (Fig 2.3). The TMEs describe a broad region of moisture exported out of the tropics. This moisture may be channelled across the midlatitudes in a narrow region known as an AR. At the head of the river exists an extratropical cyclone, where the low-level moisture flux transported by the AR impinges on coastal locations followed by broad scale ascent in the WCB.

These ideas were not without controversy however, as questions were raised regarding the credibility of the long-range moisture transport proposed to occur within ARs. A trajectory analysis presented by Bao et al. (2006), provides an example of the typical complexity of such a question.

2.3.1.1. Local Transport and Moisture Cycling

Many of the ARs (Bao et al., 2006) were noted to contain vapour from local sources, likely a result of moisture convergence associated with the WCB and the cold front of extratropical cyclones. Taking the form of small-scale moisture recycling, through evaporation from the sea surface, followed by condensation and subsequent precipitation, it is likely that water is continually lost

and refreshed ahead of the cold front. As the front moves forward the resulting water vapour track gives the appearance of a river in satellite imagery but does not share its long-range transport processes. These ideas were supported by Dacre et al. (2015) who suggested that the filamentary structures of high water-vapour content were only a result of local convergence of water vapour, existing as ‘footprints’ whilst the cyclones track northward.

It is possible to investigate these concepts in greater detail by transforming the relevant airstreams to the cyclone frame of reference (Dacre et al., 2019; Figure 2.4). A low-level moist air flow known as the ‘feeder airstream’ (FA) travels rearwards (relative to cyclone propagation) before splitting into two components just ahead of the cyclone cold front. The component that turns towards the cyclone centre is responsible for the water vapour transport to the base of the WCB, whereas the other component travels parallel to the cold front (at a speed less than the velocity of the cyclone).

Thus, as the cyclone moves poleward, a long filament of total column water vapour is left behind. This marks the cyclone ‘footprint’, as in Dacre et al. (2015) or the AR. The total transported moisture flux was found to be sensitive to the moisture content at the entrance to the feeder airstream; thus, the more moisture swept up by the cold front as it travels poleward, the stronger the AR.

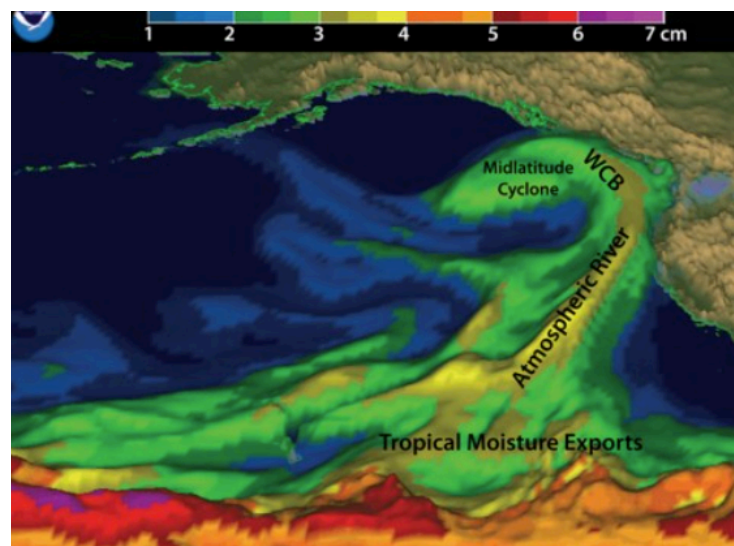


Figure 2.3 Atmospheric Rivers, Warm Conveyor Belts, Mid-Latitude Cyclones and Tropical Moisture Exports. Taken from Dettinger et al., (2015), a broad region of tropical moisture is exported across the midlatitudes in a narrow region known as an AR. At the head of the river exists an extratropical cyclone, where the low-level moisture flux transported by the AR impinges on coastal locations followed by broad scale ascent in the WCB.

2.3.1.2. Long Range Transport and Synoptic Conditions

However, some of the ARs identified by Bao et al. (2006) did indeed suggest evidence of direct poleward transport of tropical moisture, though primarily in combination with favourable synoptic-scale atmospheric conditions. For example, a weakened sub-tropical ridge within the central Pacific can permit a south-westerly low-level moisture flow from the tropics towards the US west coast. Similar results, in terms of a subtropical contribution to atmospheric moisture sources, have been found more widely across the Pacific and north Atlantic oceans (Cordeira et al., 2013; Liberato et al., 2013; Moore et al., 2012; Nayak et al., 2016; Ralph et al., 2011; Ramos et al., 2016).

Given these two different results, it is likely therefore that the majority of AR events are comprised of a combination of local moisture convergence and long-range moisture transport (Cordeira et al., 2013). Stohl et al. (2008) and Sodemann & Stohl (2013) have both been able to identify the presence of remote water vapour sources within ARs impacting on Norwegian shores. However, they have also noted that the cyclones existing along the river track were exhibiting a rapid cycling of local moisture sources (from the underlying ocean surface), thus aligning with the results of Dacre et al. (2015, 2019).

Thus, the correct conditions in the vicinity of mid-latitude cyclones can permit a flow of intense water vapour transport towards the poles, but the origins of this moisture may vary depending on the extent of water vapour transport out of the (sub) tropics and the degree of local water cycling.

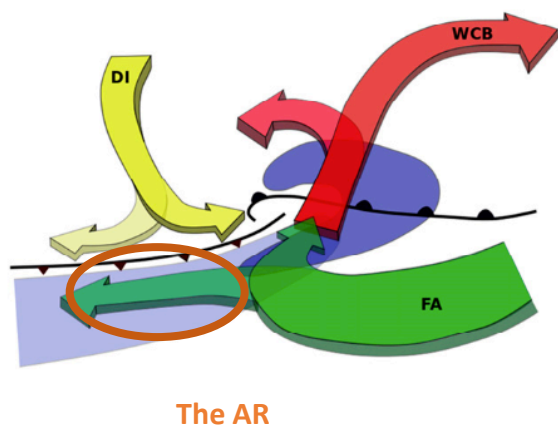


Figure 2.4 ARs and the WCB. Taken from Dacre et al. (2019), the atmospheric river exists as the ‘footprint’ of total column water vapour left behind as the cyclone moves forward i.e. it is formed locally. The AR strength is thus related to the amount of moisture swept up ahead of the cold front. There are several publications however to suggest that this is not the only method of AR formation, with evidence of tropical moisture sources. FA: Feeder Airstream. WCB: Warm Conveyor Belt. DI: Dry Intrusion.

2.3.2. Atmospheric River Formation Processes

AR formation occurs at two scales, firstly as part of the enhanced poleward water vapour flux that develops when a strong thermal gradient across a mid-latitude (synoptic-scale) cyclone cold front results in the formation of a low-level jet (Ralph et al., 2004, 2005) and secondly when (large-scale) upper level air streams (known as the Westerlies) demonstrate tight meanders (or ‘eddies’) that allows the penetration of mid-latitude troughs into subtropical latitudes. This penetration can permit the poleward water vapour transport out of the tropics and into the mid-latitudes (Ralph et al., 2020). This process, known as Rossby Wave Breaking (RWB), can also provide favourable conditions for cyclogenesis (Priestley et al., 2020) and has been associated with many extreme precipitation events across the world (de Vries, 2021).

2.4. Atmospheric River Impacts

2.4.1. Early field campaigns – moving towards an AR definition?

The combination of the CALJET field campaign (Ralph et al., 2004) and readily available microwave observations (SSM/I; Neiman et al., 2008) at the turn of the century allowed the development of the first operational definitions of an AR. The key metric in satellite data at the time was Integrated Water Vapor (the sum of water vapour content within the atmospheric column; IWV). In combination with specific geometry, a working definition was developed (Ralph et al., 2004) – for a feature to be identified as an AR it must possess a length greater than 2000km, a width less than 1000km and IWV values of greater than 20mm. The simplicity of this definition means that, nearly 20 years later, it is still a well-known approach.

The novelty of the inclusion of observational data during the US west coast field campaigns was that, in addition to the water vapour content, it was possible to measure the horizontal winds within the vicinity of ARs. The combination of water vapour content with the winds is denoted as the Integrated Water Vapor Transport (or water vapour flux; IVT). The studies of the LLJ during CALJET identified the region of intense water vapor flux existing approximately 1km aloft, perfectly aligned for the orographic enhancement of precipitation if the moist air is forced to rise (Neiman et al., 2002). The moist neutral properties of the driving air flow means that it is unlikely to resist uplift if subjected to elevated terrain (for example, the Californian coastal mountains; Ralph et al., 2005) and thus, the combination of water vapour content and driving winds provides a more accurate description of AR precipitation potential. Defined according to the similar

geometric criteria as for the IWV approach, the IVT threshold is typically taken as $250\text{kg m}^{-1} \text{s}^{-1}$ along the US west coast during the winter season.

The development of reanalysis products over the last twenty years has permitted the study of large-scale features (such as ARs) which may otherwise have been difficult to contain by observational methods alone. As well as allowing the investigation of ARs across other regions of the globe (outside of those targeted by the field campaigns and/or satellite retrieval), the development of reanalysis across historical and future periods can also provide an opportunity to study long term trends (see Section 2.5).

2.4.2. Impact Across the World

2.4.2.1. *A Global Perspective*

A global AR climatology has been developed by Guan & Waliser (2015) in which they define an Atmospheric River Detection Method (ARDM) similar to that of Ralph et al. (2004) but with a percentile specific threshold. For each season they assigned an 85th percentile IVT threshold to each grid cell across the ERA-Interim reanalysis (spanning 1997-2014), thereby isolating regions of enhanced IVT from the ‘normal’ background. This study represented the first ARDM suitable for global studies and paved the way for analysis of global AR characteristics. A brief overview of these will be given here as an introduction to more regional studies.

At any one time, an average of 11 ARs are present across the globe with around two to three of these making landfall. In striking agreement with that of Zhu & Newell (1998), ARs are found to account for over 90% of poleward water vapour transport across the mid-latitudes despite occupying less than 10% of the earth’s circumference. An overview of basic geometry, location and IVT characteristics is given in the histograms of Fig. 2.5. Points to note are an average length-to-width ratio of 6.8; much larger than the usual threshold of 2. The probability of occurrence distributions over maximum, minimum and mean latitudes verify that ARs are predominantly mid-latitude features, demonstrating a wide range of IVT magnitudes and, albeit to a smaller extent, direction angles (in each hemisphere). The direction of IVT flux is found to be largely consistent over a specific event, suggesting that ARs do indeed exist as very effective mechanisms of horizontal moisture transport across the mid-latitudes.

The global distribution of landfalling features, and their vertical profiles are given in Fig. 2.7 (from Guan & Waliser (2015)). ARs can be found across the west coasts of North America, South America and Europe, with the majority of landfalling flux concentrated at lower levels (800-900hPa). AR landfalls also occur in regions that have received less scientific attention, namely eastern Asia, Australia, New Zealand and the polar regions.

Notable seasonal variations occur across the Pacific and Atlantic ARs, with a greater number occurring in autumn and winter (defined as Sept, Oct, Nov and Dec, Jan, Feb respectively). During this time of year, a gradual shift of peak AR frequency from higher latitudes during autumn to lower latitudes across winter follows storm track movement. An overview of research is provided in the review by Gimeno et al. (2016).

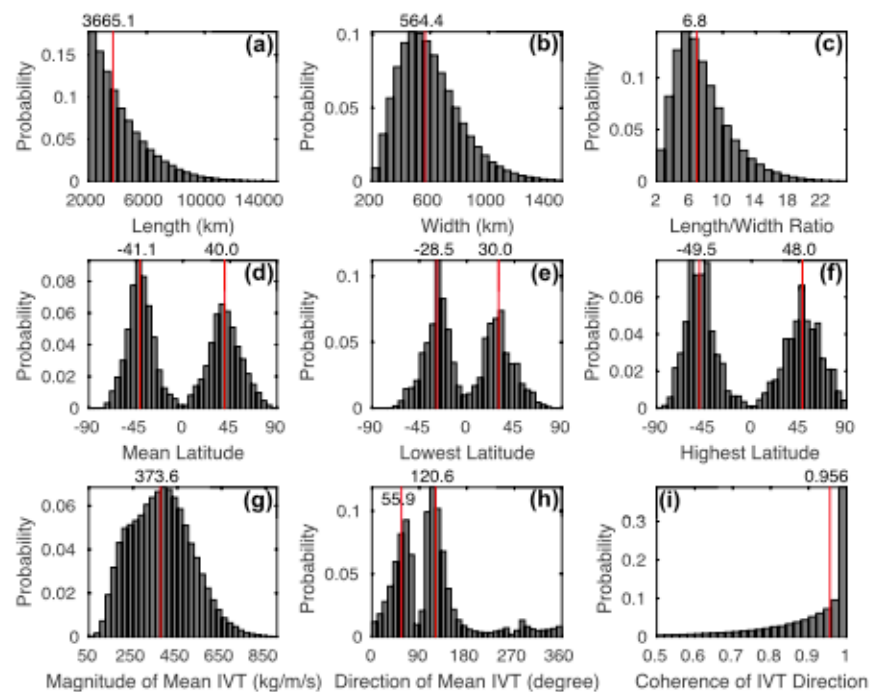


Figure 2.5 Global Properties of Atmospheric Rivers. Taken from Guan and Waliser (2015), ARs are primarily mid-latitude features demonstrating a wide range of IVT magnitudes and, albeit to a smaller extent, direction angles (in each hemisphere). The direction of IVT flux is found to be largely aligned with the direction of the mean within a specific event.

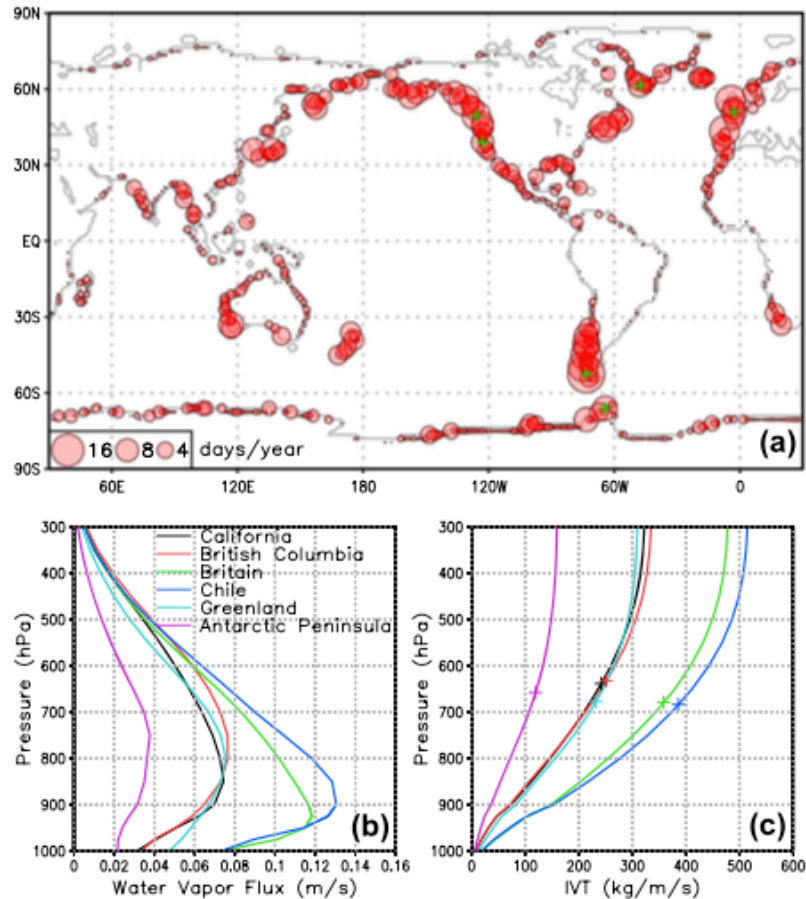


Figure 2.6. Landfalling Locations of ARs and Global Impacts. Taken from Guan & Waliser (2015), ARs are particularly numerous along the coastlines of western United States, Europe and South America. All ARs demonstrate a concentration of water vapour flux at lower levels (800-900hPa).

2.4.2.2. The United States

The west coast of the United States has been at the forefront of AR science since the discovery of the so-called ‘Pineapple-Express’ (Dettinger, 2004, 2011); a subset of ARs originating near Hawaii that can result in heavy precipitation delivered to the US West Coast during the winter season. This precipitation accounts for a notable fraction of the total annual precipitation delivered to the region, and therefore its occurrence (or not) is important from a combined flood-risk and water resources perspective.

The first climatology of ARs across the US was based on a combination of SSM/I satellite observations (and subsequent identification) across an eight-year period, with NCEP-NCAR reanalysis provided for synoptic context (Neiman et al., 2008). Whilst the results were broadly in

line with the updated (global) results of Guan & Waliser (2015), notable differences were identified in the number of detected ARs in the warm season relative to the cool season. Ralph et al. (2020) proposes these differences arise due to the AR detection method applied, and in particular, the use of IVW vs IVT as the detection metric (see Section 2.5 for further discussion of AR detection methods). This result suggests the inherent sensitivity of AR results to the detection metric applied.

The climatology of Gershunov et al. (2017) provided a perfect opportunity to compare these differences, as detection methods using both metrics were applied to the same NCEP-NCAR dataset. The explanation appears to lie with the amount of atmospheric moisture, and the typical wind distribution, across the storm seasons. In the summer, there is greater availability of atmospheric moisture, and thus typical IWV values are higher. However, the strength of atmospheric winds is reduced due to fewer intense mid-latitude storms. The IVT metric takes into account the horizontal wind strength in combination with the moisture content, and therefore removes some of the 'high moisture- low wind' events typical across the summer period. As it is the orographic enhancement of the atmospheric moisture when the AR makes landfall along the elevated terrain of the US West Coast that result in heavy precipitation (Neiman et al., 2002), a metric that is able to account for the low level winds will be more effective in picking out impactful ARs. This is an important consideration when inspecting a given climatology; what are the inherent assumptions of the detection scheme?

In general, across the US western coastline, ARs can account for up to 50% of the annual precipitation over northern California and southern Oregon, but this contribution falls to less than 20% over portions of eastern Nevada and Utah. The seasonality of the delivered precipitation is largely concentrated across the winter period, and thus ARs are particularly important for regions such as California, with the same storms dominating both water management and flood risk across the state (Dettinger, 2004, 2011). Similar figures have been presented by Lamjiri et al. (2017), who identified that 60-100% of the most extreme storms (i.e. those with return periods of greater than two years) which made landfall along the western US between 1948-2002 could be linked to the presence of an AR. In addition to precipitation, the presence of an AR can result in a doubling or more of typical wind speeds within the storms (Waliser & Guan, 2017).

2.4.2.3. *Europe*

Connections between ARs and hydrological impacts across Europe were first presented by Stohl et al. (2008) and Lavers et al. (2011). Beginning with an historical flood event along the southwestern coast of Norway, Stohl et al. (2008) identified a stream of warm, moist air originating from the sub-tropics, now known as an AR. A more complete historical analysis revealed that these long-range air streams are responsible for a notable fraction of the annual precipitation budget of south-western Norway. Similar results were found by Lavers et al. (2011), in that all ten of strongest floods to occur within a set of four study catchments across the UK could be associated with a coincident AR-like feature.

These were striking results and opened up the field for future AR studies in the northern Atlantic. At the time of writing, impacts have been linked to ARs in Spain and the Iberian Peninsula (Eiras-Barca et al., 2016; Eiras-Barca et al., 2018; Ramos et al., 2015), Madeira (Couto et al., 2012; Couto et al., 2015), additional regions of the UK (Lavers et al., 2012) and Norway (Benedict et al., 2019) and more widely across mainland Europe, including at relatively inland areas such as Poland (Lavers & Villarini, 2013a). ARs can account for up to 50% of the monthly precipitation budget along the western coastline of Europe during the winter months (see Fig. 2.7 from Lavers & Villarini, (2015)), with the strong seasonality dependence likely related to a more active North Atlantic storm track during the winter season (Catto et al., 2012).

As well as the longer term trends, the effect of ARs on annual maximum precipitation days is also striking, with regions of Norway and the Iberian Peninsula demonstrating eight out of their top ten annual maximum precipitation days associated with ARs (Lavers & Villarini, 2013a). At least across the UK, intense precipitation days across the summer do not show a strong correspondence with ARs (Champion et al., 2015), likely a result of the synoptic scale processes occurring across the year i.e. frontal vs convective driven rainfall (Allan et al., 2016).

Finally, the presence of an AR has been associated with the explosive cyclogenesis (or extreme deepening) of a passing extra tropical cyclone (Eiras-Barca et al., 2018; Zhu & Newell, 1994). These extreme extratropical cyclones can then go on to cause high-impact weather events (e.g., Storm Dennis in February 2020, which resulted in notable impacts across the western UK).

2.4.2.4. Further Afield

Over 75% of the wintertime precipitation across the subtropical central Andes (30-37°S) is delivered by a total of 4-5 heavy events on average, with synoptic analysis revealing that these heavy events could be associated with strong water vapour transport in ARs (Viale & Nuñez, 2011). Given the elevation of the sub-tropical Andes, landfalling ARs are subject to upstream blocking, which enhances precipitation over the coastal lowlands and causes abrupt drying downstream, which removes most of the AR's moisture. The warm winters associated with ARs can also result in snowmelt effects (such catchment-level processes will be discussed in Section 2.6). Further orographic details remain largely unexplored in this region, alongside analysis of the remaining South American coast.

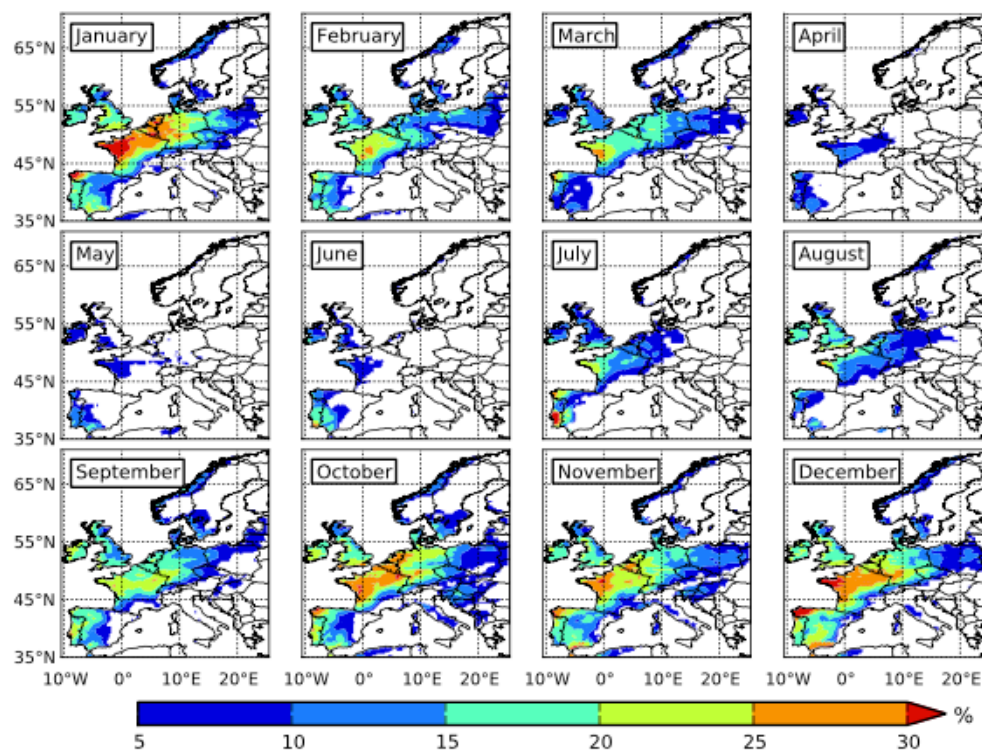


Figure 2.7 Atmospheric Rivers and European Precipitation. Taken from Lavers & Villarini, (2015), ARs can contribute up to 30% of the monthly precipitation budget along coastal areas of Europe.

ARs can induce poleward transport of warm, moist air out of the mid-latitudes towards the Arctic (Neff et al., 2014) and Antarctic (Gorodetskaya et al., 2014). This can induce heavy rainfall or snow accumulation (e.g. in 2009 and 2011 across East Antarctica; Gorodetskaya et al., 2014) affecting the subsequent surface mass balance, or conversely the advection of warm, moist air can accelerate

surface melt (e.g. in Greenland in July 2012; Neff et al., 2014). An understanding of AR processes in these regions is therefore critical for understanding changes in the cryosphere (Ralph et al., 2020).

Further afield, ARs have been reported across Australia and New Zealand (Kingston et al., 2016; Rauber et al., 2020), Western Asia including Iran and the Himalayas (Esfandiari & Lashkari, 2020; Rao et al., 2016) and Eastern Asia including Korea and Japan (Matsumoto et al., 1970; Moon et al., 2019). 78% of total precipitation and up to 94% of extreme precipitation on the western coastline of the South Island of New Zealand has recently been attributed to ARs (Prince et al., 2021). As the topic of ARs gains momentum, additional reports from across the globe are expected, linking their presence to notable impacts.

2.5. Detecting, Modelling and Forecasting Atmospheric Rivers

2.5.1. Field Campaign Development

Key in the development of AR science across the last twenty years has been the phenomenal effort dedicated to advancing the ability to measure and observe atmospheric processes. What began with a targeted field campaign in order to understand the most intense storms along the California coast (CALJET; Ralph et al., 2004), has developed into a dedicated ‘Center for Western Weather and Water Extremes’ (CW3E) and an AR Reconnaissance field campaign. Led by the Scripps Institution of Oceanography in partnership with federal, state, and local authorities, the Centre are united in their aim to research, monitor and predict the most impactful events along the US West Coast. In combination with novel satellite observations, both passive and active (Cannon et al., 2017, 2020; Neiman et al., 2008), knowledge of the large scale functioning of the water cycle, and the roles of ARs within it, has improved drastically.

Unique to the western coastline of the US has been the development of dedicated Atmospheric River Observatories (AROs), designed in line with knowledge of AR properties. As such, the observatories contain instruments to measure low-level wind and water vapour amounts, can operate under cloudy or precipitating conditions and work on a frequent enough timescale such that subtle variations in AR strength or position can be detected. What began as a pilot scheme at Bodega Bay (Russian River catchment) has developed into a ‘picket fence’ along the US West coast; a total of seven AROs through California, Oregon, and Washington. Further, in California

as an extension of the Hydrometeorology Testbed scheme (Ralph et al., 2013), the state is now monitored by over 100 sensors that keep track of snow levels, the distribution of water vapour flux, precipitation and soil moisture. The ability to construct such a network has only been possible due to, not only strong academic evidence linking AR arrival and impacts, but the engagement of key stakeholders from an early stage i.e., the Californian Dept of Water Resources and the federal Department of Energy.

Moving across to Europe, the North Atlantic Waveguide and Downstream Impact Experiment (NAWDEX; Schäfler et al., 2018) was conducted in September-October 2016 through three aircraft and enhanced ground-based observations in the UK and France. Their scientific aim was to increase physical understanding, and quantify the effects, of diabatic disturbances to the jet stream and downstream propagation across the North Atlantic. One of the multiple project aims was to look at ARs in the eastern Atlantic, helping reduce errors in the model-based representations of ARs. Others were focussed on sampling the WCB and its relationship to high-impact weather.

Results of the campaign are still developing (Schäfler et al., 2020), and the specific relevance to AR science is yet to be determined. However, given the limited observational timescale, its occurrence relatively early in the winter season, and the relatively broad aims of the study, it is likely that only a few ARs were detected, and their relevance to European impacts unclear. It is suggested therefore that a more comprehensive observational campaign in the north Atlantic is planned for the future in order to enhance understanding of the importance of north Atlantic ARs and their effects on the most extreme weather (Lavers et al., 2020).

2.5.2. Atmospheric River Detection

ARs are inherently contextual, and although a formal definition does now exist (AMS: Glossary of Meteorology), the specifics of how it is implemented in atmospheric datasets (either observational or modelled, or a combination of the two) varies on the region of interest, scientific question, and metrics available. A diagram describing the development of AR detection methods (ARDMs) is given in Table 2.1, with examples of different types of algorithms from across the world. A short summary will be given in the text for completeness.

First a characteristic variable, or metric, is chosen. Examples include the IWV or IVT. Secondly, a threshold, either absolute or relative (e.g., changing as function of location or season). Next, any geometric criteria must be considered (e.g., length and width) and possibly the orientation of the AR. The AR can then either be tracked timestep-by-timestep (i.e., a Eulerian approach) or ‘stitched’ together across multiple steps (a Lagrangian method). The required temporal threshold, namely for how long the AR must be detected, can also vary from region to region. Finally, additional complications include the running of ARDMs with or without human intervention. Some methods have discussed the application of machine learning, where the computer ‘learns’ to ‘recognise’ AR features after a period of thresholding (Chapman et al., 2019). Unsurprisingly, these steps can lead to a great deal of permutations (Table 2.1).

Evidence already exists regarding the effect of ARDM selection on scientific results. For example, Huning et al. (2017) has highlighted the differences in estimates of cumulative snowfall in the Sierra Nevada as a result of AR rainfall according to ARDMs defined according to IWV and IVT, and a similar situation has been discussed in Section 2.4. In light of these differences, the Atmospheric River Tracking Method Intercomparison Project (ARTMIP) (Shields et al., 2018) has been developed in order to quantify the possible scientific differences as a result of applying different types of algorithm. AR scientists from across the world have been invited to take part in a study where their individual algorithms are applied to common datasets and both the performances and subsequent scientific conclusions are analysed.

Early results (Lora et al., 2020; O’Brien et al., 2020; Ralph et al., 2019; Rutz et al., 2019; Zhou et al., 2021) suggest that the ARDMs tend to agree on the presence and location of the strongest ARs, with any subsequent detections largely a consequence of the restrictiveness of the individual algorithms. There are also differences when comparing the performance of global and regional algorithms, possibly a result of the latter being ‘tuned’ to the region of study. It is hoped that one day the ARTMIP catalogue will exist as a point of reference for ‘new’ AR studies where suitable algorithm(s) can be chosen based on the scientific question in mind. At the time of writing, so-called Tier 2 projects are ongoing, where ARDMs are applied to climate projection data and different reanalyses.

The occurrence of this collaboration at the same time as this PhD project exists only to highlight the topical interest in AR science and the fast pace of the associated research.

CHARACTERISTIC VARIABLE	THRESHOLD	GEOMETRIC CRITERIA	TRACKING METHOD	TEMPORAL PERSISTENCE	RUNNING METHOD
Integrated Water Vapour (IWV), Integrated Vapour Transport (IVT)	Absolute (e.g. 250 kgm-1s-1) or relative (e.g. 85th percentile)	Including AR length, width, aspect ratio etc.	Eulerian (i.e. timestep by timestep) vs Lagrangian (following the 'object?')	For example, how long must the AR make landfall?	'Static' algorithm, machine learning, objective...
Examples include, Neiman 2008 (IWV), Ralph 2004 (IWV), Ralph 2005 (IVT), Guan and Waliser (2015). For a complete details see Shields 2018.	Ralph 2004, 2005 uses IWV > 2cm and IVT > 250kgm-1s-1 respectively for ARs along US West Coast. Guan and Waliser 2015 and Lavers 2012 applied IVT 85 th percentile across global/UK region respectively.	Ralph 2004 stated an AR must possess a length greater than 2000km and a width less than 1000km. Lavers 2012 stated that the AR must be longer than 20 units of longitude.	Ralph 2004, 2005 (Eulerian), Lavers 2012 (Eulerian), Guan and Waliser 2015 (Eulerian), Ramos 2016 (Lagrangian).	Ramos 2016 (12hrs +)	Machine learning (Chapman 2019)
Algorithm relevant to this work is Lavers (2012). Algorithm details are presented here. Variable is IVT.	Relative	AR > 20 longitudinal degrees, 4.5 degree latitudinal movement permitted	Eulerian	18 hours +	Static Algorithm

Table 2.1. Atmospheric River Detection Schemes. A summary of the considerations when choosing, or developing, an AR detection method. Examples of well-known algorithms are provided in the centre row, with details of the algorithm most relevant to this work (Lavers et al. 2012) provided in the bottom row.

2.5.3. Atmospheric Rivers and Climate Change

To be able to analyse the effect of ARs in a changing climate, an ability to effectively represent them in global climate models (GCMs) is essential. This involves testing the modelled events against the observation data available and ensuring that realistic AR behaviour is captured. As the topic of AR science gains momentum, alongside an ability to observationally probe those regions of greatest error within the models, it is expected that the accuracy of modelled ARs will only improve.

The Clausius-Clapeyron relation suggests that, in a warmer world, it is reasonable to expect increased atmospheric water vapour content. However, the processes that act to transport oceanic evaporation to continental precipitation may change in terms of location, intensity and duration, thus resulting in consequences relating to both flood risk and the availability of water resources. These ideas are known as the ‘thermodynamic’ and ‘dynamic’ mechanisms respectively (Knight et al., 2017), and are jointly expected to influence the location and intensity of AR rainfall moving forward. Given that baroclinic wave activity within oceanic storm track regions is expected to increase, for example by 5-8% across the north Atlantic by the end of the 21st century (Ulbrich et al., 2008), it is reasonable to imagine a combination of a warmer, wetter atmosphere and increasingly turbulent conditions.

The first AR specific climate scenario study used the CMIP3 GCMs, and an ARDM based on IWV, to compare the historical scenario with that of the mid- and late- 21st century along the Californian coast (Dettinger, 2011). It was found that the total number of AR days did not change remarkably, but that the intensity of the events was greater. In addition, the AR ‘season’ was noted to lengthen.

Followed up by Warner et al. (2015) for the entire western US, up-to-date CMIP5 models and an ARDM based on IVT were applied to historical and end-of-century scenarios. In contrast to that of Dettinger (2011), total AR days were noted to increase by 200-300% by the end of the 21st century, alongside a corresponding rise in intensity (in terms of IVT). This could be attributed to an 11-18% increase in total AR precipitation across the US west coast, and a 15-39% increase on the most intense AR days. In combination with a fall in precipitation associated with non-AR events (Gershunov et al., 2019), the importance of ARs from a combined water resources and flood risk perspective is therefore expected to increase.

The increase in average AR IVT is largely a result of increased specific humidity, as opposed to a strengthening of low-level winds (Lavers et al., 2015). The upper level steering flows that control the landfalling latitude of ARs (Shields & Kiehl, 2016), are expected to push equatorward within a warming climate in response to subtropical jets. However, understanding how AR orientations might change, as well as wider tropospheric stability and wind shear is a region of future research. These factors in combination will affect the ability of the AR to undergo orographic enhancement.

Moving across to the Atlantic, and ARs have been shown to become stronger and more numerous under CMIP5 future scenarios Lavers et al. (2013). In particular, the high-emissions scenario suggests a doubling of AR landfalling frequency along the UK coastline. The authors suggest that these results have implications for future flood risk, however, similar to the earlier discussion, future work is required to ensure that the projected ARs are as well set-up for orographic enhancement of their transported moisture as their historical counterparts. In contrast to the results of Pacific ARs, there is tentative evidence that wind directions and strengths may change the properties of ARs in the north Atlantic (Gao et al., 2016).

2.5.4. Forecasting Potential

Numerical Weather Prediction (NWP) models assimilate real-time observations and combine with complex numerical models of the atmosphere and oceans to forecast the future weather. Most commonly, a set (or ensemble) of forecasts is produced to allow for an estimate of the uncertainty in the models and combined to give the most likely outcome. In models such as those developed at ECMWF, the spatial resolution of the NWP is around 18km, likely sufficient to resolve many local catchment characteristics across the UK. Statistical ‘downscaling’ methods, using historical observations, can also be used to calculate scenarios of local climatic conditions (e.g., precipitation, temperature) in catchments smaller than 18km or across those with a large elevation range.

ARs have been shown to play a key role in the global hydrological cycle and their combined importance at some landfalling regions in terms of both flood risk and water resources management, mean that effective forecasts are crucial. However, ARs require a lifting mechanism to generate precipitation, most commonly in the form of uplift over elevated terrain. The stability of the atmosphere within the AR is crucial to allow this uplift to occur, and the resulting

precipitation distribution will be influenced by the translation of the AR across the watersheds combined with the orientation and intensity the landfalling moisture flux relative to catchment topography. In addition, ARs are inherently narrow features, and this presents an obvious challenge in terms of forecasting potential.

The first quantitative estimate of AR precipitation potential came from Neiman et al. (2009) in which the authors used PACJET and HMT (Ralph et al., 2013) data along the California coast (focussing on the Russian River catchment) to develop a tool for precipitation forecasting based on water vapour flux. It was found that, to induce heavy rainfall capable of generating flooding, coastal observations of IWV and upslope flow must exceed 2 cm and 12.5 m/s, respectively. The Russian River catchment is unique in its wealth of data availability, both atmospheric and hydrological and provides a perfect testbed for understanding AR processes. However, a method capable of application in data sparse areas must be developed.

The Extreme Forecast Index (EFI), developed at ECMWF (Zsótér, 2006), compares the model forecast at a given location to the underlying model climatology, determining how ‘extreme’ the forecast may be. The main advantage is that the forecast is compared to the model climate, therefore automatically including all the spatial and temporal variability of the parameter within the forecast. This bypasses the need for forecast calibration, allowing users to identify weather abnormalities. It has been shown that, due to the synoptic scale processes behind the formation of intense regions of IVT (and ARs), they demonstrate a greater potential for medium range forecasting than precipitation (Lavers et al., 2014). Therefore, using the EFI in the context of IVT, may result in an increased warning lead time.

This concept has been applied to three winters across western Europe as a means of testing the usefulness of the EFI as a forecasting tool (Lavers et al., 2016). The occurrence of a positive North Atlantic Oscillation pattern (Hurrell et al., 2003) during this period was thought to be responsible for an increase in relative frequency of extratropical cyclones, and thus an increase in IVT within the storms. The EFI based on IVT was therefore found to better capture extreme precipitation forecasting than the precipitation EFI with a two-week lead time across the three-winter period, demonstrating its potential for hydrometeorological forecasting. A similar concept was later applied across the US (Lavers et al., 2016) and has been explored in greater detail more recently by Ramos et al. (2020), with particular reference to the transfer to precipitation EFI at shorter lead times.

Despite the potential of the EFI, there are still shortcomings in the ability of NWP models to accurately represent ARs especially at shorter lead times. Using the ECMWF Integrated Forecasting System (IFS) and dropsonde data from the 2018 AR Reconnaissance mission, led by CW3E, Lavers et al. (2018) identified errors in the modelled winds at the top of the planetary boundary layer, that is the boundary between the ‘free’ atmosphere and that which is influenced by terrain characteristics. This makes sense, given existing knowledge of the importance of catchment topography on controlling AR precipitation. AR shape however, was found to be well captured by existing NWP forecasts.

A later study, built on these results through the inclusion of more dropsonde data and a finer vertical resolution within the IFS (Lavers et al., 2020). This identified a cold bias across the troposphere, a dry bias in the lower troposphere and reduced modelled water vapour fluxes relative to observations. It is clear therefore that more work is to be done, spurring a recent call for an American-European observation campaign across the north Atlantic, to help identify NWP errors and aid in the development of more accurate forecasts.

2.6. The Catchment Influence

2.6.1. Orographic Precipitation

The primary importance of ARs lies with the precipitation induced when the narrow band of intense water vapour flux is forced to rise over elevated terrain, for example when making landfall along coastal areas. The CALJET field campaign revealed this flux to lie within a broader region of moist near-neutral air that is particularly susceptible to orographic lifting (Neiman et al., 2002; section 2.2).

In the context of northern California, Neiman et al. (2009) derived the first relationship between IWV (moisture content), upslope flow (wind speed) and rain rates within the context of ARs impacting on the coastal mountains. This study identified the importance of wind measurements aloft and the identification of the controlling layer of intense water vapour transport. Across the more modest terrain of the UK, it has long been recognised that orographic enhancement of rainfall, driven by low-level winds, is a key factor in precipitation distribution across upland areas (Hill et al., 1981).

A theoretical investigation of the orographic processes occurring within landfalling ARs is described by Miglietta & Rotunno (2005, 2006). A flow of nearly moist neutral air over a ridge is simulated following existing knowledge of typical AR properties and, to begin with, the Coriolis force neglected. It was found that obstacles greater than 250m in height are able to generate orographically induced precipitation. When the Coriolis force is considered, the impinging air flow will veer to the left in the Northern Hemisphere, resulting in a corridor of blocked flow running parallel to the elevated terrain. Such a phenomenon has been observed in the Sierra Nevada mountains of California, known as the Sierra Barrier Jet (SBJ; Neiman et al., 2013).

The SBJ can occur in combination with a landfalling AR, and can affect the amounts and location of precipitation induced (Neiman et al., 2014; Ralph et al., 2016). Similar such jets have been observed at additional mountain ranges across the world, e.g. the Andes (Viale & Nuñez, 2011) and are therefore an important consideration when analysing the effect of landfalling ARs on regions of elevated topography.

2.6.2. The Catchment Control?

The influence of ARs on regional and global precipitation has been extensively analysed (Gershunov et al., 2017; Guan & Waliser, 2015; Lavers & Villarini, 2015; Rutz et al., 2014) but its translation across the land-surface is defined by a number of dominant hydrological pathways and processes. Known as the catchment perceptual model (Beven, 2011) the conversion of precipitation into streamflow, and the associated timescales, are dominated by a number of stable and variable catchment factors, for example the catchment geology, aspect and soil saturation (Fig. 2.8).

The first catchment based study of ARs was carried out in the Russian River catchment of Northern California (Ralph et al., 2006) where all seven flood events since October 1997 could be linked the presence of a landfalling AR. This provided the first evidence that ARs are important flood generation processes (on top of bringing heavy precipitation). However, it was noted that not all ARs resulted in a flood, and therefore understanding why some generate stronger responses is of key importance.

The link between ARs and floods is not unique to the Russian River catchment. In particular, following so-called 'Pineapple-Express' storms (Dettinger, 2004, 2011), the Merced River near Yosemite Valley has been noted to flow nearly an order of magnitude higher as compared to any other winter storm. Across the western US more generally, ARs have been noted to contribute up to 80-100% of annual peak streamflow along the Pacific Coast and northern California, falling to 30-70% across regions of the Pacific Northwest, the Sierra Nevada, central and southern California and central Arizona (Barth et al., 2017). Moving to inland areas of eastern Montana, Wyoming, Utah, Colorado and New Mexico however, and the link with landfalling ARs and peak streamflow disappears completely. Reasons for such an observation are discussed in the following section.

Moving outside of the US, ARs have been directly linked to flooding across Europe (Couto et al., 2012; Lavers et al., 2011; Liberato et al., 2013; Ramos et al., 2015; Stohl et al., 2008), Asia (Rao et al., 2016), South America (Viale & Nuñez, 2011) and Australasia (Kingston et al., 2016). However, similar to the Russian River, it is clear that not all ARs result in notable hydrological impacts, and therefore understanding which of the hydrometeorological aspects are responsible is of particular societal value (Eiras-Barca et al., 2016).

ARs can provide a notable fraction of annual precipitation (section 2.4) and thus their relative frequency can affect the availability of water resources (Dettinger et al., 2011). Work is currently ongoing to assess this effect at the catchment scale (Oakley et al., 2018). ARs can also be associated with changes in the terrestrial landscape, as rapid runoff and soil saturation during intense storms can trigger erosion and large scale landslips (Oakley et al., 2018). Contrastingly, their absence may contribute to vegetation loss and wildfires (Albano et al., 2017).

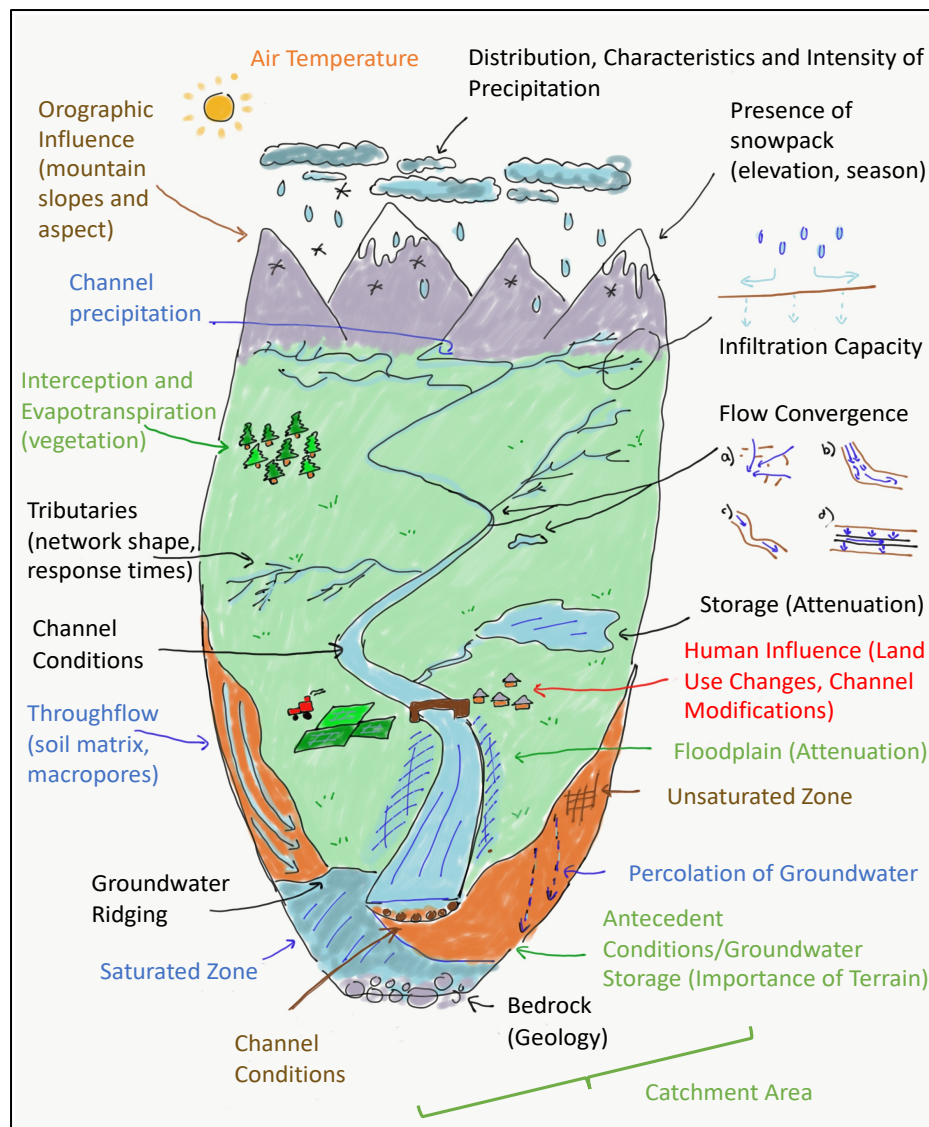


Figure 2.8 The Catchment Perceptual Model. Inspired by Beven (2011), this schematic outlines the static and variable factors to be considered when analysing flood formation. It serves to identify the complexity, and non linearity, of rainfall-runoff and explains why wealth of research is dedicated to the development of effective hydrological models. This work aims to test whether there are specific aspects of the catchment system that are particularly important for the translation of AR impacts.

2.6.3. Combining Meteorology and Hydrology

This section aims to develop a framework of meteorological and catchment specific controls that are expected to affect the impact potential of a landfalling AR. The current state of the literature in the context of these controls is provided here, alongside a graphical overview in Fig 2.11. There is a need to quantify the relative importance of these factors, particularly those associated with the land surface, if additional forecasting ability is to be obtained (Ralph et al., 2020).

2.6.3.1. Meteorological Factors

1. IVT Amounts:

Clearly one of the most important properties of a landfalling AR is the amount, and rate, at which water vapour is transported. Indeed, Ralph et al. (2013) has shown that 74% of the variance in storm total precipitation, and 61% of storm total runoff, at the Russian River catchment across a six year period can be attributed to differences in storm total water vapour transport up the catchment slope. A similar analysis, extended across the western US region for a total of 33 years of atmospheric and hydrologic data has also identifies that the water vapour amount serves as the primary control on precipitation (Albano et al., 2020).

The first quantitative thresholds suggest that the probability of an AR generating 50 mm day⁻¹ of runoff in a river on the Pacific Coast increases from 12% to 54% when daily mean water vapour transport doubles from 300 kg m⁻¹ s⁻¹ to 600 kg m⁻¹ s⁻¹. Indeed, the extreme runoff, identified by the 99th quartile of daily values, can be directly correlated with the magnitude of incoming moisture flux (Konrad & Dettinger, 2017).

When considering Atlantic ARs, although similar quantitative metrics do not yet exist, the results of Eiras-Barca et al. (2016) and Lavers & Villarini (2015) both suggest the strength of the landfalling ARs as a control on precipitation amounts. A similar conclusion was reached when looking at ARs impacting on the Atlantic island of Madeira (Couto et al., 2012; Couto et al., 2015). However, all of these studies find that most precipitation variability can be captured when the wind direction components are considered also, as discussed in the next subsection.

2. Wind Direction:

When Ralph et al. (2003) applied CALJET data to investigate variations in flood severity across adjacent coastal watersheds within the Santa Cruz mountains, they identified the presence of a rain

shadow (cast by the mountains) lying partially across the San Lorenzo catchment when an AR of a particular orientation made landfall. The result was to dampen the hydrological response in the affected catchment, as compared to its neighbour. A similar such analysis, but invoking multiple decades of streamflow and reanalysis data, has been carried out in western Washington (Neiman et al., 2011) across a series of four catchments – two within in Olympic mountains and two within the western Cascades. The result was a complex interplay between terrain topography, catchment orientations and rain shadowing, to explain the hydrological response. Catchment terrain, and its relationship to impacting ARs, is therefore an important consideration.

In an attempt to quantify the sensitivity of orographic precipitation to AR direction, a three-dimensional full-physics model of the Pacific Northwest was developed (Picard & Mass, 2017). Conditions approximating that of an AR were simulated, and the orientation of the landfalling AR was modulated in line with observational studies (e.g. Neiman et al., 2011). It was shown that precipitation totals can vary substantially with small changes in wind direction, and that the sensitivity of orographic precipitation in the Olympic Mountains to wind direction is much more strongly influenced by the presence of surrounding orography than the specific geometry of the peaks.

Considering the seasonal synoptic conditions associated with winter and summertime ARs impacting across the US west coast, it is possible to understand why it is the winter ARs that generate greater amounts of precipitation. The wintertime ARs generally demonstrate a meridional component of moisture flux, extending from the tropics to the coast, whereas the summertime ARs are much more zonally aligned. The alignment of the wintertime AR flux favours orographic enhancement along the coastal mountain ranges. In addition, the winter-time ARs show enhanced water vapour flux at approximately 1-2km aloft, coinciding with the approximate height of the Californian mountains (Neiman et al., 2002).

A similar synoptic analysis can be applied to the few ARs that have been able to penetrate inland of the coastal mountain ranges and affect south-western and southern states. Rutz et al. (2014) has identified three preferred corridors for ARs penetrating inland of the Cascades. These corridors exist as combination of synoptic patterns with the local topography; where high-elevation barriers result in AR decay and rainout, and gaps in topography can act as conduits for AR penetration into the interior (Hughes et al., 2014). Such AR orientations, in combination with terrain, may

explain the high profile event of January 2010 in Arizona, where a persistent AR broke meteorological and hydrological records across the state (Neiman et al., 2013).

Similar characteristic synoptic patterns have been identified for ARs that affect the central US (Lavers & Villarini 2013b). A characteristic trough-ridge pattern across the central states and the US East Coast permits the flow of a southerly/south-westerly orientated AR. It is ARs such as this that may possibly be responsible for the flood event in Tennessee in May 2010 (Moore et al., 2012) and during the Iowa Flood Studies campaign in April-June 2013 (Nayak et al., 2016). In Washington state, a negatively tilted low pressure system positioned to the west in the Gulf of Alaska has been associated with a particularly extreme subset of ARs to affect the region (Collow et al., 2020).

It is likely that similar orientation controls on the eastern side of the Atlantic. When attempting to explain the AR precipitation variability across western Europe, Lavers & Villarini (2015) found that models requiring just three fields worked well, namely the integrated water vapour and the 850-hPa zonal and meridional winds. Specific case studies from the island of Madeira (Couto et al., 2012; Couto et al., 2015), have identified two main synoptic patterns associated with landfalling ARs: the first corresponding to a source region in the Caribbean Sea and south-westerly flows across the island, and the second to source regions in the central to eastern Tropical Atlantic with south to south-westerly flows (more latitudinal than meridional). These types of ARs can be associated with different precipitation patterns across the upland regions of Madeira.

The ability to use large scale synoptic conditions as an indicator of landfalling AR characteristics has been applied at the Russian River catchment (Hecht & Cordeira, 2017), however they note the combined importance of mesoscale upslope moisture flux (orographic enhancement) and synoptic scale forcing (e.g., in the WCB) when determining AR precipitation potential. Additional potential lies within the concept of so-called Rossby Wave Breaking (RWB), as discussed earlier in Section 2.3 (Priestley et al., 2020). There are two regimes of RWB – anticyclonic, which are associated with a predominantly meridional jet, and cyclonic, which are associated with a zonal jet. Hu et al. (2017) have been able to link the ARs associated with these different regimes to hydrological impacts of the US west coast, and Benedict et al. (2019) has carried out a similar analysis along the Norwegian coastline. It would be of interest to extend such work more broadly across Europe, such that the relative frequency of different subsets of ARs can be identified.

3. Air Temperature:

ARs are defined by a tongue of anomalously warm water vapour flux relative to background conditions. Although the exact temperature (and moisture content) of the storms can vary depending on source region, the arrival of warm air onto coastal regions will play an important role in determining whether rain or snow will fall at a given location.

The anomalous warmth of landfalling ARs can result in a raising of the snowline and a greater proportion of precipitation falling as rain rather than snow. This can act to increase the catchment contributing area and subsequent runoff (Albano et al., 2020; Neiman et al., 2011; Neiman et al., 2013). When precipitation falls as snow, unless it melts very quickly, it will not immediately contribute to streamflow. However, when rain falls on already existing snowpack (so called rain-on-snow, or ROS, events), it can melt the top layer of snow resulting in the formation of additional runoff (Berghuijs et al., 2016). The relationship between landfalling ARs and flooding at catchments where winter snowfall is common can therefore be harder to disentangle.

The topography along the European West Coast is lower in altitude than that of the US, although some rain-on-snow flood events have been observed in the Swiss Alps possibly due to the arrival of a landfalling AR (Rössler et al., 2014). The penetration of ARs to inland communities of Europe is expected to be somewhat more likely than that across the US due to the relative height of corresponding topographies (Lavers & Villarini, 2013a, 2015) and associated rainout.

4. Atmospheric Stability and Position of the LLJ:

As discussed in earlier sections, the moist-neutral stability of ARs allows them to rise up over mountain barriers with ease (Ralph et al., 2020). The position of the LLJ relative to mountain height allows for maximum efficiency of orographic precipitation (Neiman et al., 2002), and its orientation relative to the landfalling watersheds can result in the formation of complex rain shadows (e.g. Ralph et al., 2003). The existence of so-called barrier jets (Neiman et al., 2013) can further modulate the variation of orographic precipitation.

Tsuji & Takayabu (2019) suggest the interplay between ARs and upper-level flow eddies, known as cut-off lows, can act to enhance orographic precipitation in the region where they overlap. They provide a disastrous flood event in Hiroshima during 2014 as a case study example. There is space to explore this phenomenon in other regions of the world.

5. AR Translation Speed and Characteristics:

A key control on precipitation total, aside from intensity, is the duration of rainfall. Thus, a key consideration when considering AR impacts, is the period above a given location that AR conditions can be met. At the Russian River catchment, AR conditions last 20hrs on average, with 12% lasting 30hrs or more, and further, ARs with double the mean duration can result in nearly six times greater peak streamflow and more than seven times storm-total runoff volume (Ralph et al., 2013). Lamjiri et al. (2017) has found that storm duration, more so than hourly intensities, modulate precipitation-total variability across the US west coast, with correlation coefficients spanning 0.7-0.9. Thus, AR persistence is key to extreme storms on the US west coast.

An aspect that may act to modulate the persistence of AR features is the occurrence of so-called mesoscale frontal waves (Neiman et al., 2016; Ralph et al., 2011). Instabilities in the corresponding cold front can result in a stalling, or quickening, of AR conditions overhead relative to translation speed and thus, affecting the overall duration of the event. Further, there is evidence for a set of ARs to occur in quick succession, known as an AR family (Fish et al., 2019). Using data from the AR observatory at the Russian River catchment, observations from 2004 to 2017 suggest that nearly half (47.8%) of all AR events are associated with another within a 12-hour aggregation period. This may have important implications if the landfalling position of the ARs within the family is similar.

There is space to explore the variability of AR duration, the presence of mesoscale waves and family set-up on European catchments. Do these factors affect precipitation totals and hydrological impacts in a similar way as in the US?

2.6.3.2. Catchment Factors

6. Bedrock, Soil Type and Land Use:

Interactions between the geology, soil type, and vegetation cover will affect the storage capacity, infiltration ability and subsurface transmissibility of the catchment and thus the relative effectiveness and speeds of different flow pathways. A relatively impermeable bedrock will result in limited infiltration of rainfall deep into the ground, favouring horizontal displacement of water

or the formation of saturated areas and a quick rainfall-runoff response. Contrastingly, a relatively high permeability bedrock can strongly attenuate the rainfall-runoff signal as the water is incorporated into groundwater stores. There are very limited studies analysing the impact of bedrock and groundwater on AR rainfall (Ralph et al., 2020).

Above the bedrock, the corresponding soil profile must be able to conduct the infiltrated precipitation away at the similar rate to infiltration. If this is not possible then regions of saturation may be built up within the soil profile possibly leading to lateral transport of water through the upper layers. The presence of macropores (Beven & Germann, 1982) will aid in the conduction of water through the soil profile and may exist as a result of vegetation or ecological influences.

A summary in the context of UK catchments was produced by Farquharson et al. (1978) in the form of a map of Winter Rain Acceptance Potential (WRAP). This map demonstrates the potential for soils across Britain to generate flood flows as a function of their important hydraulic properties, including soil depth, slope and permeability. There are limited studies linking soil types to AR precipitation and impact.

Finally, few catchments are exempt from human influence on some degree or another. These influences may take the form of hydraulic structures such as dams or reservoirs, or large-scale river modification schemes near regions of social importance. For example, magnification of flooding has been observed on the River Rhine in Germany, largely attributed to human modifications of the river channel, floodplains or river catchment over time, primarily for agricultural purposes (Pinter et al., 2006). In the flood-forming process, hydraulic structures are expected to act in a similar manner to natural lakes or storage areas, attenuating the flood flow response of the catchment. However, in the context of flood hazards it follows that such a structure may present a much more serious flood risk if it were to fail.

Other human influences on the run-off generating process are the modifications made to stream channels, either with the aim of decreasing flood risk to a given area (through straightening, widening, construction of relief channels etc), or through diversion of flow from one river system to another. Both these will alter the natural response of a catchment to a rainfall event and thus may lead to unexpected consequences downstream or otherwise. Historical studies of the effect of land-use change on AR impacts are limited.

7. Antecedent Soil Moisture:

The infiltration of precipitation into the soil surface and the subsequent formation of saturated areas, are key in controlling the formation of catchment runoff (Hewlett & Hibbert, 1967; Horton, 1933). In the recession period between storms, the ability of the catchment soils and bedrock to infiltrate precipitation input gradually increases as the loss of existing soil water occurs via evapotranspiration and drainage of gravity driven groundwater. The extent of this water loss will be controlled by the season, climate and vegetation content of the area. The amount of existing soil water is known as antecedent soil moisture (ASM).

The first look at catchment conditions in the context of AR impact was provided by Ralph et al., (2013) for six years of data at the Russian River catchment in northern California. In addition to their studies of AR duration, the authors found that when precursor soil moisture was less than 20%, even heavy rainfall did not lead to notable streamflow. When extending the study area across California's northern Central Valley, Neiman et al. (2014) noted the effect of an early-season AR that brought record precipitation to the region. Given the timing of AR arrival at the start of cold season, relatively dry catchment soils meant that the resulting flood impact was low.

Extending the study period back to 1950, Cao et al. (2019) has attempted to understand the connection between soil moisture, precipitation and flooding within the context of a warming western US. The results suggested that ASM is most likely controlled by antecedent precipitation (past events) as opposed to evapotranspiration, and thus any large-scale warming is expected to have minimal effect on ASM controlled events. Instead, the effect of sustained, or frequent, precipitation events can result in a wetting of the catchment and a possible 'priming' with regard to the strongest hydrological responses (Mahoney et al., 2016).

Recently, these results have been expanded on through the installation of multi-depth soil moisture sensors at a number of locations across the Russian River basin (Sumargo et al., 2021). This network has permitted the exploration of surface and surface runoff processes, and the role of evapotranspiration and recession period between storms, as a way of controlling runoff generation during AR events. This study likely acts as the first successful quantification of hydrological processes during AR storms.

Moving across to Europe, and the studies of AR impacts in the context of hydrological impacts are less common. There is evidence of antecedant soil moisture enhancing hydrological response

(e.g. Trigo et al., 2014) alongside ARs ‘priming’ the larger scale environment (Couto et al., 2015; Eiras-Barca et al., 2016). Greater data availability, including soil moisture and precipitation, would develop an understanding of the relationship between AR arrival, ASM and impacts.

8. Catchment Elevation:

Due to orographic enhancement, more precipitation falls further up the catchment slopes relative to coastal areas (Couto et al., 2015). The overall elevation of these slopes will determine both, a) the intensity of precipitation at a given location, and b) whether the precipitation falls as rain or snow. Within a warming world scenario, we may expect the relative snow fractions within high elevation catchments to fall (Bavay et al., 2013). This will have important implications for the timing and severity of AR induced floods (Curry et al., 2019).

9. Terrain Characteristics:

Terrain characteristics include the catchment slopes and their aspect. The most efficient uplift will occur when the incoming moisture flux aligns perpendicular to the catchment slopes, namely the aspect. The severity of the catchment slope will affect not only the rate of uplift (and associated precipitation generation) but also how quickly any run-off will be translated through the catchment. In addition, the location of catchment terrain, relative to near-by catchments, can result in the formation of rain-shadows.

The study of AR impacts in relation to catchment terrain has focussed primarily on the large-scale terrain gaps that allow inland penetration. The study of variability on a catchment-by-catchment scale, and a comparison between catchments based on their characteristics, is something that as yet remains unexplored in all but the most data-rich catchments (e.g., the Russian River; Sumargo et al., 2021). In this latter case, the analysis of soil moisture characteristics and runoff processes in the context of catchment terrain is something that can be possibly carried out with the data available. This may allow estimations to be made on subsurface or surface processes by using the catchments characteristics alone, perhaps paving the way for a method applicable to catchments with less data available.

10. Drainage Density:

The arrival of precipitation, and run-off, from the upper reaches of a catchment to the outlet is controlled by the drainage pattern of tributaries and river channels, acting to amplify or dampen the effect of incident storms, this in turn is largely controlled by the catchment topography (unless

there is evidence for human intervention). Variable catchment conditions, namely those that may vary with time during a storm event, include the presence of storage areas. These can initially act to attenuate and delay excess flow, however if their capacity is exceeded, this run-off will be returned to the system. Channel specific factors will dictate how efficiently water is transported away from the catchment system when runoff reaches the channel. These will include overall slope, shape and roughness which may also change with time.

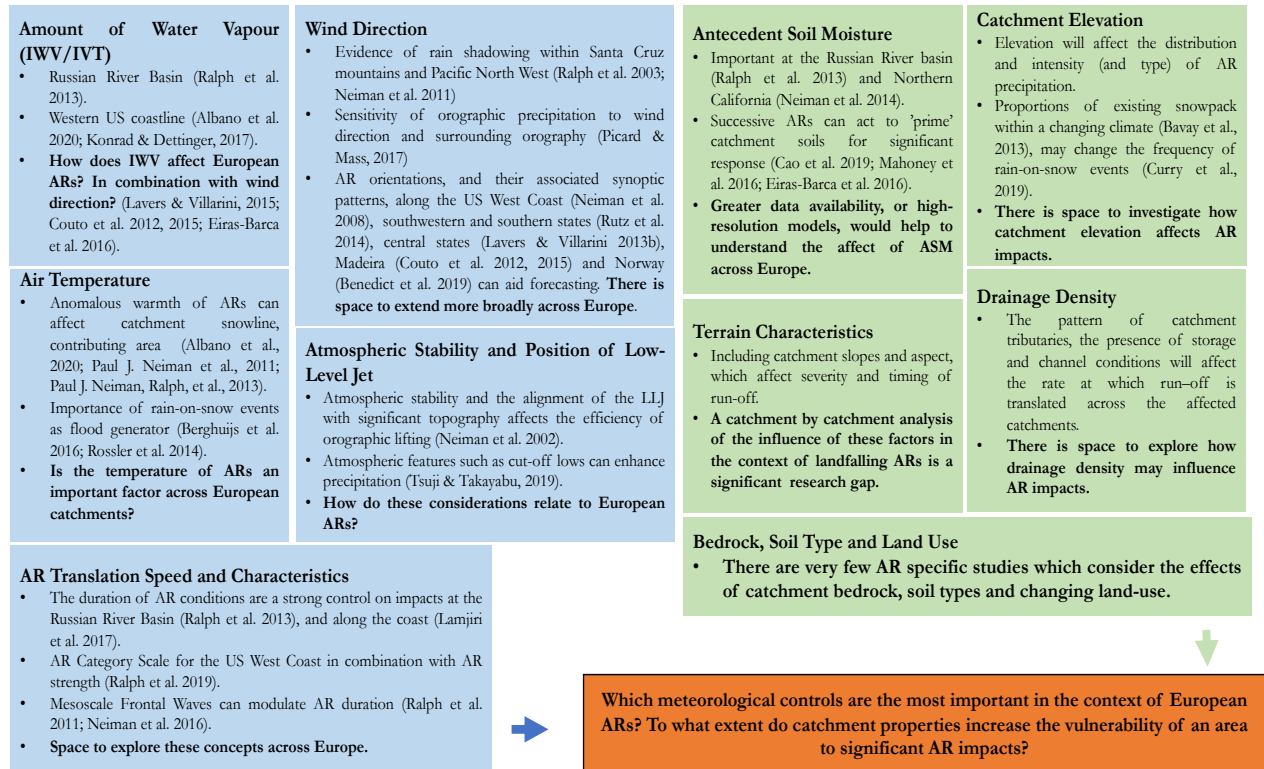


Figure 2.9. Atmospheric Rivers and the Land Surface – What do we know? This figure attempts to summarise the current literature regarding atmospheric rivers and the catchment. Although a great deal of research has been invested in understanding the meteorological processes within ARs (albeit focussed on the US West Coast), there is a contrasting lack of information when considering how catchment properties can influence (either dampen or enhance) the impacts of landfalling ARs.

2.7. Research Objectives

2.7.1. Key Research Gap

ARs are associated with some of the most extreme precipitation events across the mid-latitudes, in some cases accounting for a notable fraction of the annual precipitation budget. Accurately forecasting their landfalling location, strength and duration is key if we are to analyse the inter-annual variability of water resources and/or the risk of sustained precipitation. A great deal of

time and resources has been invested in advancing the understanding of the meteorological properties of ARs, albeit largely focused on the north Pacific (Fig. 2.9), and this has allowed identification of subtle factors that would have been impossible from satellite data alone. However, there is contrasting lack of information when considering the role that catchment properties can play in either modulating the location and intensity of the induced precipitation, and/or its translation across the landscape into run-off and streamflow.

Although ARs have been present in some of the most extreme floods ever recorded, many features arrive each winter without notable effect. In the UK for example, we can expect on average 4-5 (intense) ARs per winter period, however only a few of these may result in notable impacts. Understanding which of the events may be the most impactful, ideally at a long enough lead time to allow suitable action to be taken, is the key motivation of this thesis.

2.7.2. Thesis Aims and Objectives

The aim of this thesis therefore is to understand the role that land-surface properties play in modulating AR impact. This aim will be addressed via several objectives as outlined below:

1) How important are ARs in terms of flood generation across the UK?

The work of Lavers et al., (2012) will be enhanced, using newly available high resolution reanalysis and hydrological datasets. The performance of the AR detection method will be tested and verified in the context of such high-resolution datasets, and the study area extended across the UK. Using the Dyfi and Teifi catchments of Lavers et al., (2012) as starting points, the role of AR properties, including strength and orientation of transported moisture flux, is investigated in terms of flood response.

2) To what extent do land-surface and additional catchment properties modulate AR impact?

This work will attempt to quantify (for the first time) the relative importance of the different aspects of the land-surface in the context of a landfalling AR. A total of 22 catchment descriptors are obtained from the Flood Estimation Handbook (FEH; Institute of Hydrology, 1999) corresponding to each of the study catchments. The relationship between

these descriptors and the properties of the most impactful ARs is investigated. If a link is successfully found then an attempt will be made to build a predictive model for the properties of the most impactful ARs, based on catchment descriptors alone.

3) Can the inclusion of catchment properties help in predicting AR floods?

The role of catchment properties in controlling the most impactful ARs will be investigated. An attempt will be made to combine the results of the analysis into a predictive framework. Based on catchment properties and the characteristics of an incoming AR, is it possible to predict where the impacts will be strongest? If successful, these results will be of particular interest to the forecasting community.

Chapter 3 – Study Area, Data and Methods

3.1. Introduction

The aim of this thesis is to understand the role that land-surface properties play in modulating AR impact. This aim will be addressed via several objectives as outlined in Chapter 2 (section 2.7). The data supporting such objectives will be outlined in this chapter, alongside a description of the relevant study area. Key to the work will be the incorporation of a number of catchment or land-surface descriptors, an overview of which will also be detailed here. Specific methodology will be presented in the relevant research chapters.

3.2. Research Design

The work of this thesis is described across four research chapters. Chapter 4 is motivated directly by the findings of Lavers et al. (2012) and looks at ARs in the context of flood events at the Dyfi and Teifi catchments in western Wales. The reasoning behind differing responses at the two catchments is investigated in the context of high-resolution atmospheric and hydrological datasets. The data used in this analysis will be described later in this chapter (sections 3.4 & 3.5) alongside the statistical measures applied (section 3.6).

Chapter 5 exists to ensure the atmospheric river detection algorithm is performing appropriately and acts to test several assumptions made during the course of its development (Lavers et al. 2012). The modified algorithm is then applied across the historical period to assess the role of atmospheric rivers at a series of 81 study catchments predominantly located within the western uplands of the UK. These catchments are described within this chapter (section 3.3) and the work acts to address the first of the objectives of this thesis (Chapter 2, section 2.7).

Catchment descriptor information is obtained for each of the study catchments (section 3.3.5) and used to interpret hydrological responses to catalogue of landfalling ARs across the historical period. The relative importance of land-surface and additional catchment information in modulating AR impact is quantified, thus addressing the primary research gap and the second identified objective (Chapter 2, section 2.7). Finally, Chapter 7 looks to predict the impact

potential of ARs according to the properties of the landfalling region and acts to address the final objective of this thesis.

3.3. Study Area

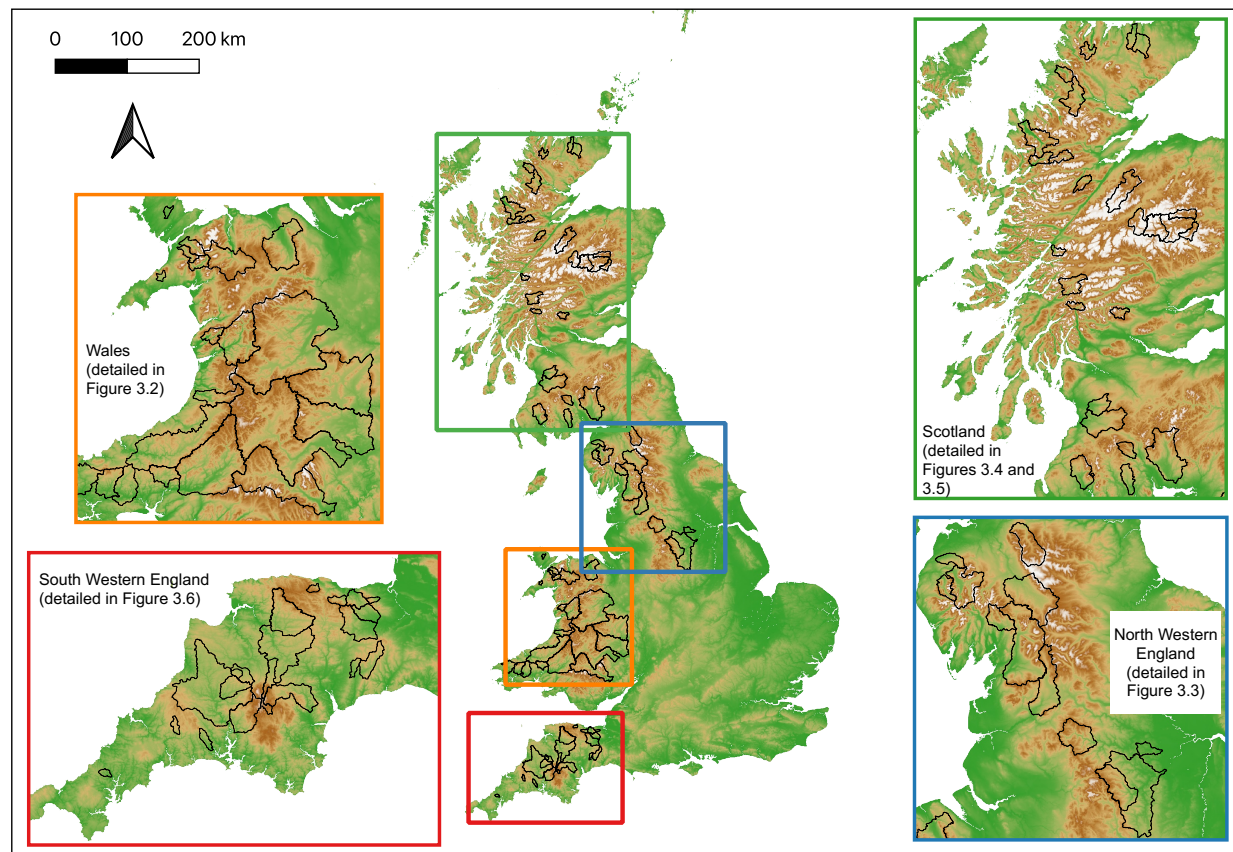


Figure 3.1. Extended Study Area. A total of 81 catchments are used to analyse the extent of AR impact on (winter) flooding. The catchments span a range of properties, including size, aspect, altitude, slope, and underlying geology. A detailed map and description of each region is provided in the following sections. Elevations are from the Institute of Hydrology Digital Terrain Model (IHDTM, Morris & Flavin, 1990, 1994).

This work intends to extend the analysis of Lavers et al. (2012), primarily through an extension of the study area across the UK. Concentrating in turn across a number of ‘hot spot’ areas of the UK, namely South Western England, Wales, North Western England and Scotland, study catchments were selected based on several requirements as detailed below:

1) Natural Flow Regime.

Catchments with a notable portion of human influence will likely demonstrate a flow regime that deviates away from natural conditions, making it harder to extract any meaningful links between ARs and hydrological response. As such, only catchments with a predominantly natural flow

regime were retained for the analysis. Along similar lines, catchments with significant attenuation according to lakes and reservoirs were rejected.

2) Suitability for Flood Studies.

This work is interested in the most extreme flows, and as such only catchments suitable for flood studies were retained. Physically, this involves the station being well gauged at high flows, both theoretically and operationally. Some gauging stations are drowned, bypassed, or undergo structural change when subject to extreme flows, thus rendering the resulting measurements of limited use. Following communication with analysts at SEPA (Scottish Environment Protection Agency), it was suggested to use only those catchments with an available 'Peak flow data' tab on the NRFA (National River Flow Archive) station page, as this ensured calibration above mean flows.

3) Topography.

Where possible, the selection of neighbouring catchments allows inspection of the influence of catchment properties on what may be presumed to be the same meteorological input. For example, the formation of rain shadows. Retaining catchments inland from the western coastline of the UK, or behind topographical barriers allows analysis of the typical propagation distance of the AR when it makes landfall. Previous work (Chapter 2, Section 2.6) has suggested that ARs can penetrate further inland when they align with favourable topographical barriers.

4) Visual Inspection.

In addition to the measures as detailed above, a visual inspection was performed of the catchment location and characteristics, data availability and any additional notes as recorded on the NRFA station page. Where possible, interactions were had with the monitoring authority analysts when submitting the data request. An example of the selection process is provided for South Western England (Table 3.1).

In total, 81 catchments were retained across the four study areas (Fig. 3.1). A detailed description of the catchments within each region is provided in the following subsections, alongside the relevant digital terrain models and catchment descriptor information (Flood Estimation Handbook; Ledingham et al., 2019).

South Western England - All Catchments								
Station number	River	Location	Year opened	Year closed	Peak flow data	Daily data	Factors affecting runoff	Urban extent
45001	Exe	Thorverton	1956		Yes	Yes	SRPGEI	0.024
45002	Exe	Stoodleigh	1960		Yes	Yes	SRPE	0.011
45003	Culm	Woodmill	1962		Yes	Yes	PGEI	0.065
45004	Axe	Whitford	1964		Yes	Yes	PGEI	0.034
45005	Otter	Dotton	1963		Yes	Yes	PGEI	0.071
45006	Quarme	Enterwell	1964	1967	No	Yes	P	0.0094
45007	Exe	Trews Weir	1996		Yes	Yes	SRPGEI	0.045
45008	Otter	Fenny Bridge	1974		Yes	Yes	P	0.053
45009	Exe	Pixton	1966		Yes	Yes	SRP	0.011
45010	Haddeo	Hartford	1973	1979	No	Yes	N	0.012
45011	Barle	Brushford	1968		No	Yes	N	0.0073
45012	Creedy	Cowley	1964		Yes	Yes	GE	0.042
45013	Tale	Fairmile	1978		Yes	Yes	N	0.079
45816	Haddeo	Upton	1993		Yes	No		0.018
45817	Unnamed St	Upton	1993		Yes	No		0.0038
45818	Withiel Flore	Bessom Brid	1992		Yes	No		0.013
46002	Teign	Preston	1956	2007	No	Yes	SRPE	0.045
46003	Dart	Austins Bridg	1958		Yes	Yes	SR	0.03
46005	East Dart	Believer	1964		Yes	Yes	N	0.0053
46006	Erme	Ermington	1973		Yes	Yes	PEI	0.066
46007	West Dart	Dunnabridge	1972		Yes	Yes	P	0.02
46008	Avon	Loddiswell	1971		Yes	Yes	SR	0.03
46013	Bovey	Bovey Parke	2004		Yes	Yes		0.018
46014	Teign	Chudleigh	2004		Yes	Yes		0.032
47001	Tamar	Gunnislake	1956		Yes	Yes	SRPEI	0.026
47002	Tamar	Werrington	1956	1961	No	Yes		0.022
47003	Tavy	Lopwell	1956	1980	No	Yes	PGEIH	0.035
47004	Lynher	Pillaton Mill	1961		Yes	Yes	P	0.033
47005	Ottery	Werrington f	1963		Yes	Yes	GE	0.027
47006	Lyd	Lifton Park	1975		Yes	Yes	SGEI	0.019
47007	Yealm	Puslinch	1963		Yes	Yes	PI	0.061
47008	Thrushel	Tinhay	1969		Yes	Yes	SH	0.019
47009	Tiddy	Tideford	1969		Yes	Yes	N	0.047
47010	Tamar	Crowford Bri	1972		Yes	Yes	SRP	0.022
47011	Plym	Carn Wood	1971		Yes	Yes	SRPGEI	0.025
47013	Withey Brook	Bastreet	1972		Yes	Yes	P	0.026
47014	Walkham	Horrabridge	1976		Yes	Yes	PI	0.019
47015	Tavy	Ludbrook	1976		Yes	Yes	N	0.035
47016	Lumburn	Lumburn Bri	1976	2002	No	Yes	N	0.026
47017	Wolf	Combe Park I	1977	1986	No	Yes	SRP	0.012
47018	Thrushel	Hayne Bridge	1988		No	Yes	N	0.022
47019	Tamar	Polson Bridg	1987		No	Yes	N	0.026
47020	Inny	Bealsmill	1988		Yes	Yes		0.027
47021	Kensley	Launceston H	2002		Yes	Yes		0.051
47022	Tony Brook	Newnham Pt	1979		Yes	Yes		0.024
47023	Tamar	Tamarstone	2010	2017	Yes	No		0.025
47024	Tavy	Tavistock Abl	1994		Yes	Yes		0.022
47025	Wolf	Germanswei	1992		Yes	Yes		0.0094
48001	Fowey	Trekeivestep	1968		Yes	Yes	SRP	0.018
48003	Fal	Tregony	1977		Yes	Yes	EI	0.05
48004	Warleggan	Trengoffe	1969		Yes	Yes	N	0.028
48005	Kenwyn	Truro	1968		Yes	Yes	N	0.076
48006	Cober	Helston Cour	1968		Yes	Yes	PGL	0.048
48007	Kenal	Ponsanooth	1968		Yes	Yes	SRPGL	0.047
48008	St Austell	Molingey	1971		No	Yes	GI	0.14
48009	St Neot	Craigshill Wc	1971		Yes	Yes	SRPE	0.038
48010	Seaton	Trebrownbri	1972		Yes	Yes	GIN	0.065
48011	Fowey	Restormel	1961		Yes	Yes	SRP	0.026
48012	Fal	Trenowth	1998		Yes	Yes		0.052
48801	Cober	Trenear	1988		Yes	Yes		0.019
48803	Carmon	Bissoe	1994		Yes	Yes		0.1
49001	Camel	Denby	1964	2019	Yes	Yes	SRPE	0.045
49002	Hayle	St Erth	1957		Yes	Yes	GI	0.06
49003	De Lank	De Lank	1966		Yes	Yes	P	0.016
49004	Gannel	Gwills	1969		Yes	Yes	GEI	0.028
49005	Bolingey Stre	Bolingey Coc	2010		Yes	Yes		0.039
49006	Camel	Camelford	2006		Yes	Yes		0.016
49007	Denby	Bodmin Dun	2015		No	Yes	SRPE	
49008	Penberth Riv	Penberth	1993		No	Yes	N	
50001	Taw	Umberleigh	1958		Yes	Yes	RP	0.024
50002	Torrige	Torrington	1962		Yes	Yes	SRPEI	0.025
50003	Taw	Sticklepath	1975		No	Yes	PG	0.0055
50005	West Okeme	Vellake	1975		No	Yes	P	
50006	Mole	Woodleigh	1965		Yes	Yes	SRPE	0.019
50007	Taw	Taw Bridge	1973		Yes	Yes	N	0.025
50008	Lew	Gribbleford E	1988		Yes	Yes	N	0.017
50009	Lew	Norley Bridg	1988		Yes	Yes	N	0.013
50010	Torrige	Rockhay Brid	1988		No	Yes	N	0.026
50011	Okement	Jacobstowe	1973		Yes	Yes	SRP	0.036
50012	Yeo	Veraby	1968	2019	No	Yes	R	0.0082
50013	Bray	Leehamford	1979		No	Yes	SP	0.0017
50014	Yeo	Collard Bridg	1995		Yes	Yes		0.017
51001	Doniford Stre	Swill Bridge	1966		Yes	Yes	N	0.043
51002	Horner Wate	West Luccon	1973		Yes	Yes	N	0.008
51003	Washford	Beggearn Hu	1966		Yes	Yes	N	0.024
52003	Halsewater	Halsewater	1961		Yes	Yes	N	0.06
52004	Isle	Ashford Mill	1962		Yes	Yes	GE	0.069
52005	Tone	Bishops Hull	1961		Yes	Yes	SP	0.059
52008	Tone	Clatworthy R	1960	1968	No	Yes	S	0.0075
52014	Tone	Greenham	1966		Yes	Yes	S	0.013
52016	Currypool Str	Currypool Fai	1971		Yes	Yes	N	0.023
52025	Hillfarrance I	Milverton	1992		Yes	Yes	E	0.051

FINAL SELECTED CATCHMENTS (SW ENGLAND)

- 45008
- 45013
- 46005
- 46014
- 47001
- 47008
- 47009
- 47015
- 48004
- 48005
- 50001
- 50006
- 50007
- 50008
- 50009
- 51001
- 51002
- 51003
- 52003
- 52005
- 52016

Table 3.1. Selection of Catchments for South Western England. Green rows correspond to selected catchments (repeated to the right of the main table). Red highlighted cells do not meet the requirements as outlined in section 3.3.

3.3.1. South Western England

Devon and Cornwall make up most of the south-western peninsula of the British Isles and are subject to the full force of the weather systems brought across the Atlantic. The population is generally confined to regions along the coast, in the form of ports, fishing towns and/or seaside resorts. Dartmoor National Park covers much of the southern half of the Devon and exists as one of the largest open spaces across the British Isles. Across the northern edge, the Exmoor National Park, so named after the River Exe which flows through its centre, consists of an area of open moorland, with dramatic cliffs falling away into the Bristol Channel. The high point of Exmoor is that of Dunkery Beacon, at 519 m. This is compared to High Willhays of Dartmoor, which stands at 621 m, and is the highest point in the UK south of Brecon Beacons.

Moving across to Cornwall and there exists an exposed series of granite intrusions gradually descending in elevation from east to west. The most eastern intrusion, and therefore the highest point within Cornwall, is known as Bodmin Moor, and sits at an elevation of 417m.

Much of the geology of South West England is characterised by igneous or metamorphic rocks. Hydrological responses are expected to be rapid in regions dominated by impermeable bedrock and limited soil cover. The primary watercourses flow from the sparsely populated central uplands towards the northern or southern coasts, depending on the watershed. The locations of many of the populated areas of Devon and Cornwall in such vulnerable positions at the mouth of the region's primary rivers have important consequences for flood risk management

As in the previous sections, a map of the study catchments is given in Fig. 3.2 alongside a summary of the key catchment descriptors (Flood Estimation Handbook, CEH; Ledingham et al., 2019) in Appendix 1. A summary of specific points to note is given here.

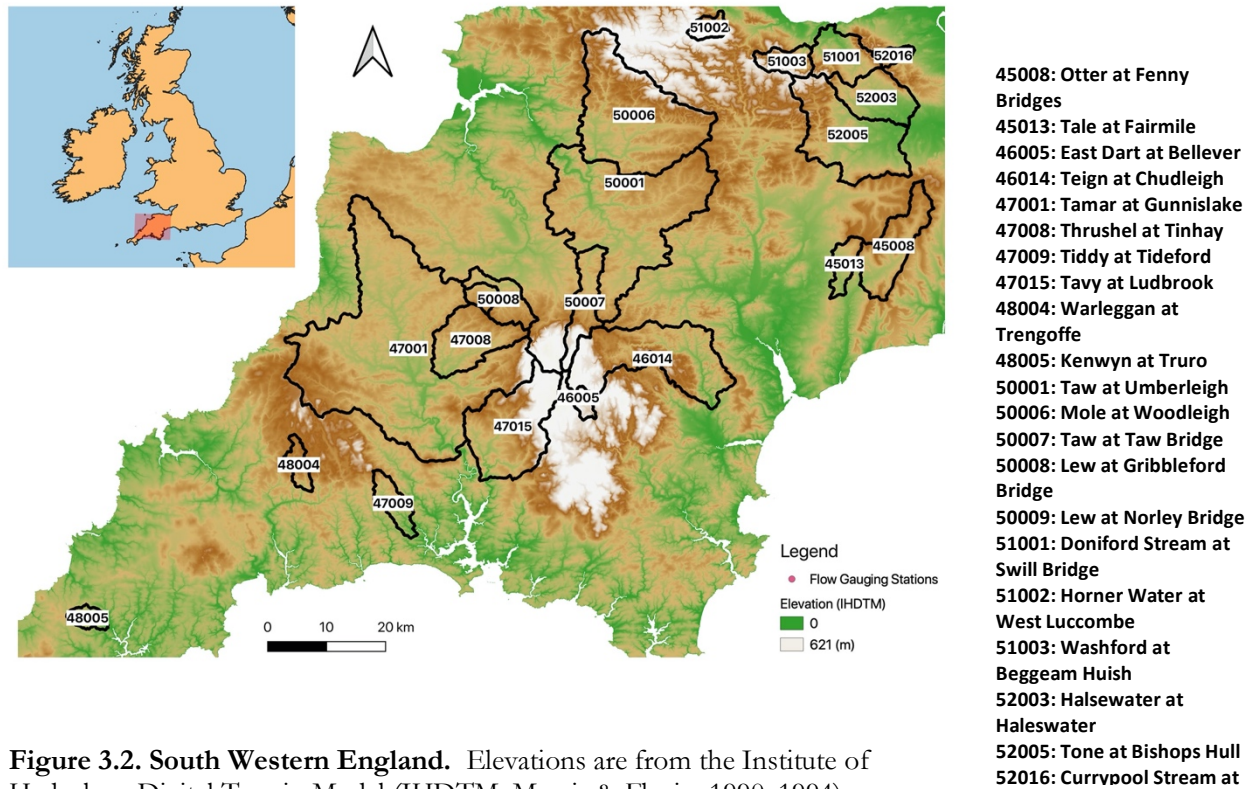


Figure 3.2. South Western England. Elevations are from the Institute of Hydrology Digital Terrain Model (IHDTM, Morris & Flavin, 1990, 1994).

The most eastern catchments can be found on the northern edge of the Devon-Somerset border, demonstrating predominantly natural flow regimes due to limited urbanisation. Moving westward into Devon, and the study catchments can be largely separated according to their respective watersheds (namely, those flowing northward towards the Bristol Channel or southward towards the South Coast). Adjacent catchments of Thrushel and Tamar are of particular interest as they are affected by the Roadford Reservoir and its subsequent water abstractions. Given their Carboniferous uplands, an element of groundwater storage at these catchments is to be expected.

3.3.2. Wales and the English Borders

Wales covers a total land area of approximately 20,000km² with a population of just over 3 million, representing around 8.5 and 5% of the respective UK totals. A country of rich environmental diversity, Wales is dominated by uplands, particularly in the north and central regions, with 25% of the total land area above 305m (Robins & Davies, 2015). Home to three of the UK's 15 National Parks, and a further five Areas of Outstanding Natural Beauty,

approximately 80% of the land surface area is devoted to agriculture, predominantly grassland and rough pasture, with an additional 12% associated with forest (Robins & Davies, 2015).

The primary mountain chains across the country consist of Snowdonia in the north, the Cambrian mountains across western central areas and the Brecon Beacons in the south. The highest elevation (1085m) is that of Yr Wyddfa (Snowdon) in the north, as compared to Cader Idris in the west (892m), Plynlimon in the centre (752m) and Pen y Fan in the south (886m). Some of the largest rivers in Wales, such as the Dyfi and Teifi, flow from the central mountain ranges to the west coast. Others, such as the Severn, Taff, Usk, and the Wye, rise in the Cambrian mountains before flowing towards the Bristol Channel (Robins & Davies, 2015).

The rivers Conwy and Clwyd rise in the northern uplands before flowing towards the Irish Sea. Due to predominant westerly, wet weather systems, Wales is one of the wettest regions of the UK, with some areas of Snowdonia receiving average annual totals of more than 3000 mm. Its geology is extraordinarily diverse (Robins & Davies, 2015), with the oldest rocks located in north Wales (Cambrian), followed by a south-west to north-east belt across central regions (Ordovician and Silurian). The bedrocks of Wales generally have limited porosity, although the Carboniferous deposits of the south and north-east demonstrate a greater ability to store and translate groundwater.

Soil cover is limited on upper ground, particularly in Snowdonia, but notable glacial outwash can be found along lower valley floors (Robins & Davies, 2015). Where soils exist, they may form groundwater driven peat bogs (e.g., Tregaron in the Teifi catchment). In general, however, high rainfall coupled with low transmissivities and limited groundwater percolation promote flashy, responsive catchments and a shallow water table.

A map of the study catchments across Wales is given in Fig. 3.3 alongside a summary of the key catchment descriptors (Flood Estimation Handbook, CEH; Ledingham et al., 2019) in Appendix 1. A summary of specific points to note is given here.

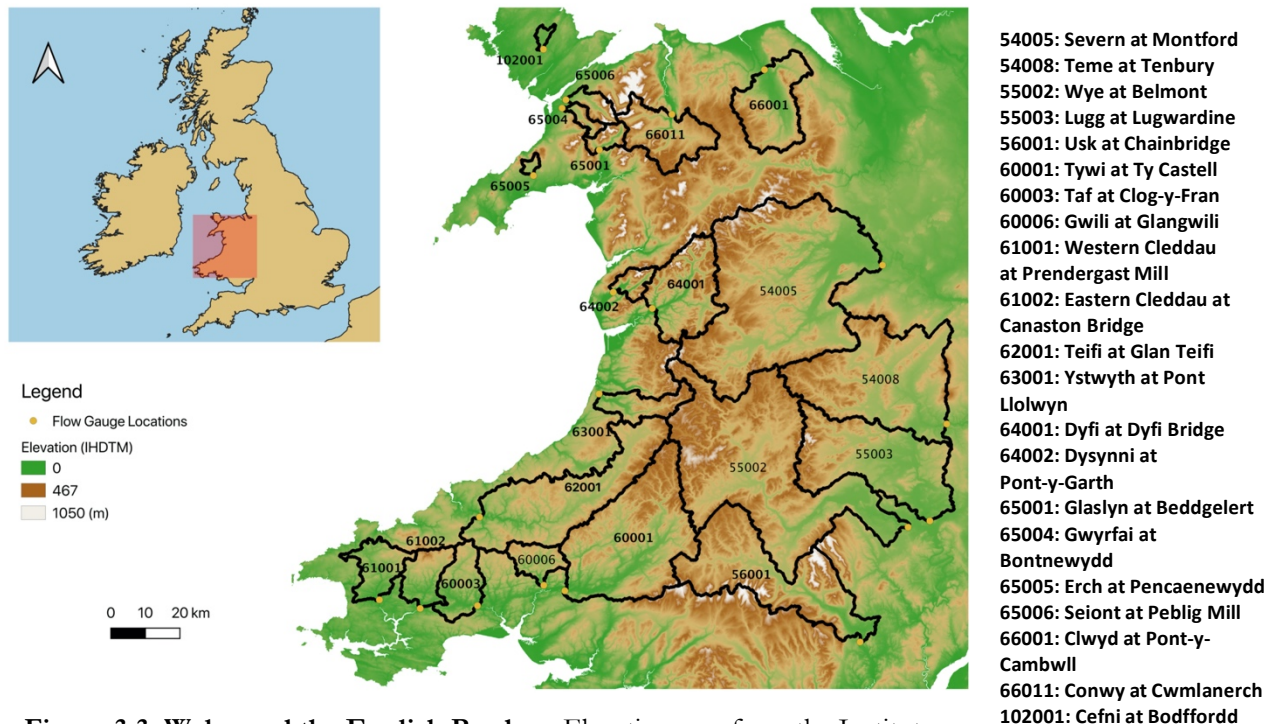


Figure 3.3. Wales and the English Borders. Elevations are from the Institute of Hydrology Digital Terrain Model (IHDTM, Morris & Flavin, 1990, 1994).

The largest catchments exist primarily along the English Borders and into southern and central Wales. Corresponding to the largest rivers of the Severn, Wye and Usk and Tywi, the sources rise primarily in the Cambrian mountains before flowing south/eastwards towards the Bristol Channel. Moving further west, and the catchments decrease in size, with the smallest found along the western coastline. As expected, these catchments demonstrate flashy flow regimes with limited permeability bedrock and predominantly natural flow regimes.

In Snowdonia, this effect is even more apparent. The presence of high elevation snowpack is also more likely during the winter months of these upland catchments; on average Snowdonia experiences around 40 days a year with an element of snowfall. This is to be compared with around 10 on the south-western coastline (Robins & Davies, 2015).

Interesting catchments to note are those of the Conwy and Clwyd. The former consists of at least four tributaries and is well-known in the area as a key factor in the development of local flood-forecasts. The location of the Clwyd catchment above fractured Carboniferous bedrock, and in combination with flood-plain storage, results in a dominant flow regime somewhat different to that of its western neighbours. That being said, the relatively populous town of St.

Asaph and the nearby A55 dual carriageway are still affected by a degree of surface water flooding nearly every winter.

3.3.3. North Western England

The study catchments largely lie within and around the Pennines and the Cumbrian mountains. The craggy, mountainous terrain of the Lake District is dominated by Ordovician and Silurian formations, falling away towards the western coastline to expose younger, Carboniferous strata. These regions are home to coal and limestone deposits, responsible for much of the historical heavy industry of the area.

The north-south orientation of the Pennine chain of mountains, sometimes referred to as the 'backbone of England' can be attributed to the axis of an anticline, defined in geological terms as an arch-like fold of the rock strata where continued weathering exposes the oldest beds at its core. As such the Pennines demonstrate a wide variety of geological features through a combination of the older, resistant bedrock towards the centre and the younger sedimentary, superficial deposits moving east and west down the flanks.

The topography of the Cumbrian mountains and the Pennine chain mark the main drainage divide in northern England; conditions to the west of the hills are considerably wetter than those found further east. In the Lake District, the near radial distribution of rivers can be noted to ultimately drain predominantly westward towards the coast and the Irish Sea, whereas those found in the Pennines will either drain west (like those in Cumbria) or east towards the North Sea. The presence of water storage in the Lake District is expected to exert an element of control on the, otherwise predominantly natural, flow regimes.

As in the previous section, a map of the study catchments is given in Fig. 3.4 alongside a summary of the key catchment descriptors (Flood Estimation Handbook, CEH; Ledingham et al., 2019) in Appendix 1. A brief summary of specific points to note are given here.

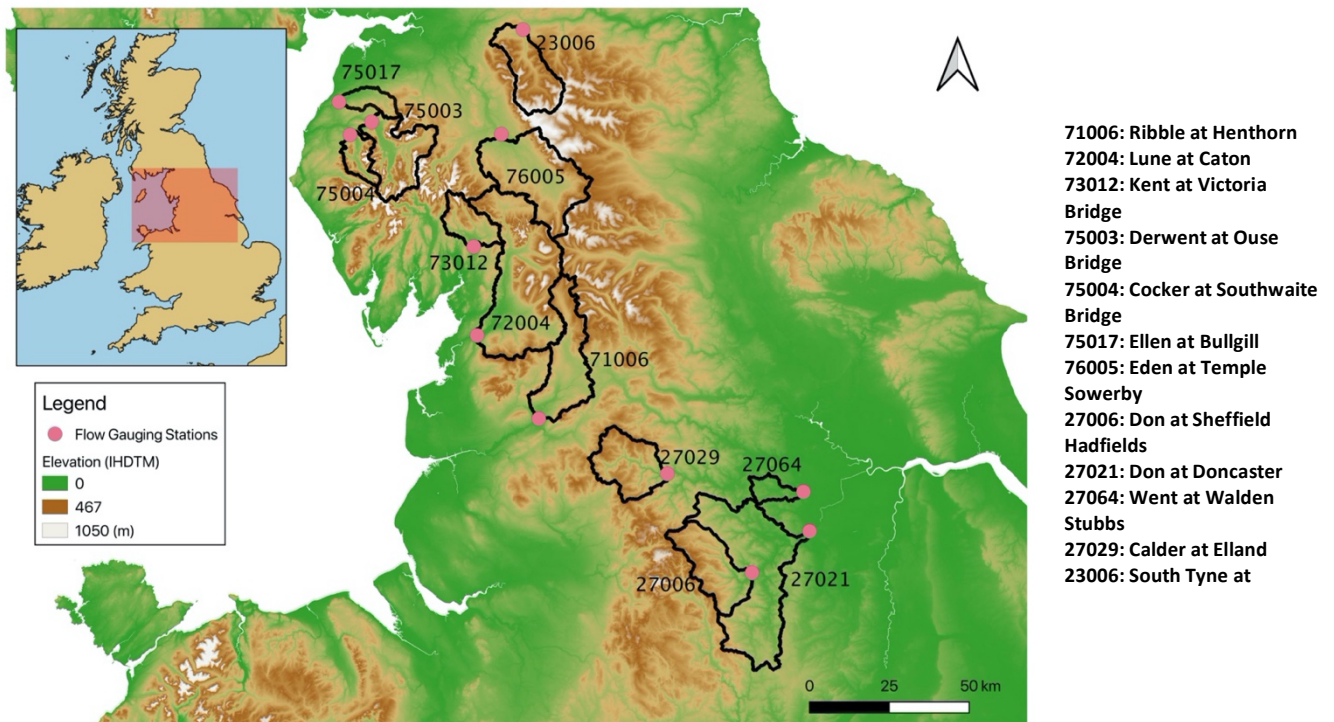


Figure 3.4. North Western England. Elevations are from the Institute of Hydrology Digital Terrain Model (IHDTM, Morris & Flavin, 1990, 1994).

Cumbria and the Lake District is region of particular interest given the history of significant events in the area upon arrival of strong winter storms (e.g., Storm Desmond in 2015). As such, particular effort has been made to select several neighbouring catchments within this region. Expected to demonstrate predominantly natural flow regimes, and existing on the western side of the Cumbrian watershed, the headwaters are heavily incised and the response times rapid. In the Pennines, catchments have been chosen within both the eastern and western watersheds. The sample also permits study of many of the largest rivers in Northern England; namely the Don and Went in the Peak District, the Lune, Ribble and Eden in the Dales and the Tyne in Northumberland.

3.3.4. Scotland

Scotland covers approximately 32% of the land-area of the UK and contains some of the most mountainous terrain found across the British Isles. It also demonstrates some of the most varied geology for an area of its size.

A notable point of reference is the so-called Highland Boundary Fault, traversing southwest to northeast from Arran on the west coast to Stonehaven in the east. Geographically, it distinguishes the region of elevated, rugged topography (the Highlands) north of the fault, from the rounded, rolling topography of the south (the Lowlands). The former contains Ben Nevis, the tallest mountain in the British Isles (standing at 1345 m above sea level). In line with the trend across other mountainous regions of the UK, the most resistant rocks are found within the Highlands and Islands of Scotland, namely north and west regions of the country. Historical volcanic activity along the Scottish coastline explains the presence of numerous volcanic and metamorphic intrusions visible within the bedrock along the Western Isles.

The western coastline of Scotland and the associated uplands are subject to the full force of Atlantic weather systems. The western highlands are some of the wettest places across the UK, recording up to 4,577 mm of annual rainfall. However, the orographic nature of this rainfall means that much of eastern Scotland is sheltered from the full force of the storms, typically recording less than 870 mm annually. As such the major drainage patterns can be classified as flowing predominantly westward towards the Atlantic, or eastward towards the North Sea, depending on the catchment's relative location to the Highland watershed.

As in the previous section, maps of the study catchments are given in Figs 3.5 and 3.6 alongside a summary of the key catchment descriptors (Flood Estimation Handbook, CEH; Ledingham et al., 2019) in Appendix 1. A brief summary of specific points to note are given here.

The southernmost catchments demonstrate natural flow regimes due to limited urbanisation and impermeable bedrock. Moving north, and the catchments can be separated according to their watershed aspect, namely whether the river they describe flows westward towards the Atlantic or eastward towards the North Sea. Given the elevation of the upland regions of many of the Scottish catchments, winter snowfall is common. For example, the catchment of Findhorn, is expected to demonstrate a very responsive flow regime but can also be affected by winter snow and ice when conditions permit.

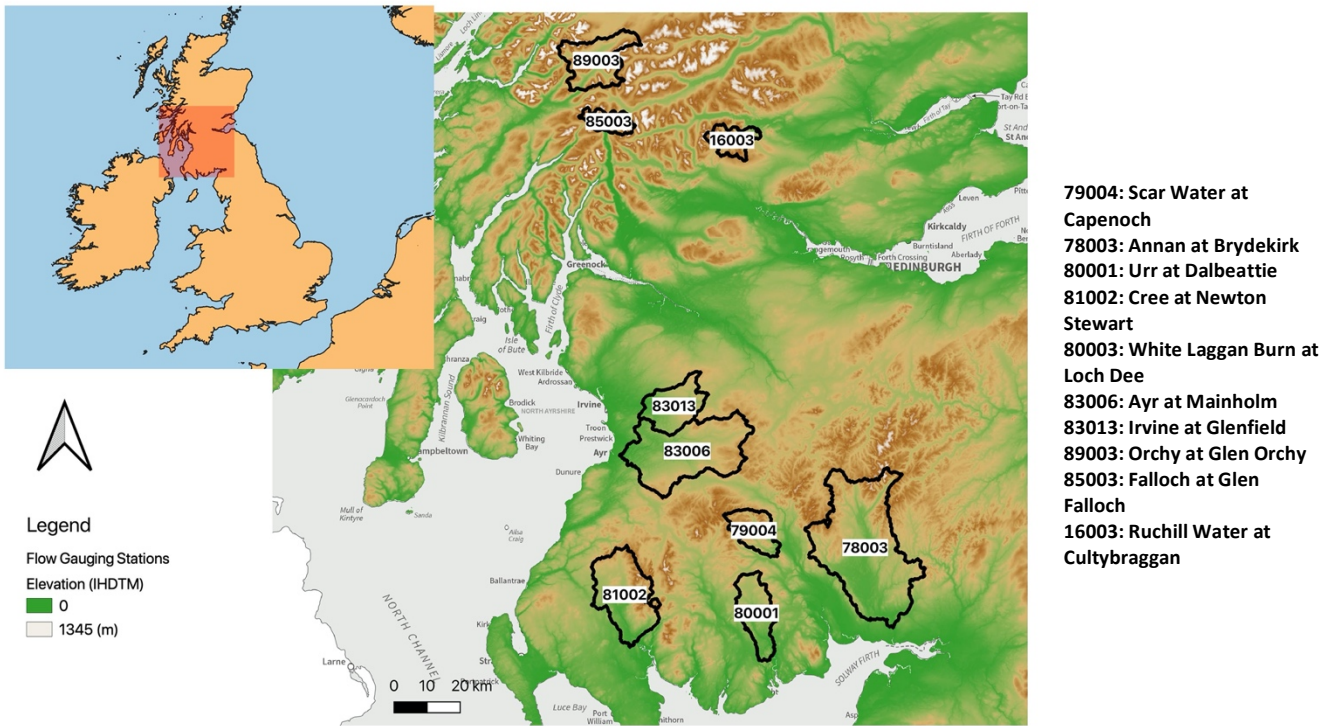


Figure 3.5. Southern Scotland. Elevations are from the Institute of Hydrology Digital Terrain Model (IHDTM, Morris & Flavin, 1990, 1994).

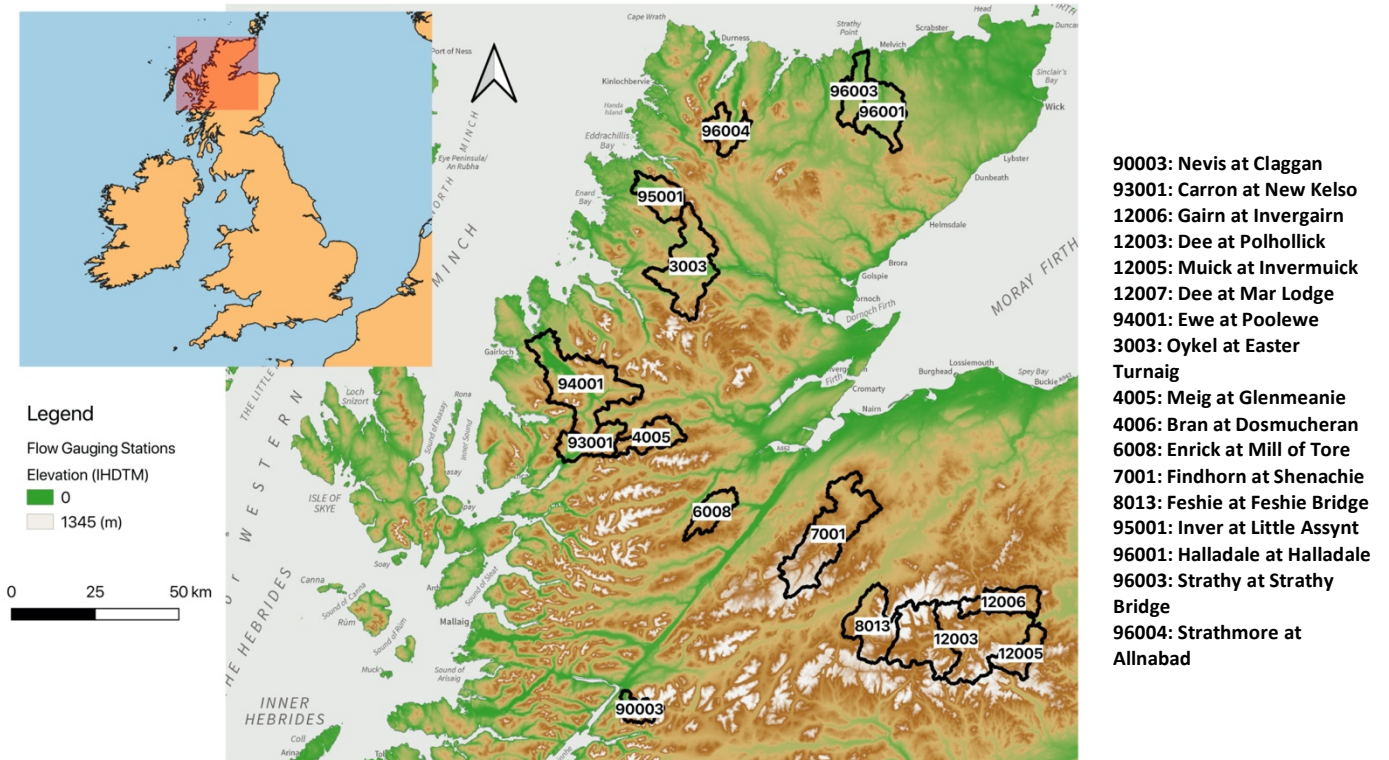


Figure 3.6. Northern Scotland. Elevations are from the Institute of Hydrology Digital Terrain Model (IHDTM, Morris & Flavin, 1990, 1994).

3.3.5. Selection of Catchment Descriptors

A series of catchment ‘descriptors’ have been extracted according to each of the study catchments. Taken from the Flood Estimation Handbook (CEH; Ledingham et al., 2019), the descriptors permit analysis of the key properties and distinctions across the study catchments. Such information was unavailable for some catchments and therefore information was sourced from the NRFA (National River Flow Archive) webpages where applicable. An overview of the chosen descriptors is given below and detailed in Appendix 1. .

3.3.5.1. Size and Configuration

These descriptors include the approximate drainage area (AREA), the longest drainage path (LDP), mean drainage path (DPLBAR) and the Shape Factor (Sf). Calculated from the Institute of Hydrology’s Digital Terrain Model (IHDTM; Morris & Flavin, 1990, 1994), the area, longest drainage path and mean drainage path in combination are able to describe both catchment size and configuration.

The Shape Factor, as developed by the Australian Rainfall and Runoff (Ball et al., 2019) goes some way to developing a metric to define catchment configuration. Approximating the catchment as an ellipse, Area, A and the Longest Drainage Path (LDP) can be written as:

$$A = \pi ab \quad (1)$$

$$LDP = 2a \quad (2)$$

where a and b are the major and minor axes of the ellipse respectively. The Shape Factor Sf is defined as:

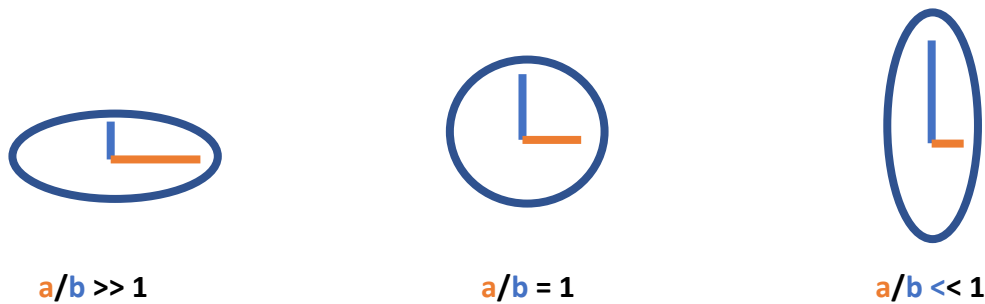
$$Sf = \frac{0.5 * LDP}{\sqrt{\text{Catchment Area}}} \quad (3)$$

Substituting for Area (1) and LDP (2) and it is possible to express Sf in terms of the axes of the ellipse:

$$Sf = \frac{0.5*(2*a)}{\sqrt{\pi ab}} = \frac{a}{\sqrt{\pi ab}} = \sqrt{\frac{a}{\pi b}} \quad (4)$$

Therefore $Sf = 1$ when $b = \frac{a}{\pi} = \frac{LDP}{2\pi}$ (5)

To understand what this means in practice, three possible catchment arrangements are suggested:



Rearranging equation (4) to give the ratio of a and b in terms of Sf:

$$\frac{a}{b} = \pi S f^2 \quad (6)$$

Therefore, the Shape Factor, Sf, can provide a measure of catchment configuration.

The distribution of the study catchments according to their area and ratio of major to minor axes (a/b), is given below (Fig. 3.7). The largest catchments are located on the English-Welsh borders and into the Pennines. South Western England is comprised of mostly smaller catchments, as are the upland regions of Snowdonia, Cumbria and northern-Scotland. All the catchments (where data was available) demonstrate axes ratios of greater than 4, suggesting an elongated shape.

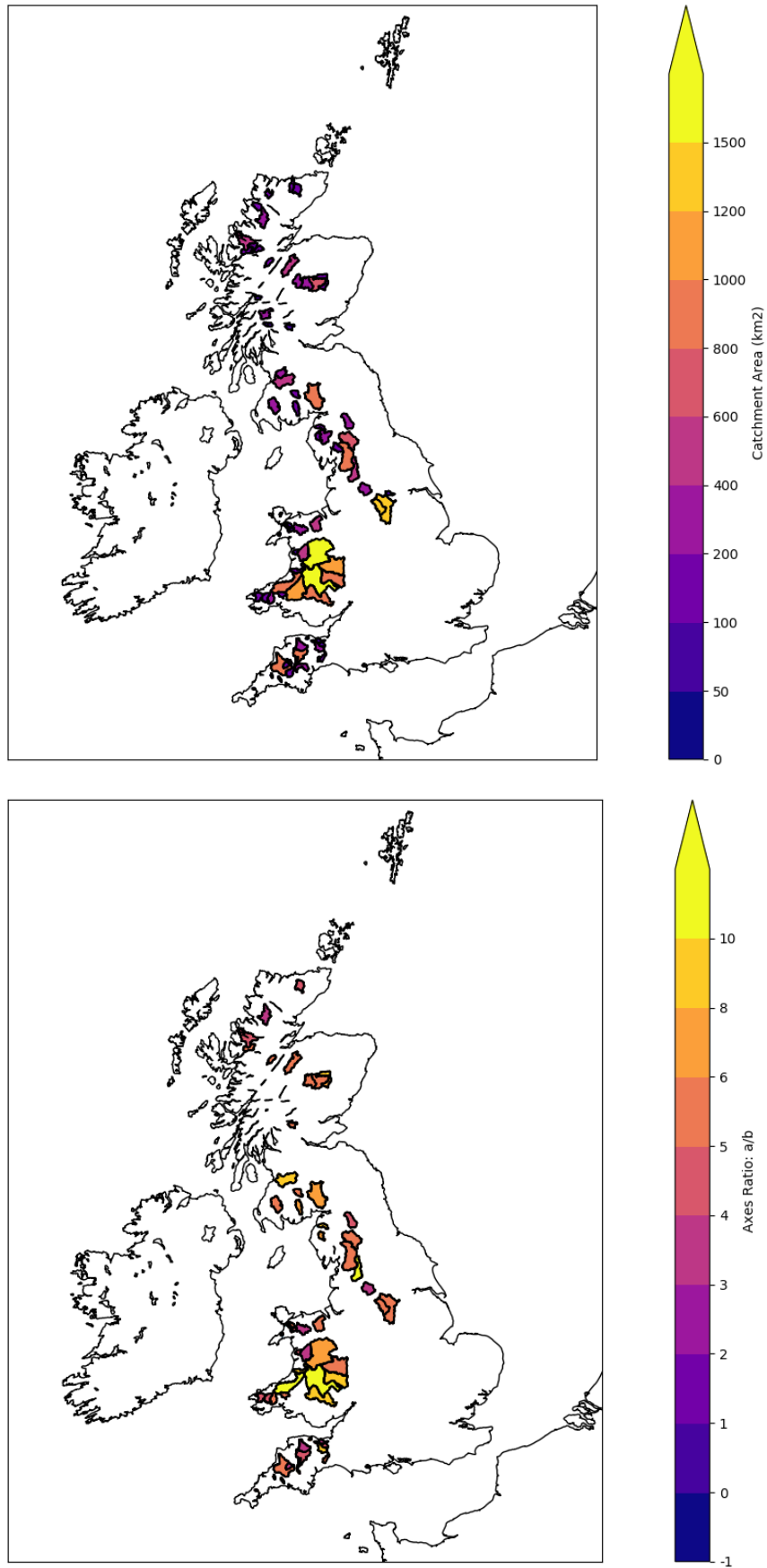


Figure 3.7. Size and Configuration. The largest catchments reside on the Welsh borders and into the Pennines. All of the study catchments have axes ratios > 4 , suggesting an elongated shape.

3.3.5.2. Altitude

Calculated from the Institute of Hydrology's Digital Terrain Model (IHDTM; Morris & Flavin, 1990, 1994), it is possible to extract the maximum (ALTMAX) and mean (ALTBAR) altitude values across the study catchments (Fig. 3.8). As expected, the highest altitudes (both max and mean) are found in the upland areas of Snowdonia, Cumbria and the Highlands of Scotland.

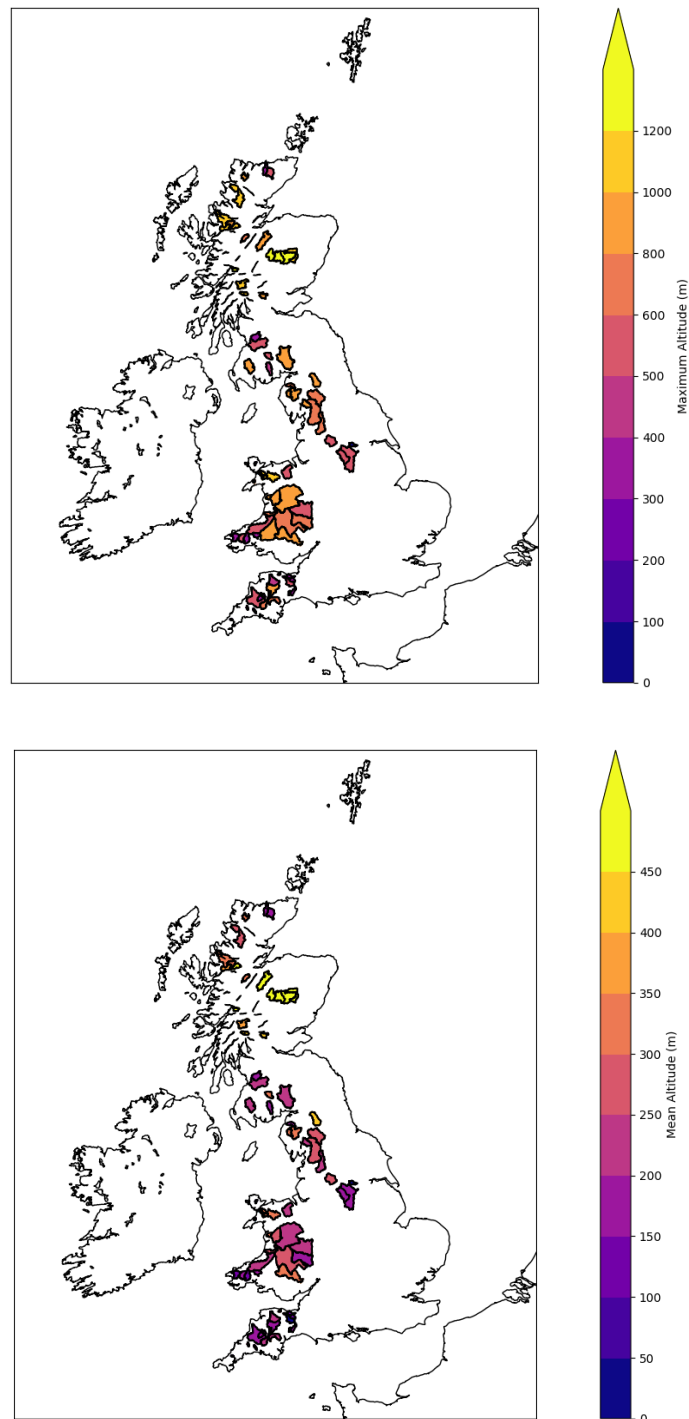


Figure 3.8. Altitude. The highest altitudes are found in the upland areas of Scotland, Cumbria and Snowdonia.

3.3.5.3. Slope and Aspect

Calculated as previously, these descriptors include the mean drainage slope (DSPBAR), mean aspect (ASPBAR) and invariability of within the aspect value (ASPVAR). The latter is provided as a number from 0-1. The closer to zero this number, the greater the variability in aspect across the catchment. The steepest catchments appear to reside in regions of mountainous terrain, with their aspect largely depending on their position relative to the relevant watershed (Fig. 3.9). The majority of ASPVAR values reside between 0.1 and 0.3, suggesting a deal of variation in aspect across the catchments, as expected.

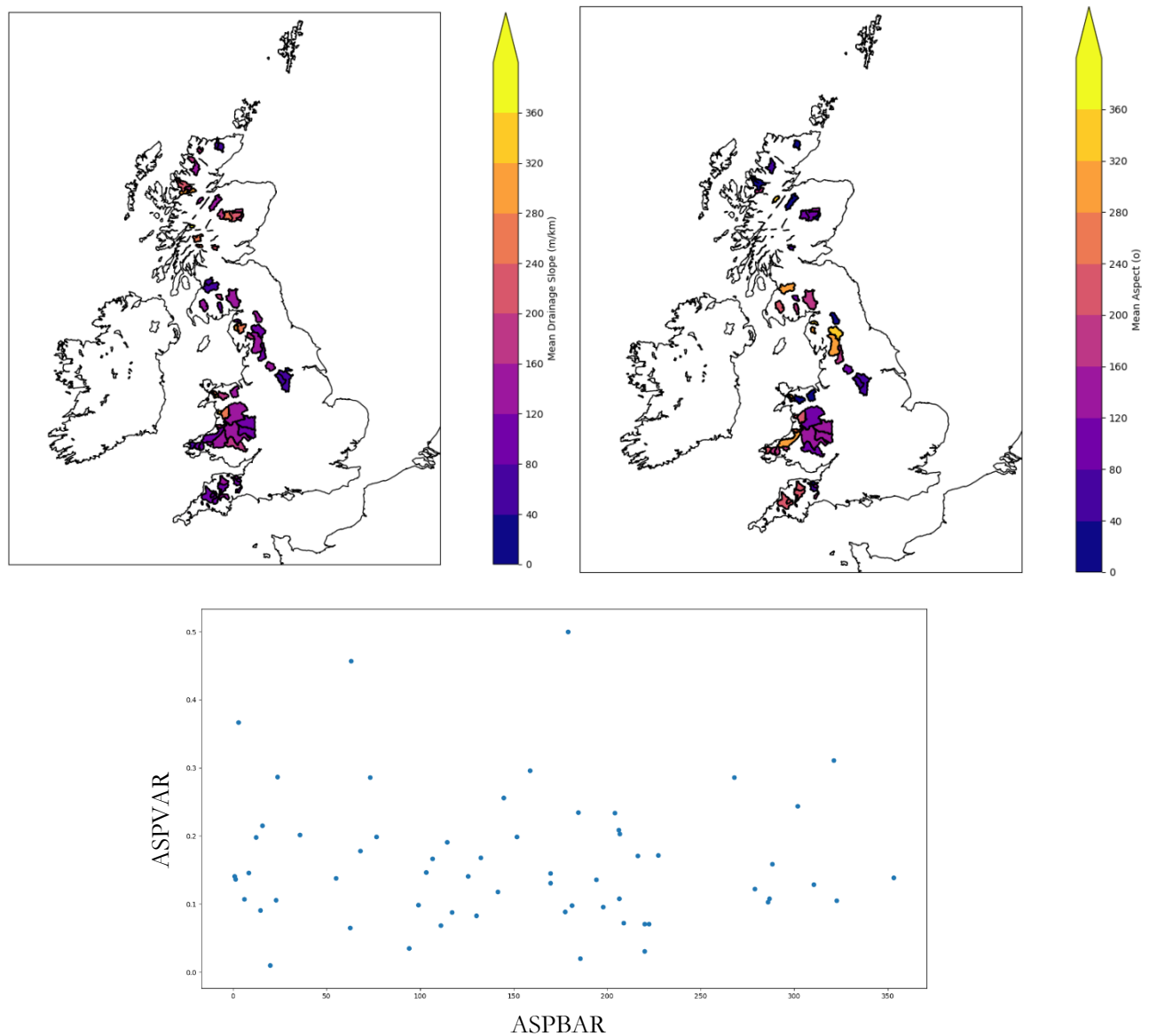


Figure 3.9. Slope and Aspect. The steepest catchments reside in regions of mountainous terrain with aspect depending on relative location to watershed. Most of the catchments show a great deal of aspect variation across their area.

3.3.5.4. Attenuation

Taken as the Flood Attenuation by Reservoirs and Lakes descriptor (FARL), values of one represent a catchment not at all influenced by lake or reservoir attenuation with decreasing values and indicating a greater influence on flows. In line with the catchment selection requirements, nearly all the study catchments show very little attenuation due lakes and reservoirs (FARL >0.95; Fig. 3.10).

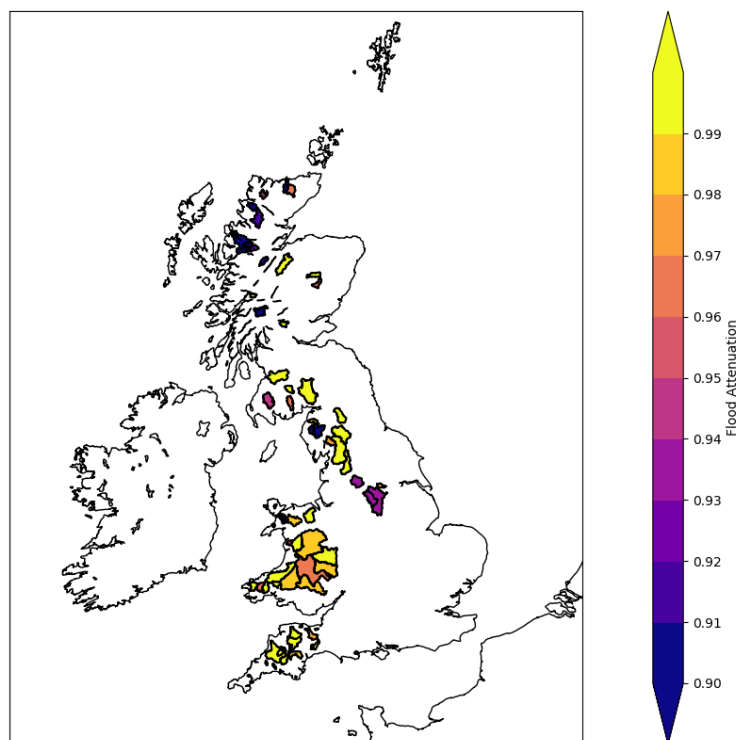


Figure 3.10. Attenuation. The majority of the test catchments show little to no attenuation due to lakes and reservoirs.

3.3.5.5. Climate and Soils

The annual average rainfall (SAAR), Base Flow Index (BFIHOST), Standard Percentage Runoff (SPRHOST) and soil moisture (PROPWET) are collated to provide a measure of typical climate and soils. SAAR indicates the typical annual rainfall recorded at the study catchments, taken across the period 1961-90 (as yet no updated values are available) and presented in units of millimetres.

The Base Flow Index and Standard Percentage Runoff are both derived from the Hydrology of Soil Types classification (HOST; Boorman et al., 1995) and can be interpreted as the a measure of the typical speed of catchment response (BFI) and the percentage of run-off hydrograph dominated by baseflow (SPR). The PROPWET descriptor provides a measure of typical soil moisture levels of the catchments, and the proportion of the time across the study period of 1961-90 that the catchment soil moisture deficit value was exceeded i.e., when soils were deemed to be 'at capacity'.

An attempt is made to combine this information across the study catchments (Fig 3.11). Annual rainfall totals are highest within the mountainous regions of the UK, in line with the orographic nature of the dominant weather systems. Nearly all catchments demonstrate SPRHOST values of less than 50%, in line with location. Soils are regularly saturated within the upland regions, in line with rainfall estimates.

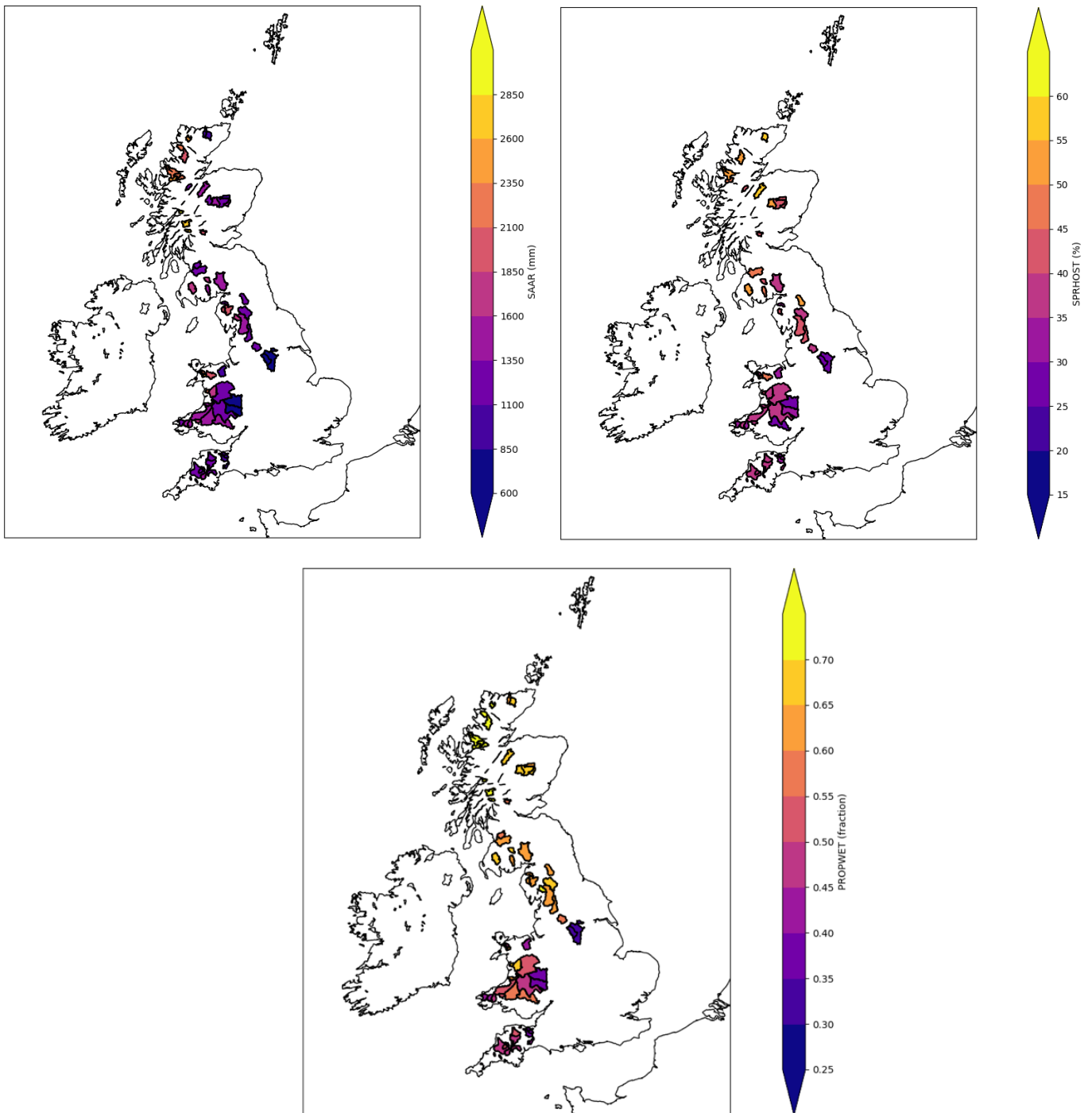


Figure 3.11. Climate and Soils. Annual rainfall totals are highest in the mountainous regions of the UK. Many catchments show SPRHOST values of less than 50%, suggesting relatively impermeable terrain. Soils are most regularly saturated in upland regions.

3.3.5.6. Land Use

Predominantly taken as the urban extent descriptor (URBEXT), this can be interpreted as the fraction of the catchment dominated by urban land-use (as of the year 2000). Shown for the study catchments (Fig. 3.12), the land use is predominantly rural, in line with the natural flow regimes. The only catchments with an element of urbanisation are those in the eastern Pennines.

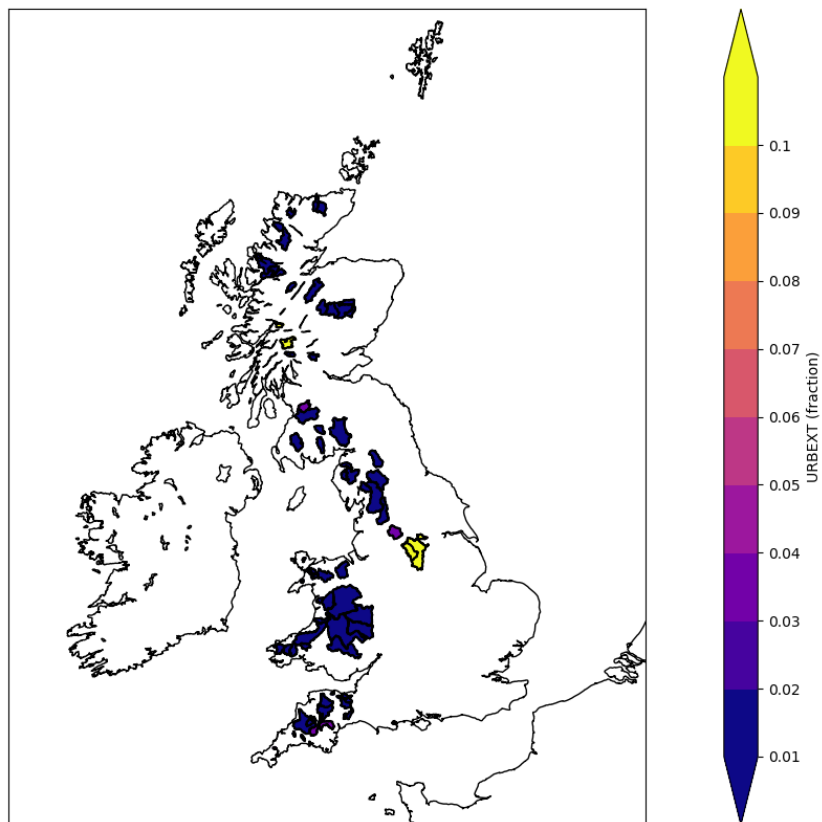


Figure 3.12. Land Use. The test catchments are predominantly rural.

3.3.5.7. Geology (Bedrock)

Taken from the NRFA website via British Geological Survey (BGS) datasets (© UKRI 2021), the proportions of the study catchments underlain by high, moderate, very low and mixed permeability bedrock are presented in Fig. 3.13. Defined in terms of aquifer potential, the data provides a measure of relative groundwater stores. The majority of the catchments in the study are underlain by very low-permeability bedrock, with limited storage available in some regions of central England, eastern Pennines and Cumbria.

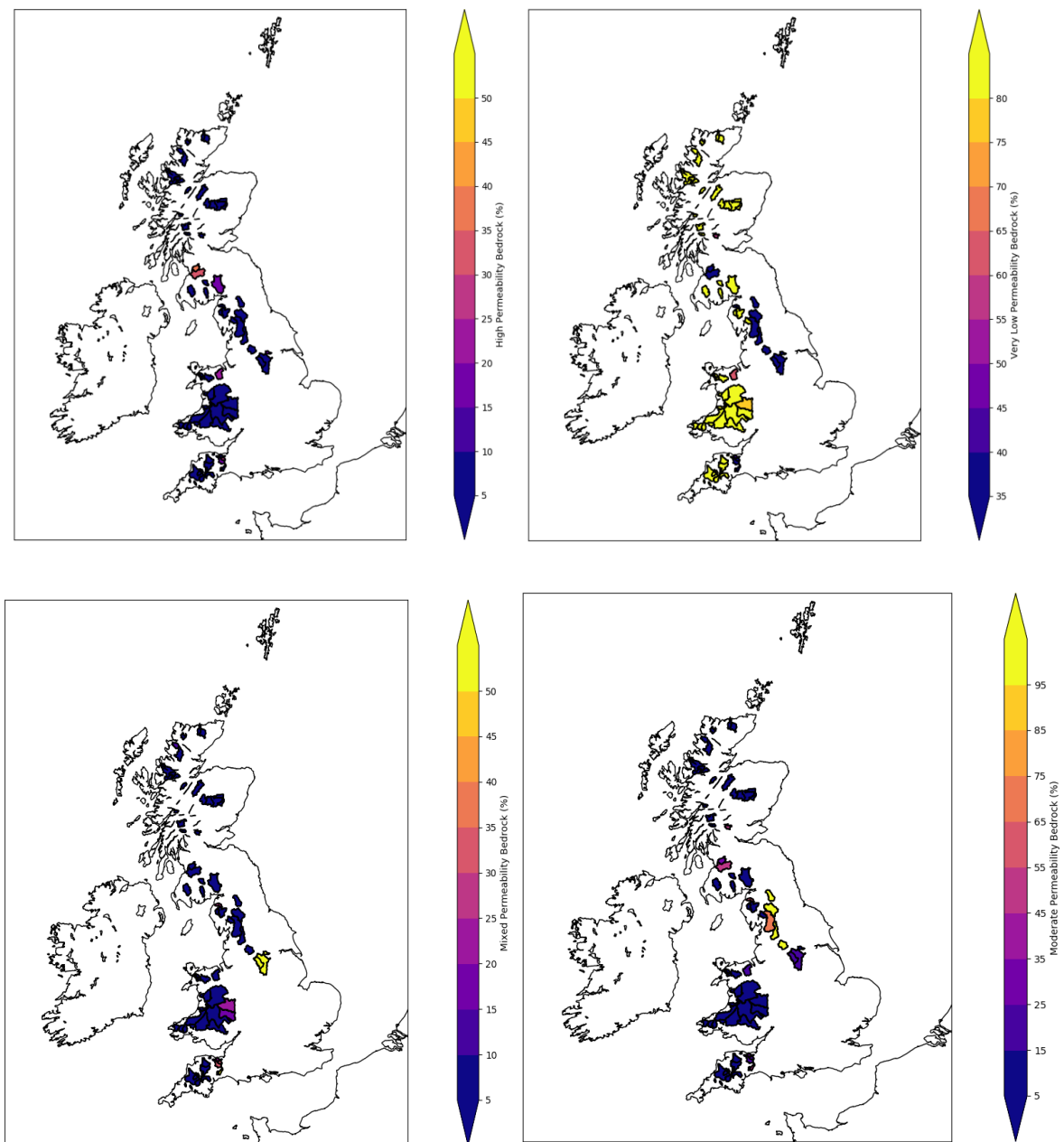


Figure 3.13. Bedrock. Most test catchments are underlain by impermeable bedrock, in line with their geographical location within the UK. .

3.4. Reanalysis Data

3.4.1. ERA5 Global Reanalysis

A key resource during this work is the recently released ECMWF ERA5 global reanalysis (Copernicus Climate Change Service Climate Data Store, 2017; Hersbach et al., 2020). A reanalysis is a dataset by which model outputs are combined with observations to produce a globally consistent ‘best estimate’ of the atmospheric properties at a given time.

ERA5 has several advantages over its predecessor, ERA-Interim (Berrisford et al., 2011), which was already held in high regard for the study of ARs (Lavers et al., 2012). It benefits from a over a decade of developments in model physics, core dynamics and data assimilation techniques, as well as invoking the latest advancements in observations, including satellite data, land surface stations and floating buoys (León, 2019). Typically, over a million observations are assimilated each day to create the reanalysis product, with the results available in near real time.

ERA5 produces as outputs, a whole suite of variables. Of relevance to the study of ARs, is the vertically integrated northward and eastward components of horizontal water vapour flux (Integrated Vapour Transport, hereon IVT). Earlier reanalyses would require the calculation of these variables from the product of specific humidity and horizontal winds, prior to integrating over the atmospheric column. The availability of these variables as direct outputs requires that, in order to calculate the total IVT, one must simply combine the orthogonal components.

The ARTMIP community (Chapter 2, section 2.5.2; Collow & Guan) has highlighted the topic of reanalyses as one of particular interest in terms of quantifying uncertainty in AR detection. When applying a Eulerian detection scheme (timestamp-by-timestamp; section 2.5.2), it is important to consider the temporal resolution of the reanalysis product. ERA5 is available at hourly resolution, to be compared with the six-hourly resolution of ERA-Interim. Whilst this provides a great deal of potential in terms of resolving temporal variability across the lifetime of the event, there is also potential for the performance of the detection scheme to be affected. The full workings of the chosen ARDM are described in the following section (3.4.2) and such concerns addressed in research Chapter 5.

In addition to the temporal resolution of the reanalysis product is its spatial resolution. The spatial resolution of ERA5 is 0.28° ($\sim 30\text{km}$) to be compared with the 0.75° of ERA-Interim and 0.625° of the NASA (National Aeronautics and Space Administration) MERRA-2 (Collow & Guan). As for the temporal resolution, the spatial resolution may also have consequences for the performance of the AR detection scheme, particularly in the case of those that search adjacent grid cells (section 2.5.2). Such a possibility will be explored in research Chapter 5.

Of primary importance when selecting a suitable reanalysis product for AR science, is the accuracy of the selected product in terms of IVT. Dropsonde measurements of IVT taken during 2020-21 AR Recon campaign in the north-eastern Pacific ³ (Chapter 2, section 2.5.1), have been compared to the estimated IVT in several reanalysis products, including MERRA-2 and ERA5 (Cobb et al., 2020). ERA5 was found to be the most reliable in terms of accuracy to the observational data, thus supporting its use in this thesis.

3.4.2. Atmospheric River Detection Method (ARDM)

The concept of ARDMs, and their inherent variability, was described in detail in Chapter 2 (section 2.5.2); the existence of ARs as synoptic scale features means that there are number of ways of approaching their detection. Many of the algorithms developed at the time of writing have been done so in accordance with respective data limitations and/or the scientific questions being posed.

The AR detection method (ARDM) as described in Lavers et al. (2012) has been identified as the most appropriate for use in this work. The reasoning is provided below:

1) Continuity

The first research objective of this thesis has been inspired by the work of Lavers et al. (2012), in that two catchments along the western coastline of Wales show remarkably different responses to landfalling ARs across the historical period (Chapter 2, section 2.7.2). As such, for continuity purposes, the detection scheme used in the original analysis is most appropriate for this study.

2) Originality and Simplicity

³ https://cw3e.ucsd.edu/arrecon_overview/

The algorithm of Lavers et al. (2012) exists as one of the original methods to detect ARs in atmospheric datasets (e.g., reanalyses) and, compared to many more modern schemes, is relatively simple in its approach. This allows for a detailed probing of its performance, which will be especially important in the context of the high spatial and temporal resolution of ERA5. Understanding the extent to which these properties of the input dataset affect the efficiency of the detection algorithm will have implication for the wider AR community (e.g., ARTMIP; Chapter 2. Section 2.5.2; Shields et al., 2018).

The ARDM as designed by Lavers et al. (2012) is described in detail in the relevant publication, however a summary will be provided here for completeness. At each available timestep in the input reanalyses, the maximum value of IVT is extracted along the coastline of mainland UK (taken as approximately 4°W and between 50° and 60°N). This maximum value is then compared to an IVT threshold; taken as ~85th percentile of the maximum IVT values to be recorded along the UK coastline over the historical period. For ERA5, this value is calculated as 486 kg m⁻¹ s⁻¹ (Fig. 3.14).

If the maximum IVT at a given timestep exceeds the threshold, then a similar procedure is carried out across the grid cells immediately to the northwest/ south/southwest/west of the original cell. The maximum IVT value across these adjacent cells is extracted and compared to the IVT threshold as previously. If the threshold condition is satisfied, then the next set of adjacent grid cells are tested. This process is repeated n times, where n is number of reanalysis grid cells along a parallel that for 20° longitude. If the IVT threshold condition is met at all n points, then the timestep is said to contain an AR affecting the UK (Lavers et al., 2012).

It has been shown that only persistent ARs induce flooding (Chapter 2, section 2.6.3) and thus only ARs that are identified across several adjacent timestamps are retained by the algorithm. Commonly, this temporal threshold is set at 18 hours (Lavers et al., 2012), which equates to 18 adjacent timesteps according to the ERA5 reanalysis. The concept of this threshold will be explored in greater detail in Chapter 5.

In addition, the ARs must be spatially persistent if they are to induce the greatest flood events. Estimating ARs to be on the order of 1000 km wide (Neiman et al., 2008), a 4.5° latitudinal movement window (approximately equal to 500 km) is applied to each AR event. Thus, the axis of the AR may move between 4.5° north or south of the initial IVT maximum across its lifetime if it is to be retained. Any ARs that do not meet this condition are immediately removed by the

detection algorithm. Finally, to be considered distinct, two AR events must be separated by at least one day (24 hours). Again, the implications of these concepts will be explored in greater detail in Chapter 5.

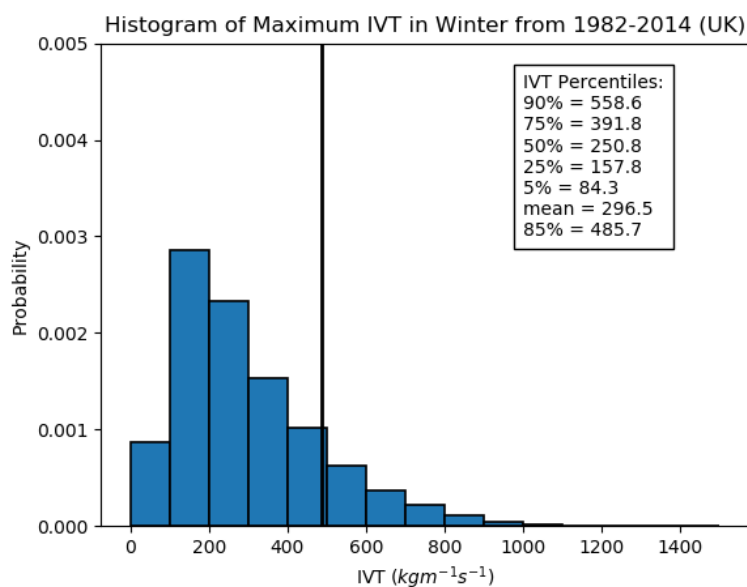


Figure 3.14. Calculation of IVT Threshold. Used in the Atmospheric River Detection Method.

3.5. Hydrological Data

3.5.1. Flow Data

High resolution (15 minute) hydrological data was obtained for each of the 81 study catchments from the relevant monitoring authorities (Environment Agency, EA – England; Natural Resources Wales, NRW– Wales; Scottish Environmental Protection Agency, SEPA – Scotland). In the case of the Dyfi and Teifi catchments, this data was provided as stage data alongside the associated rating curves (such that the flow values had to be calculated), whereas the additional catchments were provided directly as flow estimates. The requested data period was taken as 1982-2014.

For each catchment, a measure of data quality was obtained. In addition to communication with the data analysts at the relevant monitoring authority, most⁴ of the data files contained several data-quality codes alongside the measured values:

⁴ Excluding thirteen Scottish catchments where only a measure of missing data was available.

“G = good; E = estimated; S = suspect; U = unchecked; M = missing; C = complete; I = incomplete; Ed = edited; WR = within rating; NR = no rating; EX> = extrapolated upper part; EX< = extrapolated lower part; BL> = beyond upper limit; BL< = beyond lower limit; MH = weir modular (head); NH = weir non modular (head); EH = weir extremely non modular (head); MT = weir modular (tail); NT = weir non modular (tail); ET = weir extremely non modular (tail); MC = weir modular (crest); NC = weir non modular (crest); EC = weir extremely non modular (crest); -H = weir head only; RAS = rastered time stamp; A = apportioned/interpolated; D = dry; SN = snow; T = trace:”

A simple python program was developed to estimate the percentage of ‘missing’ (M), ‘estimated’ (E), ‘suspect’ (S) and ‘unchecked’ (U) data at each station across the period of interest. As this work is interested in the most extreme flooding events across the study catchments, caution was given when approaching outlier analysis. During the identification of flood events (section 3.5.2), time was given to visually inspect the evolution of several of the largest floods at each study catchment (i.e., to check the data around the time of the event was reasonable and continuous). The timestamps associated with the missing or spurious datasets were also retained.

The results of the data quality check are detailed in Appendix 2. In summary, although there is some evidence of missing data entries at several stations (e.g., 54005, 55002, 55003, 83013), there was enough continuous data at each of the stations for analysis to be carried out. As such, all 81 study catchments were retained.

3.5.2. POT Flood Selection

In order to assess the hydrological impact of ARs across the study catchments, a measure of flood events was required. Previous work suggested application of a Peaks-Over-Threshold, or POT, approach (Lavers et al., 2012), where flood events are selected on the basis of a given threshold. A common alternative is the Annual Maximum, or AMAX, method, where only the maximum flood events of each year are identified. Whilst AMAX suffers from limitations in that flood events may be missed if several events occurred within a given year, the POT approach can result in much uncertainty regarding the selection of a suitable threshold and independence window between flood events.

Application of the Lavers et al. (2012) detection algorithm across the historical period (1982-2014) to the ERA5 reanalysis, results in an average of 3-4 AR events each winter, defined as spanning October through March (Chapter 4, section 4.2.3). Given reported advantages of the POT approach over AMAX, and its use in flood selection studies (Cunderlik et al., 2004; Lang et al., 1999; Mediero et al., 2015), this work uses POT3 flood events for analysis. This equates to an average of three flood events per year, in line with the estimated occurrence of AR events. A seven-day separation criterion was applied to ensure independence of the extracted POT flood events. Summer floods were excluded because they are not normally driven by ARs (Champion et al., 2015) and are generally smaller in magnitude.

3.5.3. Rainfall Data

An attempt was made to identify appropriate rain-gauge measurements across each of the study catchments. Although initially promising for the Dyfi and Teifi catchments (Chapter 4, section 4.2.3), issues regarding station location and measurement resolution at the additional study catchments resulted in data of limited use. At the Dyfi and Teifi catchments, the 15-min precipitation data from each station was combined via a Thiessen polygon approach to obtain a measure of basin-averaged event total rainfall.

3.6. Additional Methods

3.6.1. Statistical Methods

In order to assess the distribution of AR properties, two statistical tests are proposed.

1) **T-Test:**⁵

The T-Test allows a test of the null hypothesis that two independent samples have identical means, generating the calculated t-statistic and two tailed p-value as outputs. The former quantifies the difference in means between the two samples, whilst the latter quantifies the probability of observing such a difference assuming the null hypothesis is true (i.e., that the two samples are taken from the same distribution). A low p-value therefore, typically 5% or below, allows the null hypothesis to be rejected.

⁵ https://docs.scipy.org/doc/scipy/reference/generated/scipy.stats.ttest_ind.html

2) **Levene Test:** ⁶

The Levene Test allows a test of the null hypothesis that two samples have identical variances, when normality of the data cannot be assured. As for the T-Test, a test statistic and p-value are generated as outputs of the analysis. A low p-value (<5%) allows rejection of the null hypothesis.

3.6.2. Principal Component Analysis

Principal Component Analysis (PCA) acts to reduce the dimensionality of large datasets into one that retains the variability of the original set (Jolliffe & Cadima, 2016). The aim is to extract a new set of axes to describe the dataset, along which the variance is maximised. The process also ensures orthogonality between the variables of the dataset, thus permitting application of regression methods.

In this thesis, well regarded python code⁷ has been applied to carry out PCA on the relevant datasets (Chapter 6, section 6.3.3; Galarnyk, 2021). This code acts to first standardize the original variables, such that each contributes equally to the variances within the analysis. The principal components of the data are then calculated via computation of the covariance matrix and identification of the associated eigenvectors and eigenvalues (*A Step-by-Step Explanation of Principal Component Analysis (PCA)*). The original dataset can then be recast along the Principal Component Axes permitting subsequent regression analysis or similar.

3.6.3. Random Forest Regression

Random Forest Regression (RFR) is a supervised learning algorithm that applies an ensemble-based system to building a predictive model (Liaw & Wiener, 2002). Subsets of the input data are used to build a number of decision trees based on the variables of the data. The predictions according to each decision tree are then averaged across the ‘forest’. The input data is split into so-called ‘training’ and ‘test’ subsets, where random samples of the ‘training’ set are extracted and used to build a decision tree, before applying the ‘test’ subset as a measure of performance.

⁶ <https://docs.scipy.org/doc/scipy/reference/generated/scipy.stats.levene.html>

⁷ <https://scikit-learn.org/stable/modules/generated/sklearn.decomposition.PCA.html>

Python code ⁸ was used to carry out Random Forest Regression on the datasets in this thesis (Chapter 6, section 6.4). The so-called variable ‘importance’ (Grömping, 2015; Płoński, 2020) is a way of identifying the key variables and attributing a measure of relative importance within the regression model; something that is highly non-intuitive in ‘black-box’ models such as this. A limitation of Random Forest Regression as compared to more common regression models, is that it does not perform well in the case of extrapolation (*Random Forest Regression*, 2020). As such, consideration should be given when selecting the appropriate ‘training’ dataset.

⁸ <https://scikit-learn.org/stable/modules/generated/sklearn.ensemble.RandomForestRegressor.html>

Chapter 4 – Atmospheric River Orientation Determines Flood Occurrence

4.1 Introduction

This chapter contains the work as published by Hydrological Processes in September 2020. It is reproduced here under the terms of the Creative Commons Attribution License, which permits use, distribution and reproduction in any medium, provided the original work is properly cited⁹. The section, figure references and some elements of the text have been altered in line with the format of this thesis.

4.2. Atmospheric River Orientation Determines Flood Occurrence

4.2.1. Abstract

Atmospheric Rivers (ARs) have been linked to many of the largest recorded UK winter floods. These large-scale features can be 500–800 kilometres in width but produce markedly different flood responses in adjacent catchments. Here meteorological and hydrological data is combined to examine why two impermeable catchments on the west coast of Britain respond differently to landfalling ARs. This is important to help better understand flood generation associated with ARs and improve flood forecasting and climate-change impact assessment. Analysis of 32 years of a newly available ERA5 high-resolution atmospheric reanalysis and corresponding 15-minute river flow data show that the most impactful ARs arise through a combination of the orientation and magnitude of their water vapour flux. At the Dyfi catchment, AR orientations of between 238–258° result in the strongest hydrological responses, whereas at the Teifi a range of 224–243° is preferred. This differential flood response is believed to be the result of catchment orientation and topography enhancing or suppressing orographic rainfall totals, even in relatively low-relief coastal catchments. Further to the orientation requirements, ARs must possess an average water vapour flux of 400–450 kg m⁻¹ s⁻¹ across its lifetime incident on the study catchments. Understanding the preferential properties of impactful ARs at catchments allows for the linking of large-scale synoptic features, such as ARs, directly to winter flood impacts. These results using two study catchments suggest a novel approach to flood forecasts through the inclusion of AR activity.

⁹ <https://creativecommons.org/licenses/by/4.0/>

4.2.2. Introduction

Atmospheric Rivers (ARs) are narrow regions of enhanced low-level moisture transport in mid-latitude cyclones (Browning & Pardoe, 1973; Newell, Newell, Zhu & Scott, 1992) that are responsible for most of the meridional water vapour transport across the mid-latitudes (Zhu & Newell, 1998b). These plumes of warm, moist air can generate very high rainfall totals as they cross elevated terrain and have been linked to floods in many coastal regions of the world (Barth, Villarini, Nayak & White, 2017; Dettinger, 2011; Kingston, Lavers & Hannah, 2016; Lavers et al., 2011; D. A. Lavers & Villarini, 2013; Paltan et al., 2017; Stohl, Forster, & Sodemann, 2008). The resulting hydrological impact of an AR is both dependent on the characteristics of the AR, such as its duration and intensity, and on the land surface physiography, for example, the bedrock type and terrain (Cao, Mehran, Ralph, & Lettenmaier, 2019; Hecht & Cordeira, 2017; Neiman, Schick, Ralph, Hughes, & Wick, 2011; Ralph, Neiman, Kingsmill, Persson, & White, 2003; Ralph et al., 2019).

In the UK, ARs are an important cause of floods, with some catchments having up to 80% of their largest winter floods associated with AR events (Lavers et al., 2011; Lavers, Villarini, Allan, Wood & Wade, 2012). In western Wales, however, two nearby catchments appear to respond very differently to landfalling ARs. These catchments, the Dyfi and the Teifi, are less than 70 km apart, but over the period 1979–2010 in a study of nine catchments along the west coast of Britain (Lavers et al., 2012), they demonstrated the strongest and weakest relationships between landfalling ARs and flood occurrence, respectively. Given the synoptic scale of ARs and their estimated widths of around 500–800 km, which means an AR would most likely affect both catchments, the aim of this study is to understand why these two catchments demonstrate such different hydrological responses to what may be expected a priori to be similar meteorological conditions.

Newly available high-resolution atmospheric reanalysis (ERA5; Hersbach et al., 2020) and 15-minute flow measurements are used to probe in finer detail than ever before the relationship between landfalling AR events and extreme flood events. There is particular interest in identifying the properties of AR events that may act as pointers towards impact potential. At this high atmospheric resolution, it will likely be possible to detect the evolution of the AR across the lifetime of the event, pinpointing to a greater accuracy the strength, orientation and location of the

landfalling AR water vapour flux. In addition, an increase in hydrological resolution will allow a more precise estimate of the timing and magnitude of flood response.

4.2.3. Study Areas and Data

4.2.3.1. Dyfi And Teifi Catchments

The Dyfi and Teifi catchments (Fig. 4.1) are predominantly rural catchments in western Wales. The River Dyfi (catchment area 471 km², average annual rainfall 1834 mm) flows for nearly 50 km through moorland and forestry to its mouth at the Dyfi estuary. The River Teifi (catchment area 890 km², average annual rainfall 1382 mm) flows just over 110 km from a small lake in the upland regions, through moorland to the basin of Cors Caron. From there, it flows through lowland agricultural land until its mouth at Cardigan Bay.

Both catchments have impermeable Silurian period formations predominantly, though the Teifi also includes deposits from the Ordovician. This geology, in combination with the altitude ranges found at both catchments, means that the basins are expected to respond quickly to any input rainfall. Differences to note are that the Teifi covers an area nearly twice that of the Dyfi and possesses a more elongated basin shape. The average slopes at the Teifi catchments of 10% are also somewhat shallower than the Dyfi which has a mean slope gradient of approximately 30%. Due to the location of the catchments in the uplands of the western UK, the catchments are expected to have consistently high soil moisture across the winter period (e.g. Lavers et al., 2010).

4.2.3.2. Flood Selection at the Dyfi and Teifi Catchments

Flows were calculated from 15-minute stage data at the Dyfi Bridge and Glan Teifi gauging stations (National River Flow Archive) from 1982–2014. Flood events were extracted via a Peaks-Over-Threshold (POT) analysis for the winter half-year (October–March) for POT3 flood events (on average three floods each year). Summer floods were excluded because they are not normally driven by ARs (Champion, Allan & Lavers, 2015) and they are generally smaller in magnitude. Following Lavers et al. (2012), a seven-day separation was applied to ensure independence of the flood events.

In addition to the flow data, precipitation data at a 15-minute resolution were obtained for three gauging stations in the Dyfi and four stations in the Teifi (Fig. 4.1) to help explore the effect of AR orientation and intensity on the catchment rainfall. Two stations in the near vicinity of the Dyfi and a single station nearby the Teifi were also considered. Rainfall estimates were combined according to Thiessen polygons to obtain a measure of basin-averaged AR event total rainfall.

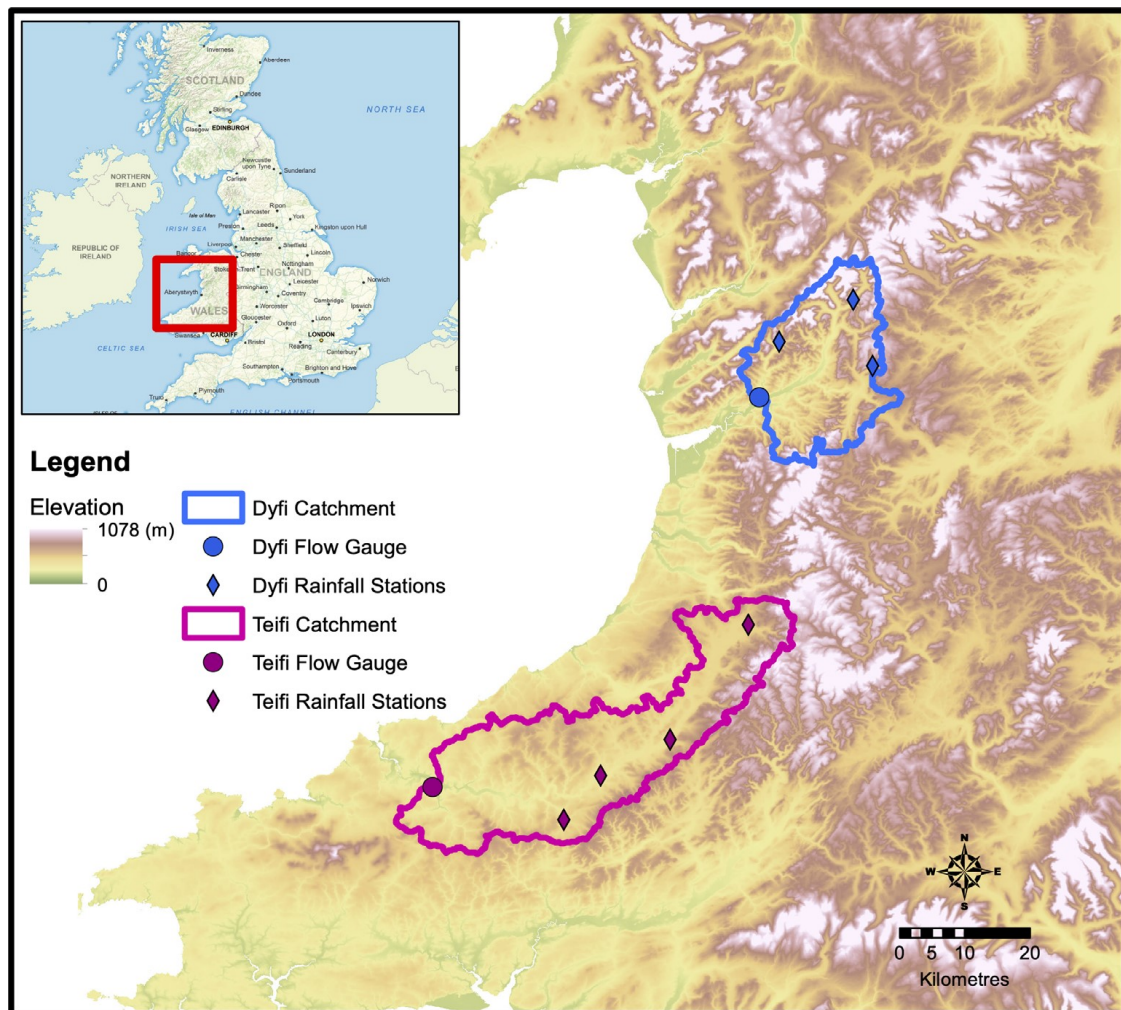


Figure 4.1 The location of the Dyfi and Teifi catchments in Wales. The locations of the flow gauges and precipitation stations are highlighted by the circle and diamond markers respectively. Elevations are from the Institute of Hydrology Digital Terrain Model (IHDTM, Morris & Flavin, 1990, 1994).

4.2.3.3. AR Detection Method

Persistent AR events across the winters of 1982–2014 were extracted from the ERA5 reanalysis (Hersbach et al., 2020) at hourly timesteps. ERA5 has a spatial resolution of approximately 0.28 x

0.28 degrees, around a third finer than datasets used in previous analyses (Lavers et al., 2012). The eastward and northward components of the water vapour flux were retrieved across the UK and combined to calculate the vertically integrated horizontal water vapour transport (hereon Integrated Vapour Transport; IVT), and its associated orientation.

Following the steps described by Lavers et al. (2012), at each timestep, the maximum value of IVT along the British coastline (taken as approximately 4°W) was extracted and tested against a threshold of 500 kg m⁻¹ s⁻¹. If exceeded, a similar procedure was carried out at the adjacent grid cells in an attempt to trace the IVT plume back across the Atlantic. An AR was identified if the plume could be traced continuously over a distance of more than 20° longitude and for at least 18 hours.

Across the 1982–2014 time period, a total of 107¹⁰ persistent winter ARs were detected (an average of 3–4 ARs per winter). The discrepancy between the frequency of AR events found herein and in Lavers et al. (2012), where an average frequency of 8–10 events per winter was detected, has arisen as a result of the increased ability to detect atmospheric variability in the hourly ERA5 data. For example, temporary drops in IVT along the axis of the AR (Ralph, Neiman, Kiladis, Weickmann & Reynolds, 2011) across the lifetime of the ARs, possibly due to secondary frontal waves, may have led to a reduced number of ARs being identified. For each AR event, the average IVT magnitude and orientation values were extracted from the ERA5 grid squares containing the location of gauging stations at the Dyfi and Teifi catchments.

4.2.4. Results and Discussion

4.2.4.1. *Atmospheric Rivers and POT3 Flood Events*

A POT flood was said to be associated with an AR event if the flood occurred within the three days immediately following AR arrival. For the POT3 floods at the Dyfi, 34 out of a possible 96 floods could be linked to ARs. For the Teifi, only 13 of 96 floods could be attributed to ARs. Of the POT3 floods that occurred at both the Dyfi and the Teifi, only 11 were found to be associated with the same AR. It is evident therefore, that the majority of AR events do not affect the catchments in the same way (Table 5.1).

¹⁰ Within 4.5° of the Dyfi and Teifi catchments i.e., passing overhead.

	Dyfi Catchment		Teifi Catchment	
	AR	No AR	AR	No AR
POT3 Flood	34	62	13	83
No POT3 Flood	73	N/A	94	N/A

Table 4.1. Matrix of AR Occurrence. At the Dyfi catchment, 34 out of the 107 ARs passing overhead result in a POT3 flood. At the Teifi catchment this value falls to 13 out of 107. As such, it is clear that the majority of ARs do not affect catchments in the same way.

The Dyfi Catchment

The distributions of POT3 and non-POT3 AR samples in terms of their landfalling properties are shown in Fig. 4.2 for the Dyfi catchment. Two statistical tests were employed to assess the mean and spread of the two samples; these are the T-Test and Levene Test, respectively. The T-Test is used to test the null hypothesis that the two samples have equal means and the Levene test is used to test the null hypothesis that the two samples have equal variances. A significant p-value (of less than 0.05) allows us to reject the null hypothesis.

In addition, a two-sample Kolmogorov-Smirnov (KS) Test was used to test the null hypothesis that the two samples are drawn from the same (continuous) distribution. The KS test is non parametric and therefore makes no assumptions regarding the distributions of our samples, however an apparent weakness lies within its ability to detect differences when the samples differ in the extreme values (distribution tails).

In terms of IVT orientation (panel a), the boxplots suggest that the non-POT3 ARs demonstrate a wide range of possible orientations, from 205–310° when considering the entire sample. Conversely, the POT3 flood AR sample demonstrates a much smaller range of 220–280°. Furthermore, by only considering the central 50% of the relevant distributions (i.e., between the upper and lower quartiles), the bulk of the POT3 flood generating ARs have been found to demonstrate orientations of between 238–258° as compared to 230–268° for the non-POT3 flood generating AR sample.

Using the Levene test, significant differences are identified between the spread of the two distributions, providing statistical evidence for a preferential orientation of impactful ARs. In terms of IVT magnitude (panel b), the mean IVT for the POT3 events is $536 \text{ kg m}^{-1} \text{ s}^{-1}$ compared to $479 \text{ kg m}^{-1} \text{ s}^{-1}$ for the non-AR group. Using the T-Test, it is possible to show that these means are significantly different at the 99% significance level (p-value of 0.007). Hence, the ARs associated with POT3 floods tend to possess greater IVT magnitudes.

The KS test does not return a significant result (p value < 0.05) when looking at the distribution of AR orientations as this is likely due to the samples differing primarily in the extremes i.e. at the Dyfi there is a narrow range of orientations that generate the most significant floods. In agreement with the T and Levene Tests, the POT3 flood generating ARs are significantly different in terms of IVT magnitude than those not linked to POT3 floods (p-value 0.046).

The sensitivity of the results to different flood thresholds, in particular the POT1 sample, has been investigated. At the Dyfi, a narrower preferential range is found (248-258*) with a significant Levene Test result. However, the smaller sample sizes adversely affect the robustness of our statistical tests in general, and so we choose to focus on the POT3 sample in this study.

The combined relationship between the AR orientation and magnitude for the POT3 correlated sample and non-related POT3 events are shown in panel c of Fig. 4.2. Within the preferential orientation ranges identified above, it is possible to identify the mean IVT for the POT3 events to be $500 \text{ kg m}^{-1} \text{ s}^{-1}$ compared to $440 \text{ kg m}^{-1} \text{ s}^{-1}$ for the non-AR group (panel d), with all POT3 flood generating ARs existing above a threshold of $400 \text{ kg m}^{-1} \text{ s}^{-1}$. Using the T-Test, the means of the relevant distributions can be shown to be different at the 90% significance level (p value of 0.06), however the likelihood of these results changing through a widening of the preferential orientation range to include more AR events, should be noted.

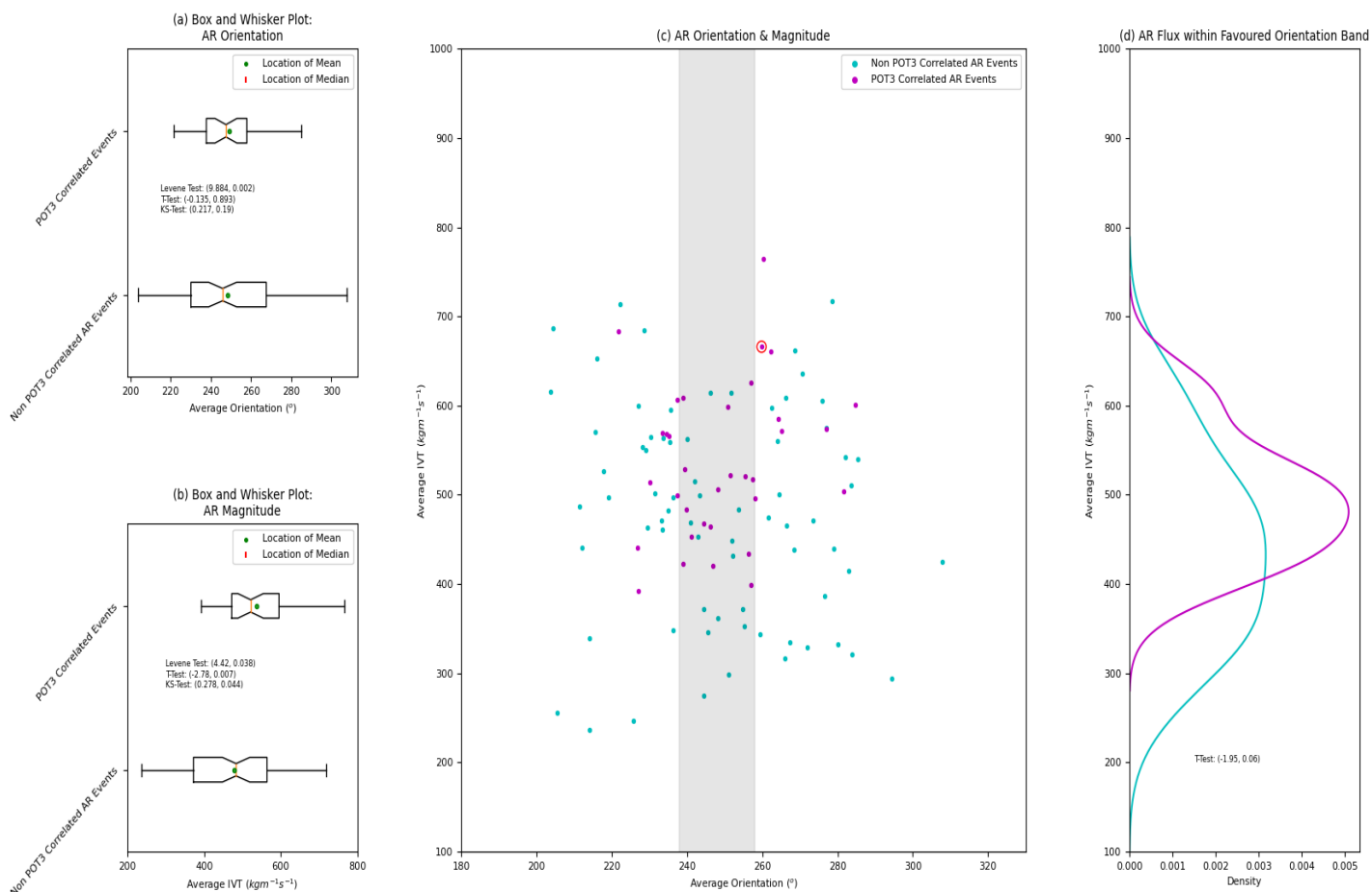


Figure 4.2 The distribution of IVT orientation (panel a) and magnitude (panel b) of POT3 correlated and non-POT3 correlated ARs at the Dyfi catchment. The relevant distributions are described in terms of box and whisker plots; the whiskers correspond to the 5th and 95th percentiles, the boxes bound the 25th and 75th percentiles, and the dot and line within the boxes represent the mean and median respectively. Statistical results in the format (test-statistic, p-value) are given in the legend of each subplot. The AR resulting in the most severe POT3 flood is highlighted by a red ring.

Panels (a) and (b) show the POT3 related ARs to exist preferentially in a subset of possible orientation and magnitude ranges. The Levene and T-Tests support the interpretation of preferential orientation and magnitude ranges for ARs that are correlated to POT3 floods. A possible weakness may exist in the KS test in terms of detecting changes in the extremes of the samples, possibly explaining the lack of significant results in terms of AR orientation. The preferential orientation band is extracted from the bounds of the box plots as 238–258°. Combining the orientation and magnitude dependencies in a simple scatter plot (panel c) and extracting the properties of the AR events to fall within the preferential orientation window (panel d), a threshold in magnitude of 400–450 kg m⁻¹ s⁻¹ for the POT3 flood generating events can be identified.

The Teifi Catchment

As for the Dyfi, at the Teifi catchment (Fig. 4.3), in terms of orientation (panel a), the boxplots referring to the non-POT3 ARs demonstrate a wide range of possible orientations, from 205–310° when considering the entire sample. The similarity to the results for the non-POT3 related ARs of

the Dyfi is in line with an expectation of the same AR events impacting the catchments across the study period (given the typical width of landfalling AR events to be on the order of 500–800 km).

Conversely, the POT3 flood AR sample demonstrates a much smaller range of 205–260°. As for the Dyfi catchment, the existence of a narrower distribution of the AR POT3 floods suggests a preferential orientation. Furthermore, by only considering the central 50 % of the distribution (i.e., between the upper and lower quartiles), it is possible to identify the central half of the POT3 flood generating ARs to exist between 224–243° as compared to 233–266° for the non-POT3 sample. The Levene Test again provides statistical evidence that the spread of the POT3 and non-POT3 AR distributions are different at the 95% significance level. Similar to the findings at the Dyfi catchment, the average IVT of the POT3 ARs is greater than that of the non-POT3 sample, 567 $\text{kg m}^{-1} \text{s}^{-1}$ compared to 515 $\text{kg m}^{-1} \text{s}^{-1}$ (panel b). The smaller sample sizes may at least partly explain the absence of a significant difference in these means; the Teifi catchment demonstrated fewer POT3 correlated ARs as compared to the Dyfi. In agreement with earlier results, the KS test suggests that the POT3 flood generating ARs are significantly different in terms of IVT orientation than those not linked to POT3 floods (p-value 0.026).

At the Teifi catchment when considering a similar analysis for the POT1 floods, an orientation range similar to that above is found, however the statistical analyses are much less robust. This is likely a result of the sample sizes (only seven ARs can be correlated to POT1 floods at the Teifi).

The combined relationship between the AR orientation and magnitude for the POT3 correlated sample and non-related POT3 events are shown in panel c of Fig.4.3. Within the preferential orientation ranges identified above, the mean IVT for the POT3 events can be identified as 567 $\text{kg m}^{-1} \text{s}^{-1}$ compared to 530 $\text{kg m}^{-1} \text{s}^{-1}$ for the non-AR group (panel d), with all POT3 flood generating ARs existing above the 450 $\text{kg m}^{-1} \text{s}^{-1}$ threshold. As compared to the Dyfi catchment, there appears to be less of a skew towards stronger magnitude IVT ARs when considering the most impactful events. This is primarily a result of small sample sizes at the Teifi catchment as a visual trend is apparent.

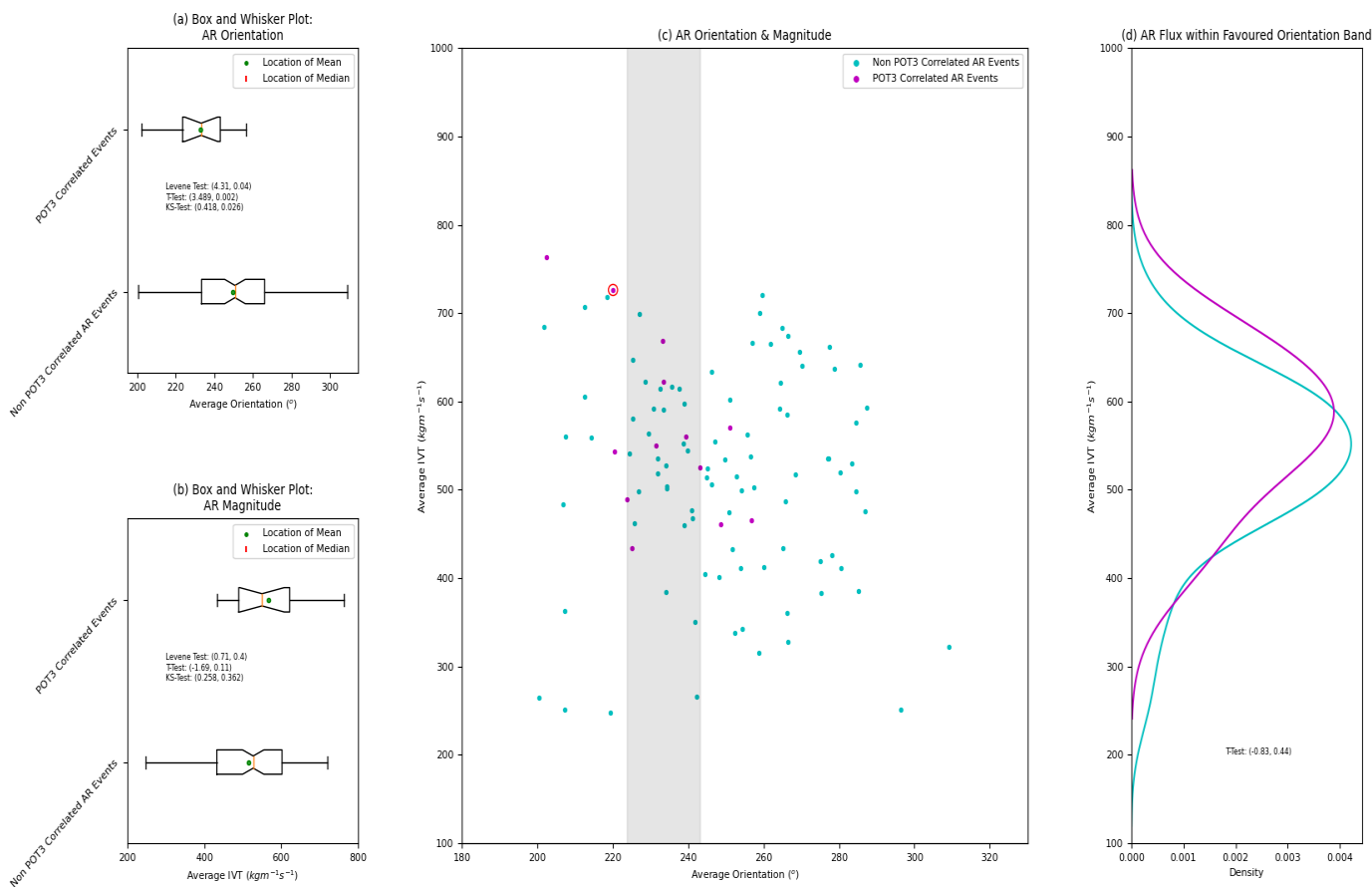


Figure 4.3 The distribution of IVT orientation (panel a) and magnitude (panel b) of POT3 correlated and non-POT3 correlated ARs at the Teifi catchment. The relevant distributions are described in terms of box and whisker plots; the whiskers correspond to the 5th and 95th percentiles, the boxes bound the 25th and 75th percentiles, and the dot and line within the boxes represent the mean and median respectively. Statistical results in the format (test-statistic, p-value) are given in the legend of each subplot. The AR resulting in the most severe POT3 flood is identified by a red ring.

Panel (a) shows the POT3 related ARs to exist preferentially in a subset of possible orientation ranges. The results of the Levene, KS and T-tests support this interpretation. A preferential orientation band of 224-243° for the POT3 flood generating ARs is identified. Although the POT3 flood generating ARs show a similar skew towards stronger IVT magnitudes, this result is less clear in the statistical tests than for the Dyfi catchment (Fig. 4.2). This could be due to the smaller sample sizes at the Teifi catchment as compared to the Dyfi. Combining the orientation and magnitude dependencies (panel c) and extracting the properties of the AR events to fall within the preferential orientation window (panel d), it is possible to identify a similar threshold in magnitude of 400-450 kg m⁻¹ s⁻¹ for the POT3 flood generating events.

4.2.4.2. Case Study Application: AR of 10th - 11th February 2002

The findings of the previous section are exemplified in a case study. Fig. 4.4 shows the evolution of overhead IVT flux component (both the total magnitude and zonal (eastward) and meridional (northward) components) and flow/precipitation observations at the Dyfi and Teifi catchments

across the month of February 2002. The incident AR (highlighted by the shaded section in Fig. 4.4) was found to demonstrate an average magnitude of $506 \text{ kg m}^{-1} \text{ s}^{-1}$ at the Dyfi catchment and $551 \text{ kg m}^{-1} \text{ s}^{-1}$ at the Teifi. The average orientation of landfalling flux was calculated as 248° at the Dyfi and 247° at the Teifi. In line with the findings of the previous section, and the presence of AR orientation as a primary control on AR impact potential, the AR results in stronger response at the Dyfi catchment as compared to the Teifi.

4.2.5. Conclusions and Future Work

This study has used high-resolution datasets to link the large-scale atmospheric conditions directly to local flood peaks. The main control on impactful ARs at these two flashy catchments in western Wales has been found to be the orientation of the incoming IVT relative to catchment topography. At the Dyfi catchment, the bulk of the POT3 flood generating ARs demonstrate average IVT flux orientations of $238\text{--}258^\circ$ across their lifetimes, whereas at the Teifi a range of $224\text{--}243^\circ$ is preferred. These results are summarised in the Fig. 4.5 schematic.

It is suggested that, at the Dyfi catchment, surrounded by the mountains of Snowdonia, ARs that follow the main river channel have the most impact potential in terms of flood generation and magnitude. This seems to be the result of “rainout” as the AR hits the higher elevation land at the head of the valley (Ralph et al., 2003). When the ARs have an IVT above $400\text{--}450 \text{ kg m}^{-1} \text{ s}^{-1}$, the largest floods (POT3 and above) can occur. In the Teifi, which is a less mountainous catchment, this effect is also apparent. This is attributed to the topographic effect of the northern edge of the catchment lowlands and/or IVT into the upland regions.

A next step is to confirm the processes and establish the strength of this effect at a national level. Several limitations and restrictions inherent to the current AR detection algorithm are likely to be filtering out legitimate ARs, as several POT3 floods at these catchments showed traces of precursor AR events. For example, the algorithm is unlikely to be currently detecting ARs with secondary frontal wave activity. It is likely therefore that some AR events are missing when dealing with high-resolution input data such as ERA5. This does not alter the result reported here, but points the way in terms of the next step for further refinement; if work can be done to increase the resilience and effectiveness of the detection algorithm and if preferential AR orientations can be calculated for a greater variety of catchments, then this offers great potential for the improved forecasting of extreme flood events (Lavers, Pappenberger & Zsoter, 2014; Ramos, Sousa, Dutra,

& Trigo, 2020). In the future, forecasts based on likely AR properties could improve the identification of damaging storms, potentially reducing impact to people and property.

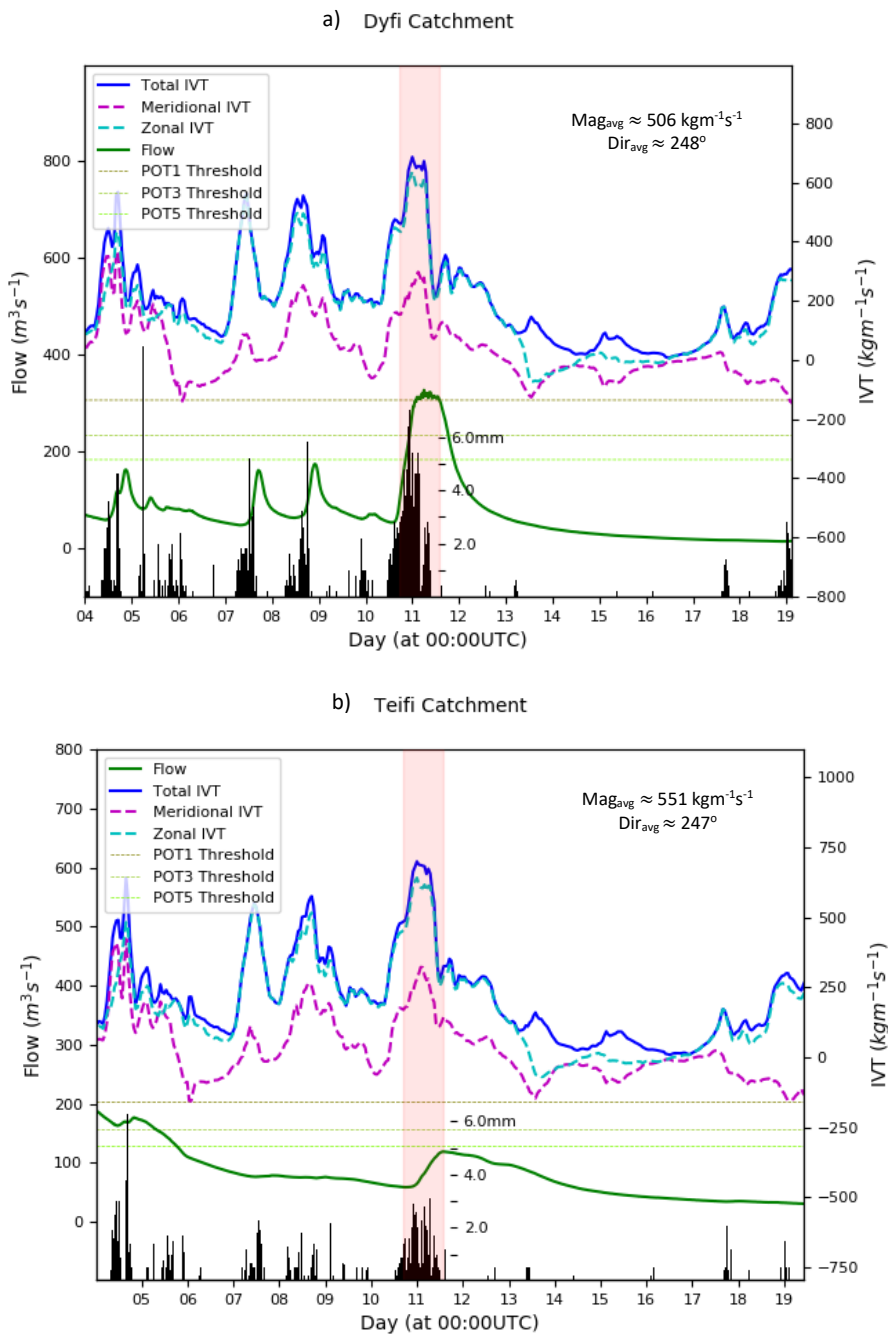


Figure 4.4. Time series analysis of landfalling IVT, rainfall and flow patterns at the Dyfi and Teifi catchments in response to an AR on the 11th of February 2002 (red shaded region).

The average magnitude and orientation properties of the AR are shown. The difference in flood responses between the catchments can be explained through the AR magnitude and orientation. The AR orientation of 247° sits outside the preferential range identified at the Teifi catchment of $224\text{--}243^\circ$ but inside that of the Dyfi ($238\text{--}258^\circ$).

A stronger impact on flow is observed at the Dyfi compared to the Teifi, despite the average IVT magnitude at the Dyfi being smaller than that at the Teifi. This suggests AR orientation is an important control on rainfall occurrence, and therefore flood response

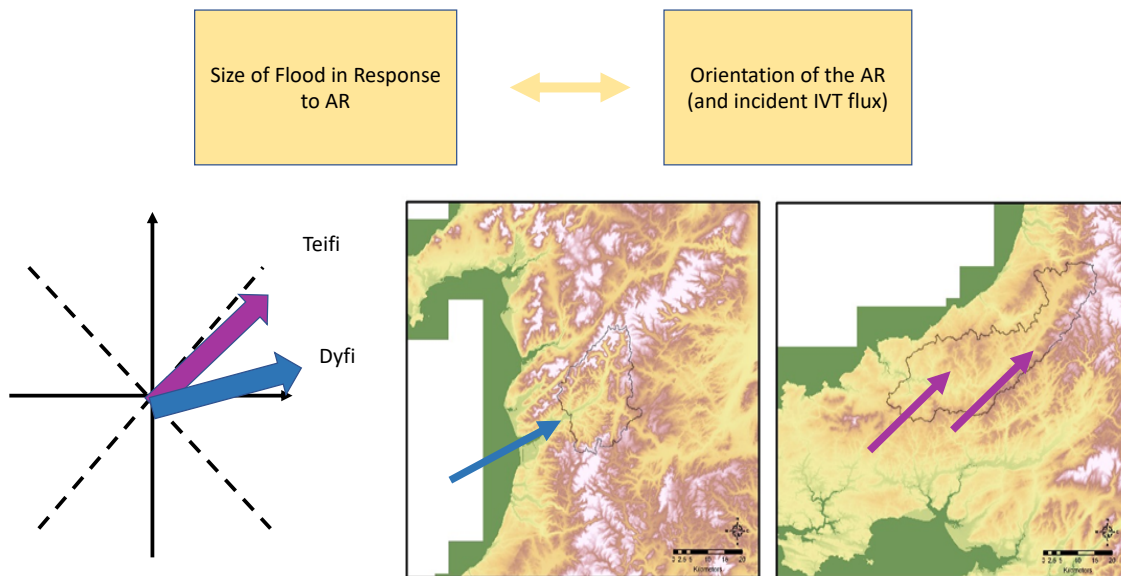


Figure 4.5. Summary schematic of the conclusions. The primary control on AR impact lies with the orientation of the landfalling flux relative to catchment slopes. Physically, this can be interpreted as the efficiency of orographic enhancement of the landfalling AR and the amount of precipitation induced. When the orientation of the AR is preferable, the extent of response lies with the amount of moisture transported towards the catchment i.e., the IVT magnitude. The ARs associated with the largest floods possess average IVT magnitudes above $400\text{-}450\text{kgm}^{-1}\text{s}^{-1}$. Elevations are from the Institute of Hydrology Digital Terrain Model (IHDTM, Morris & Flavin, 1990, 1994).

4.3. Summary

In summary, this published work has demonstrated the importance of AR orientation when considering the most impactful events. This orientation has been associated with the land surface properties of the catchments of interest, and likely relates to the rainfall generation process within the AR events themselves.

Chapter 5 – Verification of Atmospheric River Detection Method

5.1 Introduction

The aim of this chapter is to test (and ultimately improve) the performance of the Lavers et al. (2012) AR detection algorithm in the context of high resolution datasets, such as the ERA5 reanalysis, in line with concerns raised in the previous chapter (Chapter 4, section 4.2.5). In addition, the assumptions made in previous sections of this thesis, for example regarding AR width and latitudinal movement (Chapter 3, section 3.4.2), will be verified. Thus, this chapter acts to ensure that (1) all appropriate AR events across the study period are successfully extracted by the detection algorithm, and that (2) appropriate key properties of the ARs are retained for further analysis.

The structure of the chapter is outlined the schematic below (Fig. 5.1). At first, the focus will be on improving the Lavers et al. (2012) AR detection algorithm, culminating in a test of performance using the Dyfi and Teifi catchments (Section 5.2). The assumptions surrounding AR width, AR landfalling location and the typical variation of properties, namely AR strength and/or orientation, across AR lifetime will then sequentially be tested (Section 5.3). Finally, the evolution of the properties of the AR will be inspected as it propagates inland. In combination, these ideas will go some way towards determining a typical ‘region of influence’ of the AR.

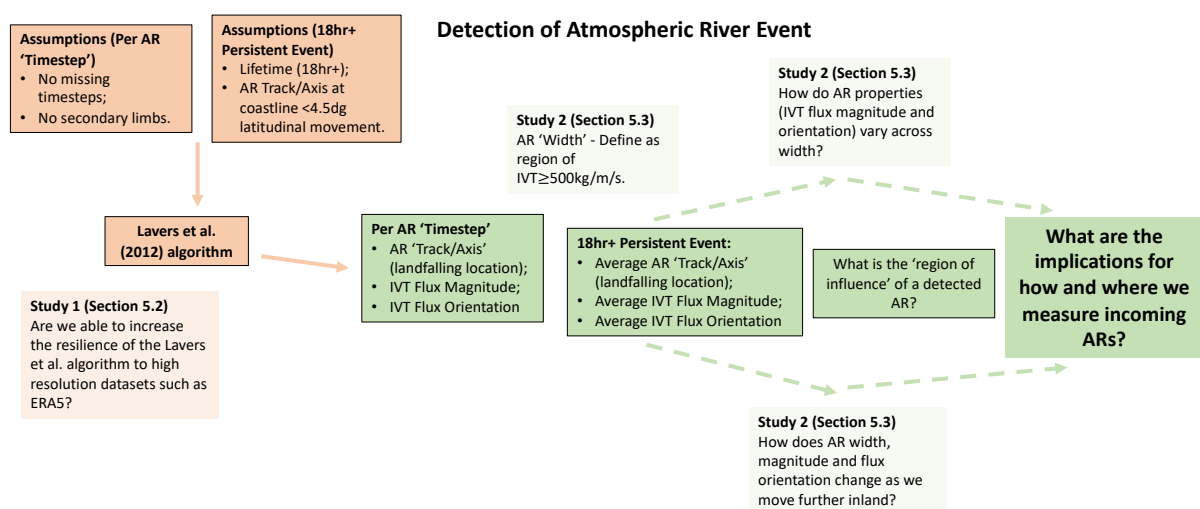


Figure 5.1. Chapter Summary. This schematic provides an outline the structure of the analysis. First, the resilience and robustness of the Lavers et al. (2012) algorithm will be increased, particularly in the context of high spatial and temporal resolution datasets. The assumptions and thresholds used to determine AR impact potential are then tested to calculate the typical ‘region of influence’ of a landfalling AR.

5.2. Improving the Detection Algorithm

5.2.1. Rationale

It was hypothesised in Chapter 4, that the relatively weak AR-POT3 flood associations noted at the Dyfi and Teifi catchments, as compared to those reported by Lavers et al. (2012), may arise from the higher resolution reanalysis input dataset (ERA5 is hourly, as compared to ERA-Interim's six-hourly timestamps). The justification for such a hypothesis is supported by several examples given below.

- 1) **Resolution:** One definition of a persistent AR is one that can be detected for 18 hours or more (Lavers et al., 2012). Given the temporal resolution of ERA5 as compared to ERA-Interim, this equates to an AR track being detected at 18 consecutive timestamps, as compared to just three. If any one of these 18 timestamps returns a negative detection, then the entire feature is removed.

Further, the spatial resolution of ERA5 is more than twice that of ERA-Interim. Thus, rather than the AR track at a given timestamp consisting of around 30 adjacent grid points, for ERA5 it is closer to 80. The spatial and temporal requirements applied by the detection algorithm are therefore far more stringent when using high-resolution input data.

- 2) **Mesoscale Frontal Waves and Secondary Limbs:** Mesoscale Frontal Waves (Neiman et al., 2016; Ralph et al., 2011; Fig. 5.2) can result in a stalling, or quickening, of AR conditions overhead relative to the overall propagation speed. The landfalling region can therefore experience ebbs and flows in the delivered atmospheric moisture (IVT) over the lifetime of an AR. The ebbs of IVT flux may result in a non-detection by the AR algorithm.

Secondary limbs, defined as plumes of IVT existing separate to the main AR axis (Fig. 5.2), may act to push the algorithm 'off-course' and away from the main IVT track. As a result, insufficient spatial geometry may also result in a missed AR detection.

- 3) **AR Duration:** In addition to algorithm performance at a single timestamp, it is likely that ARs of durations below 18 hours may still have the power to be impactful, especially in steep, flashy catchments or when arriving on the back of wet conditions.

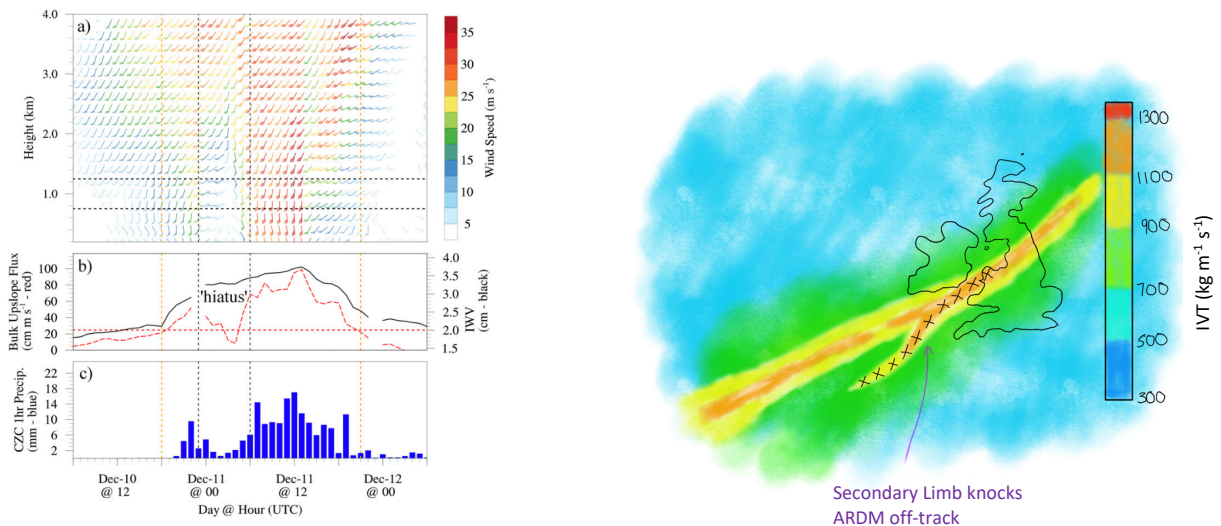


Figure 5.2. Mesoscale Frontal Waves and Secondary Limbs. The left-hand panel is taken from Martin et al. (2019) and shows the overhead flux evolution of an extreme AR that made landfall in northern California during December 2014. The measurements were taken using a nearby Atmospheric River Observatory (ARO), and it is possible to identify the temporary drop in IVT flux associated with a mesoscale frontal wave. From the measurements, it is estimated that MFWs are of durations around three hours. The right-hand panel shows a schematic of a secondary AR limb occurring alongside a main AR track. The high resolution of the ERA5 input reanalysis increases the susceptibility of the chosen AR detection algorithm to be thrown off track.

5.2.2. Algorithm Modifications

The Lavers et al. (2012) algorithm has been updated and refined in line with the possible issues presented above. A description of the modifications are discussed below.

- **Mesoscale Frontal Waves and/or Missing Timesteps:** A tolerance to several missing timesteps within a given AR event is developed within the ARDM. Using the typical MFW duration to be on the order of three hours (Martin et al., 2019; Ralph et al., 2011b), it is suggested that up to three consecutive timesteps can be missing within a chain of AR detections before the entire feature is removed (Fig. 5.3). This is also expected to include other sources of missing timesteps, for example, small-scale atmospheric variability.

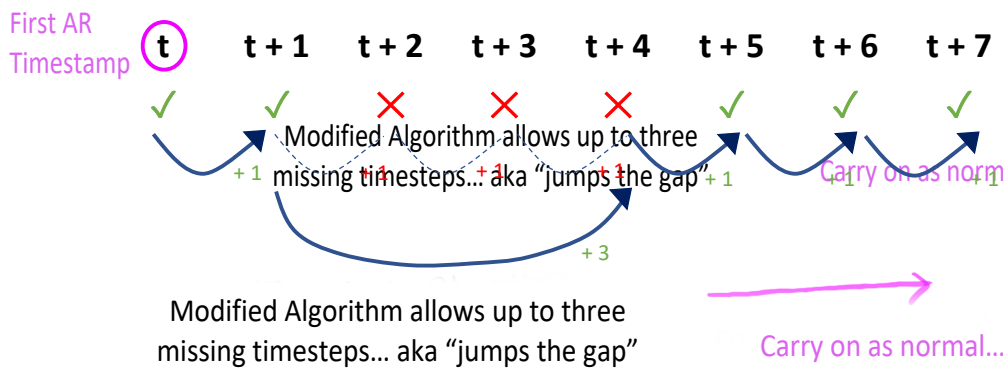


Figure 5.3. Missing Timestep Modifications. The modified algorithm permits the absence of up to three consecutive timesteps within a chain of AR timesteps. This is in line with expected MFW duration and is expected to be sufficient for other sources of atmospheric variability.

- Secondary Limbs: ARs are large scale features and, despite the extra information gained from the higher resolution reanalysis, it is likely that such information is not essential for their detection alone. As such the algorithm is modified to detect every ‘third’ grid cell (as opposed to adjacent cells), as outlined in Fig. 5.4. This equates to around 26 ‘adjacent’ grid cells (totalling 20 longitudinal degrees). The high-resolution dataset is retained however for later analysis of the detected ARs.

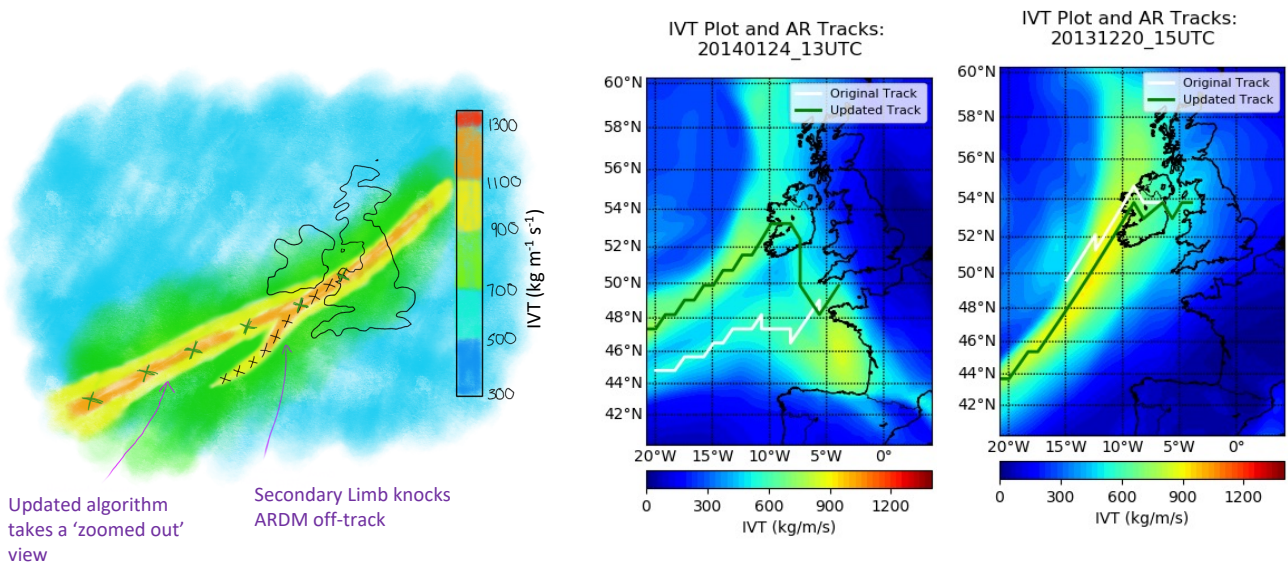


Figure 5.4. Secondary Limb Modifications. In line with the earlier analysis of Lavers et al. (2012), the detection algorithm is modified to search every ‘third’ grid cell, i.e., it takes a ‘zoomed out’ view of the AR and is less likely to be caught out by small scale variation.

- **AR Duration:** The required temporal threshold for retained AR events is sequentially relaxed, from 18 hours in three-hourly intervals down to nine hours. As such, a total of four AR catalogues are generated, corresponding to ARs of duration 9+hrs, 12+hrs, 15+hrs and 18+hrs respectively. Fig. 5.5 shows the number of reported ARs in each of the catalogues over the study period. Table 5.1 shows the number of matching ARs within each catalogue.

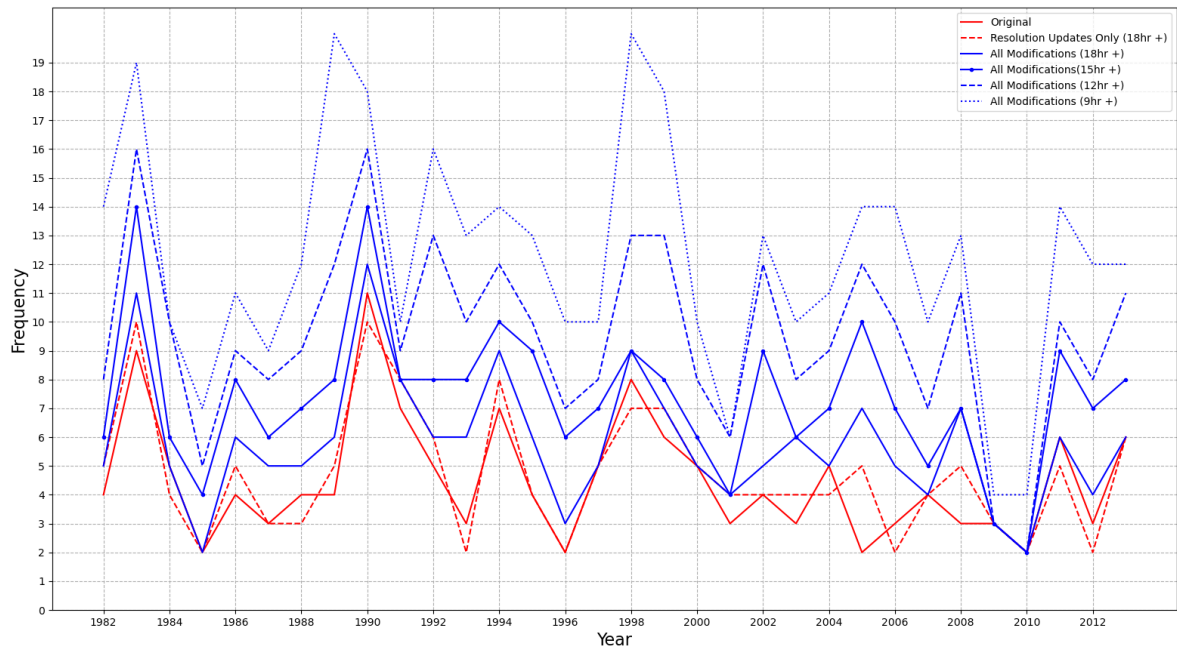


Figure 5.5. Updated AR Catalogues. As the modifications are applied to the AR detection algorithm, and the temporal threshold is relaxed, a greater number of AR events over the study period (1982-2014) are detected.

		Comparison of ARs as detected within the ERA5 reanalysis (1982-2014)					
		Lavers et al. (2012)	Resolution Updates Only (Duration 18hr+)	All Modifications (Duration 18hr+)	As previous (Duration 15hr+)	As previous (Duration 12hr+)	As previous (Duration 9hr+)
Lavers et al. (2012)	151		137	142	151	151	151
Resolution Updates Only (Duration 18hr+)	158			158	158	158	158
All Modifications (Duration 18hr+)	192				192	192	192
As previous (Duration 15hr+)	243					243	243
As previous (Duration 12hr+)	312						312
As previous (Duration 9hr+)	399						

Table 5.1. Matching Events Within the Modified Algorithms. The second column gives the total number of ARs as detected by each algorithm over the 1982-2014 period, with the contingency table presenting the number of matching events.

5.2.3. Application to the Dyfi and Teifi catchments

In order to test whether the algorithm modifications have made any improvement in terms of AR detection, the number of POT3 floods within the Dyfi and Teifi catchments that can be explained by the ARs in the updated catalogues are analysed. The results are then compared to those within previous analyses (Chapter 4) and to those reported by Lavers et al. (2012).

It is clear that the modifications have increased the ability of the algorithm to detect impactful ARs (Table 5.2). Keeping the temporal threshold at 18+ hours, and comparing the results to those presented in Chapter 5, the modified algorithm can account for an increase of six AR associated floods at the Dyfi catchment and one at the Teifi. As the temporal requirements are relaxed from 18+ hours down to 9+ hours, a further 26 POT3 floods can be associated ARs at the Dyfi catchment. This equates to a total of 63% of POT3 floods associated with persistent ARs of duration nine hours or above (up from 35% in Chapter 4). At the Teifi catchment, and as the temporal threshold is relaxed, a further 21 POT3 floods can be associated with ARs. This totals as 35% of POT3 floods at the Teifi associated with persistent ARs of duration nine hours or above (up from 14% in Chapter 4). These updated figures are similar to those presented in Lavers et al. (2012) for historical POT1 floods.

DYFI CATCHMENT (POT3 FLOODS)					
AR Start Date < 3 days pre-flood	Lavers Original	Mod (18hrs+)	Mod (15hrs+)	Mod (12hrs+)	Mod (9hrs+)
	34/96 35%	40/96 41%	43/96 45%	53/96 55%	60/96 63%
	TEIFI CATCHMENT (POT3 FLOODS)				
AR Start Date < 3 days pre-flood	Lavers Original	Mod (18hrs+)	Mod (15hrs+)	Mod (12hrs+)	Mod (9hrs+)
	13/96 14%	14/96 15%	17/96 18%	25/96 26%	34/96 35%

Table 5.2. AR-Flood Correlations according to the Modified Algorithm. A modified algorithm, and a relaxation of the temporal threshold, allows for detection of a greater number of impactful ARs. With a temporal threshold of 9+ hrs, it is possible to associate 63% of POT3 floods at the Dyfi with ARs, and 35% of floods at the Teifi.

To test whether the preferential orientations and/or IVT thresholds as identified in Chapter 4 for impactful ARs remain valid, a distribution analysis for the ARs correlated to POT3 floods (and otherwise) within each of the AR catalogues is carried out. The results for the nine hours or above duration ARs are given in Fig. 5.6, with the upper and lower plots referring to the results of the Dyfi and Teifi catchments respectively.

Originally presented in Chapter 4, the distribution of the properties of ARs associated with POT3 floods, and otherwise, are described in terms of box and whisker plots (Fig. 5.6); the whiskers correspond to the 5th and 95th percentiles, the boxes bound the 25th and 75th percentiles, and the dot and line within the boxes represent the mean and median respectively of the relevant distribution. Statistical results in the format (test-statistic, p-value) are given in the legend of each subplot. The orientation (if applicable) and magnitude dependencies are combined in a simple scatter plot (panel c) and the properties of the AR events to fall within the preferential orientation window extracted (panel d).

At the Dyfi Catchment, a preferential orientation of the most impactful ARs is identified. At 239° to 263°, the lower limit of the range agrees with the results presented in Chapter 4 (238-258°), however the upper limit is slightly wider. When the modified algorithm is applied with a temporal threshold of 18+hrs (Table 5.2), a similar preferential range is extracted. This suggests that the additional ARs detected by the modified algorithm, and associated with POT3 floods, are at the upper end of the original preferential orientation range.

At the Teifi Catchment, the preferential orientation band for impactful ARs is identified as 222° to 246°. This is similar to that identified in Chapter 4 (224-243°), however the (statistical) evidence for the presence of this band is weaker within the modified catalogues (Table 5.2). That is, the additional (low duration) flood-forming ARs identified do not show sufficient evidence for a preferential orientation.

However, there is evidence for those ARs associated with floods at the Teifi to be systematically stronger. Perhaps it is possible to suggest therefore, that the Teifi catchment is ‘flux dominated’ when considering AR impacts, as opposed to ‘orientation dominated’ at the Dyfi. In addition, it is likely that low-duration ARs are the most impactful at the Teifi when arriving to wet antecedent conditions (given existing knowledge of the relative sizes of the two catchments and

their run-off processes) and therefore deducing impacts on the basis of AR properties alone, is likely to be more complex.

For both the Dyfi and Teifi catchments, IVT magnitudes of around $450 \text{ kg m}^{-1} \text{ s}^{-1}$ and above are identified for the most impactful ARs. At the Dyfi this IVT threshold must be met, in addition to the orientation requirements, if an AR is to be particularly impactful. Conversely at the Teifi catchment, the IVT strength is the dominating factor, and for an AR to pose a threat it must simply have an average IVT magnitude of above $450 \text{ kg m}^{-1} \text{ s}^{-1}$. A summary of distribution results according to each of the AR catalogues is given in Table 5.3.

Dyfi Catchment					
	Original	18+ hrs	15+ hrs	12+ hrs	9+ hrs
Preferential Orientation Band?	(238, 258)	(238, 263)	(238, 263)	(239, 264)	(239, 263)
IVT Threshold?	448	453	447	454	447
Teifi Catchment					
	Original	18+ hrs	15+ hrs	12+ hrs	9+ hrs
Preferential Orientation Band?	(222, 246)	(233, 245)	N/A	N/A	N/A
IVT Threshold?	546	468	475	434	422

Table 5.3. Distribution Results according to each AR catalogue. In terms of preferential orientation ranges, very similar results are found within each of the AR catalogues when considering impactful ARs at the Dyfi catchment. The IVT threshold of impactful ARs is calculated as consistently around $450 \text{ kg m}^{-1} \text{ s}^{-1}$ (in line with the results as presented in Chapter 4). There is little to no statistical evidence for preferential orientation bands when considering (short duration) impactful ARs at the Teifi catchment within the modified catalogues, however the impactful ARs do show evidence of being systematically stronger. This IVT threshold is calculated as slightly higher than that of the Dyfi.

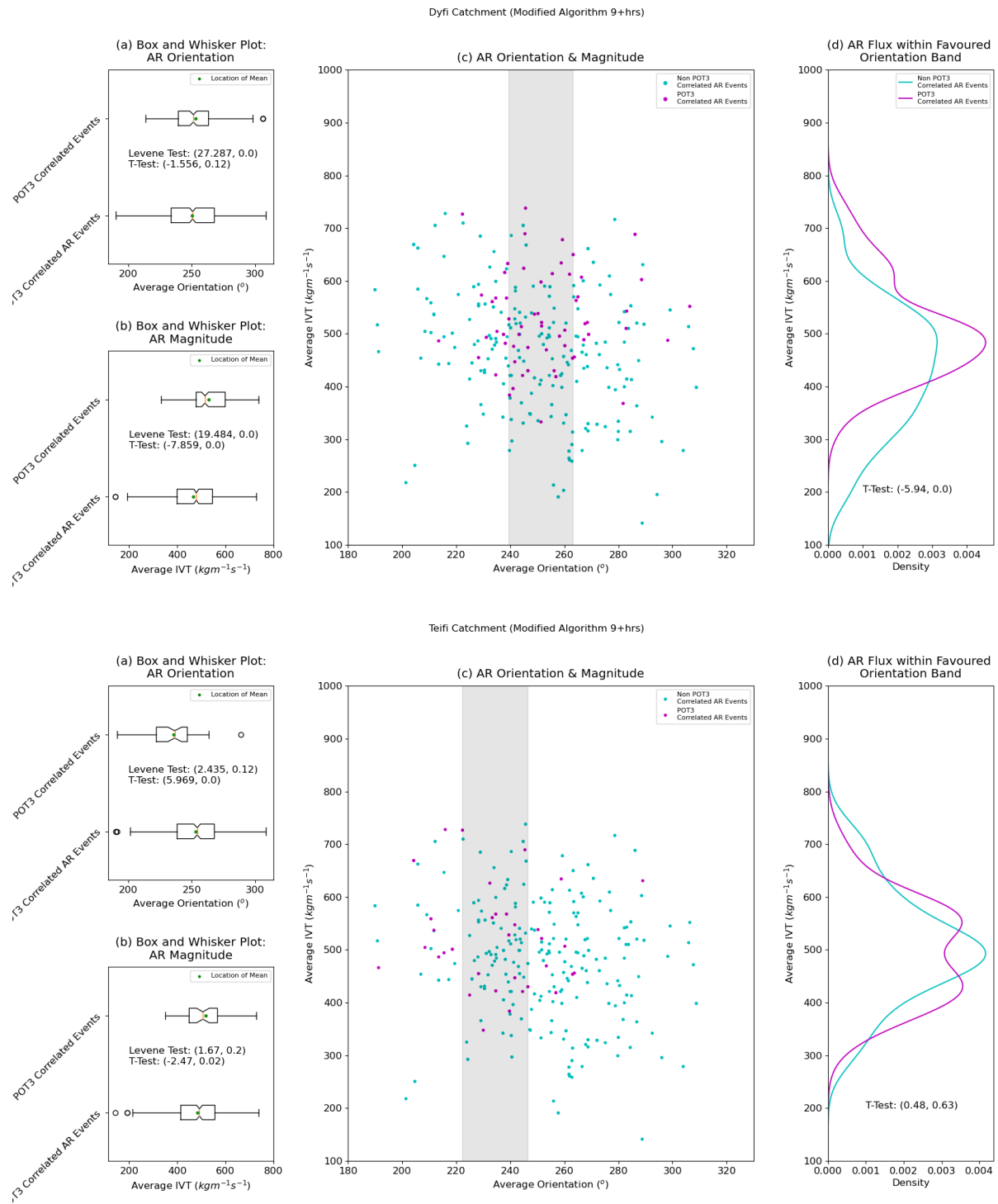


Figure 5.6. Distribution Results according to the Modified Algorithm. The distribution of IVT orientation (panel a) and magnitude (panel b) of POT3 correlated and non-POT3 correlated ARs at the Dyfi and Teifi catchments are given in the upper and lower plots respectively. The relevant distributions are described in terms of a box and whisker visualisation; the whiskers correspond to the 5th and 95th percentiles of the relevant distribution, the boxes bound the 25th and 75th percentiles, and the dot and line within the boxes represent the mean and median respectively. Statistical results in the format (test-statistic, p-value) are given in the legend of each subplot. The orientation (if applicable) and magnitude dependencies are combined in a simple scatter plot (panel c) and the properties of the AR events to fall within the preferential orientation window extracted (panel d). The results according to the modified algorithm and a temporal threshold of 9+ hours are compared to the original results of Chapter 4. At the Dyfi catchment, the updated results are found to align with those of Chapter 4; a preferential orientation of impactful ARs can be identified. At the Teifi catchment however, the identification of a preferential band weakens, and overall AR strength appears to dominate the likelihood of a POT3 flood response.

5.3. AR Properties According to the Modified Algorithm

5.3.1. Rationale

Previous work (Chapter 4, Lavers et al., 2012) has made several assumptions regarding AR structure and behaviour in order to effectively process a large number of events. This section intends to verify whether these assumptions are accurate.

ARs have been estimated as typically 1000km in width (Neiman et al., 2008) and thus a 4.5° latitudinal movement window was applied by Lavers et al. (2012) when deducing persistent events - 4.5° is approximately equal to 500km, and thus even if the central axis of the AR moves by 4.5° or less, AR conditions may still be observed above a given location. This section will use the modified AR detection algorithm developed to analyse the typical width of persistent ARs across the UK, thus verifying that the 4.5° movement window is appropriate moving forward. In addition, the evolution of the measured width as a function of AR lifetime will be investigated, in addition to inspecting the relationship between AR width and transported water vapour. Are the most impactful ARs of relatively larger width, or vice versa?

The AR detection algorithm (section 5.2.2) returns an estimate of the AR axis; a path of maximum IVT flux. From this axis, the landfalling location of the AR is calculated, averaged across the lifetime of the event. This section intends to verify the accuracy of this estimate through a quantification of the extent that an AR axis moves across its lifetime. Is it possible to relate this movement to other properties of the AR, e.g., its strength, overall width etc. In addition, what is the typical distribution of the ARs, in terms of their landfalling location? Are some regions of the UK more 'prone' to the presence of an AR than others?

Finally, the distribution of AR properties across the width of the AR will be analysed. Cross sections will be extracted both as the AR makes landfall and as it propagates inland. A picture of how the moisture flux is distributed around the AR axis will be developed, alongside understanding how this distribution may change over the lifetime of the event. These questions in combination, will ultimately help in extracting the most meaningful information from landfalling ARs and deducing the regions affected.

5.3.2. Data Extraction

The workings of the (updated) AR detection algorithm is detailed earlier sections of this work (sections 3.3.2 & 5.2.2), but a summary will be provided here for completeness. At each timestamp, the algorithm searches between 50 and 60°N at approximately 4°W for the maximum IVT value. If this value is above $500 \text{ kg m}^{-1} \text{ s}^{-1}$ then it sequentially tracks back the AR axis via every-third grid cells until it spans 20° in longitude. For the event to be labelled as persistent, the AR axis must be identified in a minimum number of sequential timestamps. The algorithm will allow up to three missing timestamps, so long as there is evidence for the AR axis either side of the missing region (this is in line with Mesoscale Frontal Waves and other phenomenon, as described in the previous section of the chapter). The temporal threshold applied in this analysis has been taken as nine hours, equating to a total of nine sequential timestamps.

A typical AR can be identified in the ERA5 reanalysis (Fig. 5.7). The AR axis, as defined by the detection algorithm, is highlighted via the white trace. The landfalling location of the AR is taken according to first point of the axis track; identified in Fig. 5.7 as the dark shaded grid square. The average landfalling location of an AR, and hence the point from where the 4.5° assumption is applied, is calculated via averaging the landfalling locations across the individual timestamps.

In order to calculate the AR width, it is necessary to decide a value of IVT whereupon AR conditions are no longer met. A natural such limit, taken from the AR detection algorithm, is $500 \text{ kg m}^{-1} \text{ s}^{-1}$. However, evidence exists for AR impacts to be observed when the overhead IVT flux is below this, for example along the US West Coast the AR threshold is often taken as $250 \text{ kg m}^{-1} \text{ s}^{-1}$ (Gershunov et al., 2017).

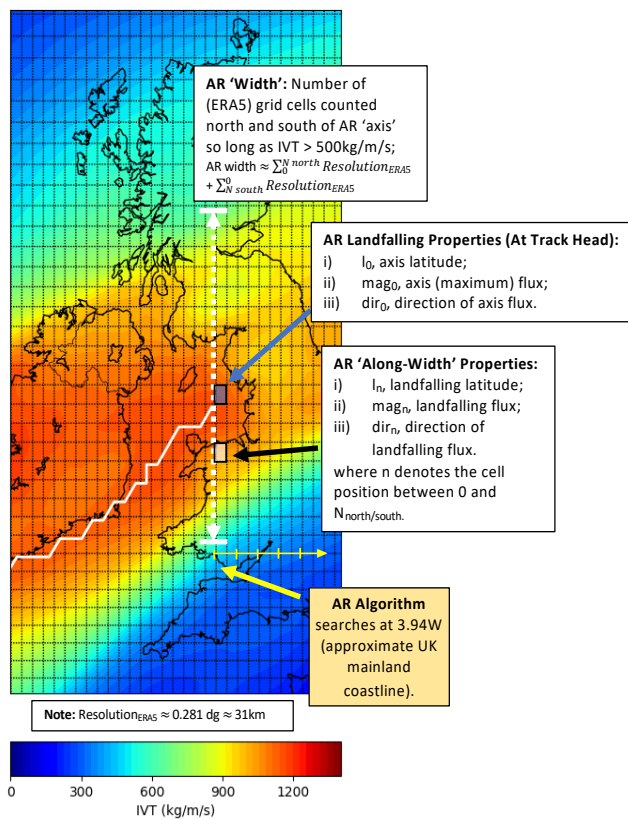
As such, this chapter will investigate the results according to both thresholds, summing the total number of grid squares north and south of the AR axis where the IVT threshold is met to obtain estimates AR width (see the white shaded squares in Fig. 5.7). In order to build up a cross sectional view of IVT magnitude and orientation across the width of the AR, the relevant properties will be extracted from each grid square during this process.

It should be noted that the resulting 'width' is in fact the width along the vertical axis, and not the actual width. For simplicity, the term width shall continue to be used. In addition, the

‘threshold’ or ‘limit’ used to determine the AR width should be noted as independent to that used in the mechanics of the ARs detection algorithm.

In addition to calculating the AR widths at their landfalling (coastal) locations, the process is sequentially repeated through application of the AR detection algorithm at increasingly inland locations (Fig. 5.7), namely moving eastward from approximately 4°W to 4°E. This will allow analysis of the evolution of AR properties as the feature moves across the UK.

British Coastline (approx. 4W)



Moving Inland...

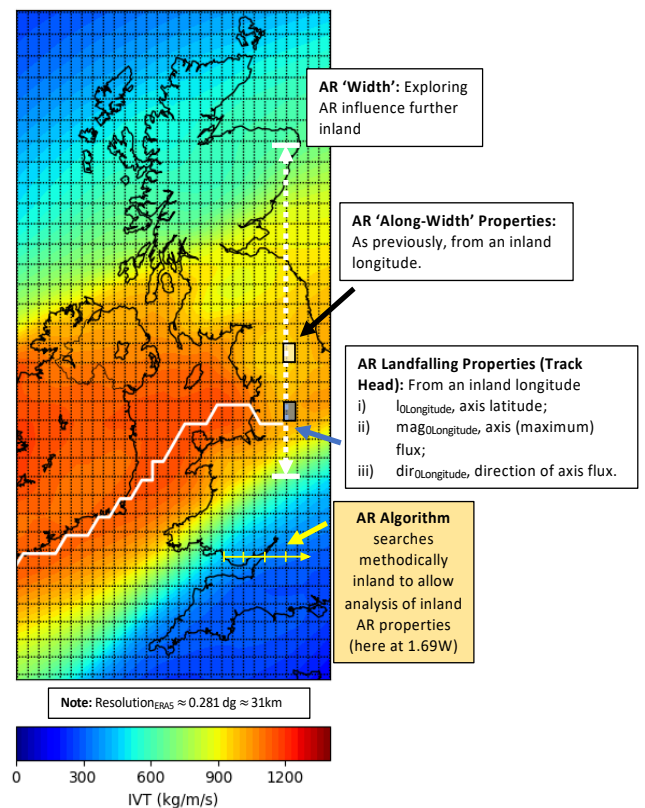


Figure 5.7. Atmospheric River Variability. A schematic to describe the process of extracting AR width and IVT magnitude and orientation properties. The left-hand plot shows this process for coastal ARs (where the algorithm searches at 4°W) with the right-hand plot describing the process for inland propagating ARs.

5.3.3. AR Axis

When considering the average landfalling location of the ARs within the chosen catalogue (Fig. 5.8a), the presence of a slightly southerly bias can be observed. That is, ARs are more frequently detected at the ‘southern’ end of the UK. Within each of these AR events, the average movement of the axis across their lifetime is just over 100km (Fig. 5.8b). The typical values of

moisture flux transmitted along the AR axes are strongly correlated to the landfalling location of the AR (Fig. 5.8c); that is, the more southerly ARs are associated with stronger IVT values at their centreline. This observation may explain the increase in AR detections at the southern latitudes.

5.3.4. AR Width

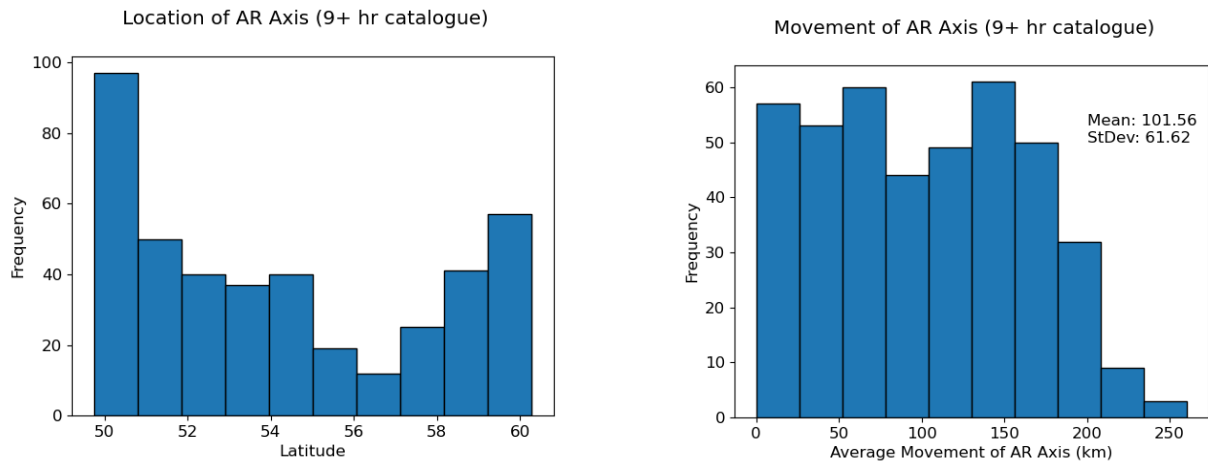
5.3.4.1. Importance of Threshold Selection

The calculated widths for the ARs in the chosen catalogue are strongly dependent on the IVT threshold applied (Fig. 5.9, panels a and c). Using the $500 \text{ kg m}^{-1} \text{ s}^{-1}$ threshold, an average width of 539 km is obtained, with a standard deviation across the sample of 232 km (equivalent to around 40% of the mean). For a threshold of $1000 \text{ kg m}^{-1} \text{ s}^{-1}$, an average value of 1291 km is calculated, with a standard deviation across the sample of 341 km (closer to 26% of the mean value).

Considering the variability in the calculated AR width across the lifetime of each individual event (Fig. 5.9, panels b and d), it is found that the average change in AR width is around 170 km and 190 km when calculated according to the $500 \text{ kg m}^{-1} \text{ s}^{-1}$ and $250 \text{ kg m}^{-1} \text{ s}^{-1}$ thresholds respectively. Further inspection reveals that the maximum width across an individual event is typically recorded around 20-40% of the way through the lifetime (Fig. 5.10).

The question arises as the best way to interpret this information in the context of deducing the typical region of influence of an AR event. The widths of the most impactful ARs at the Dyfi and Teifi catchments are calculated according to the two IVT thresholds, via the method described in section 5.3.2 (Fig. 5.9, panels e and f). When applying the $500 \text{ kg m}^{-1} \text{ s}^{-1}$ threshold, this width is found to be 567 km at the Dyfi and 705 km at the Teifi. When considering the $250 \text{ kg m}^{-1} \text{ s}^{-1}$ threshold, these figures rise to 1300 km and 1480 km respectively.

The 4.5° movement window is developed based on an assumed AR width of approximately 1000 km. The estimates provided here, for the most impactful ARs at the Dyfi and Teifi, likely exist as an upper and lower estimate of region of influence of typical AR events, given the IVT threshold applied. Also considering the observed variability within the historical composites (Fig. 5.9, panels a and c), it is proposed that this estimate of 1000 km is reasonable for the majority of cases of AR events to affect the UK.



a) Slight southerly bias for the average landfalling position of historical ARs.

b) On average, each AR demonstrates 100km of latitudinal movement of the AR axis across its lifetime.

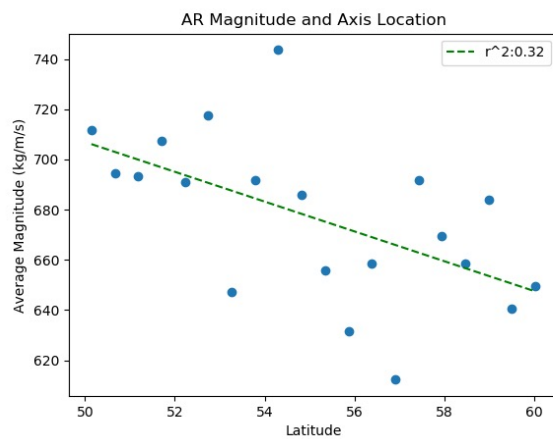


Figure 5.8. Atmospheric River Landfalling Locations. The average landfalling locations of the ARs in the updated catalogue are inspected (a), alongside the average movement of each AR axis over their lifetime (b) and how the location of the landfalling AR relates to its average strength (c). There is a slight southerly bias of landfalling ARs, likely a result of the stronger IVT magnitudes typically observed at the southern latitudes. The small latitudinal movement displayed by each AR event suggests that ARs are indeed relatively static and persistent features.

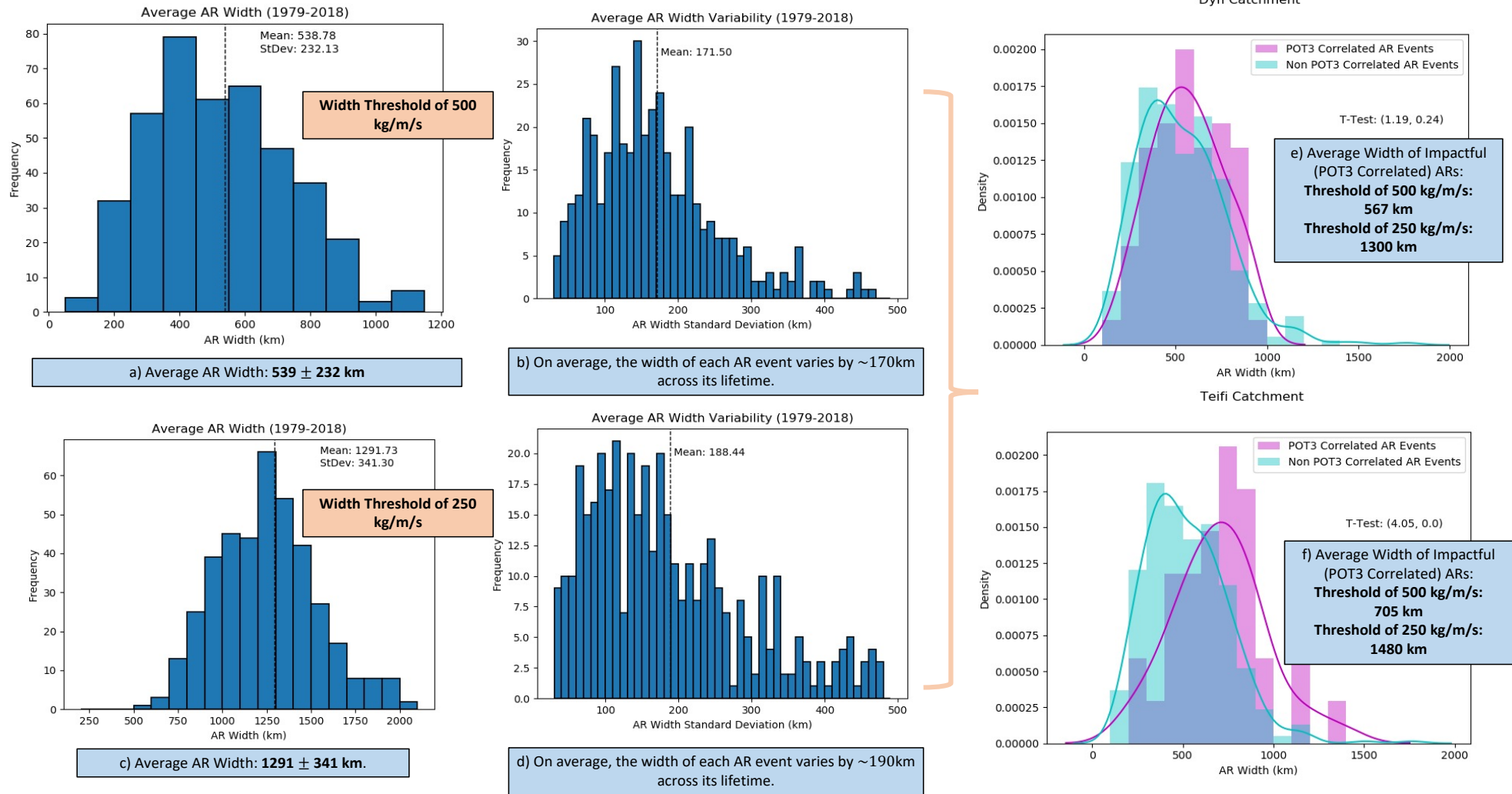


Figure 5.9. Atmospheric River Width. The average width of the ARs in the test catalogue are calculated according to IVT thresholds of 500 and 250 kg/m/s (panels a and c respectively). The average width variation displayed by a given AR across its lifetime is also calculated according to the different thresholds (panels b and d). A test of the typical width of impactful ARs at the Dyfi and Teifi (panels e and f), suggests that a typical AR width of 1000 km is reasonable. A such the 4.5° movement threshold suggested by Lavers et al. (2012) is sensible.

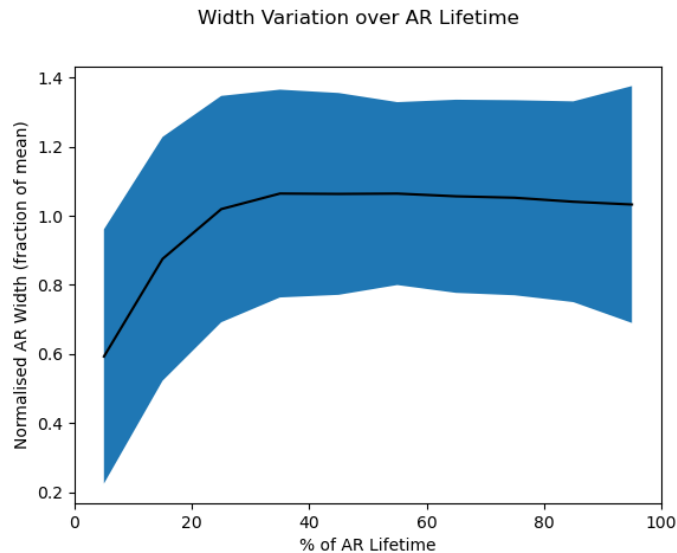


Figure 5.10. Width Variation over Lifetime. The largest AR width is typically observed 20-40% of the way through their lifetime.

5.3.4.2. Relation to AR Properties

The work described in this subsection tests the relationship between AR width and additional properties. Are the strongest ARs associated with the widest widths, or perhaps vice versa, as the atmospheric moisture is ‘channelled’ into a narrower feature? The association between the width of an AR and its landfalling location will also be tested. That is, is there evidence to suggest that ARs in the north systematically narrower than those found further south, or vice versa? These questions in combination will help deduce the most useful properties from a forecasting perspective.

There appears to be little to no relationship between the width of an AR and its landfalling location (Fig. 5.11a). That is, ARs demonstrate a range of widths independent of where they make landfall. However, differences in width can account for nearly 40% of the variance in AR magnitude (Fig. 5.11b). That is, the strongest ARs are systematically wider than their weaker counterparts and a width estimate can provide a rough estimate of AR strength. This result may suggest that IVT falls off uniformly each side of the AR axis, such that the greater the strength at the axis, the greater the total width (when calculated according to a fixed threshold).

Using the Dyfi and Teifi catchments as an example (Fig. 5.9, panels e and f), the most impactful ARs at the Dyfi (i.e., those associated with POT3 floods) appear to be slightly wider than those that result in little to no impact, however, using a T-Test (the results of which are given in the

figure legend) there is no statistical evidence for such a statement. At the Teifi however, a statistically significant difference is obtained between the widths of those impactful ARs as compared to those with little to no impact. That is, the ARs associated with POT3 floods at the Teifi catchment are statistically wider than those that are not.

Given the findings of Section 5.2.3, where IVT magnitude is deduced as a stronger control on AR impact potential at the Teifi than the Dyfi, these results are reasonable. At the Dyfi catchment, where the orientation of the incoming AR is much more important, the strength of the AR (and thus the width) can be thought of as a secondary consideration.

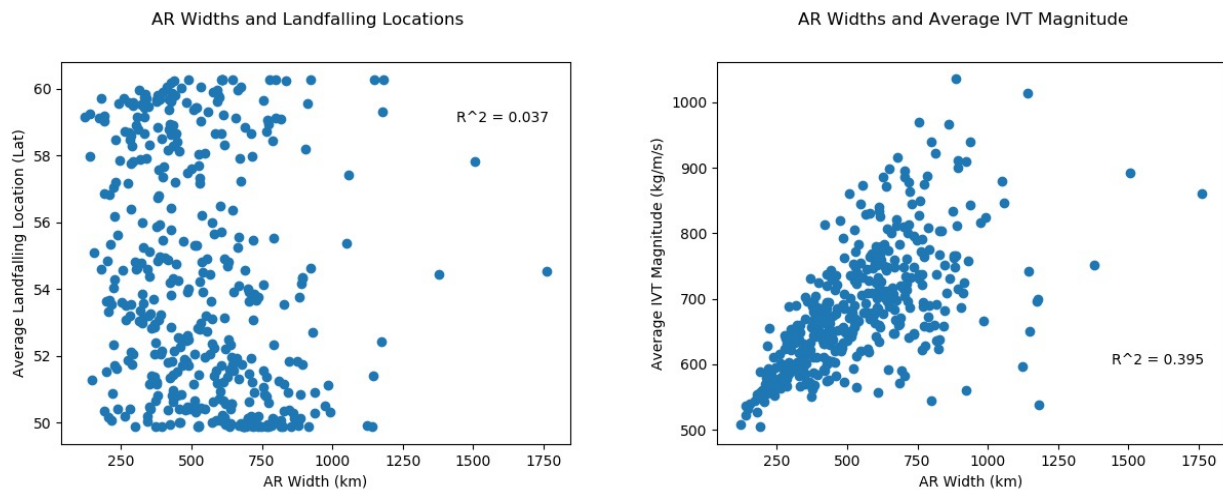


Figure 5.11. AR Width and Additional Properties. There appears to be little evidence of a link between the width of an AR and its landfalling location, that is, ARs of all different widths are observed at all latitudes. However, a stronger relationship exists between the AR width and average IVT strength transported by the AR. In fact, differences in width can account for nearly 40% of the variance in strength. The strongest ARs are systematically wider than their weaker counterparts.

5.3.5. AR Cross Sections

5.3.5.1. Coastal ARs

This section inspects the cross-sectional distribution of ARs making landfall along the coastline of mainland UK, in terms of their IVT magnitude and orientation. Results are initially presented for a single case study - storm Desmond - which made landfall in December 2015 alongside its associated AR (Fig. 5.10a). The left-hand panel describes the evolution of IVT magnitude over the lifetime of the storm – with the colours of each cross-section corresponding to a separate timestamp (following a rainbow colour-scheme). The black dashed line corresponds to the average cross section (over all timesteps) with the cross marker denoting the location of the AR axis at each timestamp.

The AR grows in both width and strength as it passes overhead, with a gradual southernly drift of the axis centreline. Moving away from the axis, and the observed IVT strength falls off rather dramatically. In fact, the strongest IVT values are observed within $\pm 1.5^\circ$ of the axis. In contrast, IVT orientation (Fig. 5.10a, right hand panel) appears relatively uniform over the width of the AR, demonstrating only a slight anticlockwise shift in orientation as the AR moves overhead. Perhaps this is in line with the expectation of ARs arriving in combination with cyclonic storm systems; as the storm passes overhead, the cold front, and its associated tail of moisture (the AR), swings anticlockwise.

To investigate the extent to which the case study results are representative of the historical catalogue, the average cross section of each AR event is stacked on a normalised axis. To normalise the y-axis, the average values of IVT strength/orientation at each AR centreline are subtracted from the associated cross section. To normalise the x-axis, the average landfalling location of each AR (at the AR centreline) is subtracted from the associated cross section. This allows a stacking of all cross sections of the ARs within the catalogue (Fig. 5.10b).

The average value of the stack is identified by the solid black trace (Fig. 5.10b) and the associated standard deviation by the blue shading. The results of the historical composite are similar to those identified in the single case study. Whilst IVT orientation remains relatively constant over the width of the AR, IVT magnitude drops off rapidly once moving away from the AR centreline. The bulk of the AR IVT flux can be contained within a typical width of around $4\text{--}5^\circ$.

5.3.5.2. *Inland ARs*

In this final sub-section, the aim is to investigate how AR properties change as the AR moves inland. The earlier analysis is repeated at sequentially inland locations, moving one grid cell at a time, until 4°E is reached (by which point, it is reasonable to assume that the AR had passed over the UK).

The results for Storm Desmond are given in Fig. 5.13. The results according to each longitude follow a rainbow colour-scheme, with the westernmost and easternmost traces corresponding to the red and purple traces respectively. Peak IVT magnitude falls as the AR moves inland, with the latitude of the track axis steadily drifting northward. IVT orientation remains consistent over the width of the AR, but drifts slightly clockwise as the event progresses.

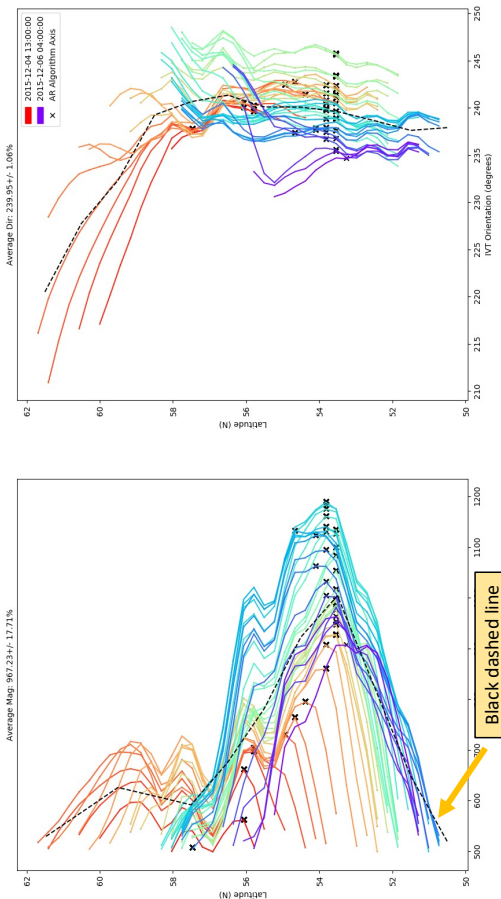
The distribution of IVT magnitude and orientation at each longitude are stacked by applying the same methodology of Fig. 5.12, to produce a historical composite for all landfalling ARs across the historical period (Fig. 5.13b). The axes are once again normalised to account for differences in landfalling location and average IVT magnitude/orientation. For reference, the axes are normalised according to the values at 4°W. This allows an inspection of how AR properties change, relative to the coastal values, as they propagate inland. The colour-scheme is as for the storm Desmond case study. From this composite it is suggested that IVT magnitude falls by $100 \text{ kg m}^{-1} \text{ s}^{-1}$ as the AR passes over the UK with the corresponding orientation swinging clockwise.

How do AR properties (IVT flux magnitude and orientation) vary across width?

1. Take the average distribution (black dashed line) for each AR event;
2. Normalise the latitudinal axis;
 - $lat_{norm} = lat - lat_0$
3. Normalise the Magnitude and Orientation Axes;
 - $mag_{norm} = mag - mag_0$
 - $dir_{norm} = dir - dir_0$
4. Stack the historical AR distribution and calculate mean/variability.

Storm Desmond: 2015-12-04

Storm Desmond: 2015-12-04
Duration: 40
Average Width: 23.12°± 5.06%



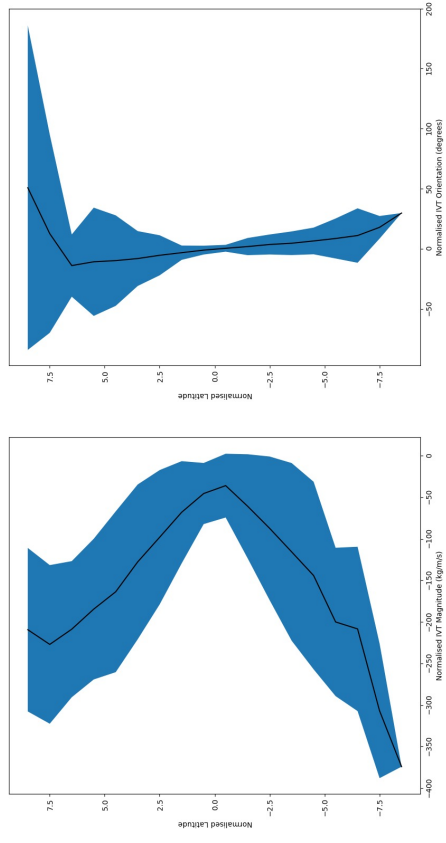
Black dashed line shows AVERAGE flux distribution over AR lifetime

It is from this distribution that we calculate the average properties at a given location (in our analyses up until now)...

a

Historical AR Sample (1982-2014)

Average Distribution of Historical ARs and Variability in their Properties



Black solid line is average AR distribution. Blue shading shows standard deviation of the historical sample (188 events)

b

Figure 5.12. Coastal Atmospheric River Cross Section. Panel (a) shows the distribution of IVT magnitude and orientation across the width of the AR associated with Storm Desmond. The dashed black line shows the average IVT and orientation distribution across the lifetime of the event. The average distributions all ARs are stacked to produce a historical composite (panel (b)). AR IVT magnitude falls rapidly from the axis centreline, whereas IVT orientation remains relatively uniform.

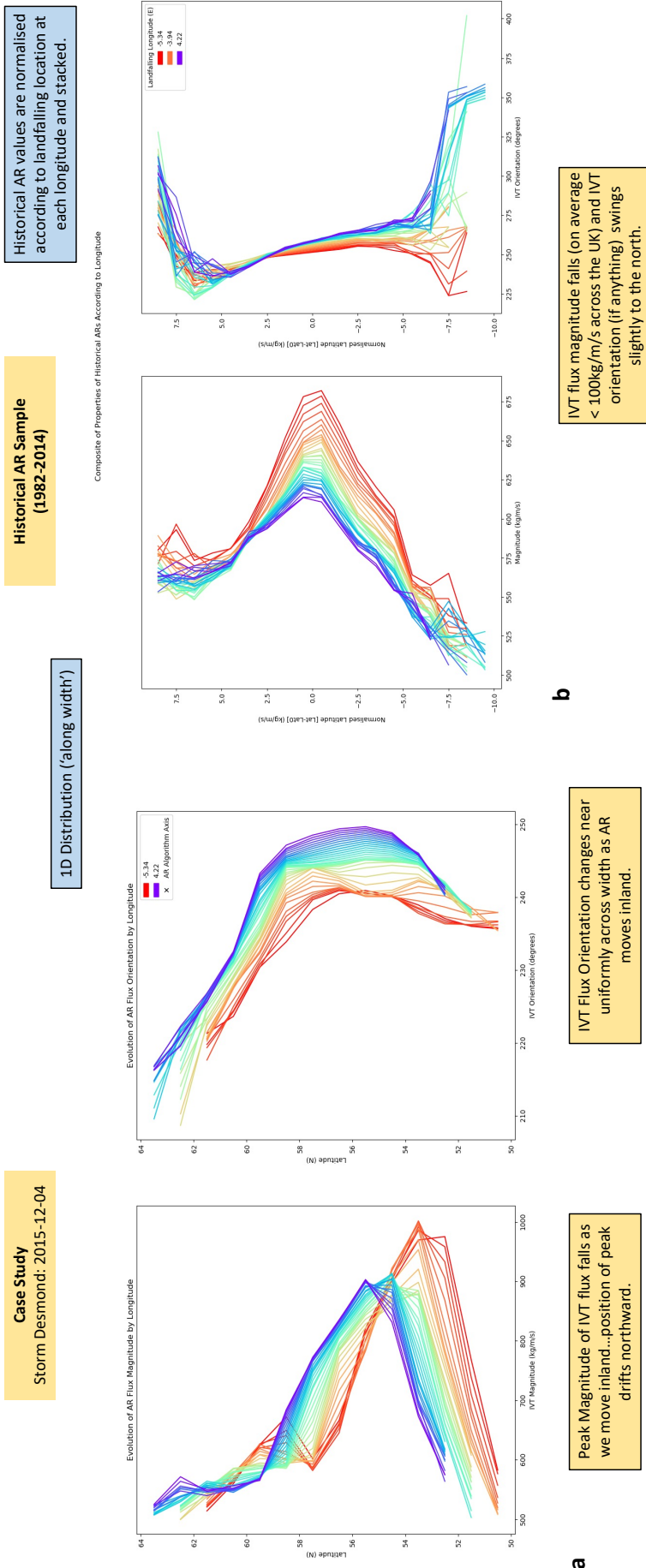


Figure 5.13. Inland Atmospheric River Cross Sections. An inspection of how AR properties (IVT magnitude and orientation) change as the AR moves inland for storm Desmond (a) and the historical composite (b). The strength of the AR falls by about $100\text{kg m}^{-1} \text{s}^{-1}$ as the feature passes over the UK and the orientation swings clockwise.

5.4. Conclusions

The aim of this chapter has been to improve the performance of the Lavers et al. (2012) AR detection algorithm in the context of high spatial and temporal resolution datasets such as ERA5. In its previous state (Chapter 4, section 4.2.5), it was likely to be removing legitimate ARs on the basis of sub-threshold IVT values and/or missing timesteps. Such variability has been attributed to physical phenomena such as Mesoscale Frontal Waves and secondary IVT limbs, and several adjustments to the Lavers et al. (2012) AR detection algorithm have been implemented in response.

The modified algorithm has been applied to the Dyfi and Teifi catchments; investigating its ability to detect further flood generating ARs as compared to its original counterpart. The orientation and strength of the additionally detected ARs are inspected with regard to the preferential bands/IVT thresholds presented in Chapter 4.

In addition to the algorithm adjustments, several assumptions regarding AR width, landfalling location and the cross sectional distribution of IVT magnitude and/or orientation have been verified. This process will ensure that, moving forward, (1) as many appropriate ARs as possible are successfully detected, (2) their most representative properties are being extracted (for use in further analysis) and (3) those regions most likely at risk from a given AR event are successfully identified.

The main findings of this chapter can be summarised as follows:

- There is merit in updating the original 2012 detection algorithm in line with higher resolution datasets. There is also room for some flexibility with regard to the duration of AR events; that is, even ‘short’ duration ARs can still be impactful.

The updated algorithm is recommended for future analyses and, in order to detect the greatest number of possible ARs, a temporal persistence threshold of nine hours or more.

- The width of an AR is strongly dependent on the ‘threshold’ used to calculate AR conditions. Using thresholds of $500 \text{ kg m}^{-1} \text{ s}^{-1}$ and $1000 \text{ kg m}^{-1} \text{ s}^{-1}$, the average widths of the catalogue are calculated as 539 km and 1291 km respectively (albeit with standard

deviations of near 40% and 25% respectively). The width of an AR appears to be strongly correlated with its strength (or vice versa).

AR width could be considered to determine its impact, especially in the cases where a catchment is sensitive to AR strength.

- However, when inspecting the widths of the most impactful AR at the Dyfi and Teifi catchments, an estimate of 1000 km is sensible.

In most cases, the 4.5° latitudinal movement assumption is appropriate. For consistency therefore, it will be applied in future analyses.

- The latitudinal movement of a typical AR track is small compared to the typical width of the AR i.e., ARs are relatively stationary when they make landfall.

This is in line with expectations and only acts to highlight the role that ARs can play in the delivery of heavy, persistent rainfall to their landfalling locations.

- The bulk of AR flux is concentrated within $\pm 2^\circ$ of the AR axis. The orientation of the flux is relatively uniform across the AR centreline.

An AR is detected on the basis of the conditions at its centreline, however, if the region of interest is towards edge of the feature then the conditions overhead should be expected to be less severe.

- The peak AR flux falls by about $100 \text{ kg m}^{-1} \text{ s}^{-1}$ as it makes its way across the UK. The AR orientation swings slightly clockwise.

Whilst the majority of ARs pose the greatest threat to coastal locations, the strongest ones may be able to deliver intense water vapour flux to inland regions. If conditions are favourable, i.e., with AR orientation and catchment terrain, then notable impacts may still result.

Chapter 6 – Atmospheric Rivers and the Catchment

6.1. Introduction

The majority of poleward movement of water vapour across the mid-latitudes can be explained through the existence of atmospheric rivers (ARs; [Gimeno et al., 2016](#); [Newell et al., 1992](#)). Characterised by lengths much greater than their widths, they are often located within the warm sector of extratropical cyclones, where the occurrence of a low-level jet just ahead of the cyclone's cold front, coinciding with warm, moist air provided by the AR, result in a region of enhanced water vapour flux ([Browning & Pardoe, 1973](#); [Ralph et al., 2005](#)). When the AR makes landfall and the moisture rich air is forced to rise, heavy and persistent precipitation can result, especially when impinging upon mountainous areas ([Neiman et al., 2008](#)).

The majority of AR research to-date has focussed on the western USA, where the inter-annual variability of ARs is particularly important from water resources perspective, as well as a flood hazard ([M. D. Dettinger et al., 2011](#)). Across the western coastline of Europe, ARs can account for up to 50% of the monthly precipitation budget during the winter months and have been directly linked to floods across the UK, Iberia and Norway, as well as further afield in regions of Asia, South America and Australasia ([M. D. Dettinger et al., 2011](#); [Kingston et al., 2016](#); [D. A. Lavers et al., 2011](#); [Ralph et al., 2006](#); [Ramos et al., 2015](#); [Viale & Nuñez, 2011](#)). However, many ARs arrive each year without resulting in notable effects, and therefore understanding why this is the case is essential for effective impact-based forecasts ([Eiras-Barca et al., 2021](#)).

The recent AR Categorisation Scale initially suggested for the US West Coast ([Ralph, Rutz, et al., 2019](#)), and later extended to Europe ([Eiras-Barca et al., 2021](#)), invokes a combination of (maximum) overhead Integrated Water Vapour Transport (IVT) and duration to infer a category spanning 1 through 5. However, there is additional evidence that AR orientation relative to catchment topography is also an important consideration ([Griffith et al., 2020](#); [Neiman et al., 2011](#); [Ralph et al., 2003](#)). Further, there is contrasting lack of research when considering the role that additional catchment properties can play in either modulating the location and intensity of induced precipitation and/or its translation across the landscape into runoff and streamflow. Here we look at the role of ARs as historical flood-generators at a series of 81 test catchments along the western coastline of the UK. We are able to quantify, for the first time, the relative role of land-surface properties in determining the most impactful ARs.

The research questions of this chapter are detailed below:

- How important are ARs across the UK uplands in terms of wintertime flood generation?
- Is it possible to identify certain characteristics of the most impactful ARs e.g., IVT strength and/or orientation?
- To what extent can the identification of preferential AR properties be explained through the inclusion of land-surface properties?
- How important are antecedent conditions and storm duration in controlling the most extreme events?
- Is it possible to predict the properties of the most impactful ARs based on catchment descriptors alone?

6.2. How Important Are ARs across the UK?

6.2.1. Rationale

The aim of this section is to understand the role of ARs on wintertime flooding across the UK. The original set of catchments posed by Lavers et al. (2012), in their analysis of AR influence across the UK, has been extended (Chapter 3, Section 3.2; Figure 3.1).

The 81 study catchments have been selected on the basis of several requirements, including minimal urbanisation and effective gauging at high flows (Chapter 3, Section 3.2). They can be organised into four broad regions of the UK: south-western England, Wales and the English Borders, north-western England, and Scotland, and span a range of catchment properties, including size, elevation, aspect, slope and underlying geological conditions.

Persistent AR events across the winters of 1982–2014 were extracted from the ERA5 reanalysis at hourly timesteps using the modified Lavers et al. (2012) AR detection algorithm (Chapter 5; Section 5.2). At each of the study catchments, the percentage of POT3 floods occurring within three days following the arrival of a persistent AR was extracted. For each catchment therefore, the AR sample could be split into two groups; those associated with a POT3 flood and those

without. A total of four AR catalogues were applied; corresponding to minimum AR durations of 9, 12, 15 and 18 hours respectively.

The properties of the ARs (namely, magnitude and orientation) associated with (and without) a POT3 flood were inspected. For each of the AR properties, two statistical tests were employed to assess the mean and spread of the two samples: these being the T-Test and Levene Test, respectively.

The T-Test is used to test the null hypothesis that the POT3 and non-POT3 correlated samples have equal means and the Levene test used to test the assumption of equal variances. A significant p-value (of less than 0.05) can allow a rejection of the null hypotheses, and permit identification of statistical differences between the two samples. In addition to the distribution analyses, the combined influence of AR magnitude and orientation was assessed through a simple scatter plot.

The following methodology was applied as a way of extracting the key information across a number of catchments:

- A significant Levene Test suggests a preferential orientation band for the most impactful ARs. In this case, the catchment can be labelled as **Orientation Dominated**. The preferential orientation band is extracted as the 25th and 75th percentile of the POT3 correlated sample (namely, the upper and lower bands of the box in the box and whisker plot; upper left panel of Fig. 6.1).

The distribution of the POT3 correlated ARs and otherwise **within the preferential band** in terms of IVT magnitude is assessed through a simple scatter plot (central and right-hand panels in Figure 6.1). A minimum IVT threshold for the most impactful events is extracted according to the 25th percentile of the POT3 correlated sample.

- If the Levene test returns a non-significant result, the IVT magnitudes are inspected. A positive T-Test suggests that the ARs correlated to POT3 flood events at the catchment are systematically stronger than those that are not. In this case, the catchment is deemed to be **Flux Dominated**. The 25th percentile of the POT3 correlated sample is used to calculate the minimum IVT threshold for the most impactful events (the lower band of the box in the box and whisker plot; lower left panel of Fig. 6.1).

- If **neither** the Levene or T-Test return statistically difference results, then no further meaningful information is extracted, and the catchment is removed from all subsequent stages of the analysis.

Catchments are therefore identified according to whether they demonstrate an orientation- or flux-dominated response to landfalling ARs. In the former case, a preferential orientation band and IVT threshold is extracted. In the latter case, only an IVT threshold is retained. Those catchments that do not show evidence for either orientation or flux-dominated responses are removed from the analysis. This equates to a total of 11 catchments, thus reducing the number of study catchments to 70. It should be noted that the IVT threshold extracted from this process is independent to that used in the mechanics of the AR detection algorithm, which is always kept at $500 \text{ kg m}^{-1} \text{ s}^{-1}$.

The full results according to each catchment are presented in Appendix 3 and a summary table of the number of catchments within which a preferential subset of ARs could be identified is provided below (Table 6.1), according to each of the AR catalogues. The shortest duration AR catalogue (9+ hours) is able to detect the greatest number of impactful ARs, and as such the number of catchments within which a preferential subset of ARs can be identified is maximised.

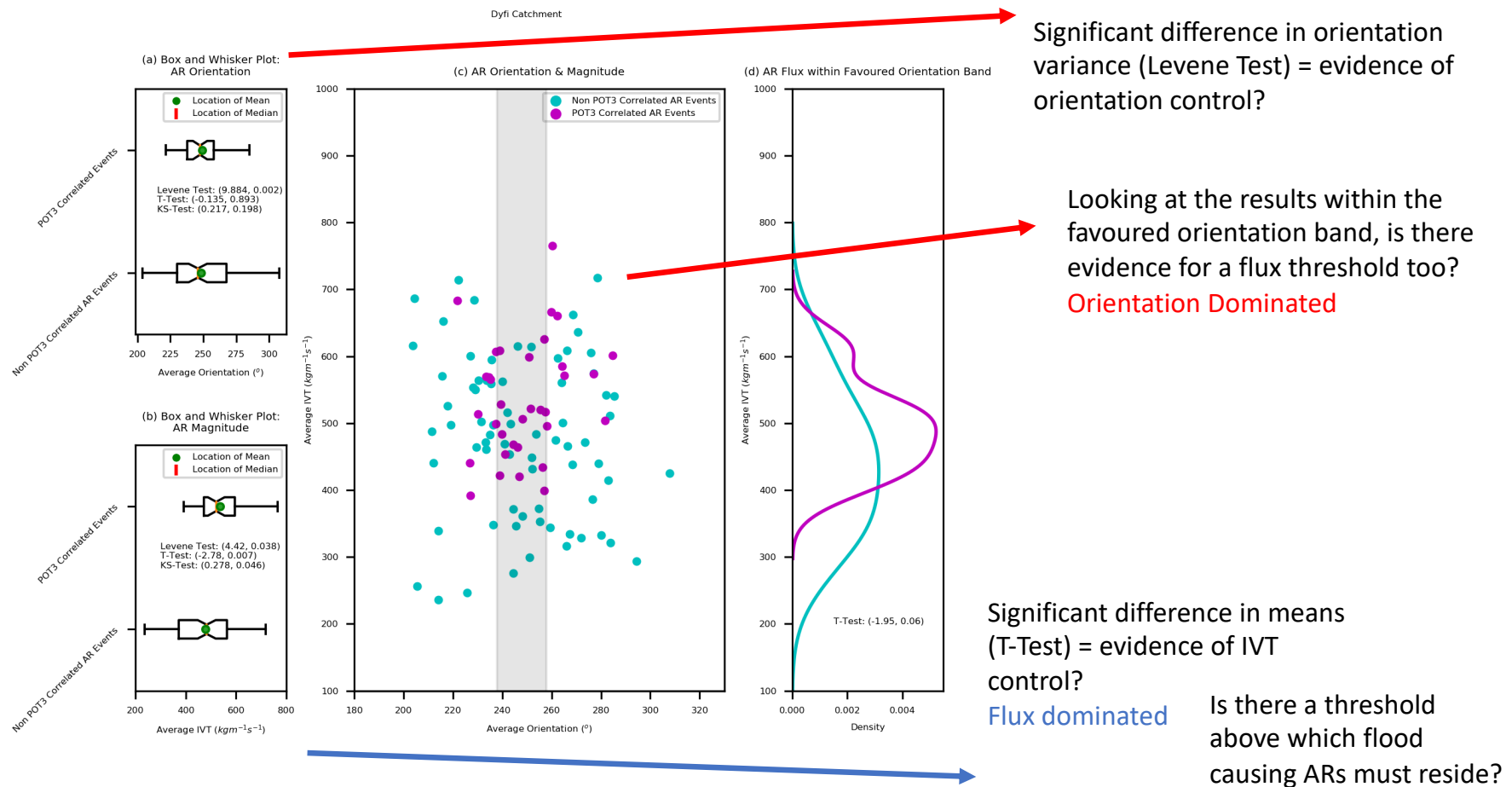


Figure 6.1. Orientation and Flux Dominated Catchments. Given the number of catchments within the study, it has been necessary to propose a standardised way of extracting distribution information. Using the results of the Dyfi catchment as an example (Chapter 4; Figure 4.2), catchments are identified as either orientation or flux dominated based on the distribution of their POT3, and non POT3, correlated ARs.

AR Minimum Duration	9 hr	12 hr	15 hr	18 hr
Number of catchments at which a subset of ARs could be identified via statistical means (i.e., T/Levene Test)	70	65	62	53

Table 6.1. AR Catalogues and catchments with a preferential subset of ARs. If a significant result was identified for either the Levene or T-Test, a preferential subset of ARs was identified.

6.2.2. AR-Flood Relationships at Orientation and Flux Dominated Catchments

The first intention of this chapter is to develop a broad understanding of the importance of ARs during the formation of extreme floods across the study catchments. The percentage of POT3 floods at each of the study catchments associated with persistent ARs of duration nine hours or more is inspected (Fig. 6.2). This particular AR catalogue is chosen to maximise the number of impactful ARs. The catchments where no significant AR-flood relationship could be found (Table 6.1) are highlighted in red.

The strongest relationships are found within the upland regions of Cumbria, Snowdonia, Devon and north-western Scotland, suggesting that orography is a key control on AR impact. However, in line with earlier work, there are markedly different results demonstrated across adjacent catchments. This suggests that the presence of an AR alone is insufficient to result in a flood. The following sections will attempt to understand why this may be the case.

6.2.2.1. Preferential Orientation Bands

It is possible to compare the preferential orientation bands extracted from orientation dominated catchments to the large-scale topography (Fig. 6.3). Although many adjacent catchments are found to be similar in their preferential AR orientations, for example those across south Wales and Cumbria, there are some differences. For example, the catchments in south-western England demonstrate a change in preferential AR orientation when moving from Cornwall through Devon. It is likely therefore, that a subtle interplay between local catchment slopes and large-scale topography exists, to drive the most efficient rainout, with the overall catchment elevation and subsequent rain shadowing effects also playing a role. Thus, in line with earlier conclusions, the simple presence of an AR alone is not enough to generate a flood.

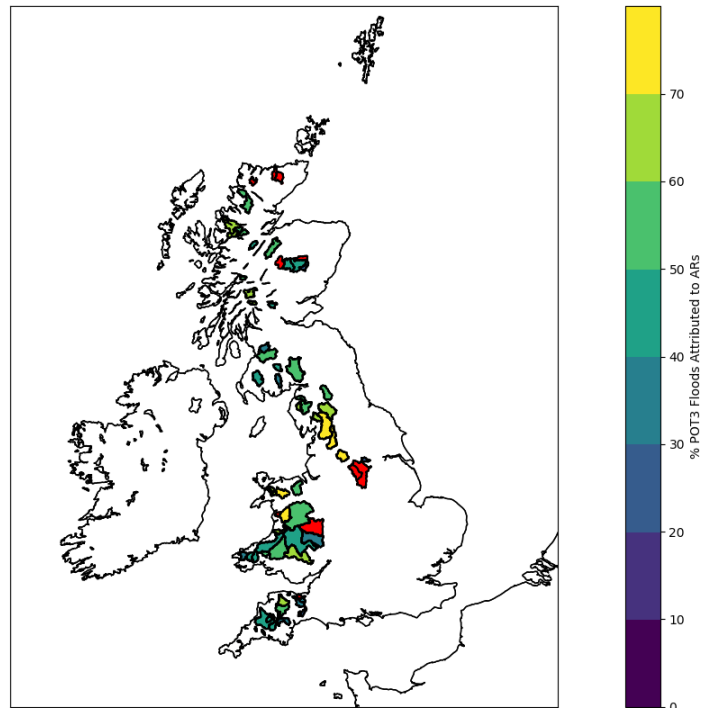


Figure 6.2. Percentage of POT3 floods associated with ARs of duration 9hr +. Atmospheric Rivers are responsible for many of the largest (POT3) floods at a wide range of catchments across the study period. Strongest correlations are noted in Wales and north-western England and, in line with earlier research, nearby catchments demonstrate markedly different results. Thus, the simple presence of an AR alone is an insufficient condition for a notable flood. Catchments where no significant relationship between ARs and winter floods are highlighted in red.

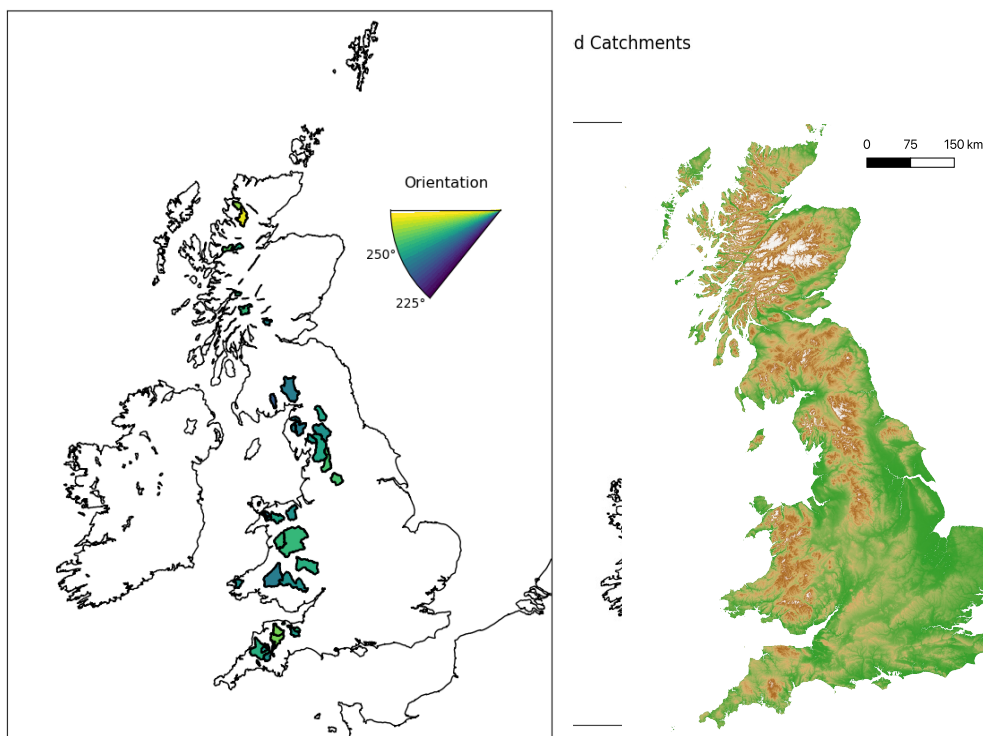


Figure 6.3. Orientation Dominated Catchments. The majority of catchments in the study require a specific orientation of AR if the largest floods are to be generated. Although some nearby catchments demonstrate similar preferential orientations, some do not. A subtle interplay between local catchment slopes and large-scale topography is expected to control the most efficient rainout.

6.2.2.2. IVT Thresholds

The IVT thresholds for impactful ARs, at both flux and orientation dominated catchments, can be compared to the average IVT values for all landfalling ARs across the study period (Fig. 6.4). Moving northward and the magnitude of the calculated IVT thresholds fall. Such observations are in line with the expected climatology, in that the atmosphere cools as we move northward in line with its typical moisture content.

The most impactful ARs in the southernmost catchments are systematically stronger than the average. Subtracting these average value from the IVT threshold (Fig. 6.4), and it is clear that almost all of the catchments in south-western England require ARs to be (on average) 60-80 $\text{kg m}^{-1} \text{s}^{-1}$ stronger than the mean value. Moving northward, into Wales and Cumbria, and the difference in strength between the impactful ARs and the average values is reduced.

Perhaps in this case, as the surrounding topography increases in elevation, the orientation of the incident AR plays a greater role, and as such the strength alone is insufficient to result in a flood. In addition, the uplift generated by the lower relief topography is reduced as compared to more northern catchments and thus a stronger AR is required to generate significant precipitations.

The catchments across Scotland demonstrate scattered results in terms of AR strength as compared to average. Again, this is likely a reflection of the complex interplay between large-scale topographic controls and internal slopes, and as such, deciding whether an AR will be impactful based on its strength alone is less helpful.

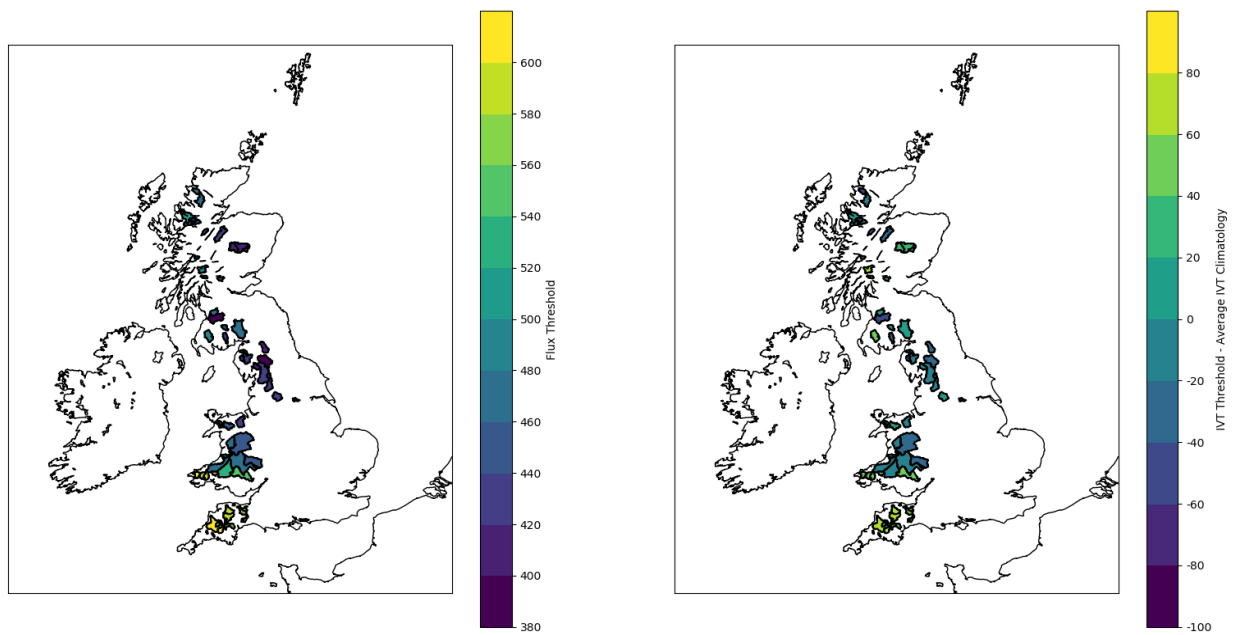


Figure 6.4. IVT Thresholds. There is a decreasing trend within the IVT threshold results moving northward (LHS), in line with the expected AR climatology (central). Comparing the IVT thresholds to the average AR climatology, it is possible to deduce the strength of the most impactful ARs as compared to average. The strongest results are found in the southernmost catchments.

6.3. Incorporation of Catchment Properties

6.3.1. Rationale

The previous section has demonstrated that different types of AR, in terms of orientation and strength, are particularly impactful at different catchments. However, nearby catchments show notable differences in the properties of these ARs, and it has been proposed that the surrounding topography may play a role. This section intends to test whether the inclusion of a variety of catchment properties can help in understanding these results.

6.3.2. Refining the Descriptor Dataset

A total of 22 catchment descriptors are collated according to each of the study catchments (Chapter 3, Section 3.2). It is likely that several of the descriptors are highly correlated, for example catchment elevation and average slope severity. One of the assumptions of many regression methods, or any other machine learning tool, is that the independent variables are

uncorrelated. A simple correlation matrix will help in deducing the most strongly correlated variables (Fig. 6.5).

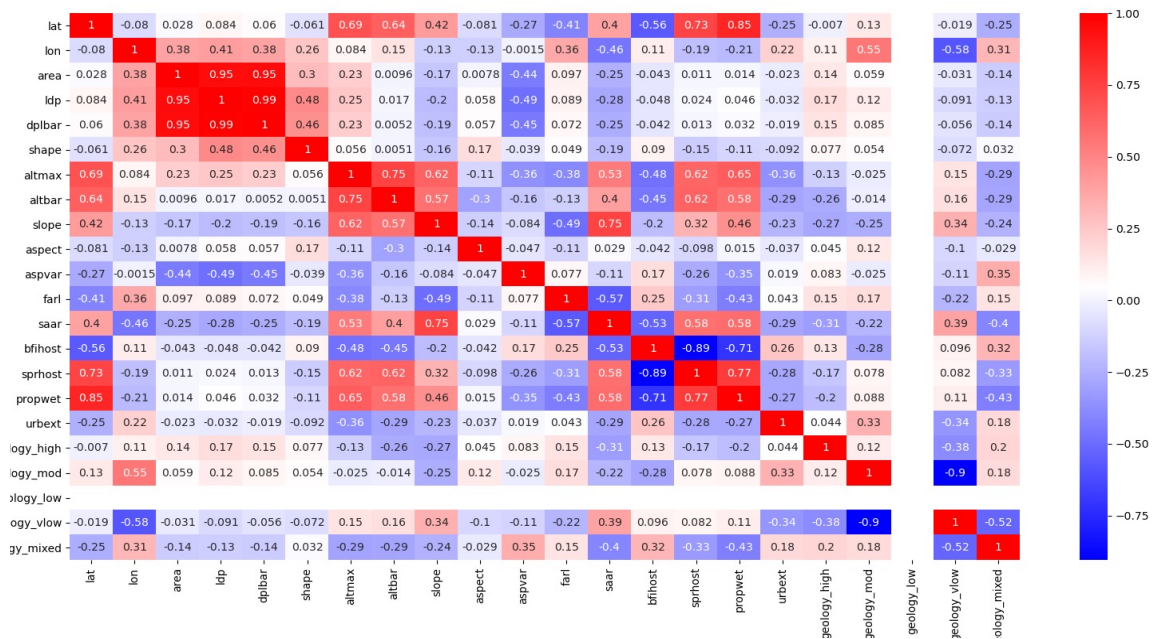


Figure 6.5. Correlation Matrix of all Catchment Descriptors. Using the Pearson Correlation coefficient, highly correlated descriptors are removed.

Choosing to remove catchments with strong correlation values but ensuring that a well-rounded description of the catchment is retained, the 22 descriptors are refined to a final five – catchment latitude, area, maximum altitude, BFIHOST and the percentage of impermeable bedrock (Fig. 6.6), whilst retaining the key characteristics of the original dataset. However, several of these descriptors remain correlated to each other to some extent and thus, to apply a regression model or similar, new ways of describing the dataset will be required.

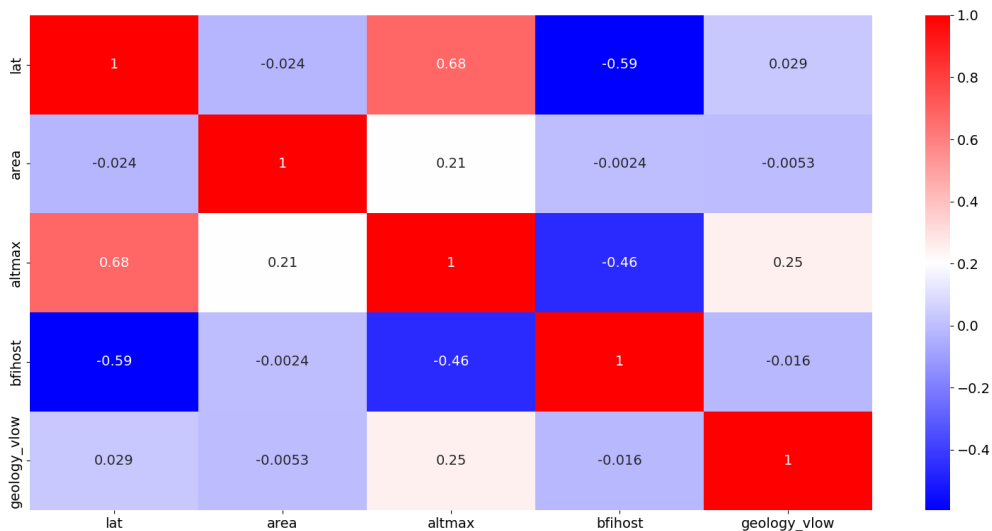


Figure 6.6. Final Descriptor Variables. The retained catchment descriptors include the catchment latitude, area, maximum altitude (elevation), the proportion of underlying impermeable bedrock and the soil responsiveness (BFIHOST).

6.3.3. Principal Component Analysis – Linking the Descriptors to AR Properties

Principal Component Analysis is primarily a dimensionality reduction technique (Chapter 3, section 3.6.2). It allows an identification the so-called ‘principal components’ of a dataset, which can be thought of a new set of axes to describe the data, created from a linear combination of the original axes. Each of the principal components extracted during the process are orthogonal, and therefore, by projecting the original dataset onto the new axes it is possible to ensure independence between the ‘new’ descriptors of the dataset. This is an essential requirement for many regression models and permits a test of the relationship between the ‘new’ variables and catchment descriptors.

The principal components (PCs) of the descriptor dataset are detailed below (Fig. 6.7). Using only the first three PCs, it is possible to describe over 85% of the variance of the original dataset. In fact, the first PC (PC1) alone, accounts for nearly half (44%) of the total variance.

A so-called loading plot allows an identification of the driving components of each PC (Fig. 6.7). PC1 appears to be dominated by the latitude (‘lat’) and maximum catchment altitude (‘altmax’). PC2 is driven predominantly by the extent of impermeable geology (‘geology’), and PC3 is controlled by the catchment area (‘area’).

By projecting the original dataset onto the first three principal components, it is possible to identify to what extent they explain the variation of a dependent variable. In this case, the IVT threshold (Section 6.2.2). Known as a score plot, potential drivers of the threshold can be identified in terms of PCs (Fig. 6.8). A summary of the main findings is given below.

- PC1 displays a relatively linear relationship with the IVT threshold. Thus, those catchments with higher IVT threshold are associated with larger (positive) values of PC1, and therefore lower altitudes and latitudes (i.e., towards the south of the UK). This conclusion is supported by earlier results, in that the highest IVT thresholds are observed at the southernmost catchments with the gentlest terrain (Fig. 6.4).
- The pink and cyan points of PC2 are located towards the bottom end of the scale. That is, both the highest IVT and average IVT values are associated with the most permeable catchments (or at least those with the smallest proportions of underlying impermeable

bedrock). Geographically, these points likely correspond to the permeable catchments in Devon and the Pennines.

- Finally, nearly all catchments correspond to negative PC3 values, albeit with some evidence of a linear relationship. Thus, the smallest catchments are associated with the higher IVT thresholds in the majority of cases. A reflection on why this may be the case is beneficial – the smallest catchments within the sample are found within Devon and Cornwall (Chapter 3, Fig. 3.7), which may be driving the observed link to IVT.

From a physical standpoint, this may refer to the gentler terrain found in the southern regions of the UK, and the additional methods of flood formation found within these catchments. Perhaps also, the smallest catchments are subject to only a portion of the overhead AR, and the relative effect between the edge of the AR and the AR axis impacting the catchment is more apparent.

PC	Proportion Variance	Cumulative Variance	LAT	AREA	ALTMAX	BFIHOST	Geology (% of Very Low Permeability Bedrock)
1	0.44	0.44	-0.596	-0.147	-0.589	0.525	-0.016
2	0.21	0.65	0.059	-0.146	-0.215	-0.244	-0.932
3	0.20	0.85	-0.171	0.949	0.070	0.142	-0.213
4	0.10	0.95	-0.373	0.137	-0.376	-0.799	0.251
5	0.05	1.00	-0.688	-0.195	0.679	-0.079	-0.149

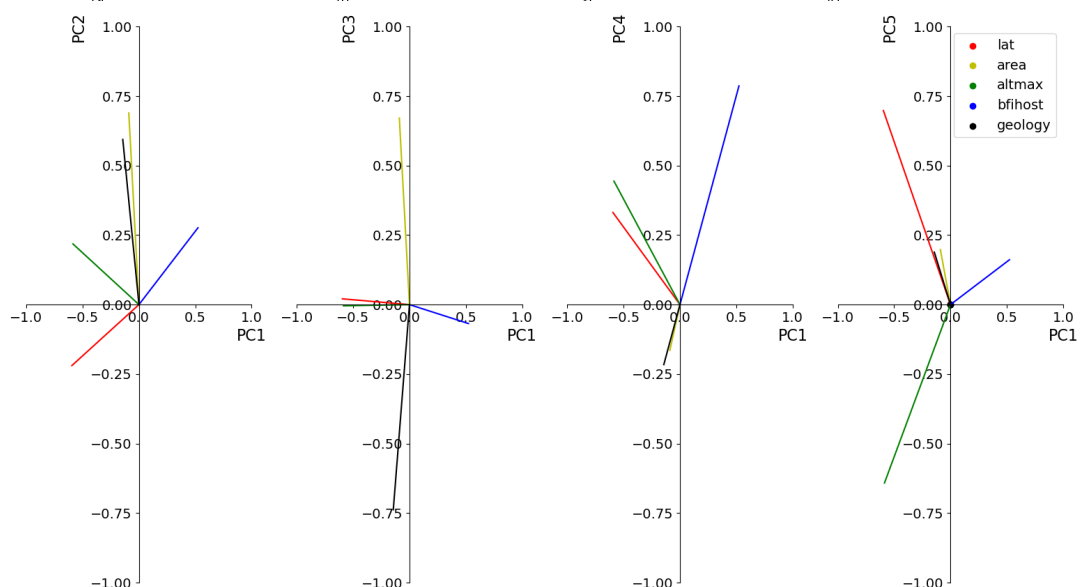


Figure 6.7. Principal Component Analysis and Loading Plots. The first principal component (PC1) accounts for 44% of the variance in the catchment descriptor dataset (upper panel). The loading plots (lower panel) allow identification of the drivers of PC1: catchment latitude and maximum elevation. Following a similar process, PCs 2 and 3 are driven by the impermeable geology and catchment area respectively accounting for around 20% of the variance each. Using the first three PCs alone therefore, it is possible to account for 85% of the variance in the independent dataset.

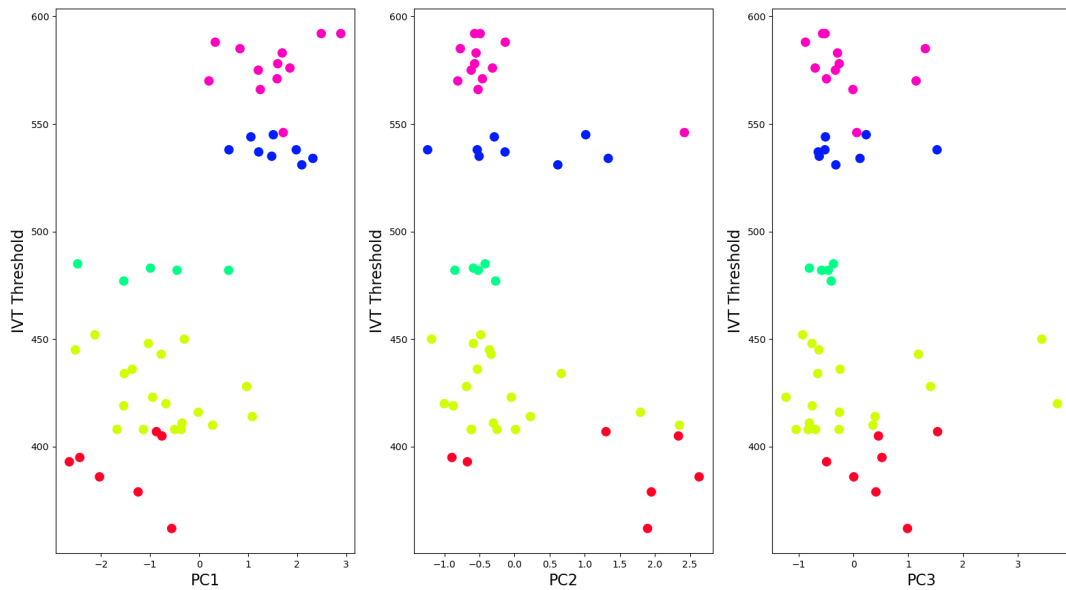


Figure 6.8. Score Plot According to IVT Threshold. The IVT Threshold results, in terms of their relevant catchment descriptors, are projected onto the first three Principal Component axes. The markers have been coloured according to IVT threshold to help with visual interpretation of the results. There appears to be traces of a positive linear correlation with IVT threshold along PC1, however any such relationships are more subtle within PCs 2 and 3.

6.3.4. One Dimensional Descriptor Relationships

Principal component analysis suggests therefore, that catchment latitude and elevation are key controls on the minimum strength of the most impactful ARs (the IVT threshold). The distribution of results in terms of these catchment descriptors alone are inspected.

The distribution of flux vs orientation dominated catchments in terms of their maximum altitude reveals that, for catchments above 400-600m, AR orientation is the controlling variable for AR impact (Fig. 6.9), i.e., orientation-dominated catchments. When considering the relationship between IVT threshold and altitude, there is some evidence of a negative association; that is, for those catchments of higher elevation, a lower IVT threshold is required (Fig 6.9). Such result is likely a reflection of the relative amounts of uplift generated at catchments of differing elevation.

The distribution of results according to geology and catchment area are harder to disentangle (Fig. 6.10), particularly as many of the catchments are underlain entirely by impermeable geology or possess areas of below 500km². However, there is some evidence of a positive trend between the IVT threshold and BFIHOST – suggesting that as the groundwater component of the catchment increases, the IVT threshold for impactful ARs increases.

This latter result aligns with the geological control as mentioned previously. The more permeable catchments, i.e., those with a lower percentage of underlying bedrock, can be expected to demonstrate a greater proportion of groundwater. These catchments likely include those in Devon and Cumbria (section 3.3.5.7).

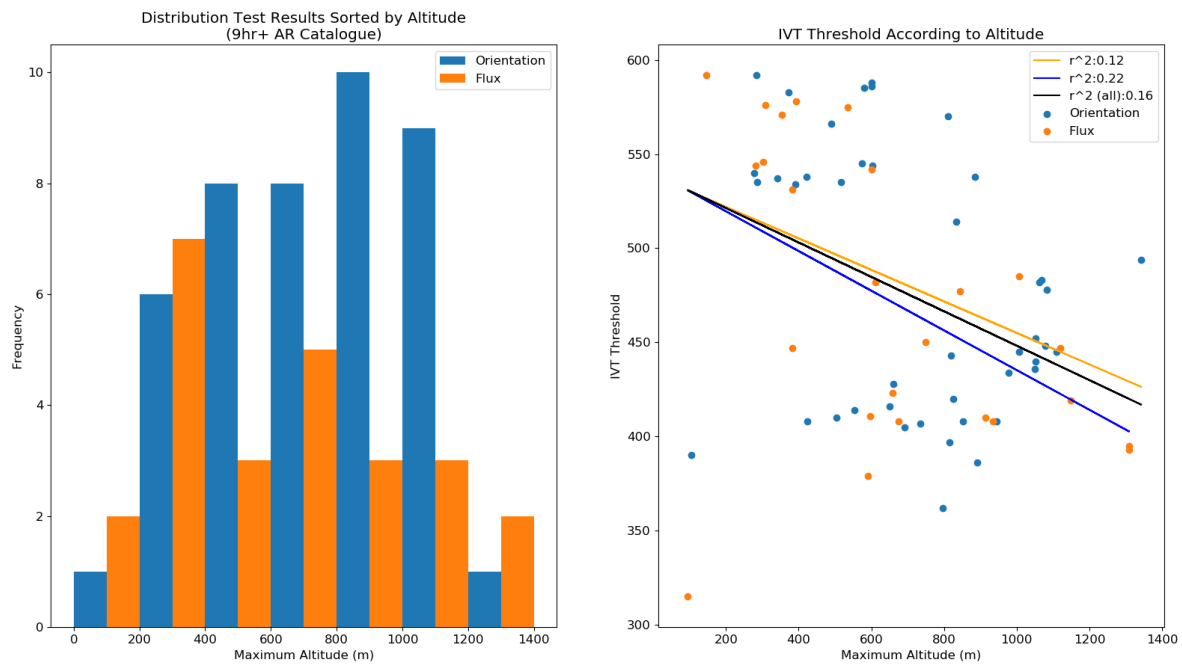


Figure 6.9. Catchment Altitude. Above 400-600m, the presence of orientation-dominated catchments increases relative to flux-dominated catchments. Intuitively, there is evidence that IVT threshold falls as catchment elevation increases.

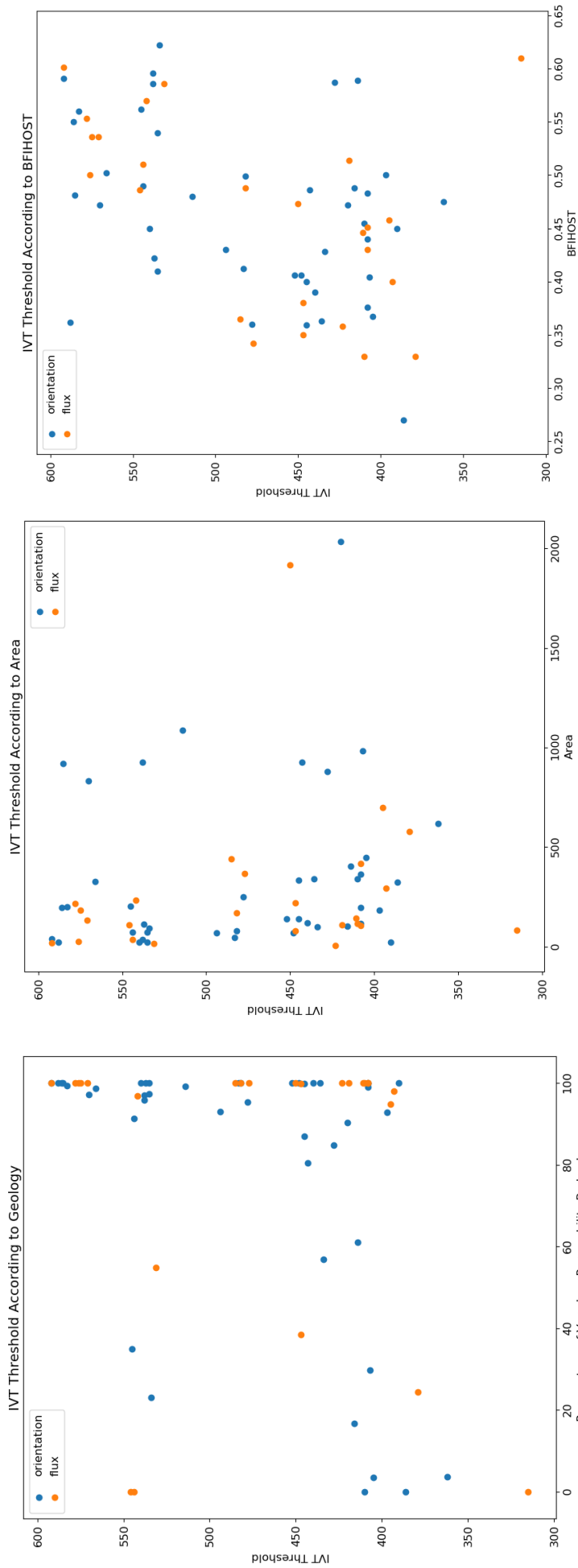


Figure 6.10. Catchment Geology, Area and BFIHOST. These plots are used to test for trends regarding the IVT threshold and the additional catchment descriptors. Whilst relationships are hard to disentangle within the plots associated with geology and catchment area, there is some evidence of a positive linear relationship between the IVT threshold and BFIHOST. That is, as the groundwater component of the soils increase, so does the IVT threshold.

6.3.5. Event Specific Descriptors

6.3.5.1. Storm Duration

To assess the role of storm duration, a comparison between the results according to the different AR catalogues is undertaken. First, the strength of the overall flood-AR relationships are inspected, before comparing the calculated IVT thresholds of the most impactful ARs.

At the majority of catchments, overall flood-AR percentages (i.e., the percentage of POT3 floods associated with persistent ARs) fall when moving from the 9+hr and 18+hr duration AR catalogues (Fig. 6.11). Therefore, although many floods are associated with long duration, persistent ARs, others can be linked to much shorter duration events. In fact, it is the smallest and steepest catchments, such as several in Snowdonia and the Lake District, that demonstrate the largest decrease in flood-AR percentage as the AR duration threshold is increased, suggesting that it is these catchments which are particularly susceptible to shorter duration, flashy AR events.

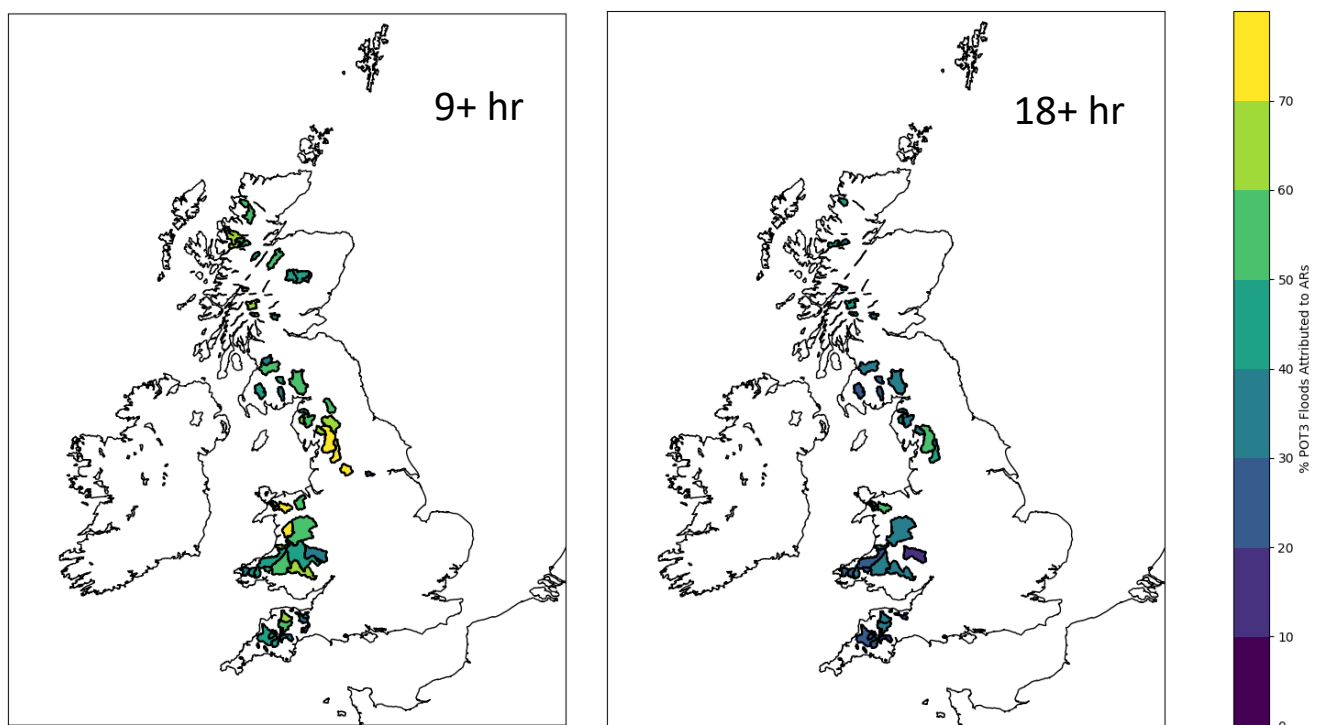


Figure 6.11. AR Duration – Flood Correlation. Moving from the 9 to 18hr + catalogue, the percentage of POT3 floods associated with ARs typically falls. This suggests that lower duration ARs can still be impactful, particularly in steep, flashy catchments.

Next, the IVT thresholds are calculated according to the impactful ARs within each catalogue (Fig. 6.12). An important aspect to note is that the sample sizes of impactful ARs at each catchment are falling as the AR duration increases, and as such there may be more uncertainty in the calculated AR thresholds (Table 6.1).

At many catchments, the IVT threshold is found to increase with duration. This may have been considered counter-intuitive; it was perhaps expected that a lower IVT delivery over a longer period would be similarly impactful. However, the opposite appears to be the case according to these results; a longer duration AR must possess a stronger average IVT than its shorter duration AR counterpart, if the strongest floods are to be observed.

Perhaps this result points towards the fact that ARs are rarely constant over the longest timescales. Many ARs arrive in so-called ‘families’ (Fish et al., 2019), whereupon multiple events arrive in short succession. The AR detection algorithm used in this analysis combines ARs that arrive within less than 24 hours of one another i.e., it will typically join together such AR families. As such, for the longest duration events, an overall ebb and flow in overhead IVT flux may be occurring, similar to the mesoscale frontal wave phenomenon as described in Chapter 5 (Section 5.2.1) but on a longer timescale.

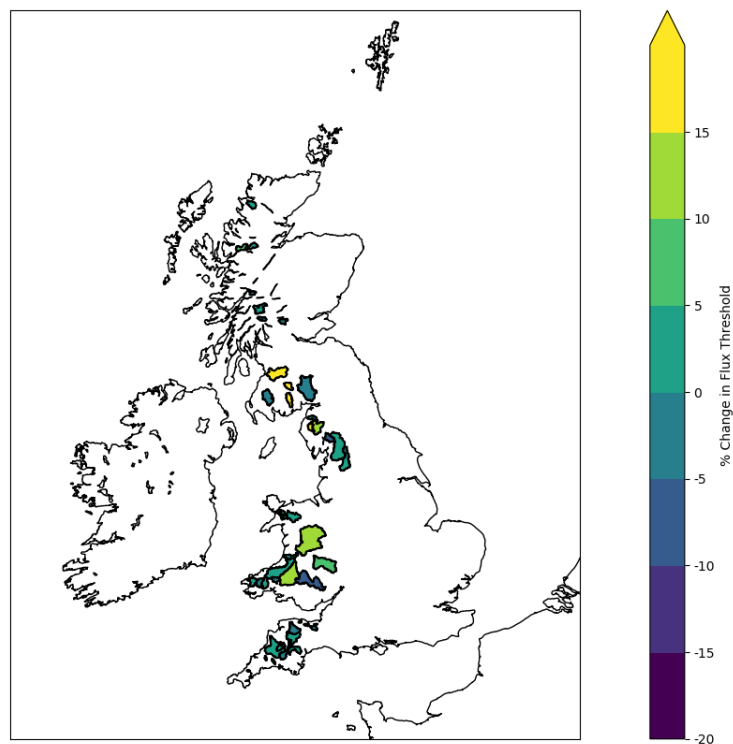


Figure 6.12. AR Duration – IVT Threshold. Somewhat counter-intuitively, an increase in IVT threshold is observed at many catchments as AR duration increases; possibly a reflection of the likely ebb and flow of overhead IVT flux during the longest duration events. Many ARs arrive in ‘families’ and the AR detection algorithm used in this analysis combines together ARs arriving within 24-hours of each other.

6.3.5.2. *Initial Flow Conditions*

The final aim of this section is to investigate the importance of initial flow conditions in shaping the hydrological response of an AR. The 75th percentile of the winter (October to March) flows is calculated at each of the study catchments to assess such conditions. Using the 9hr + catalogue, the landfalling ARs at each catchment are organised as to whether they arrive during 'low' (<75th percentile) or 'high' (> 75th percentile) flow conditions. This allows a comparison of the average IVT thresholds according to the ARs within each group. The 75th percentile was chosen to ensure sufficient sample sizes within each subset, although it is appreciated that any threshold will be somewhat subjective. A discussion on the advantages and disadvantages of taking this approach to assessing antecedent conditions shall be given in Chapter 7 (section 7.4.2).

The majority of catchments show a fall in IVT threshold needed to cause a POT3 flood when comparing the ARs that arrive during high to low flow conditions, with typical values of around 10-15% decrease across Wales and northern England (Fig. 6.13). There are several catchments in Scotland that demonstrate a 35-40% decrease in IVT threshold at high flows.

These results are largely intuitive - assuming the initial flow estimate can be applied as a proxy for catchment wetness, the catchment is expected to be more responsive under 'high' flow conditions. Thus, a weaker AR is required to bring about a similar magnitude hydrological response. The relative changes of IVT threshold across the study catchments, can be used to assess the regions where antecedent wetness matters the most.

Conversely, the results can also help in the identification of catchments where a consideration of initial flow is less important, i.e., where there has been no meaningful change, or even an increase in IVT threshold, when comparing the corresponding results at low and high flows respectively. These catchments include the Lugg along the Welsh borders, many of the smaller catchments in Devon and Cornwall, the Eden in Cumbria, the Urr in southern Scotland and the Orchy within the Scottish Highlands. In addition, it is expected that antecedent conditions are less important in the smaller catchments.

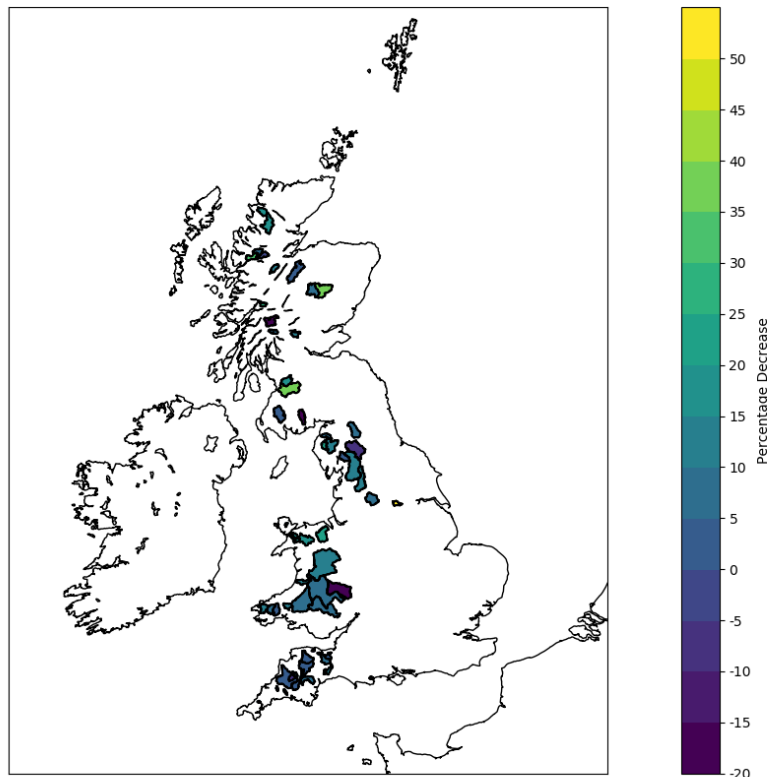


Figure 6.13. Initial Flow and IVT Threshold. Many catchments experience a drop in IVT threshold of around 10-15% when comparing values calculated according to low and high flow conditions respectively. Where no notable difference is found, it can be inferred that immediate river flow considerations are less important.

6.4. Calculating the IVT Threshold from Catchment Properties

In order to bring the results of this chapter together, a predictive model for IVT threshold is developed based on catchment descriptors alone. The projection of the catchment data on the Principal Component Axes (Section 6.3) ensures that the data along each axis are independent; an essential requirement for many regression models.

A key consideration when building a predictive model is the likely relationship between the independent and dependent variables. There is little evidence for strong linear relationships between the IVT threshold and Principal Components (Section 6.3) and, as such, a typical linear regression model is unlikely to be suitable in this case.

Random Forest Regression is a supervised learning algorithm that uses a so-called ensemble learning method to build up a predictive model (Chapter 3, section 3.6.3). The ensemble consists of multiple machine learning algorithms, in this case a collection of decision trees (aka the ‘forest’). A collection of ‘Decision Nodes’, which are based on the Principal Components, will lead to a selection of ‘Leaf Nodes’ that act to predict the IVT threshold. In this study, a total of 10 trees are chosen for the Forest ensemble.

To avoid overfitting, the catchment dataset is split into what are commonly known as ‘train’ and ‘test’ subsets. The ‘train’ dataset is used to build the predictive model, and the ‘test’ dataset to provide an independent test of performance. The relative sizes of the test and train dataset are set at 0.25 and 0.75 respectively. This equates to approximately 17 catchments against 51, as the further two catchments did not show statistical evidence for a preferential subset of ARs (Table 6.1).

As the test and train datasets are selected via a random process, by definition, they will be different each time the model is developed. In order to test its robustness, the model building process is carried out a total of 20 times. This equates to a total of 20 different ‘test’ and ‘train’ datasets, and a corresponding model build.

In general, in the predictive models built through the process match the observed data well, with an R^2 value of approx. 0.79 ± 0.18 (Fig. 6.14). The variables (PCs) with the strongest predictive power – hereon referred to as their ‘importance’ – are also identified. PC1 is the strongest predictor in all the models (with a relative importance of 0.88 ± 0.04), with PC5 and PC3 accounting for a further 0.057 and 0.028 respectively. These results in combination suggests that the predictive model is relatively robust with regard to changes in the test and train datasets.

Variable	Importance (mean)	Importance (std)
PC1	0.875	0.039
PC5	0.057	0.020
PC3	0.028	0.030
PC4	0.021	0.013
PC2	0.019	0.008

R^2 (mean)	R^2 (std)
0.787	0.179

Figure 6.14. Multiple Model Builds. Across the 20 model builds, the results regarding feature importance are relatively robust (left-hand panel) and the predictive model describes the test data well (right-hand panel).

A single model is selected from the collection of builds for descriptive purposes, therefore. With an R^2 value of 0.848 and PC1, PC5 and PC3 the most important descriptor variables in order of importance, the predicted IVT thresholds are found to align well with the observed values (Fig. 6.15). That is, catchment descriptors alone have been successfully applied to deduce the required strength of an impactful AR. In combination with the catchment elevation (Section 6.3.4; Fig 6.9), it is possible to deduce whether AR orientation should be an additional consideration.

For illustrative purposes, two of the ten decision trees that make up the model are presented (Fig. 6.16). Beginning at the first ‘decision node’, where the path left or right depends on the value of a particular principal component (e.g., $PC1 \leq -0.616$ for Estimator 0 and $PC1 \leq -0.601$ for Estimator 5), it is possible to follow the tree until a ‘leaf node’ is obtained, whereupon the IVT threshold is estimated. The estimates from each of the 10 trees in the model form an ensemble, which is averaged to give the final IVT threshold. The model is then retained for future use. Future work may include an analysis of the results ensemble produced by the model.

Prior to the results of this work, it would have been possible to provide an educated guess as to the contributions of different catchment properties in the development of a flood response to ARs, but without a measure of their relative importance. The results presented in the previous sections have gone some way to quantifying this; calculating the relative orientation and/or strength of an impactful AR based on the land-surface properties of the area of interest. Such results can act to enhance existing flood forecasting tools.

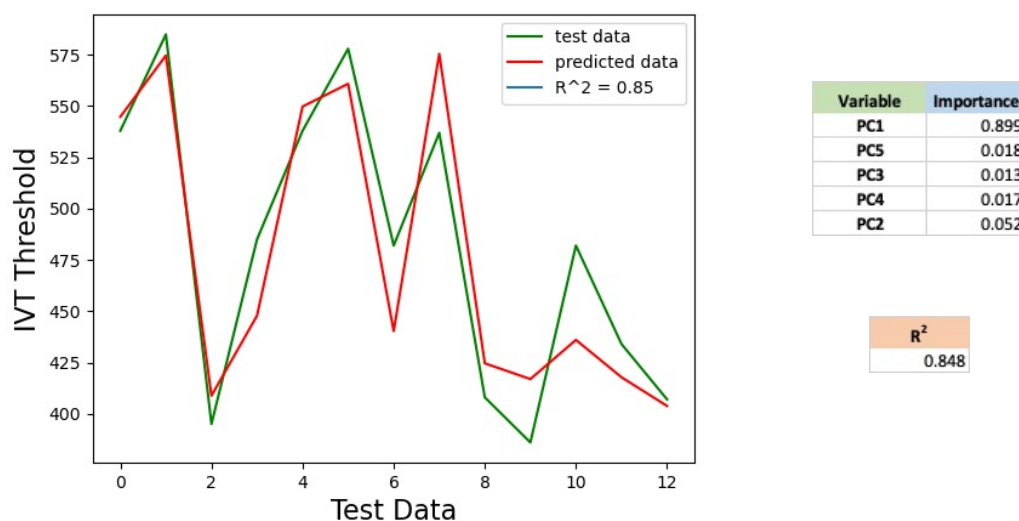


Figure 6.15. Single Model Build (example). This model predicts the test data with an R^2 of 0.85 (a good fit). PC1 accounts for nearly 90% of the importance within the model, followed by PC5 and PC3.

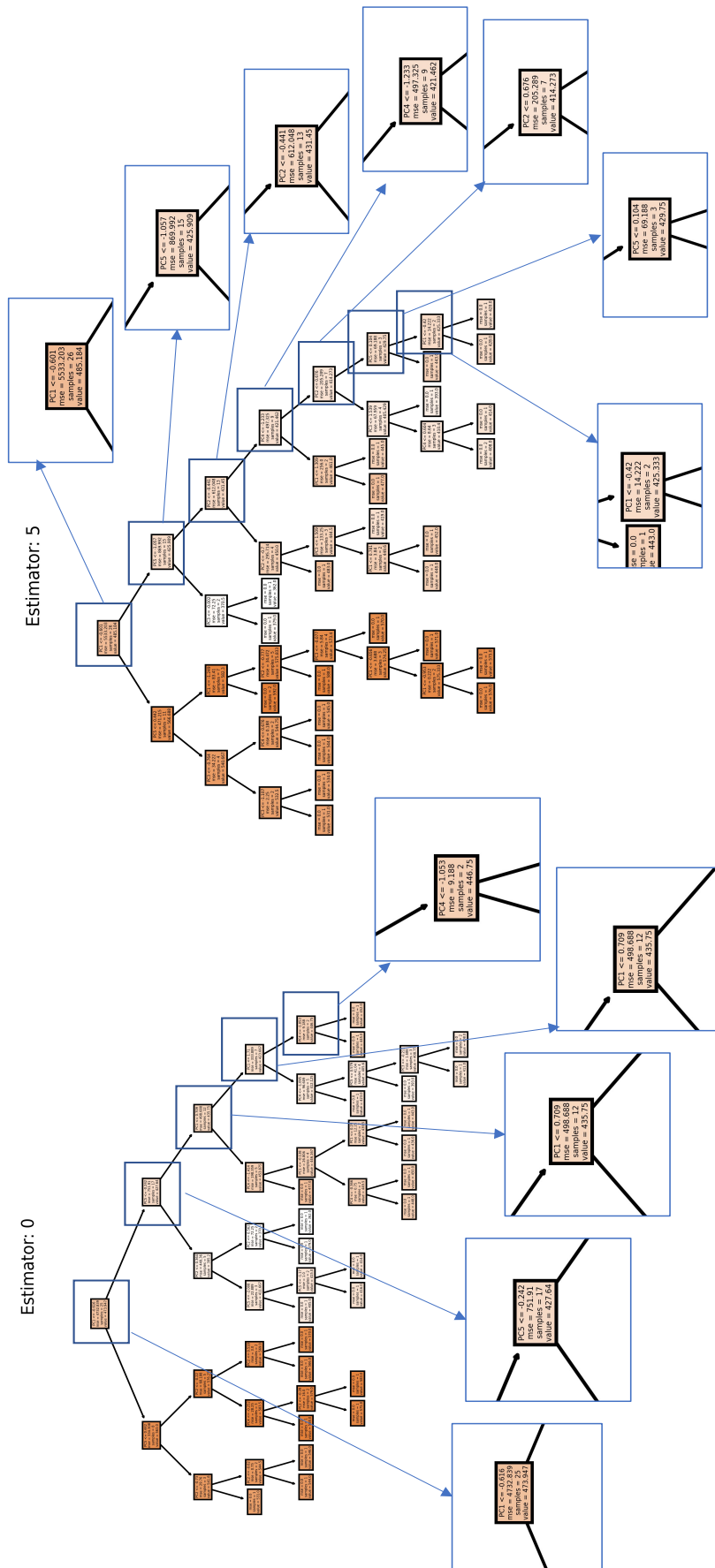


Figure 6.16. Example Trees from the Forest. The model contains a total of ten decision trees with the forest, two of which are presented here. The zoomed in panels show that each decision node refers to a principal component. The model follows the decision nodes until a leaf node is reached and the IVT threshold is predicted.

6.5. Conclusions

In this chapter, the relationship between ARs and extreme (POT3) winter flooding has been explored across a total of 81 catchments located predominantly along the western UK mainland coastline. The aim was to understand the extent that ARs influence extreme flood generation and whether their impact is in turn influenced by the land-surface characteristics of the landfalling area. The role of AR duration and antecedent soil wetness in terms of influencing the hydrological response to AR, was also quantified.

The orientations and/or IVT strengths of the most impactful ARs at each of the study catchments have been extracted. Subsequently referring to each catchment as either ‘orientation’ or ‘flux’ dominated, it has been possible to search for a link between those catchments with a clear, preferential AR trajectory and their land-surface properties. Further, the factors controlling the required strength of an AR has been investigated.

This chapter has intended to address a research gap concerning the influence of catchment level properties on the most impactful ARs. Its final conclusions are detailed below:

- There is evidence for AR impact across a wide range of catchments across the UK. Indeed, when considering persistent ARs of duration of 9hrs and above, ARs can account for up to 70% of POT3 floods across the historical (1982-2010) period in some upland areas of the UK.

This therefore acts as additional evidence that ARs are a clear flood-generator across the UK uplands in the winter months.

- However, in line with previous results (Chapters 2 and 4), nearby catchments appear to respond very differently to the same set of ARs.

The simple presence of an AR is alone insufficient for an intense hydrological response.

- Evidence exists of preferential orientations and/or minimum IVT magnitude thresholds for the most impactful ARs across the study catchments. These requirements are different for each catchment. Using feature selection and Principal Component Analysis, the results have been analysed in the context of catchment descriptors. The elevation of a catchment appears to be a key control on the presence (or not) of a preferential AR

orientation; this is in line with earlier hypotheses regarding the most efficient rainout and/or rain-shadowing effects. The location (in terms of latitude) and elevation in combination appear to influence the IVT threshold for the most impactful ARs. This is in addition to information regarding the underlying geology and soils, and the catchment area.

Catchments with maximum elevations of 400-600m and above are more likely to require a specific orientation of AR if the strongest hydrological responses are to be observed. The IVT threshold for impactful ARs falls moving from the southernmost catchments further north, in line with the expected climatology and the typical elevation. To a lesser degree, catchment area, geology and soils will also influence the IVT threshold.

- Using Random Forest Regression, a predictive model for the IVT threshold has been developed on the basis of the catchment descriptors alone. Over 20 test runs, this model demonstrates a mean R^2 value of 0.79 ± 0.18 . Catchment latitude and elevation are key predictors in this model.

This may provide a method to extend the AR analysis presented here to ungauged, or previously unexplored, catchments, but such a potential requires further work.

- AR duration and the initial flow conditions at the time of AR arrival are important modulators of the IVT required to generate a POT3 flood. In the majority of cases, the required IVT increases as the AR duration increases, likely a result of ebbs and flow in the overhead IVT flux during the longest duration events. In contrast, the required IVT falls when the AR arrives on the backdrop of 'high' versus 'low' flow conditions.

AR properties alone are not sufficient to predict AR impact. In many cases, the initial flow of the catchment at the time of AR arrival will modulate the predicted values.

Chapter 7 Bringing it All Together: An AR Impacts Prediction Framework and Discussion of Results

7.1 Introduction

For the first time, it has been possible to quantify the relative contributions of catchment properties in modulating AR impact (Chapter 6, section 6.3.3). Combined into a predictive model (section 6.4), the existence of preferential orientation bands and/or IVT thresholds have been calculated across the set of study catchments.

This chapter aims to combine this information in the form of an AR impact framework, which will act to identify the catchments most likely affected by an incoming AR of given orientation, strength and landfalling location. This framework is then tested in the context of several high-profile storms of the last decade.

Finally, a critical assessment and discussion regarding the results of this thesis is undertaken. The key aims and objectives shall be reassessed and the successes, and possible limitations, of the thesis are explored. The latter will be used to decide upon the most effective directions of future work, as outlined in the Conclusions chapter (Chapter 8).

7.2. A Proposed AR Prediction Framework

The ERA5 reanalysis dataset allows for a near real time availability of atmospheric properties (Copernicus Climate Change Service Climate Data Store (CDS), 2017; Chapter 3, section 3.3.1). The magnitude and orientation of IVT flux overhead of a given point are relatively easy to calculate, and as such the suggested framework will be based on these variables.

Preferential orientation bands and IVT thresholds (Chapter 6, section 6.2.2) are used to develop a simple scoring system (Fig. 7.1), which will act to translate the properties (orientation and strength) of a landfalling AR into severity of impact potential at a given catchment. Scores of zero, one, two or three are returned, as a measure of the relative impact severity from least (0) to greatest (3). This scoring allows comparison of anticipated impact across the study region.

Previous work of this type includes the AR Categorisation Scale as initially posed by Ralph et al. (2019) for those features impacting the US West Coast, later extended to European regions by Eiras-Barca et al., (2021). This scale uses a combination of (maximum) overhead IVT magnitude and duration to infer an AR category spanning 1 through 5. A category 1 AR is primarily beneficial, providing essential moisture recharge during the winter months, whilst a category 5 AR may be strong and/or persistent enough to present a notable hazard. Previous work regarding tropical cyclone (TC) flooding in the Philippines (Macalalad et al., 2021), proposed a simple checklist method concerning TC trajectory, season and expected rainfall totals. Identified as key controls on the extent of expected flooding, such an idea was suggested as useful in regions of limited data and/or forecasting resources.

The AR framework is therefore developed in line with such approaches, aiming to produce as output a numerical value of expected impact. The key variables of AR impact potential (magnitude and orientation) are assessed in the form of a flow chart. Equal weighting is applied to both orientation and flux dominated catchments, such that they result in the same 'maximum' score, despite a different number of decision stages (Fig 7.1). Simplicity and transparency were a key consideration when developing the framework, in pursuit of an effective test of performance. It is expected that any such tool will be developed and possibly modified as the research progresses.

A test of the framework will take place in the context of several high-profile AR storms. Occurring within the last decade, these storms exist outside of the catalogue used in previous stages of the analysis, and thus provide an independent test of results. For simplicity, information regarding AR duration or antecedent flow conditions will not be directly included and will instead be presented alongside the results of the framework. The effectiveness of the framework will be analysed through the inclusion of hydrological data following AR arrival. The maximum flow within three days of AR arrival is retained and compared to POT1, 3 and 5 thresholds, calculated in the same way as in previous stages of this work (Chapter 3, section 3.4).

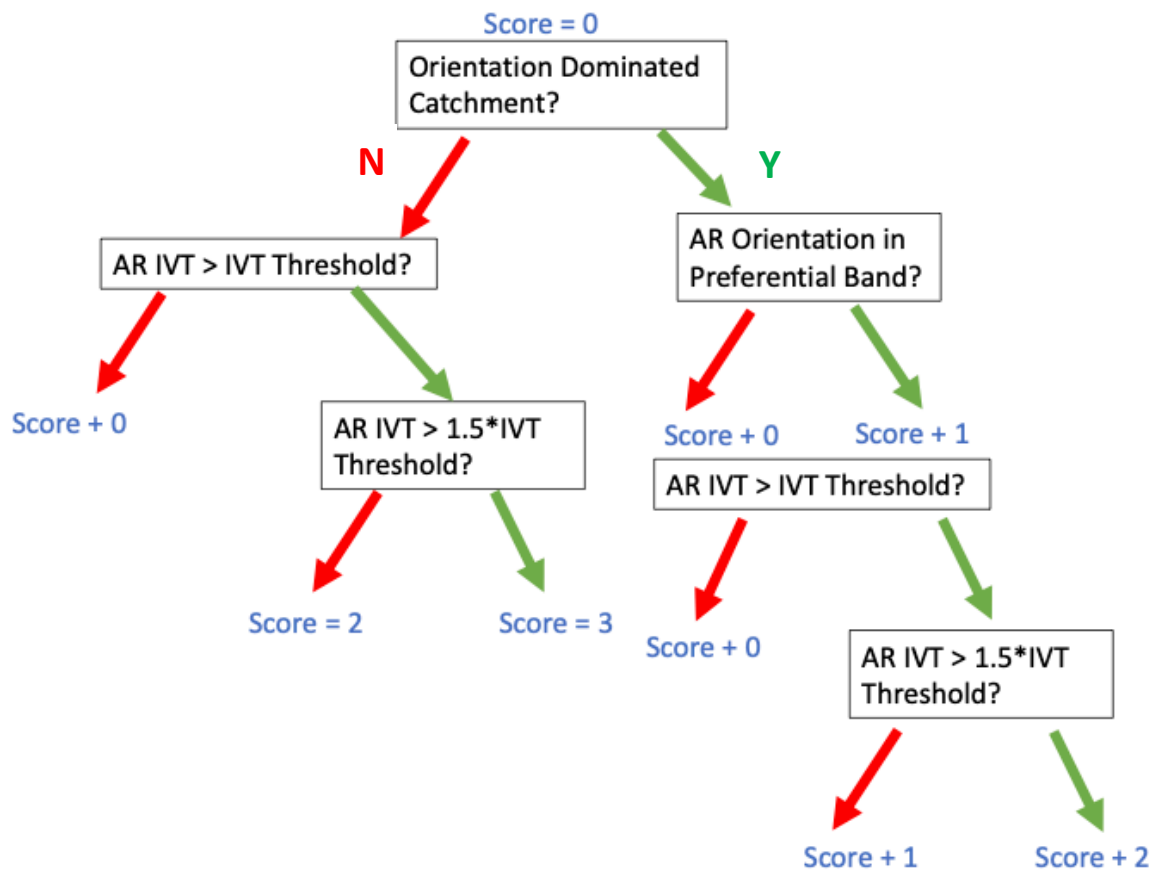


Figure 7.1. The Proposed AR Impacts Framework. Using information regarding AR orientation and strength, a simple scoring system is proposed. The relevant preferential orientation bands and IVT thresholds were deduced in Chapter 6 for the study region. For simplicity, information regarding AR duration and/or antecedent flow conditions has not been included. This instead will be presented alongside the results of the framework.

7.3.1. Storm Desmond: 3rd-8th December 2015

Storm Desmond, and its associated AR tail, made landfall on the western coastline of the UK on the 5th of December 2015 with a total lifetime of approximately 39 hours. It set a new 24-hour rainfall record (as over 341mm of rain were recorded in Honister Pass in Cumbria) and brought winds of up to 112 mph (recorded in the Scottish Highlands). The worst affected areas were predominantly Cumbria, parts of Lancashire and the Scottish borders. It is estimated that approximately 5000 homes were internally flooded across the north-west of England, although the disruption caused by road blockages, landslides and power outages were much further reaching. The total damage has been estimated at over £870 million with at least three reported fatalities.

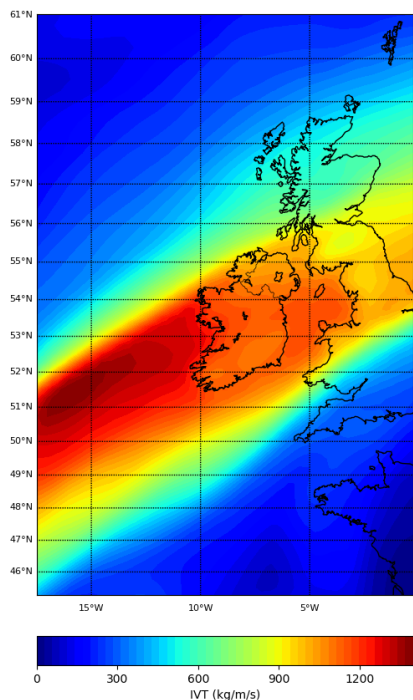


Figure 7.2. Storm Desmond. The Integrated Vapour Transport as calculated from ERA5 reanalysis on the 5th of December 2015 1300UTC. The atmospheric river associated with Storm Desmond can be easily identified, with the peak of the flux centered on northern England (average landfalling location 57.5°).

The AR associated with storm Desmond can be easily identified within the overhead IVT flux taken during the peak of the storm (Fig. 7.2). The strongest AR IVT flux falls across Cumbria and northern England. With an average landfalling location of 57.5°, and considering the landfalling latitude shown in Fig. 7.2, it is possible to deduce that the axis of the AR drifts northward over its lifetime (and as such the duration of overhead AR conditions at a given location will likely to be less than the total lifetime of the AR). The antecedent river flow conditions at the time of the AR arrival are expressed as a percentile of historical winter flow (Fig.7.3a). Many of the rivers in Cumbria and southern Scotland were flowing at very high levels, as were many in Snowdonia and north-western Wales.

The AR impacts framework (Fig 7.3b) predicts the strongest response in regions of Cumbria and north Wales (score level 2, out of a possible 3). This is in line with the observed maximum flows in the following three days (Fig 7.3c); Cumbria and northern England experienced floods of magnitude greater than POT1, in line with historical evidence. The full results are given in Table 7.1.

The framework is able to identify many catchments, primarily located across the northwest of England and north Wales, that are susceptible to the IVT strength and orientation demonstrated by Storm Desmond (Table 7.1). In combination with high antecedent river flows, typically >95th

percentile, many of these catchments demonstrate intense floods in response (POT1 or POT3). Understanding the relative difference in flood magnitudes, especially within those catchments demonstrating similar antecedent flows, when subject to the same 'score' AR is a region for future consideration.

It is possible to highlight several catchments where the performance of the framework has been less accurate, either where a particular impact has been implied but not observed (e.g., 27029 and 16003), or vice versa (e.g, 55002). These catchments can be identified as the Calder at Elland (Fig. 3.3), Ruchill Water at Cultybraggan (Fig. 3.4) and the Wye at Belmont (Fig 3.2) respectively.

Located in the Pennines, Scottish Highlands and Welsh Borders respectively, these catchments can all be identified as eastward flowing. As such the orientation of the catchments may be expected to be less susceptible to the direct orographic enhancement of AR moisture, perhaps instead susceptible to a spill-over effect as the moisture is forced upward by catchments to the west. A detailed analysis of the framework's performance on eastward and westward orientated catchments is therefore highlighted as a region of future work.

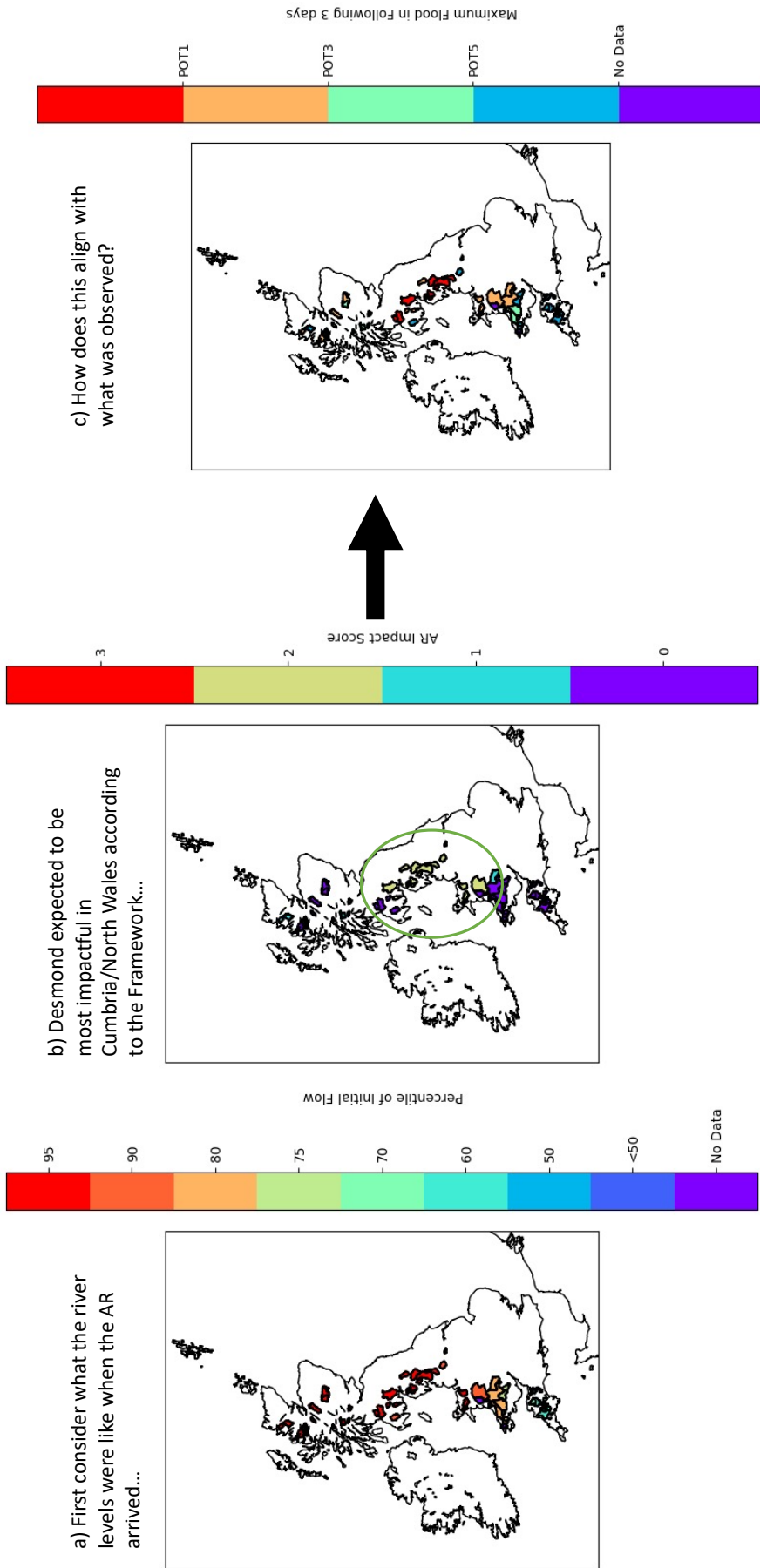


Figure 7.3. Storm Desmond Impacts. Panel (a) shows the river levels at the time of storm arrival expressed as a percentile of winter flows. In the main, rivers in northern England, southern Scotland and north Wales were flowing at very high levels. Panel (b) shows the score extracted from the AR impacts framework based on the magnitude and orientation of the storm only. Panel (c) shows the observed maximum flow in the following 3 days in terms of POT1, 3 and 5 thresholds. The largest floods were observed in Cumbria, in line with historical evidence.

Storm Desmond										Storm Clara										Storm Dennis									
Catchment Code	% Decrease in IWT Threshold at High Flows (Fig. 6.13)	Initial Flow Score	Percentile Equivalent	AR Framework Score	Max Flow Score	Flood Equivalent	Catchment Code	% Decrease in IWT Threshold at High Flows (Fig. 6.13)	Initial Flow Score	Percentile Equivalent	AR Framework Score	Max Flow Score	Flood Equivalent	Catchment Code	% Decrease in IWT Threshold at High Flows (Fig. 6.13)	Initial Flow Score	Percentile Equivalent	AR Framework Score	Max Flow Score	Flood Equivalent									
65004	23.4	7	>95%	2	3	PO11	23006	4.1	7	>95%	2	3	PO11	27054	49.0	7	>95%	3	3	PO11									
65006	10.7	7	>95%	2	3	PO11	27029	2.1	7	>95%	2	3	PO11	52002	0.8	7	>95%	3	3	PO11									
71006	9.8	7	>95%	2	3	PO11	65001	11.8	7	>95%	2	3	PO11	61002	3.5	7	>95%	3	3	PO11									
73001	5.6	7	>95%	2	3	PO11	65004	22.4	7	>95%	2	3	PO11	64008	9.2	7	>95%	3	3	PO11									
73002	4.5	7	>95%	2	3	PO11	65011	13.4	7	>95%	2	3	PO11	64009	9.2	7	>95%	3	3	PO11									
73003	6.5	7	>95%	2	3	PO11	71006	3.6	7	>95%	2	3	PO11	81003	12.8	6	90.95%	2	1	PO12									
73004	6.5	7	>95%	2	3	PO11	73006	3.6	7	>95%	2	3	PO11	81005	31.1	6	90.95%	3	0	<PO12									
73007	3.8	7	>95%	2	3	PO11	73012	15.2	7	>95%	2	3	PO11	81007	2.1	6	80.90%	3	0	<PO12									
73008	10.7	7	>95%	2	3	PO11	75001	3.2	7	>95%	2	3	PO11	81008	1.6	2	80.90%	3	0	<PO12									
73009	4.1	7	>95%	2	3	PO12	75002	3.7	7	>95%	2	3	PO12	81009	2	2	80.90%	3	0	<PO12									
73010	11.8	7	>95%	2	3	PO12	75003	32.7	7	>95%	2	2	PO13	81010	2	2	80.90%	3	0	<PO12									
73011	11.8	7	>95%	2	3	PO12	81006	23.7	7	>95%	2	2	PO13	83006	4.8	2	50.45%	2	0	<PO12									
73012	13.4	7	>95%	2	3	PO12	83007	21.1	6	90.95%	2	1	PO15	83008	3.2	7	>95%	2	3	PO11									
73013	13.4	7	>95%	2	3	PO12	83009	31.1	6	90.95%	2	1	PO15	86004	13.9	7	>95%	2	3	PO11									
73014	48.6	7	>95%	2	3	PO12	83010	1.1	6	90.95%	2	1	PO15	86005	3.1	7	>95%	2	3	PO11									
73015	7.1	7	>95%	2	3	PO12	83011	5.0	5	80.90%	2	3	PO15	86006	1.9	7	>95%	2	3	PO11									
73016	6.1	6	90.95%	2	1	PO12	75005	49.0	4	75.80%	2	3	PO11	86007	1.7	7	>95%	2	3	PO11									
73017	7.2	9	>95%	2	1	PO12	55002	32.1	2	60.70%	2	2	PO13	86008	6.1	7	>95%	2	3	PO11									
73018	2.6	6	90.95%	2	0	<PO12	55003	0.7	1	No Data	2	1	No Data	86009	4.6	7	>95%	2	1	PO12									
73019	14.5	9	>95%	1	2	PO12	55006	15.2	1	No Data	2	1	No Data	86010	8.6	7	>95%	2	1	PO12									
73020	32.1	5	80.90%	1	1	PO12	46001	15.2	1	No Data	2	1	No Data	86011	2.0	7	>95%	1	3	PO11									
73021	32.1	5	80.90%	1	1	PO12	49001	1.9	7	>95%	1	0	<PO12	86012	3.7	7	>95%	2	1	PO12									
73022	10.7	7	>95%	1	0	<PO12	49002	3.9	7	>95%	1	0	<PO12	86013	3.1	7	>95%	2	1	PO12									
73023	28.5	7	>95%	1	0	<PO12	49003	1.3	7	>95%	1	2	PO13	86014	9.6	7	>95%	2	1	PO12									
73024	6.1	6	90.95%	1	0	<PO12	49004	1.3	7	>95%	1	2	PO13	86015	9.6	7	>95%	2	1	PO12									
73025	27.7	6	90.95%	1	0	<PO12	55001	2.1	7	>95%	1	2	PO13	86016	2.1	7	>95%	2	1	PO12									
73026	32.2	9	>95%	1	0	<PO12	55002	48.6	2	>95%	1	2	PO13	86017	2.1	7	>95%	2	1	PO12									
73027	32.2	9	>95%	1	0	<PO12	55003	48.6	2	>95%	1	2	PO13	86018	2.1	7	>95%	2	1	PO12									
73028	32.2	9	>95%	1	0	<PO12	55004	48.6	2	>95%	1	2	PO13	86019	2.1	7	>95%	2	1	PO12									
73029	32.2	9	>95%	1	0	<PO12	55005	48.6	2	>95%	1	2	PO13	86020	2.1	7	>95%	2	1	PO12									
73030	32.2	9	>95%	1	0	<PO12	55006	48.6	2	>95%	1	2	PO13	86021	2.1	7	>95%	2	1	PO12									
73031	32.2	9	>95%	1	0	<PO12	55007	48.6	2	>95%	1	2	PO13	86022	2.1	7	>95%	2	1	PO12									
73032	32.2	9	>95%	1	0	<PO12	55008	48.6	2	>95%	1	2	PO13	86023	2.1	7	>95%	2	1	PO12									
73033	32.2	9	>95%	1	0	<PO12	55009	48.6	2	>95%	1	2	PO13	86024	2.1	7	>95%	2	1	PO12									
73034	32.2	9	>95%	1	0	<PO12	55010	48.6	2	>95%	1	2	PO13	86025	2.1	7	>95%	2	1	PO12									
73035	32.2	9	>95%	1	0	<PO12	55011	48.6	2	>95%	1	2	PO13	86026	2.1	7	>95%	2	1	PO12									
73036	32.2	9	>95%	1	0	<PO12	55012	48.6	2	>95%	1	2	PO13	86027	2.1	7	>95%	2	1	PO12									
73037	32.2	9	>95%	1	0	<PO12	55013	48.6	2	>95%	1	2	PO13	86028	2.1	7	>95%	2	1	PO12									
73038	32.2	9	>95%	1	0	<PO12	55014	48.6	2	>95%	1	2	PO13	86029	2.1	7	>95%	2	1	PO12									
73039	32.2	9	>95%	1	0	<PO12	55015	48.6	2	>95%	1	2	PO13	86030	2.1	7	>95%	2	1	PO12									
73040	32.2	9	>95%	1	0	<PO12	55016	48.6	2	>95%	1	2	PO13	86031	2.1	7	>95%	2	1	PO12									
73041	32.2	9	>95%	1	0	<PO12	55017	48.6	2	>95%	1	2	PO13	86032	2.1	7	>95%	2	1	PO12									
73042	32.2	9	>95%	1	0	<PO12	55018	48.6	2	>95%	1	2	PO13	86033	2.1	7	>95%	2	1	PO12									
73043	32.2	9	>95%	1	0	<PO12	55019	48.6	2	>95%	1	2	PO13	86034	2.1	7	>95%	2	1	PO12									
73044	32.2	9	>95%	1	0	<PO12	55020	48.6	2	>95%	1	2	PO13	86035	2.1	7	>95%	2	1	PO12									
73045	32.2	9	>95%	1	0	<PO12	55021	48.6	2	>95%	1	2	PO13	86036	2.1	7	>95%	2	1	PO12									
73046	32.2	9	>95%	1	0	<PO12	55022	48.6	2	>95%	1	2	PO13	86037	2.1	7	>95%	2	1	PO12									
73047	32.2	9	>95%	1	0	<PO12	55023	48.6	2	>95%	1	2	PO13	86038	2.1	7	>95%	2	1	PO12									
73048	32.2	9	>95%	1	0	<PO12	55024	48.6	2	>95%	1	2	PO13	86039	2.1	7	>95%	2	1	PO12									
73049	32.2	9	>95%	1	0	<PO12	55025	48.6	2	>95%	1	2	PO13	86040	2.1	7	>95%	2	1	PO12									
73050	32.2	9	>95%	1	0	<PO12	55026	48.6	2	>95%	1	2	PO13	86041	2.1	7	>95%	2	1	PO12									
73051	32.2	9	>95%	1	0	<PO12	55027	48.6	2	>95%	1	2	PO13	86042	2.1	7	>95%	2	1	PO12									
73052	32.2	9	>95%	1	0	<PO12	55028	48.6	2	>95%	1	2	PO13	86043	2.1	7	>95%	2	1	PO12									
73053	32.2	9	>95%	1	0	<PO12	55029	48.6	2	>95%	1	2	PO13	86044	2.1	7	>95%	2	1	PO12									
73054	32.2	9	>95%	1	0	<PO12	55030	48.6	2	>95%	1	2	PO13	86045	2.1	7	>95%	2	1	PO12									
73055	32.2	9	>95%	1	0	<PO12	55031	48.6	2	>95%	1	2	PO13	86046	2.1	7	>95%	2	1	PO12									
73056	32.2	9	>95%	1	0	<PO12	55032	48.6	2	>95%	1	2	PO13	86047	2.1	7	>95%	2	1	PO12									
73057	32.2	9	>95%	1	0	<PO12	55033	48.6	2	>95%	1	2	PO13	86048	2.1	7	>95%	2	1	PO12									
73058	32.2	9	>95%	1	0	<PO12	55034	48.6	2	>95%	1	2	PO13	86049	2.1	7	>95%	2	1	PO12									
73059	32.2	9	>95%	1	0	<PO12	55035	48.6	2	>95%	1	2	PO13	86050	2.1	7	>95%	2	1	PO12									
73060	32.2	9	>95%	1	0	<PO12	55036	48.6	2	>95%	1	2	PO13	86051	2.1	7	>95%	2	1	PO12									
73061	32.2	9	>95%	1	0	<PO12	55037	48.6	2	>95%	1	2	PO13	86052	2.1	7	>95%	2	1	PO12									
73062	32.2	9	>95%	1	0	<PO12	55038	48.6	2	>95%	1	2	PO13	86053	2.1	7	>95%	2	1	PO12									
73063	32.2	9	>95%	1	0	<PO12	55039	48.6	2	>95%	1	2	PO13	86054	2.1	7	>95%	2	1	PO12									
73064	32.2	9	>95%	1	0	<PO12	55040	48.6	2	>95%	1	2	PO13	86055	2.1	7	>95%	2	1	PO12									
73065	32.2	9	>95%	1	0	<PO12	55041	48.6	2	>95%	1	2	PO13	86056	2.1	7	>95%	2	1	PO12									
73066	32.2	9	>95%	1	0	<PO12	55042	48.6	2	>95%	1	2	PO13	86057	2.1	7	>95%	2	1	PO12									
73067	32.2	9	>95%	1	0	<PO12	55043	48.6	2	>95%	1	2	PO13	86058	2.1	7	>95%	2	1	PO12									
73068	32.2	9	>95%	1	0	<PO12	55044	48.6	2	>95%	1	2	PO13	86059	2.1	7	>95%	2	1	PO12									
73069	32.2	9	>95%	1	0	<PO12	55045	48.6	2	>95%	1	2	PO13	86060	2.1	7	>95%	2	1	PO12									
73070	32.2	9	>95%	1	0	<PO12	55046	48.6	2	>95%	1	2	PO13	86061	2.1	7	>95%	2	1	PO12									
73071	32.2	9	>95%	1	0	<PO12	55047	48.6	2	>95%	1	2	PO13	86062															

7.3.2. Storms Ciara and Dennis: 8-9th and 15-16th February 2020

February 2020 currently stands as the wettest February on record for most of the UK (*Record Breaking Rainfall - Met Office*), largely driven by the arrival of storms Ciara and Dennis less than one week apart. When storm Ciara hit overnight on the 8th of February, gusts of up to 97mph were recorded off the coast of the Isle of Wight and, in combination with an intense band of rainfall, it drove rivers to record levels across parts of north Wales, northern England and the Scottish borders. There was widespread travel disruption and hundreds of properties were flooded across Northern England and North Wales. In total, the AR associated with storm Ciara persisted for 17 hours, with an average axis location of 54.5°N.

There was little time to recover before storm Dennis (and its associated AR) made landfall on the 15th of February. Nearly a month's worth of rain fell in the south Wales Valleys in less than 24 hours, this on the back of increasingly saturated conditions from the week prior. The most severe weather warning – a red 'danger to life' warning – was issued by the Met Office for regions of south Wales, with amber and yellow warnings in place for much of England, Wales and southern Scotland. Estimates put the number of internally flooded properties upward of 500, many of whom were in a similar position the week before. At least five fatalities were reported during the combined arrival of Storms Ciara and Dennis. Arriving with a more southerly trajectory (average axis location of 50°N), the AR associated with storm Dennis persisted for a total of 38 hours, gradually drifting northward over its lifetime.

It is possible to extract the typical overhead IVT flux during storms Ciara and Dennis (Fig. 7.4), where the different shapes and sizes of ARs are apparent. Ciara resulted in the delivery of short duration, intense atmospheric moisture to regions of Snowdonia and northern England, whilst Dennis resulted in more sustained delivery to more southerly catchments.

The results of the AR impact framework for Storms Ciara and Dennis are presented (Fig. 7.5 and 7.6 respectively). The left-hand panels describe the antecedent river flows at the time of AR arrival, the central panels describe the results of our AR impact framework, and the right-hand panels present the maximum recorded floods in the three-days following AR arrival. The full results are given in Table 7.1.

At the time of arrival of Storm Ciara, rivers in Cumbria, southern Scotland and south Wales were at very high levels (>90th percentile). According to the AR impacts framework, the AR was expected to be most impactful in Cumbria and north Wales, with additional effects in southern Scotland (risk score 2 out of a possible 3). The observed floods in the following three days match up well with these combined predictions.

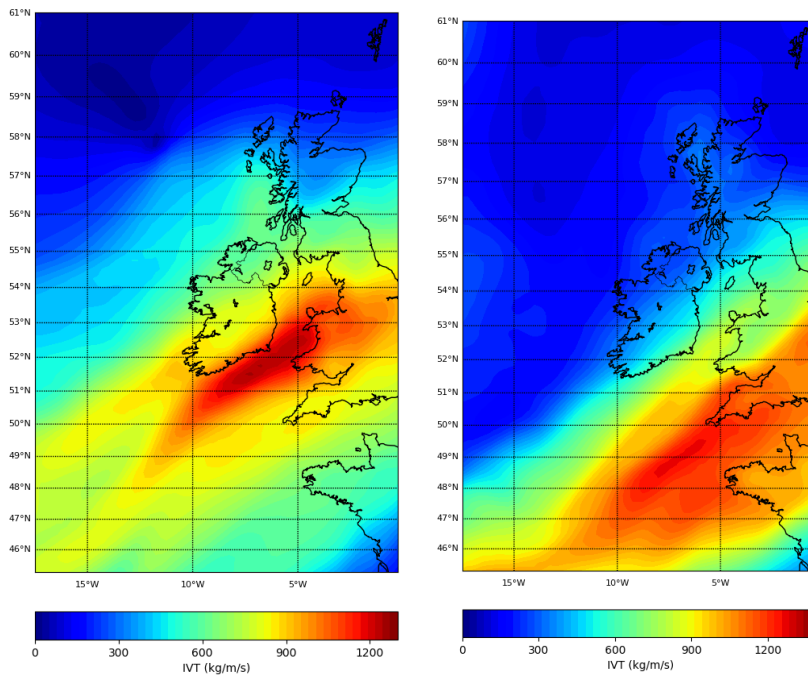


Figure 7.4. Storms Ciara and Dennis. The Integrated Vapour Transport as calculated from ERA5 reanalysis on the 9th of February 2020 0700UTC (left-hand panel; Storm Ciara) and the 16th of February 2020 0200UTC (right-hand panel; Storm Dennis). Where storm Ciara delivered high-intensity, short duration moisture flux to regions of north and western Wales, storm Dennis was centred on parts of south-Wales and Cornwall and resulted in more sustained rainfall.

By the time Storm Dennis arrived a week later, nearly all rivers across the UK were flowing very high (Fig 7.6a). Soils were likely saturated, and many catchments primed to respond strongly to any additional rainfall. Dennis brought persistent rainfall to southern catchments and the AR impacts framework flags up several catchments in south Wales with a maximum impact score of three. These regions are in line with the historical accounts of the strongest impacts following the storm. Combining the framework predictions with antecedent catchment conditions allows effective communication of those regions most likely to demonstrate the strongest hydrological response to the incoming AR.

It is possible to identify many catchments across northern England and south Wales that were correctly predicted by the framework to be susceptible to intense hydrological impacts during storms Ciara and Dennis respectively (Table 7.1). Understanding the sensitivity of the study catchments to initial flows however, particularly when subject to a similar ‘score’ AR, is a region of further study.

Several catchments are identified as being poorly predicted by the framework, either in terms of minimal flood response when subject to a high score AR on high initial flow conditions, or vice versa. Examples during Storm Ciara include the Dee at Polhollick in northeastern Scotland (12003; Fig. 3.5) and East Dart at Bellever in Devon (46005; Fig. 3.6) for the former case, and Wye at Belmont (55002; Fig 3.2) in the latter.

During Storm Dennis, it is possible to identify a number of catchment subject to a score three AR (the maximum possible score), with moderate antecedent flow conditions that do not generate a notable flood. Examples include the Dee at Polhollick once more (12003; Fig 3.5), Findhorn at Shenachie in the Scottish Highlands (7001; Fig 3.5), Scar Water at Capenoch in southwestern Scotland (79004; Fig 3.4) and nearby Ayr at Mainholm (83006; Fig. 3.4).

Similar to the results of storm Desmond, many of the catchments identified above show an eastward aspect. That is, they are unlikely to be directly responsible for the orographic enhancement of atmospheric moisture within ARs, which ultimately triggers the rainfall. Instead, they are more likely to be subject to the rain shadowing effects of the AR rising over western catchments. Understanding the performance of the framework, and ultimately the rainfall generation processes, at these types of catchments is a region of further work.

Another aspect to bear in mind is overhead translation speed of the AR. Given the known landfalling location of storm Dennis, and its subsequent passage northward over its lifetime, it is unlikely that the north-western catchments of Scotland were subject to AR conditions for the entirety of the AR duration. Perhaps the conditions they did experience were indeed score three on the framework scale, but that these conditions did not persist for long enough to generate a notable flood event.

Understanding how the assumptions and methodology of the AR framework perform in these types of situations will be essential for enhancing its operational potential.

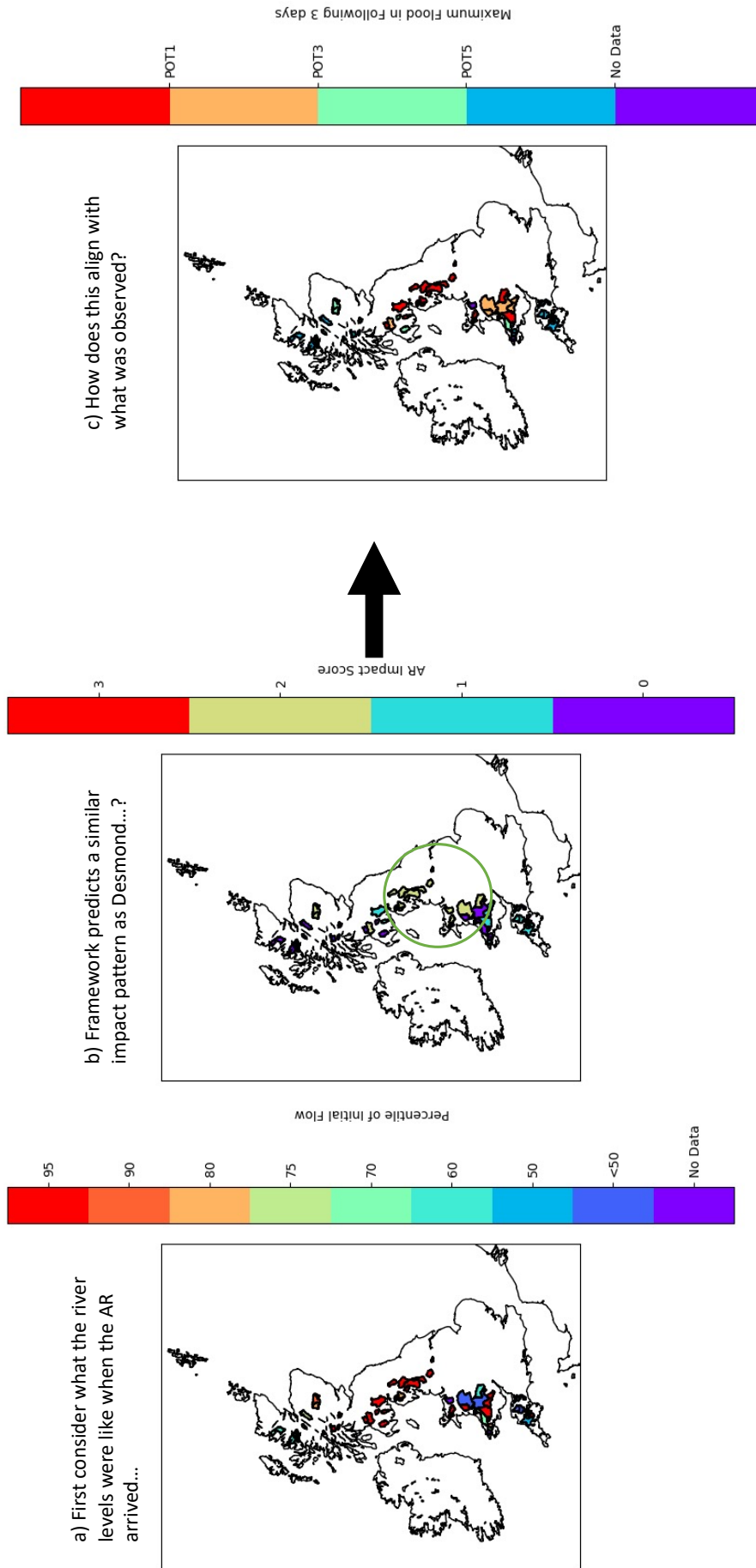


Figure 7.5. Storm Ciara Impacts. Panel (a) shows the river levels at the time of storm arrival expressed as a percentile of winter flows. In the main, rivers in northern England and south Wales were flowing at very high levels. Panel (b) shows the score extracted from the AR impacts framework based on the magnitude and orientation of the storm only. Panel (c) shows the observed maximum flow in the following 24hours in terms of POT1, 3 and 5 thresholds. The strongest floods were observed in northern England and across Wales.

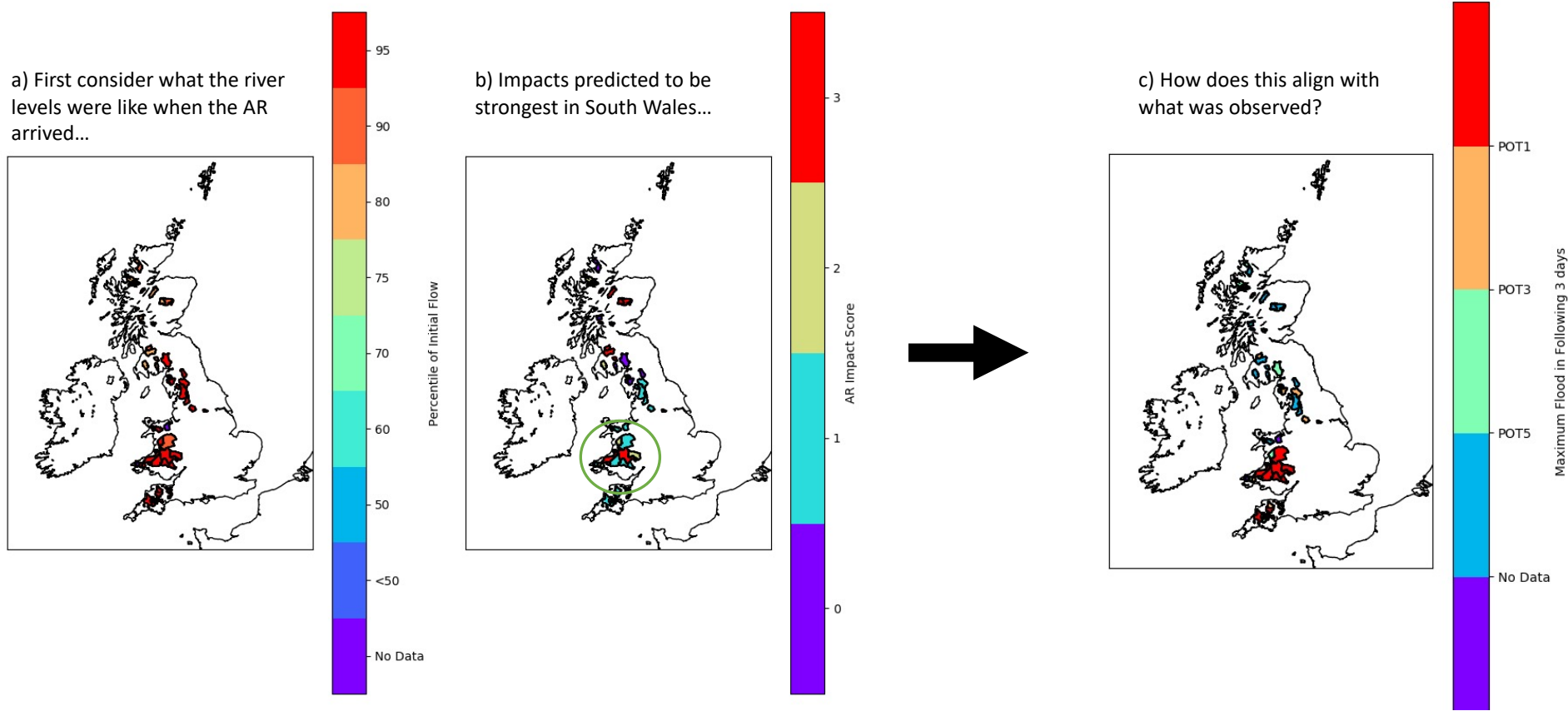


Figure 7.6. Storm Dennis Impacts. Panel (a) shows the river levels at the time of storm arrival expressed as a percentile of winter flows. As expected from Storm Ciara not long previously, river levels were high across the country. Panel (b) shows the score extracted from the AR impacts framework based on the magnitude and orientation of the storm only. Panel (c) shows the observed maximum flow in the following 24hours in terms of POT1, 3 and 5 thresholds. The strongest floods are found in south Wales, in line with historical evidence.

7.3.3. Storm Christoph: 19-20th January 2021

Storm Christoph made the headlines earlier this year when it brought nearly a month's worth of rainfall to regions of Cheshire, Lancashire, Greater Manchester and north-eastern Wales. Arriving alongside a particularly persistent AR, which then subsequently stalled over the UK for several days, it drove the rivers Mersey, Bollin and Dee to record breaking levels. Over 3,000 people were evacuated from their homes but in general the impact to property was lower than anticipated, likely attributed to the ongoing flood defences within many of the affected areas. However, the disruption and mental turmoil were exacerbated due to the storm arriving on the backdrop of the Covid-19 global pandemic.

The IVT flux magnitude demonstrated by the storm is much lower than those of the previous case studies (Fig. 7.7). Hydrological information was unavailable at the time of writing, and therefore only the results of the impacts framework are presented (i.e., based on AR magnitude and orientation alone; Fig. 7.8).

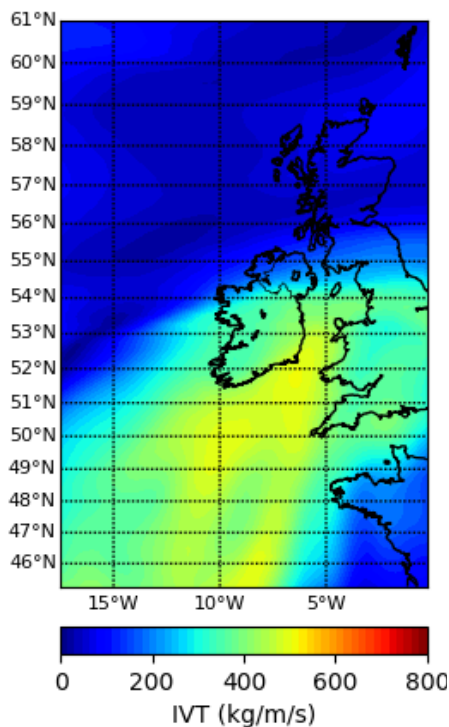


Figure 7.7. Storm Christoph. The Integrated Vapour Transport as calculated from ERA5 reanalysis on the 19th of January 2021 1200UTC. The relative magnitude of this storm is lower than the previous case studies.

The AR Framework is able to identify regions of south Wales and the Welsh borders as being particularly at risk from the AR alone. It is important to highlight that this storm was impactful due to its stationarity (Fig. 7.9), despite the AR being weaker than many studied so far. Perhaps the steep, flashy catchments within the study region (for example, in north-western Wales and

upland regions of Cumbria) were most effective at channelling the (low intensity) generated runoff through the river basin. In regions surrounding the Welsh borders and into central England, where rivers typically respond more slowly, perhaps the effects of Christoph compounded over the lifetime of the event. Such an event will be discussed further in this chapter (section 7.4.3).

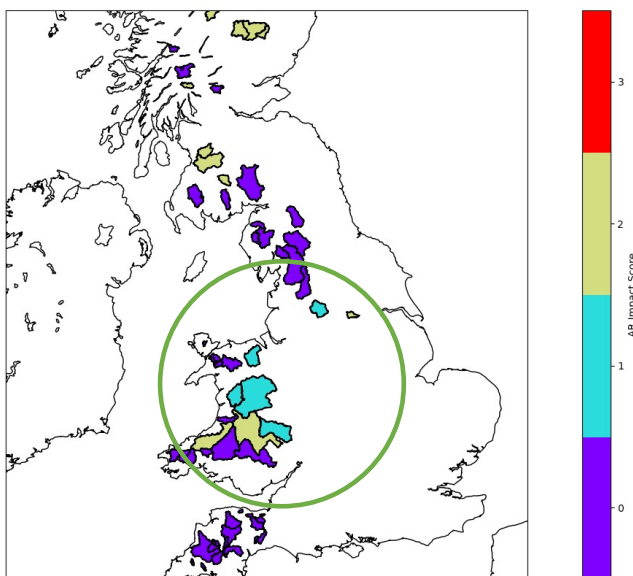


Figure 7.8. Storm Christoph Impacts. The score as calculated from the impact framework. From the AR properties alone, catchments in central England, the Welsh borders and the southern Welsh Valleys are highlighted as being particularly at risk.

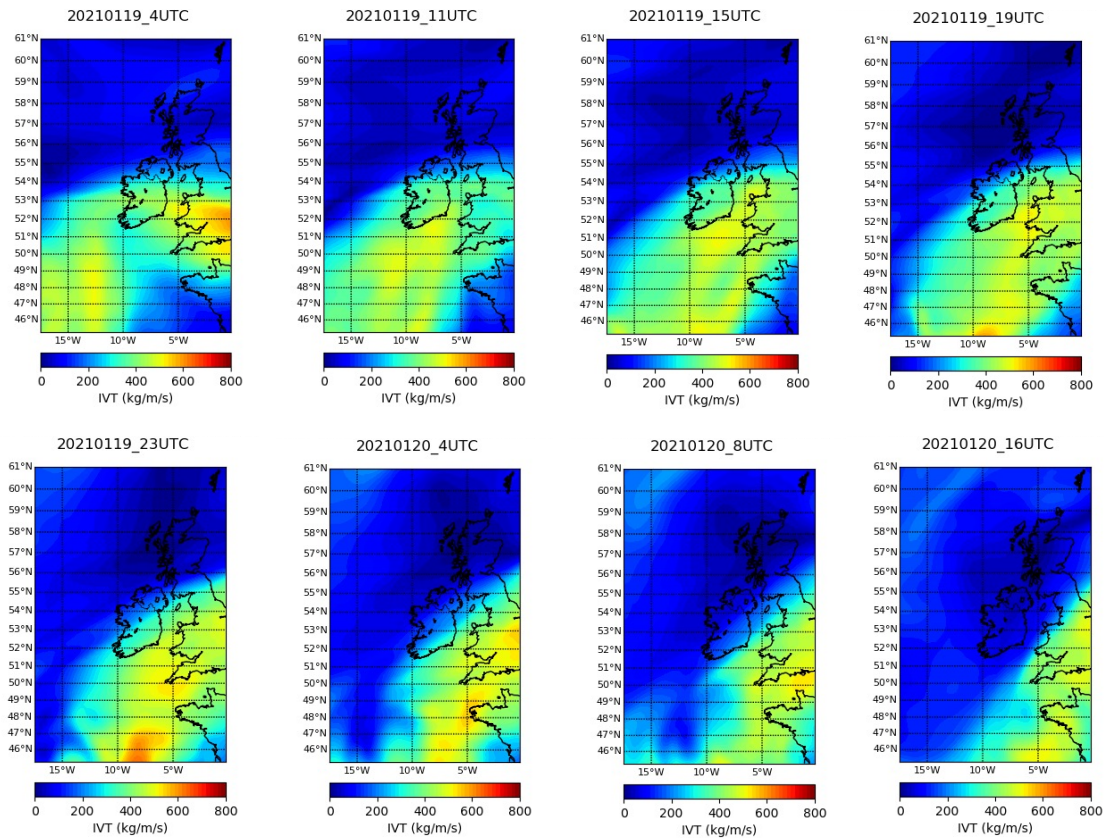


Figure 7.9. Storm Christoph Algorithm Performance. It is suggested that the properties of the AR associated with Storm Christoph make it difficult for the AR detection algorithm to work efficiently. Storm Christoph was likely impactful due to low-intensity atmospheric moisture transport being delivered over a long period of time (at least 36-hours as presented above).

7.4. Discussion

This section presents a critical analysis of the main findings of this thesis. The extent to which the results have been successful in addressing the identified research gap will be discussed, alongside how they may align with any similar such studies. Any obvious shortcomings, or gaps, within the analysis are addressed in terms of motivation for additional analyses in the future.

7.4.1. How important are ARs in flood generation across the UK?

This thesis has confirmed that ARs are indeed important flood drivers across the western UK, accounting for up to 70% of POT3 winter floods across the historical period. Such results are in line with the anticipated drivers of precipitation across the UK (Browning et al., 1973; Burt & Howden, 2013; Hill et al., 1981; Maraun et al., 2009). The peak of annual rainfall along the west

coast tends to occur during the winter, driven by frontal and orographic rainfall. The intensity of the rainfall is expected to increase with altitude (Couto et al., 2015), and year-to-year variability by the strength of large scale drivers such as the NAO (Burt & Howden, 2013). Previous work has been able to link the relative frequency of ARs and winter storms to the phase of the NAO and other such climate modes (Benedict et al., 2019; D. A. Lavers et al., 2012).

It should be noted that extreme precipitation is generally an essential, but not sufficient, condition for extreme flooding. The role of antecedent soil moisture has long been identified as an important control (Berghuijs et al., 2019). Along the western coastline of the UK, the timing of maximum antecedent soil moisture and extreme precipitation align across the winter period, thus the largest annual floods tend to occur at this time of year. In contrast, eastern and southern areas of the UK receive their maximum precipitation totals during summertime, convective events, but as the associated soil moisture tend to be lower at this time of year, such events do not necessarily result in significant flood impacts.

We have found the strongest correlations between AR presence and extreme floods within the upland areas of the UK. Such a result is likely driven by the combined influence of altitude (resulting in more generated rainfall) and saturated, shallow soils (resulting in a smaller influence of antecedent soil moisture). However, the final correlations presented in this thesis remain somewhat lower than that presented by [Lavers et al., \(2012\)](#) and suggestions for why this may be so are presented below.

1) The Detection Algorithm

There are several aspects of the ERA5 reanalysis, as compared to the previously studied ERA-Interim, including its high spatial and temporal resolution, that affect the ability of the Lavers et al. (2012) algorithm to detect persistent ARs (Chapter 5, section 5.2). As such, several adjustments were made to the detection algorithm in Chapter 5. By applying the updated AR catalogue to the Dyfi and Teifi catchments, the percentage of POT3 winter floods associated with ARs at the two study catchments could be increased (section 5.2.3).

2) POT Flood Section

A separation period of 7-days is required between extracted POT floods to ensure independence (Chapter 3, Section 3.4). However, for the smallest and flashiest of catchments, this window may in fact be too long, and as such, there is a chance that some flood events are

being neglected. However, given the variation in response times of catchments across the UK, and particularly those expected within the sample used in later stages of this work (Chapter 6), it was decided to retain the 7-day window for consistency.

In Chapter 6, the initial analysis was extended to include a total 81 catchments, located mostly along the western half of the UK (Chapter 3, section 3.3). This permitted an overview of the role of ARs in generating extreme winter floods at a variety of catchments of different shapes and sizes. The highest percentage of POT3 floods associated with ARs, were noted in upland regions of Cumbria, Snowdonia, Devon, and north-western Scotland. However, there exist several caveats in these results that are worth exploring.

1) Seasonality

Only the winter period has been analysed in this work, and therefore it is not possible to say anything about the typical impact of ARs across the summer months. Justified through the larger magnitude river flows typically demonstrated across the winter months, and the greater frequency of frontal storm systems arriving from across the Atlantic, there may be space to repeat a similar such analysis for the summer period (even just to ensure that little impact is found as per the work of Champion et al., 2015).

2) Minimal Urbanisation

The study catchments have been selected largely on basis of natural flow regimes (Chapter 3, section 3.4.1), and therefore minimal urbanisation. An element of hydrological modelling may permit the analysis of AR impacts in urbanised areas, where the influence of sub-surface drainage and surface flow is all the more important. It is likely that runoff and flood generation will be more extreme in urbanised areas, where the natural percolation of rainfall into the soil surface is limited.

3) The Detection Algorithm

Although improvements have been made to the AR detection algorithm, it remains unlikely to be able to pick up every possible AR. ARs are inherently qualitative features, coming in many different shapes and sizes. In the development of the algorithm, several assumptions have been made about many of these features, and it is important to bear them in mind when interpreting the results. Storm Christoph for example in the previous section, has not been picked up well by the algorithm due to its comparatively weak IVT flux, however it was still impactful given its persistence over slower responding catchments.

In summary, this section should act to highlight the importance of context in interpreting the presented results. It can be said with some confidence that ARs (defined according to the detection algorithm developed in Chapter 5) can be shown to play an important role in influencing some of the most extreme floods across the winter season at many regions across the UK. Their influence appears to be strongest in upland, western areas of the UK, in line with existing knowledge of how ARs work – i.e., that orographic uplift is key to extracting their atmospheric moisture.

However, it remains unlikely that all possible AR events are detected, just as all possible floods are extracted, and thus there is room to possibly probe those catchments where the strength of the AR-POT3 flood relationship is the lowest. In these cases, it may indeed be that the catchment is unresponsive to typical ARs, or it may be due to missing floods and/or AR events in line with the assumptions addressed previously.

7.4.2. How important are catchment properties in modulating the most impactful ARs?

This thesis has identified preferential orientations and/or strengths of landfalling ARs that result in the most severe impacts. To what extent these results can be explained by the inclusion of land-surface properties has then been investigated.

The higher the catchment, the more likely it is that a specific orientation of AR will be required to generate significant precipitation. Such a result is intuitive when considering the most efficient orographic rainout (Griffith et al., 2020; Miglietta & Rotunno, 2005; Neiman et al., 2011; Ralph et al., 2003). The role of latitude is likely complementary, in that elevation across the western UK tends to increase as we move northward. The role of settled snow, and the arrival of an AR in triggering its melting, is likely only a consideration in the most northern catchments. The Met Office, estimates that the UK experiences on average 15.6 days of settled snow across the uplands, and thus identifying ARs that arrive during such periods, is an area of future work and would expect to be possible within our existing datasets.

Additional land-surface properties identified in this work as important for controlling AR impact include the underlying geology, the catchment area and the extent of base flow (via BFIHOST). It is likely that most of these parameters relate to the degree of importance of antecedent soil moisture within the catchment. For example, a catchment with more permeable soils, a higher

degree of baseflow and larger area will likely require the alignment of high moisture content with peak rainfall to result in a flood. Or rather, increased rainfall totals relative to a smaller, impermeable, flashy catchment (and hence, the increased IVT required within the most impactful ARs; section 6.3).

The role of antecedent soil moisture (ASM) has been assessed through the use of antecedent river flow as a proxy. Although reasonable in the smallest of catchments within the study, it may not be as applicable for the larger members of the sample. An alternative could have been to have used the soil moisture estimates direct from the reanalysis, or a similar gridded product, and average over the catchment area, especially as previous research has identified antecedent precipitation as possibly ‘priming’ the soils to the arrival of an AR (Cao et al., 2019; Mahoney et al., 2016). However, it is well known that rainfall radar does not work well in regions of orographic rainfall (Fairman Jr et al., 2015), and hence the decision was made in this work to select the most straightforward approach based on the observational data.

The hydrometeorological monitoring along the US western coastline to the arrival of landfalling ARs, is a method that permits an understanding of the sub-surface hydrology of ARs and the development and suitable parametrisation of associated hydrological models (Sumargo et al., 2021). Such a system would be invaluable across the UK and, as such, the role of ASM in controlling AR impacts is identified as an important area of future work.

The AR duration has also been considered, albeit with its own set of assumptions. Of particular consideration is the fact that ARs are not static over their lifetime, either in terms of their landfalling position or in terms of the moisture they channel. As discussed during the framework performance analysis of Storm Christoph (section 7.3.3), it is likely that the longest duration ARs in fact consist of a number of distinct AR features that have been ‘joined’ together by the AR detection algorithm (i.e., AR ‘families’; Fish et al., 2019)

Therefore, it is suggested that, if AR duration is to be properly studied, the algorithm may need to be altered once more. Further, an AR drifting heavily northward or southward during its lifetime can be expected to pass overhead of an affected area relatively quickly, especially given the relatively rapid fall off in transmitted IVT flux when moving away from the AR axis (Chapter 5, section 5.3.5). A fall in IVT magnitude will likely translate to a reduction in rainfall generation. Such results could be investigated through the inspection of rainfall gauges and/or radar.

An overarching assumption of this thesis has been the method used to extract the properties of the most impactful ARs (if applicable) at the test catchments. It was decided, to ensure a consistent approach, that the results of the 81 additional study catchments be organised according to whether they demonstrated a preferential orientation of incoming ARs (whereupon they are deemed to be ‘orientation dominated’) or strength (‘flux dominated’). Indeed, possibly the first caveat in the results of this thesis, is that the catchments that did not meet at least one of these conditions were immediately discarded. This equates to just over one-tenth of the original sample size (according to the 9 hr + AR catalogue; Table 6.1).

For those catchments that remained, a total of 22 (static) catchment descriptors (Chapter 3, Section 3.2) were obtained that, in combination, provide an overview of key characteristics of the study region (CEH; Ledingham et al., 2019). Many of these descriptors were derived from gridded digital terrain models and are therefore subject to averaging and estimations accordingly. It should be noted here that, although the chosen descriptors are sufficient and appropriate for use, there are many additional descriptors that could have been used. Indeed, many of the chosen descriptors were neglected in the Principal Component Analysis and associated feature selection (Chapter 6, Section 6.3) and as such perhaps only the most representative characteristics could have been chosen from the beginning.

Finally, given the study catchments were chosen primarily on the basis of their natural flow regime and suitability for flood studies, their properties do not span the entire range of descriptors for UK based catchments e.g., many of the catchments are below 500km² in size as the majority of larger catchments are modified in some way and/or contain a degree of urbanisation. Thus, the (unavoidable) bias of the sample selection should be appreciated when interpreting the results.

7.4.3. Can the inclusion of catchment properties help in predicting AR floods?

The UK has seen a number of advances in the field of flood forecasting since of 2007 summer floods. Organisational restructuring has resulted in the development of a dedicated flood forecasting centre, based at the UK Met Office. Here, the results of ensemble numerical weather prediction models are combined with hydrological models to formulate an assessment of risk. A large part of this process is the clear and effective communication of the flood and its uncertainty to those that can act, at sufficient lead time. Indeed, the forecasts should be viewed

as only ‘part of the story’ (Stephens & Cloke, 2014), where communication, planning, governance and spending should be of equal importance.

Therefore, given the different types of impactful ARs identified across the UK, there is motivation for trying to combine the information into an easily communicated operational-style framework. That is, given an incoming AR of known strength, orientation, duration and landfalling location, is it possible to infer its impact across the study region?

Previous work of this type includes the AR Categorisation Scale as initially posed by Ralph et al. (2019) for those features impacting the US West Coast, later extended to European regions by Eiras-Barca et al., (2021). However, it has been shown, through the work presented in this thesis, that nearby areas can demonstrate different hydrological responses to similar overhead AR conditions. This result appears to be particularly relevant in western regions of the UK, where many catchments are small, steep, and flashy.

The preferential orientation bands and IVT thresholds calculated within this thesis have therefore been combined to create a sequential scoring system, denoted as the AR impacts framework (Figure 7.1). This framework can be applied to either orientation or flux dominated catchments and intends to exist complementary to that of Ralph et al. (2019). Whilst the AR Categorisation system presents a method of distinguishing between the most beneficial and hazardous ARs, particularly at the continental and/or national level, the AR impacts framework developed in this work permits an estimate of relative impacts at the catchment scale.

The framework is applied to several notable case studies of the last decade (section 7.3). Although the initial results are promising, there is space to refine the method in future analysis.

1) Reanalysis vs Forecast?

The framework is currently based on reanalysis data and as such it has been possible to extract AR properties (magnitude and orientation) over the lifetime of the event above the catchment of interest. Applying the method to forecast data will be a whole different challenge. The results will likely depend on factors such as the lead time, how well the AR magnitude and orientation are forecast, the intrinsic variability of the AR itself and uncertainty in its landfalling location. There is likely to be a balance between the forecast uncertainty at longer lead times against the increased preparation time for those areas at risk. The performance of the AR algorithm on operational forecast data will also need to be

considered; it will be essential to ensure a reliable and robust method of detecting ARs in forecast data.

2) Event Specific Conditions

The framework at the time of writing does not include the AR duration and/or catchment initial conditions. There is evidence presented in earlier stages of this work (Chapter 6, section 6.3.5) that both variables can modulate the impactful potential of ARs. Additional work is needed, in line with earlier suggestions regarding rainfall and/or soil moisture data (section 7.5.2) to quantify these factors. In the meantime, the initial flow data and AR duration over the regions of interest, alongside the framework results, can provide a reasonable idea of likely catchment response.

3) Storm Christoph

Without prior knowledge of storm Christoph being particularly impactful in parts of north-west England, it was unlikely to have been flagged as high-risk AR by the framework. Its average IVT magnitude is lower than that of Storms Desmond, Ciara and Dennis and as such was difficult to detect through the (modified) algorithm. Intrinsic to the AR detection algorithm is an IVT threshold of above $500 \text{ kg m}^{-1} \text{ s}^{-1}$, and to obtain a framework estimate for the storm, the threshold had to be lowered to $400 \text{ kg m}^{-1} \text{ s}^{-1}$.

The impact of Storm Christoph lies with the fact that the, albeit relatively low magnitude, IVT flux persisted for several days and resulted in notable rainfall totals in regions where the catchments are slightly more slowly responding than in upland western regions. As such, the rainfall was unable to be quickly translated through the catchment and compounded over the lifetime of the storm. This case study is included in this analysis therefore to highlight the intricacies of forecasting impacts over multiple catchments with different methods of flood generation.

4) Catchment Orientation

It is likely that the rainfall generation processes between those catchments with a predominantly westward aspect is different to those with an easterly aspect, when considering AR events (sections 7.3.1 and 7.3.2). Additional analyses of the framework's performance in the context of these catchments will be important in terms of its operational potential.

7.5. Conclusions

This chapter has attempted to bring together the results of this thesis in an operational style framework. The framework has been applied to several high-profile storms of the last decade to assess its performance, and a wider discussion of the results has been undertaken, highlighting any possible shortcomings or regions of future analysis. The conclusions of this chapter are summarised below.

- An AR impacts framework based on AR IVT magnitude and orientation has been developed. This framework has been applied to several high-profile storms of the last decade.

There is merit in creating such a summary tool and in the main, areas most strongly affected are predicted well.

- Information regarding the average AR landfalling location, duration and antecedent catchment conditions are presented alongside the framework.

There is space to quantify the effect of these factors and build them into the prediction tool.

- The results have been critically assessed in the context of existing knowledge and in terms of the methods and data used.

Although the results of this thesis are promising, several avenues exist for future, more detailed work.

Chapter 8 – Conclusions and Further Work

8.1. Context

The aim of this thesis has been to understand the role that land-surface properties play in modulating the impact of landfalling ARs. Can their inclusion help in explaining the differing hydrological responses of the Dyfi and Teifi catchments as presented in Lavers et al., (2012)? And, from an operational perspective, do they further our ability to identify the most impactful events? The results of this thesis are first discussed in the context of original research objectives, before addressing their operational potential. The chapter concludes with suggestions of future work.

8.2. Overall Conclusions

8.2.1. How important are ARs in flood generation across the UK?

This work has quantified the role of ARs in extreme winter flood generation across a series of 81 study catchments, located primarily along the western half of mainland UK. When considering persistent ARs of duration 9 hours and above, up to 70% of historical POT3 floods can be aligned with the arrival of an AR within the three days prior. The strongest relationships are typically found in upland regions of the UK, including the highlands of Scotland, Cumbria and Snowdonia (Chapter 6, section 6.2).

However, nearby catchments appear to demonstrate different responses to what may be expected to be similar meteorological input, suggesting that the presence of an AR alone is insufficient to result in a notable flood. This result, in line with that of Lavers et al. (2012), acts as the motivation for the inclusion of additional information.

The use of newly available high-resolution atmospheric reanalysis has permitted a critical analysis of the performance of the Lavers et al. (2012) detection algorithm. The increased temporal and spatial resolution of ERA5 as compared to the reanalyses applied in previous analyses, has motivated the inclusion of several adjustments and additions to ensure the efficiency and robustness of the algorithm moving forward.

Detailed in Chapter 5 (section 5.2), these adjustments include an element of tolerance to missing detections within an AR event and a consideration of additional limbs of strong moisture flux existing independent to the main AR axis. In addition, it is suggested that ARs of duration 9 hours and above can still be impactful, particularly at the smallest and flashiest of catchments.

The modified detection algorithm has been tested in the context of the Dyfi and Teifi catchments, where its ability to detect a greater number of impactful ARs was noted (Chapter 5, section 5.2.3). As such, the updated algorithm is strongly suggested for future analyses and carried forward into the following research chapters (Chapters 6 and 7).

8.2.2. How important are catchment properties in modulating the most impactful ARs?

Preferential subsets of impactful ARs are noted at 70 of the original 81 study catchments (for the 9 hr + AR catalogue; Chapter 6, section 6.2). These subsets may refer to ARs of preferential orientation and/or minimum strength, herein referred to ‘orientation’ and ‘flux’ dominated catchments respectively. These results suggest that different ‘types’ of ARs are particularly impactful at different ‘types’ of catchments. It is suggested that these preferential properties may relate to the topography of the catchments concerned (Chapter 4).

As such, a total of 22 (static) catchment descriptors are used to help understand these results (Chapter 6, section 6.3). Feature selection tools have been used to deduce the most efficient way of describing the 81 study catchments, and Principal Component Analysis (PCA) applied to test the strength of relationship between specific catchment properties and AR characteristics (section 6.3). The main findings are summarised below:

- Catchment latitude and elevation are the most important properties when considering impactful ARs. Catchments with maximum elevations above 400-600 m are most likely to demonstrate a preferential orientation, in line with physical interpretations (e.g., where the preferential orientation aligns with the most efficient rainout). The required IVT strength of the most impactful ARs falls with both latitude and elevation (e.g., it is largest in the southernmost catchments of the UK with the gentlest terrain). These factors in combination align with knowledge regarding AR processes; the heaviest rainfall is generated when the warm, moist air of the AR is forced to rise over elevated terrain.
- The strongest ARs are required in catchments with the most permeable bedrock, likely due to a greater fraction of storm water infiltrating into the soil surface. In addition, the

extent of groundwater (in terms of BFIHOST), correlates positively with the required strength of the most impactful ARs.

- The strongest ARs are required in the smallest of catchments, perhaps driven by the catchments of Devon and Cornwall. In these southernly regions, the terrain is lower and subject to a wider variety of flood formation mechanisms.

In addition to the static analysis, two event specific factors are collated: AR duration and antecedent catchment conditions. In the latter case, river levels at the time of AR arrival are used as a proxy for catchment wetness. The level is compared to the 75th percentile of historical winter flows, where a reading above and below this value is taken as ‘high’ and ‘low’ flow conditions respectively.

- At the majority of catchments, ARs arriving during low flow conditions are required to be between 10-15% stronger than those arriving during high flow conditions (section 6.3.5). It is also possible to identify those catchments where initial flow conditions are of minimal effect.
- Perhaps counter-intuitively, ARs of longer duration (18 hours or more) are required to be comparatively stronger than those of lower duration (9 hours or more) to induce a notable hydrological impact. This result may relate to the fact that ARs are rarely constant over their lifetime, and in fact, the longest events typically consist of a ‘family’ of shorter duration events (section 6.3.5).

By applying Random Forest Regression and machine learning (Chapter 3, section 3.6), a predictive model has been developed to predict the minimum strength of the most impactful ARs, based on catchment properties alone (Chapter 6, section 6.4). Catchment location and elevation are key predictors of this model, in line with earlier results. This provides great potential to extend the analysis presented in this thesis to previous unexplored, and even ungauged, catchments.

8.2.3. Can the inclusion of catchment properties help in predicting AR floods?

The results of this thesis are combined in an AR Impacts Prediction Framework, inspired by the work of Ralph et al. (2019) and Eiras-Barca et al., (2021) for the US West Coast and European regions respectively. Whilst the referenced methods mentioned rely solely on AR orientation and

duration to predict impacts on a national scale, the framework presented in this thesis suggests the inclusion of AR orientation and minimum AR strength to explain the catchment level variations in hydrological response.

The framework is applied to several high-profile case studies of the last decade, existing outside the catalogue used in earlier analyses, as an independent test of performance. Although there is space to develop the tool (Chapter 7, section 7.4.3; Section 8.4), the initial results are promising. The framework is able to identify the catchments most likely at risk through an AR of given strength and orientation which, in combination with river levels at the time of AR arrival, permit a prediction of extent of hydrological response.

8.3. Operational Impact

8.3.1. Existing Operational Tools

The Extreme Forecast Index developed at ECMWF (EFI, Lavers et al., 2016; Chapter 2, section 2.5.4) and based on IVT has been shown to have potential for hydrometeorological forecasting. As such, the tool has been on trial at the UK Flood Forecasting Centre (based at the UK Met Office in combination with the Environment Agency) across recent winters.

As discussed previously, the work of Ralph et al. (2019) and Eiras-Barca et al., (2021) provide an accessible, large-scale method of classifying ARs. In particular, it acknowledges the role of ‘beneficial’ events, essential in providing essential winter recharge in the form of low-intensity or short duration features. It should hopefully be clear from the results provided in this thesis that not all the ARs expected to impact the UK’s shores each winter will be hazardous.

8.3.2. The Inclusion of Atmospheric Rivers

It is suggested from the work built up during the course of this thesis, that inclusion of AR events in operational flood forecasting tools across the UK will be beneficial. This could initially take the form of a consideration of IVT thresholds, and the typical terrain of the expected landfalling location of the AR. Whilst the framework is developed (section 8.4), a simple cataloguing of notable events could be built up, identifying key storm characteristics and regions of impact. This work will be made all the more straightforward through the near real-time

availability of ERA5. Further discussion as to the inclusion of ARs in operational flood forecasting, will be given in the following section.

8.4. Intentions for Further Work

8.4.1. Develop

- **Catchments:** There remains space to explore the results in the context of additional UK based catchments, including those on either side of the highest watersheds (Chapter 7, section 7.4.3), those where no preferential subsets of ARs are found (section 7.4.1) and in those that demonstrate deviations away from a natural flow regime (7.4.1). This may occur in the form of more urbanised catchments, or in those containing storage areas. The aim is test to what extent the ideas presented in this thesis are applicable more broadly across the UK.
- **Antecedent Soil Wetness:** There remains space to explore the assumptions made regarding antecedent catchment conditions, and the accuracy of initial flow estimations (section 7.5.2). Additional (gridded) soil moisture information could be sourced and averaged over the area of the catchment. If the initial flow estimate is found to be appropriate, then a modulation of the ‘high/low’ flow threshold (Chapter 6, section 6.3.5) can be performed, to test the sensitivity of results to such a value.
- **POT Flood Assumptions:** It is likely that POT flood events are missed in the smaller, flashier catchments due to the 7-day independence criterion applied by the POT flood extraction scheme (Chapter 7, section 7.4.1). As such, this window could be modified in line with expected catchment response times.
- **Detection Algorithm:** The longest duration ARs presented in this thesis likely consist of a number of individual AR events arriving within 24 hours of one another (section 7.4.2), and as such a robust analysis of the effect of AR duration has been challenging (Chapter 6, section 6.3.5). Further modifications can be made to the algorithm to address this.
- **Seasonality:** The analyses presented in this thesis occur across the winter season only (Chapter 7, section 7.4.1). There is space to repeat the analysis for the summer season (even if to ensure that ARs are of minimal influence, as per the work of Champion et al., 2015). It will also be possible to explore the typical synoptic conditions associated with ARs of different orientation, which may be useful from a forecasting perspective (Chapter 2, section 2.6.3.1).

8.4.2. Operationalise

- **Region of Influence:** The results of Chapter 5 (section 5.3) give reason to suspect that the ‘region of influence’ of an impactful AR may be less than originally assumed. The width of an AR is found to correlate strongly with the strength at its axis (section 5.3.4), with the maximum moisture flux falling off rapidly moving away from the centreline (section 5.3.5). These ideas will be important from an operational perspective, and inclusion into the AR framework could be useful.
- **Forecast Data:** How well are IVT strength and orientation predicted in typical products? This question will align well with the possibility of a European AR field campaign (Lavers et al., 2020). The analysis of synoptic conditions associated with differing AR orientations may aid this process.
- **Detection Method:** The extent to which the current AR detection algorithm can be applied to forecast data will need to be investigated (Chapter 7, section 7.4.3).
- **Antecedent Conditions:** To what extent is it appropriate to include antecedent catchment conditions into an impact prediction tool, such as that presented in this thesis (section 7.2)?
- **Real-time test/benchmarking:** The ideas of this thesis should be tested in the context of a ‘real life’ storm season, perhaps in combination with the Flood Forecasting Centre. The AR prediction framework aims to provide a method to identify the most ‘impactful’ ARs, as opposed to the ‘strongest’ ARs. However, in order to test its usefulness, it will need to be compared against methods such as the EFI (in terms of lead time) and hydrological modelling results of NWP precipitation (in terms of impact). To be useful, it will need to aid these existing forecasting tools, either in terms of the identification of preferential orientation bands, or via minimum required AR strengths.

8.4.3. Extend

- **Study Area:** To what extent are the ideas presented in this thesis useful in other regions of Europe (e.g., Iberia) and the world (e.g., New Zealand; Prince et al., 2021).
- **Observational Methods:** Develop AROs across the coastline of western Europe?

8.5. Final Remarks

Typical methods of flood forecasting involve complex downscaling processes, with elements of uncertainty introduced at each stage. The presence of ARs as synoptic-scale features increases their potential for earlier identification in forecast products (Lavers et al., 2014), with the work presented here acting to directly link their observed properties to catchment level impacts. As the climate warms, and ARs are expected to become stronger and more numerous (Lavers et al., 2015), understanding the processes behind the strongest events will be essential for adequate preparation. The most effective forecasting tools will require a consideration of the subtle interplay between the land-surface and the AR itself.

References

- A Step-by-Step Explanation of Principal Component Analysis (PCA)*. (n.d.). Built In. Retrieved 3 August 2021, from <https://builtin.com/data-science/step-step-explanation-principal-component-analysis>
- Albano, C. M., Dettinger, M. D., & Harpold, A. A. (2020). Patterns and Drivers of Atmospheric River Precipitation and Hydrologic Impacts across the Western United States. *Journal of Hydrometeorology*, 21(1), 143–159. <https://doi.org/10.1175/JHM-D-19-0119.1>
- Albano, C. M., Dettinger, M. D., & Soulard, C. E. (2017). Influence of atmospheric rivers on vegetation productivity and fire patterns in the southwestern U.S. *Journal of Geophysical Research: Biogeosciences*, 122(2), 308–323. <https://doi.org/10.1002/2016JG003608>
- Allan, R. P., Lavers, D. A., & Champion, A. J. (2016). Diagnosing links between atmospheric moisture and extreme daily precipitation over the UK: LINKING ATMOSPHERIC MOISTURE AND UK PRECIPITATION. *International Journal of Climatology*, 36(9), 3191–3206. <https://doi.org/10.1002/joc.4547>
- Bao, J.-W., Michelson, S. A., Neiman, P. J., Ralph, F. M., Wilczak, J. M., Bao, J.-W., Michelson, S. A., Neiman, P. J., Ralph, F. M., & Wilczak, J. M. (2006). Interpretation of Enhanced Integrated Water Vapor Bands Associated with Extratropical Cyclones: Their Formation and Connection to Tropical Moisture. *Monthly Weather Review*, 134(4), 1063–1080. <https://doi.org/10.1175/MWR3123.1>
- Barth, N. A., Villarini, G., Nayak, M. A., & White, K. (2017). Mixed populations and annual flood frequency estimates in the western United States: The role of atmospheric rivers. *Water Resources Research*, 53(1), 257–269. <https://doi.org/10.1002/2016WR019064>
- Bauer, P., Thorpe, A., & Brunet, G. (2015). The quiet revolution of numerical weather prediction. *Nature*, 525(7567), 47–55. <https://doi.org/10.1038/nature14956>
- Bavay, M., Grünewald, T., & Lehning, M. (2013). Response of snow cover and runoff to climate change in high Alpine catchments of Eastern Switzerland. *Advances in Water Resources*, 55, 4–16. <https://doi.org/10.1016/j.advwatres.2012.12.009>

- Benedict, I., Ødemark, K., Nipen, T., & Moore, R. (2019). Large-Scale Flow Patterns Associated with Extreme Precipitation and Atmospheric Rivers over Norway. *Monthly Weather Review*, *147*(4), 1415–1428. <https://doi.org/10.1175/MWR-D-18-0362.1>
- Berghuijs, W. R., Harrigan, S., Molnar, P., Slater, L. J., & Kirchner, J. W. (2019). The Relative Importance of Different Flood-Generating Mechanisms Across Europe. *Water Resources Research*, *55*(6), 4582–4593. <https://doi.org/10.1029/2019WR024841>
- Berghuijs, W. R., Woods, R. A., Hutton, C. J., & Sivapalan, M. (2016). Dominant flood generating mechanisms across the United States: Flood Mechanisms Across the U.S. *Geophysical Research Letters*, *43*(9), 4382–4390. <https://doi.org/10.1002/2016GL068070>
- Berrisford, P., Dee, D., Poli, P., Brugge, R., Fielding, K., Fuentes, M., Kallberg, P., Kobayashi, S., Uppala, S., & Simmons, A. (2011). *The ERA-Interim archive, version 2.0*.
- Beven, K. J. (2011). *Rainfall-runoff modelling: The primer*. John Wiley & Sons, Ltd.
- Bjerknes, V. F. (1910). Synoptical representation of atmospheric motions. *Quarterly Journal of the Royal Meteorological Society*, *36*(155), 267–286.
- Boorman, D., Hollis, J. M., & Lilly, A. (1995). *Hydrology of soil types: A hydrologically-based classification of the soils of United Kingdom*. Institute of Hydrology.
- Browning, K. A., Hardman, M. E., Harrold, T. W., & Pardoe, C. W. (1973). The structure of rainbands within a mid-latitude depression. *Quarterly Journal of the Royal Meteorological Society*, *99*(420), 215–231. <https://doi.org/10.1002/qj.49709942002>
- Browning, K. A., & Harrold, T. W. (1970a). Air motion and precipitation growth at a cold front. *Quarterly Journal of the Royal Meteorological Society*, *96*(409), 369–389. <https://doi.org/10.1002/qj.49709640903>
- Browning, K. A., & Harrold, T. W. (1970b). Air motion and precipitation growth at a cold front. *Quarterly Journal of the Royal Meteorological Society*, *96*(409), 369–389. <https://doi.org/10.1002/qj.49709640903>
- Browning, K. A., & Pardoe, C. W. (1973). Structure of low-level jet streams ahead of mid-latitude cold fronts. *Quarterly Journal of the Royal Meteorological Society*, *99*(422), 619–638. <https://doi.org/10.1002/qj.49709942204>

- Burt, T. P., & Howden, N. J. K. (2013). North Atlantic Oscillation amplifies orographic precipitation and river flow in upland Britain. *Water Resources Research*, *49*(6), 3504–3515.
<https://doi.org/10.1002/wrcr.20297>
- Cannon, F., Cordeira, J. M., Hecht, C. W., Norris, J. R., Michaelis, A., Demirdjian, R., & Ralph, F. M. (2020). GPM Satellite Radar Observations of Precipitation Mechanisms in Atmospheric Rivers. *Monthly Weather Review*, *148*(4), 1449–1463. <https://doi.org/10.1175/MWR-D-19-0278.1>
- Cannon, F., Ralph, F. M., Wilson, A. M., & Lettenmaier, D. P. (2017). GPM Satellite Radar Measurements of Precipitation and Freezing Level in Atmospheric Rivers: Comparison With Ground-Based Radars and Reanalyses. *Journal of Geophysical Research: Atmospheres*, *122*(23).
<https://doi.org/10.1002/2017JD027355>
- Cao, Q., Mehran, A., Ralph, F. M., & Lettenmaier, D. P. (2019). The Role of Hydrological Initial Conditions on Atmospheric River Floods in the Russian River Basin. *Journal of Hydrometeorology*, *20*(8), 1667–1686. <https://doi.org/10.1175/JHM-D-19-0030.1>
- Catto, J. L., Jakob, C., Berry, G., & Nicholls, N. (2012). Relating global precipitation to atmospheric fronts: FRONTS AND PRECIPITATION. *Geophysical Research Letters*, *39*(10), n/a-n/a.
<https://doi.org/10.1029/2012GL051736>
- Champion, A., Allan, R. P., & Lavers, D. A. (2015). Atmospheric rivers do not explain UK summer extreme rainfall. *Journal of Geophysical Research: Atmospheres*, *120*(14), pp.6731–6741.
- Champion, A. J., Allan, R. P., & Lavers, D. A. (2015). Atmospheric rivers do not explain UK summer extreme rainfall. *Journal of Geophysical Research: Atmospheres*, *120*(14), 6731–6741.
<https://doi.org/10.1002/2014JD022863>
- Chapman, W. E., Subramanian, A. C., Delle Monache, L., Xie, S. P., & Ralph, F. M. (2019). Improving Atmospheric River Forecasts With Machine Learning. *Geophysical Research Letters*, *46*(17–18), 10627–10635. <https://doi.org/10.1029/2019GL083662>
- Cobb, A., Delle Monache, L., & Ralph, F. M. (2020). *Atmospheric river integrated vapor transport ground truth: Dropsonde observations compared to reanalyses*. 2020, A179-0001.
- Collow, A. B. M., Mersiovsky, H., & Bosilovich, M. G. (2020). *Large-Scale Influences on Atmospheric River Induced Extreme Precipitation Events Along the Coast of Washington State*. 15.

- Collow, A., & Guan, B. (n.d.). *ARTMIP Tier 2 Reanalysis Discussion*. 13.
- Copernicus Climate Change Service Climate Data Store (CDS). (2017). *Copernicus Climate Change Service (C3S): ERA5: Fifth generation of ECMWF atmospheric reanalyses of the global climate*.
- Cordeira, J. M., Ralph, F. M., & Moore, B. J. (2013a). The Development and Evolution of Two Atmospheric Rivers in Proximity to Western North Pacific Tropical Cyclones in October 2010. *Monthly Weather Review*, *141*(12), 4234–4255. <https://doi.org/10.1175/MWR-D-13-00019.1>
- Cordeira, J. M., Ralph, F. M., & Moore, B. J. (2013b). The Development and Evolution of Two Atmospheric Rivers in Proximity to Western North Pacific Tropical Cyclones in October 2010. *Monthly Weather Review*, *141*(12), 4234–4255. <https://doi.org/10.1175/MWR-D-13-00019.1>
- Couto, F. T., Salgado, R., & Costa, M. J. (2012). Analysis of intense rainfall events on Madeira Island during the 2009/2010 winter. *Natural Hazards and Earth System Sciences*, *12*(7), 2225–2240. <https://doi.org/10.5194/nhess-12-2225-2012>
- Couto, F. T., Salgado, R., Costa, M. J., & Prior, V. (2015). Precipitation in the Madeira Island over a 10-year period and the meridional water vapour transport during the winter seasons. *International Journal of Climatology*, *35*(13), 3748–3759. <https://doi.org/10.1002/joc.4243>
- Cunderlik, J. M., Ouarda, T. B. M. J., & Bobée, B. (2004). Determination of flood seasonality from hydrological records / Détermination de la saisonnalité des crues à partir de séries hydrologiques. *Hydrological Sciences Journal*, *49*(3), 11. <https://doi.org/10.1623/hysj.49.3.511.54351>
- Curry, C. L., Islam, S. U., Zwiers, F. W., & Déry, S. J. (2019). Atmospheric Rivers Increase Future Flood Risk in Western Canada's Largest Pacific River. *Geophysical Research Letters*, *46*(3), 1651–1661. <https://doi.org/10.1029/2018GL080720>
- Dacre, H. F., Clark, P. A., Martinez-Alvarado, O., Stringer, M. A., & Lavers, D. A. (2015a). How do atmospheric rivers form? *Bulletin of the American Meteorological Society*, *96*(8), 1243–1255. <https://doi.org/10.1175/BAMS-D-14-00031.1>
- Dacre, H. F., Clark, P. A., Martinez-Alvarado, O., Stringer, M. A., & Lavers, D. A. (2015b). How Do Atmospheric Rivers Form? *Bulletin of the American Meteorological Society*, *96*(8), 1243–1255. <https://doi.org/10.1175/BAMS-D-14-00031.1>

- Dacre, H. F., Martínez-Alvarado, O., & Mbengue, C. O. (2019). Linking Atmospheric Rivers and Warm Conveyor Belt Airflows. *Journal of Hydrometeorology*, 20(6), 1183–1196.
<https://doi.org/10.1175/JHM-D-18-0175.1>
- de Vries, A. J. (2021). *A global climatological perspective on the importance of Rossby wave breaking and intense moisture transport for extreme precipitation events*. 33.
- Dettinger, M. (2004). *Fifty-Two Years of "Pineapple-Express Storms Across the West Coast of North America*. 20.
- Dettinger, M. (2011). Climate Change, Atmospheric Rivers, and Floods in California - A Multimodel Analysis of Storm Frequency and Magnitude Changes1: Climate Change, Atmospheric Rivers, and Floods in California - A Multimodel Analysis of Storm Frequency and Magnitude Changes. *JAWRA Journal of the American Water Resources Association*, 47(3), 514–523.
<https://doi.org/10.1111/j.1752-1688.2011.00546.x>
- Dettinger, M. D., Ralph, F. M., Das, T., Neiman, P. J., & Cayan, D. R. (2011). Atmospheric Rivers, Floods and the Water Resources of California. *Water*, 3(2), 445–478.
<https://doi.org/10.3390/w3020445>
- Dettinger, M., Ralph, F. M., & Lavers, D. A. (2015). Setting the Stage for a Global Science of Atmospheric Rivers. *Eos, Earth and Space Science News*, 96, 1–4.
- Eckhardt, S., Stohl, A., Wernli, H., James, P., Forster, C., & Spichtinger, N. (2004). A 15-year climatology of warm conveyor belts. *Journal of Climate*, 17(1), 218–237. [https://doi.org/10.1175/1520-0442\(2004\)017<0218:AYCOWC>2.0.CO;2](https://doi.org/10.1175/1520-0442(2004)017<0218:AYCOWC>2.0.CO;2)
- Eiras-Barca, J., Brands, S., & Miguez-Macho, G. (2016). Seasonal variations in North Atlantic atmospheric river activity and associations with anomalous precipitation over the Iberian Atlantic Margin. *Journal of Geophysical Research: Atmospheres*, 121(2), 931–948.
<https://doi.org/10.1002/2015JD023379>
- Eiras-Barca, J., Lorenzo, N., Taboada, J., Robles, A., & Miguez-Macho, G. (2018). On the relationship between atmospheric rivers, weather types and floods in Galicia (NW Spain). *Natural Hazards and Earth System Sciences*, 18(6), 1633–1645. <https://doi.org/10.5194/nhess-18-1633-2018>
- Eiras-Barca, J., Ramos, A. M., Algarra, I., Vázquez, M., Dominguez, F., Miguez-Macho, G., Nieto, R., Gimeno, L., Taboada, J., & Ralph, F. M. (2021). European West Coast atmospheric rivers: A

- scale to characterize strength and impacts. *Weather and Climate Extremes*, *31*, 100305.
<https://doi.org/10.1016/j.wace.2021.100305>
- Eiras-Barca, J., Ramos, A. M., Pinto, J. G., Trigo, R. M., Liberato, M. L. R., & Miguez-Macho, G. (2018). The concurrence of atmospheric rivers and explosive cyclogenesis in the North Atlantic and North Pacific basins. *Earth System Dynamics*, *9*(1), 91–102. <https://doi.org/10.5194/esd-9-91-2018>
- Esfandiari, N., & Lashkari, H. (2020). Identifying atmospheric river events and their paths into Iran. *Theoretical and Applied Climatology*, *140*(3–4), 1125–1137. <https://doi.org/10.1007/s00704-020-03148-w>
- Fairman Jr, J. G., Schultz, D. M., Kirshbaum, D. J., Gray, S. L., & Barrett, A. I. (2015). A radar-based rainfall climatology of Great Britain and Ireland. *Weather*, *70*(5), 153–158.
<https://doi.org/10.1002/wea.2486>
- Farquharson, F., Mackney, D., Newson, M., & Thomasson, A. (1978). Estimation of run-off potential of river catchments from soil surveys. *Special Survey*.
- Fish, M. A., Wilson, A. M., & Ralph, F. M. (2019). Atmospheric River Families: Definition and Associated Synoptic Conditions. *Journal of Hydrometeorology*, *20*(10), 2091–2108.
<https://doi.org/10.1175/JHM-D-18-0217.1>
- Galarnyk, M. (2021, February 3). *PCA using Python (scikit-learn)*. Medium.
<https://towardsdatascience.com/pca-using-python-scikit-learn-e653f8989e60>
- Gao, Y., Lu, J., & Leung, L. R. (2016). Uncertainties in Projecting Future Changes in Atmospheric Rivers and Their Impacts on Heavy Precipitation over Europe. *Journal of Climate*, *29*(18), 6711–6726.
<https://doi.org/10.1175/JCLI-D-16-0088.1>
- Gershunov, A., Shulgina, T., Clemesha, R. E. S., Guirguis, K., Pierce, D. W., Dettinger, M. D., Lavers, D. A., Cayan, D. R., Polade, S. D., Kalansky, J., & Ralph, F. M. (2019). Precipitation regime change in Western North America: The role of Atmospheric Rivers. *Scientific Reports*, *9*(1), 9944.
<https://doi.org/10.1038/s41598-019-46169-w>

- Gershunov, A., Shulgina, T., Ralph, F. M., Lavers, D. A., & Rutz, J. J. (2017). Assessing the climate-scale variability of atmospheric rivers affecting western North America. *Geophysical Research Letters*, *44*(15), 7900–7908. <https://doi.org/10.1002/2017GL074175>
- Gimeno, L., Dominguez, F., Nieto, R., Trigo, R., Drumond, A., Reason, C. J. C., Taschetto, A. S., Ramos, A. M., Kumar, R., & Marengo, J. (2016). Major Mechanisms of Atmospheric Moisture Transport and Their Role in Extreme Precipitation Events. *Annual Review of Environment and Resources*, *41*(1), 117–141. <https://doi.org/10.1146/annurev-environ-110615-085558>
- Gorodetskaya, I. V., Tsukernik, M., Claes, K., Ralph, M. F., Neff, W. D., & Lipzig, N. P. M. V. (2014). The role of atmospheric rivers in anomalous snow accumulation in East Antarctica. *Geophysical Research Letters*, *41*(17), 6199–6206. <https://doi.org/10.1002/2014GL060881>
- Griffith, H. V., Wade, A. J., Lavers, D. A., & Watts, G. (2020). Atmospheric river orientation determines flood occurrence. *Hydrological Processes*, *34*(23), 4547–4555.
- Grömping, U. (2015). Variable importance in regression models. *WIREs Computational Statistics*, *7*(2), 137–152. <https://doi.org/10.1002/wics.1346>
- Guan, B., & Waliser, D. E. (2015). Detection of atmospheric rivers: Evaluation and application of an algorithm for global studies. *Journal of Geophysical Research: Atmospheres*, *120*(24), 12514–12535. <https://doi.org/10.1002/2015JD024257>
- Hecht, C. W., & Cordeira, J. M. (2017). Characterizing the influence of atmospheric river orientation and intensity on precipitation distributions over North Coastal California: ARs and Precipitation Over North Coastal CA. *Geophysical Research Letters*, *44*(17), 9048–9058. <https://doi.org/10.1002/2017GL074179>
- Hersbach, H., Bell, B., Berrisford, P., Hirahara, S., Horányi, A., Muñoz-Sabater, J., Nicolas, J., Peubey, C., Radu, R., Schepers, D., Simmons, A., Soci, C., Abdalla, S., Abellan, X., Balsamo, G., Bechtold, P., Biavati, G., Bidlot, J., Bonavita, M., ... Thépaut, J. (2020). The ERA5 Global Reanalysis. *Quarterly Journal of the Royal Meteorological Society*, *qj.3803*. <https://doi.org/10.1002/qj.3803>
- Hewlett, J. D., & Hibbert, A. R. (1967). Factors affecting the response of small watersheds to precipitation in humid areas. *Forest Hydrology*, *1*, 275–290.

- Hill, F. F., Browning, K. A., & Bader, M. J. (1981). Radar and raingauge observations of orographic rain over south Wales. *Quarterly Journal of the Royal Meteorological Society*, *107*(453), 643–670.
<https://doi.org/10.1002/qj.49710745312>
- Horton, R. E. (1933). The role of infiltration in the hydrologic cycle. *Eos, Transactions American Geophysical Union*, *14*(1), 446–460. <https://doi.org/10.1029/TR014i001p00446>
- Hu, H., Dominguez, F., Wang, Z., Lavers, D. A., Zhang, G., & Ralph, F. M. (2017). Linking Atmospheric River Hydrological Impacts on the U.S. West Coast to Rossby Wave Breaking. *Journal of Climate*, *30*(9), 3381–3399. <https://doi.org/10.1175/JCLI-D-16-0386.1>
- Hughes, M., Mahoney, K. M., Neiman, P. J., Moore, B. J., Alexander, M., & Ralph, F. M. (2014). The Landfall and Inland Penetration of a Flood-Producing Atmospheric River in Arizona. Part II: Sensitivity of Modeled Precipitation to Terrain Height and Atmospheric River Orientation. *Journal of Hydrometeorology*, *15*(5), 1954–1974. <https://doi.org/10.1175/JHM-D-13-0176.1>
- Huning, L. S., Margulis, S. A., Guan, B., Waliser, D. E., & Neiman, P. J. (2017). Implications of Detection Methods on Characterizing Atmospheric River Contribution to Seasonal Snowfall Across Sierra Nevada, USA: Atmospheric River Detection and Snowfall. *Geophysical Research Letters*, *44*(20), 10,445–10,453. <https://doi.org/10.1002/2017GL075201>
- Hurrell, J. W., Kushnir, Y., Ottersen, G., & Visbeck, M. (2003). An overview of the North Atlantic Oscillation. In J. W. Hurrell, Y. Kushnir, G. Ottersen, & M. Visbeck (Eds.), *Geophysical Monograph Series* (Vol. 134, pp. 1–35). American Geophysical Union. <https://doi.org/10.1029/134GM01>
- Institute of Hydrology. (1999). *Flood estimation handbook*.
- Jolliffe, I. T., & Cadima, J. (2016). Principal component analysis: A review and recent developments. *Philosophical Transactions of the Royal Society A: Mathematical, Physical and Engineering Sciences*, *374*(2065), 20150202. <https://doi.org/10.1098/rsta.2015.0202>
- Kalnay, E., Kanamitsu, M., Kistler, R., Collins, W., Deaven, D., Gandin, L., Iredell, M., Saha, S., White, G., Woollen, J., Zhu, Y., Chelliah, M., Ebisuzaki, W., Higgins, W., Janowiak, J., Mo, K. C., Ropelewski, C., Wang, J., Leetmaa, A., ... Joseph, D. (1996). The NCEP/NCAR 40-Year Reanalysis Project. *Bulletin of the American Meteorological Society*, *77*(3), 437–472.
[https://doi.org/10.1175/1520-0477\(1996\)077<0437:TNYRP>2.0.CO;2](https://doi.org/10.1175/1520-0477(1996)077<0437:TNYRP>2.0.CO;2)

- Kendon, M., McCarthy, M., Jevrejeva, S., Matthews, A., Sparks, T., & Garforth, J. (2021). State of the UK Climate 2020. *International Journal of Climatology*, *41*(S2), 1–76. <https://doi.org/10.1002/joc.7285>
- Kingston, D. G., Lavers, D. A., & Hannah, D. M. (2016). Floods in the Southern Alps of New Zealand: The importance of atmospheric rivers: Atmospheric Rivers and Floods in New Zealand. *Hydrological Processes*, *30*(26), 5063–5070. <https://doi.org/10.1002/hyp.10982>
- Knight, J. R., Maidens, A., Watson, P. A. G., Andrews, M., Belcher, S., Brunet, G., Fereday, D., Folland, C. K., Scaife, A. A., & Slingo, J. (2017). Global meteorological influences on the record UK rainfall of winter 2013–14. *Environmental Research Letters*, *12*(7), 074001. <https://doi.org/10.1088/1748-9326/aa693c>
- Knippertz, P., & Wernli, H. (2010). A lagrangian climatology of tropical moisture exports to the northern hemispheric extratropics. *Journal of Climate*, *23*(4), 987–1003. <https://doi.org/10.1175/2009JCLI3333.1>
- Konrad, C. P., & Dettinger, M. D. (2017). Flood Runoff in Relation to Water Vapor Transport by Atmospheric Rivers Over the Western United States, 1949–2015. *Geophysical Research Letters*, *44*(22), 11,456–11,462. <https://doi.org/10.1002/2017GL075399>
- Lanjiri, M. A., Dettinger, M. D., Ralph, F. M., & Guan, B. (2017). Hourly storm characteristics along the U.S. West Coast: Role of atmospheric rivers in extreme precipitation: Storm Characteristics in U.S. West Coast. *Geophysical Research Letters*, *44*(13), 7020–7028. <https://doi.org/10.1002/2017GL074193>
- Lang, M., Ouarda, T. B. M. J., & Bobée, B. (1999). Towards operational guidelines for over-threshold modeling. *Journal of Hydrology*, *225*(3), 103–117. [https://doi.org/10.1016/S0022-1694\(99\)00167-5](https://doi.org/10.1016/S0022-1694(99)00167-5)
- Lavers, D. A., Allan, R. P., Villarini, G., Lloyd-Hughes, B., Brayshaw, D. J., & Wade, A. J. (2013). Future changes in atmospheric rivers and their implications for winter flooding in Britain. *Environmental Research Letters*, *8*(3), 034010. <https://doi.org/10.1088/1748-9326/8/3/034010>
- Lavers, D. A., Allan, R. P., Wood, E. F., Villarini, G., Brayshaw, D. J., & Wade, A. J. (2011). Winter floods in Britain are connected to atmospheric rivers. *Geophysical Research Letters*, *38*(23), n/a–n/a. <https://doi.org/10.1029/2011GL049783>

- Lavers, D. A., Ingleby, N. B., Subramanian, A. C., Richardson, D. S., Ralph, F. M., Doyle, J. D., Reynolds, C. A., Torn, R. D., Rodwell, M. J., Tallapragada, V., & Pappenberger, F. (2020). Forecast errors and uncertainties in atmospheric rivers. *Weather and Forecasting*, WAF-D-20-0049.1.
<https://doi.org/10.1175/WAF-D-20-0049.1>
- Lavers, D. A., Pappenberger, F., Richardson, D. S., & Zsoter, E. (2016). ECMWF Extreme Forecast Index for water vapor transport: A forecast tool for atmospheric rivers and extreme precipitation. *Geophysical Research Letters*, *43*(22), 11,852–11,858.
<https://doi.org/10.1002/2016GL071320>
- Lavers, D. A., Pappenberger, F., & Zsoter, E. (2014). Extending medium-range predictability of extreme hydrological events in Europe. *Nature Communications*, *5*(1), 5382.
<https://doi.org/10.1038/ncomms6382>
- Lavers, D. A., Ralph, F. M., Richardson, D. S., & Pappenberger, F. (2020). Improved forecasts of atmospheric rivers through systematic reconnaissance, better modelling, and insights on conversion of rain to flooding. *Communications Earth & Environment*, *1*(1), 39.
<https://doi.org/10.1038/s43247-020-00042-1>
- Lavers, D. A., Ralph, F. M., Waliser, D. E., Gershunov, A., & Dettinger, M. D. (2015). Climate change intensification of horizontal water vapor transport in CMIP5. *Geophysical Research Letters*, *42*(13), 5617–5625. <https://doi.org/10.1002/2015GL064672>
- Lavers, D. A., Rodwell, M. J., Richardson, D. S., Ralph, F. M., Doyle, J. D., Reynolds, C. A., Tallapragada, V., & Pappenberger, F. (2018). The Gauging and Modeling of Rivers in the Sky. *Geophysical Research Letters*, *45*(15), 7828–7834. <https://doi.org/10.1029/2018GL079019>
- Lavers, D. A., & Villarini, G. (2013a). The nexus between atmospheric rivers and extreme precipitation across Europe. *Geophysical Research Letters*, *40*(12), 3259–3264. <https://doi.org/10.1002/grl.50636>
- Lavers, D. A., & Villarini, G. (2013b). Atmospheric Rivers and Flooding over the Central United States. *Journal of Climate*, *26*(20), 7829–7836. <https://doi.org/10.1175/JCLI-D-13-00212.1>
- Lavers, D. A., & Villarini, G. (2015). The relationship between daily European precipitation and measures of atmospheric water vapour transport. *International Journal of Climatology*, *35*(8), 2187–2192.
<https://doi.org/10.1002/joc.4119>

- Lavers, D. A., Villarini, G., Allan, R. P., Wood, E. F., & Wade, A. J. (2012). The detection of atmospheric rivers in atmospheric reanalyses and their links to British winter floods and the large-scale climatic circulation. *Journal of Geophysical Research: Atmospheres*, *117*(D20).
<https://doi.org/10.1029/2012JD018027>
- Lavers, D. A., Waliser, D. E., Ralph, F. M., & Dettinger, M. D. (2016). Predictability of horizontal water vapor transport relative to precipitation: Enhancing situational awareness for forecasting western U.S. extreme precipitation and flooding. *Geophysical Research Letters*, *43*(5), 2275–2282.
<https://doi.org/10.1002/2016GL067765>
- Lavers, D., Prudhomme, C., & Hannah, D. M. (2010). Large-scale climate, precipitation and British river flows: Identifying hydroclimatological connections and dynamics. *Journal of Hydrology*, *395*(3–4), 242–255. <https://doi.org/10.1016/j.jhydrol.2010.10.036>
- Ledingham, J., Archer, D., Lewis, E., Fowler, H., & Kilsby, C. (2019). Contrasting seasonality of storm rainfall and flood runoff in the UK and some implications for rainfall-runoff methods of flood estimation. *Hydrology Research*, *50*(5), 1309–1323. <https://doi.org/10.2166/nh.2019.040>
- León, J. A. P. (2019, April 15). *Global reanalysis: Goodbye ERA-Interim, hello ERA5* [Text]. ECMWF.
<https://www.ecmwf.int/en/newsletter/159/meteorology/global-reanalysis-goodbye-era-interim-hello-era5>
- Liaw, A., & Wiener, M. (2002). *Classification and Regression by randomForest*. *2*, 5.
- Liberato, M. L. R., Ramos, A. M., Trigo, R. M., Trigo, I. F., Durán-Quesada, A. M., Nieto, R., & Gimeno, L. (2013). Moisture Sources and Large-Scale Dynamics Associated With a Flash Flood Event. In J. Lin, D. Brunner, C. Gerbig, A. Stohl, A. Luhar, & P. Webley (Eds.), *Geophysical Monograph Series* (pp. 111–126). American Geophysical Union. <https://doi.org/10.1029/2012GM001244>
- Lora, J. M., Shields, C. A., & Rutz, J. J. (2020). Consensus and Disagreement in Atmospheric River Detection: ARTMIP Global Catalogues. *Geophysical Research Letters*, *47*(20), e2020GL089302.
<https://doi.org/10.1029/2020GL089302>
- Macalalad, R. V., Badilla, R. A., Cabrera, O. C., & Bagtasa, G. (2021). Hydrological Response of the Pampanga River Basin in the Philippines to Intense Tropical Cyclone Rainfall. *Journal of Hydrometeorology*, *22*(4), 781–794. <https://doi.org/10.1175/JHM-D-20-0184.1>

- Mahoney, K., Jackson, D. L., Neiman, P., Hughes, M., Darby, L., Wick, G., White, A., Sukovich, E., & Cifelli, R. (2016). Understanding the Role of Atmospheric Rivers in Heavy Precipitation in the Southeast United States. *Monthly Weather Review*, *144*(4), 1617–1632.
<https://doi.org/10.1175/MWR-D-15-0279.1>
- Maraun, D., Rust, H. W., & Osborn, T. J. (2009). The annual cycle of heavy precipitation across the United Kingdom: A model based on extreme value statistics. *International Journal of Climatology*, *29*(12), 1731–1744. <https://doi.org/10.1002/joc.1811>
- Martin, A. C., Ralph, F. M., Wilson, A., DeHaan, L., & Kawzenuk, B. (2019). Rapid Cyclogenesis from a Mesoscale Frontal Wave on an Atmospheric River: Impacts on Forecast Skill and Predictability during Atmospheric River Landfall. *Journal of Hydrometeorology*, *20*(9), 1779–1794.
<https://doi.org/10.1175/JHM-D-18-0239.1>
- Matsumoto, S., Yoshizumi, S., & Takeuchi, M. (1970). On the Structure of the “Baiu Front” and the Associated Intermediate-scale Disturbances in the Lower Atmosphere. *Journal of the Meteorological Society of Japan. Ser. II*, *48*(6), 479–491.
https://doi.org/10.2151/jmsj1965.48.6_479
- Mediero, L., Kjeldsen, T. R., Macdonald, N., Kohnova, S., Merz, B., Vorogushyn, S., Wilson, D., Albuquerque, T., Blöschl, G., Bogdanowicz, E., Castellarin, A., Hall, J., Kobold, M., Kriauciuniene, J., Lang, M., Madsen, H., Onușluel Gül, G., Perdigão, R. A. P., Roald, L. A., ... Pórarinnsson, Ó. (2015). Identification of coherent flood regions across Europe by using the longest streamflow records. *Journal of Hydrology*, *528*, 341–360.
<https://doi.org/10.1016/j.jhydrol.2015.06.016>
- Miglietta, M. M., & Rotunno, R. (2005). Simulations of Moist Nearly Neutral Flow over a Ridge. *Journal of the Atmospheric Sciences*, *62*(5), 1410–1427. <https://doi.org/10.1175/JAS3410.1>
- Miglietta, M. M., & Rotunno, R. (2006). Further Results on Moist Nearly Neutral Flow over a Ridge. *Journal of the Atmospheric Sciences*, *63*(11), 2881–2897. <https://doi.org/10.1175/JAS3793.1>
- Miles, M. K. (1962). Wind, temperature and humidity distribution at some cold fronts over SE. England. *Quarterly Journal of the Royal Meteorological Society*, *88*(377), 286–300.
<https://doi.org/10.1002/qj.49708837708>

- Moon, H., Kim, J., Guan, B., Waliser, D. E., Choi, J., Goo, T.-Y., Kim, Y., & Byun, Y.-H. (2019). The Effects of Atmospheric River Landfalls on Precipitation and Temperature in Korea. *Atmosphere. Korean Meteorological Society*, 29(4), 343–353. <https://doi.org/10.14191/ATMOS.2019.29.4.343>
- Moore, B. J., Neiman, P. J., Ralph, F. M., & Barthold, F. E. (2012a). Physical Processes Associated with Heavy Flooding Rainfall in Nashville, Tennessee, and Vicinity during 1–2 May 2010: The Role of an Atmospheric River and Mesoscale Convective Systems*. *Monthly Weather Review*, 140(2), 358–378. <https://doi.org/10.1175/MWR-D-11-00126.1>
- Moore, B. J., Neiman, P. J., Ralph, F. M., & Barthold, F. E. (2012b). Physical Processes Associated with Heavy Flooding Rainfall in Nashville, Tennessee, and Vicinity during 1–2 May 2010: The Role of an Atmospheric River and Mesoscale Convective Systems. *Monthly Weather Review*, 140(2), 358–378. <https://doi.org/10.1175/MWR-D-11-00126.1>
- Morris, D. G., & Flavin, R. W. (1990). A digital terrain model for hydrology. *Proc 4th International Symposium on Spatial Data Handling*, 1, pp 250-262.
- Morris, D. G., & Flavin, R. W. (1994). Sub-set of the UK 50 m by 50 m hydrological digital terrain model grids. *NERC, Institute of Hydrology, Wallingford*.
- Nayak, M. A., Villarini, G., & Bradley, A. A. (2016). Atmospheric Rivers and Rainfall during NASA's Iowa Flood Studies (IFloodS) Campaign. *Journal of Hydrometeorology*, 17(1), 257–271. <https://doi.org/10.1175/JHM-D-14-0185.1>
- Neff, W., Compo, G. P., Ralph, F. M., & Shupe, M. D. (2014). Continental heat anomalies and the extreme melting of the Greenland ice surface in 2012 and 1889. *Journal of Geophysical Research: Atmospheres*, 119(11), 6520–6536. <https://doi.org/10.1002/2014JD021470>
- Neiman, P. J., Hughes, M., Moore, B. J., Ralph, F. M., & Sukovich, E. M. (2013). Sierra Barrier Jets, Atmospheric Rivers, and Precipitation Characteristics in Northern California: A Composite Perspective Based on a Network of Wind Profilers. *Monthly Weather Review*, 141(12), 4211–4233. <https://doi.org/10.1175/MWR-D-13-00112.1>
- Neiman, P. J., Moore, B. J., White, A. B., Wick, G. A., Aikins, J., Jackson, D. L., Spackman, J. R., & Ralph, F. M. (2016). An Airborne and Ground-Based Study of a Long-Lived and Intense

- Atmospheric River with Mesoscale Frontal Waves Impacting California during CalWater-2014. *Monthly Weather Review*, 144(3), 1115–1144. <https://doi.org/10.1175/MWR-D-15-0319.1>
- Neiman, P. J., Ralph, F. M., Moore, B. J., Hughes, M., Mahoney, K. M., Cordeira, J. M., & Dettinger, M. D. (2013). The Landfall and Inland Penetration of a Flood-Producing Atmospheric River in Arizona. Part I: Observed Synoptic-Scale, Orographic, and Hydrometeorological Characteristics. *Journal of Hydrometeorology*, 14(2), 460–484. <https://doi.org/10.1175/JHM-D-12-0101.1>
- Neiman, P. J., Ralph, F. M., Moore, B. J., & Zamora, R. J. (2014). The Regional Influence of an Intense Sierra Barrier Jet and Landfalling Atmospheric River on Orographic Precipitation in Northern California: A Case Study. *Journal of Hydrometeorology*, 15(4), 1419–1439. <https://doi.org/10.1175/JHM-D-13-0183.1>
- Neiman, P. J., Ralph, F. M., White, A. B., Kingsmill, D. E., & Persson, P. O. G. (2002). The Statistical Relationship between Upslope Flow and Rainfall in California's Coastal Mountains: Observations during CALJET. *Monthly Weather Review*, 130, 25.
- Neiman, P. J., Ralph, F. M., Wick, G. A., Lundquist, J. D., & Dettinger, M. D. (2008). Meteorological Characteristics and Overland Precipitation Impacts of Atmospheric Rivers Affecting the West Coast of North America Based on Eight Years of SSM/I Satellite Observations. *Journal of Hydrometeorology*, 9(1), 22–47. <https://doi.org/10.1175/2007JHM855.1>
- Neiman, P. J., Schick, L. J., Ralph, F. M., Hughes, M., & Wick, G. A. (2011). Flooding in Western Washington: The Connection to Atmospheric Rivers. *Journal of Hydrometeorology*, 12(6), 1337–1358. <https://doi.org/10.1175/2011JHM1358.1>
- Neiman, P. J., White, A. B., Ralph, F. M., Gattas, D. J., & Gutman, S. I. (2009). A water vapour flux tool for precipitation forecasting. *Proceedings of the Institution of Civil Engineers - Water Management*, 162(2), 83–94. <https://doi.org/10.1680/wama.2009.162.2.83>
- Newell, R. E., Newell, N. E., Zhu, Y., & Scott, C. (1992). Tropospheric rivers? - A pilot study. *Geophysical Research Letters*, 19(24), 2401–2404. <https://doi.org/10.1029/92GL02916>
- Oakley, N. S., Cannon, F., Boldt, E., Dumas, J., & Ralph, F. M. (2018). Origins and variability of extreme precipitation in the Santa Ynez River Basin of Southern California. *Journal of Hydrology: Regional Studies*, 19, 164–176. <https://doi.org/10.1016/j.ejrh.2018.09.001>

- Oakley, N. S., Lancaster, J. T., Hatchett, B. J., Stock, J., Ralph, F. M., Roj, S., & Lukashov, S. (2018). A 22-Year Climatology of Cool Season Hourly Precipitation Thresholds Conducive to Shallow Landslides in California. *Earth Interactions*, 22(14), 1–35. <https://doi.org/10.1175/EI-D-17-0029.1>
- O'Brien, T. A., Payne, A. E., Shields, C. A., Rutz, J., Brands, S., Castellano, C., Chen, J., Cleveland, W., DeFlorio, M. J., Goldenson, N., Gorodetskaya, I. V., Díaz, H. I., Kashinath, K., Kawzenuk, B., Kim, S., Krinitskiy, M., Lora, J. M., McClenny, B., Michaelis, A., ... Zhou, Y. (2020). Detection Uncertainty Matters for Understanding Atmospheric Rivers. *Bulletin of the American Meteorological Society*, 101(6), E790–E796. <https://doi.org/10.1175/BAMS-D-19-0348.1>
- Paltan, H., Waliser, D., Lim, W. H., Guan, B., Yamazaki, D., Pant, R., & Dadson, S. (2017). Global Floods and Water Availability Driven by Atmospheric Rivers: Global Hydrology and ARs. *Geophysical Research Letters*, 44(20), 10,387-10,395. <https://doi.org/10.1002/2017GL074882>
- Picard, L., & Mass, C. (2017). The Sensitivity of Orographic Precipitation to Flow Direction: An Idealized Modeling Approach. *Journal of Hydrometeorology*, 18(6), 1673–1688. <https://doi.org/10.1175/JHM-D-16-0209.1>
- Płoński, P. (2020, June 29). *Random Forest Feature Importance Computed in 3 Ways with Python*. MLJAR Automated Machine Learning. <https://mljar.com/blog/feature-importance-in-random-forest/>
- Priestley, M. D. K., Dacre, H. F., Shaffrey, L. C., Schemm, S., & Pinto, J. G. (2020). The role of secondary cyclones and cyclone families for the North Atlantic storm track and clustering over western Europe. *Quarterly Journal of the Royal Meteorological Society*, 146(728), 1184–1205. <https://doi.org/10.1002/qj.3733>
- Prince, H. D., Cullen, N. J., Gibson, P. B., Conway, J., & Kingston, D. G. (2021). A Climatology of Atmospheric Rivers in New Zealand. *Journal of Climate*, 34(11), 4383–4402. <https://doi.org/10.1175/JCLI-D-20-0664.1>
- Ralph, F. M. (1999). *The California Land-falling Jets Experiment (CALJET): Motivation, Strategy, and Description of a Flooding Event*. 16.
- Ralph, F. M., Coleman, T., Neiman, P. J., Zamora, R. J., & Dettinger, M. D. (2013). Observed Impacts of Duration and Seasonality of Atmospheric-River Landfalls on Soil Moisture and Runoff in Coastal

- Northern California. *Journal of Hydrometeorology*, 14(2), 443–459. <https://doi.org/10.1175/JHM-D-12-076.1>
- Ralph, F. M., Cordeira, J. M., Neiman, P. J., & Hughes, M. (2016). Landfalling Atmospheric Rivers, the Sierra Barrier Jet, and Extreme Daily Precipitation in Northern California's Upper Sacramento River Watershed. *Journal of Hydrometeorology*, 17(7), 1905–1914. <https://doi.org/10.1175/JHM-D-15-0167.1>
- Ralph, F. M., Dettinger, M. D., Rutz, J. J., & Waliser, D. E. (2020). *Atmospheric Rivers* (1st ed.). Springer International Publishing.
- Ralph, F. M., Intrieri, J., Andra Jr, D., Atlas, R., Boukabara, S., Bright, D., Davidson, P., Entwistle, B., Gaynor, J., & Goodman, S. (2013). The emergence of weather-related test beds linking research and forecasting operations. *Bulletin of the American Meteorological Society*, 94(8), 1187–1211.
- Ralph, F. M., Neiman, P. J., Kiladis, G. N., Weickmann, K., & Reynolds, D. W. (2011a). A Multiscale Observational Case Study of a Pacific Atmospheric River Exhibiting Tropical–Extratropical Connections and a Mesoscale Frontal Wave. *Monthly Weather Review*, 139(4), 1169–1189. <https://doi.org/10.1175/2010MWR3596.1>
- Ralph, F. M., Neiman, P. J., Kiladis, G. N., Weickmann, K., & Reynolds, D. W. (2011b). A Multiscale Observational Case Study of a Pacific Atmospheric River Exhibiting Tropical–Extratropical Connections and a Mesoscale Frontal Wave. *Monthly Weather Review*, 139(4), 1169–1189. <https://doi.org/10.1175/2010MWR3596.1>
- Ralph, F. M., Neiman, P. J., Kingsmill, D. E., Persson, P. O. G., & White, A. B. (2003). The Impact of a Prominent Rain Shadow on Flooding in California's Santa Cruz Mountains: A CALJET Case Study and Sensitivity to the ENSO Cycle. *JOURNAL OF HYDROMETEOROLOGY*, 4, 22.
- Ralph, F. M., Neiman, P. J., & Rotunno, R. (2005). Dropsonde Observations in Low-Level Jets over the Northeastern Pacific Ocean from CALJET-1998 and PACJET-2001: Mean Vertical-Profile and Atmospheric-River Characteristics. *Monthly Weather Review*, 133(4), 889–910. <https://doi.org/10.1175/MWR2896.1>

- Ralph, F. M., Neiman, P. J., & Wick, G. A. (2004). Satellite and CALJET Aircraft Observations of Atmospheric Rivers over the Eastern North Pacific Ocean during the Winter of 1997/98. *MONTHLY WEATHER REVIEW*, *132*, 25.
- Ralph, F. M., Neiman, P. J., Wick, G. A., Gutman, S. I., Dettinger, M. D., Cayan, D. R., & White, A. B. (2006). Flooding on California's Russian River: Role of atmospheric rivers. *Geophysical Research Letters*, *33*(13), L13801. <https://doi.org/10.1029/2006GL026689>
- Ralph, F. M., Rutz, J. J., Cordeira, J. M., Dettinger, M., Anderson, M., Reynolds, D., Schick, L. J., & Smallcomb, C. (2019). A Scale to Characterize the Strength and Impacts of Atmospheric Rivers. *Bulletin of the American Meteorological Society*, *100*(2), 269–289. <https://doi.org/10.1175/BAMS-D-18-0023.1>
- Ralph, F. M., Wilson, A. M., Shulgina, T., Kawzenuk, B., Sellars, S., Rutz, J. J., Lamjiri, M. A., Barnes, E. A., Gershunov, A., Guan, B., Nardi, K. M., Osborne, T., & Wick, G. A. (2019). ARTMIP-early start comparison of atmospheric river detection tools: How many atmospheric rivers hit northern California's Russian River watershed? *Climate Dynamics*, *52*(7–8), 4973–4994. <https://doi.org/10.1007/s00382-018-4427-5>
- Ramos, A. M., Nieto, R., Tomé, R., Gimeno, L., Trigo, R. M., Liberato, M. L. R., & Lavers, D. A. (2016). Atmospheric rivers moisture sources from a Lagrangian perspective. *Earth System Dynamics*, *7*(2), 371–384. <https://doi.org/10.5194/esd-7-371-2016>
- Ramos, A. M., Sousa, P. M., Dutra, E., & Trigo, R. M. (2020). Predictive skill for atmospheric rivers in the western Iberian Peninsula. *Natural Hazards and Earth System Sciences*, *20*(3), 877–888. <https://doi.org/10.5194/nhess-20-877-2020>
- Ramos, A. M., Trigo, R. M., Liberato, M. L. R., & Tomé, R. (2015). Daily Precipitation Extreme Events in the Iberian Peninsula and Its Association with Atmospheric Rivers. *Journal of Hydrometeorology*, *16*(2), 579–597. <https://doi.org/10.1175/JHM-D-14-0103.1>
- Random Forest Regression: When Does It Fail and Why?* (2020, May 22). Neptune.Ai. <https://neptune.ai/blog/random-forest-regression-when-does-it-fail-and-why>
- Rao, P. C., Shinde, A. S., & Jaswal, A. K. (2016). *Intense Precipitation causing Floods over Himalayan Region of Northern India – A case study on Role of Atmospheric Rivers*. 10.

- Rauber, R. M., Hu, H., Dominguez, F., Nesbitt, S. W., McFarquhar, G. M., Zaremba, T. J., & Finlon, J. A. (2020). Structure of an Atmospheric River Over Australia and the Southern Ocean. Part I: Tropical and Midlatitude Water Vapor Fluxes. *Journal of Geophysical Research: Atmospheres*, *125*(18), e2020JD032513. <https://doi.org/10.1029/2020JD032513>
- Robins, N. S., & Davies, J. (2015). *Hydrogeology of Wales*. British Geological Survey (Natural Environment Research Council).
- Rössler, O., Froidevaux, P., Börst, U., Rickli, R., Martius, O., & Weingartner, R. (2014). Retrospective analysis of a nonforecasted rain-on-snow flood in the Alps – a matter of model limitations or unpredictable nature? *Hydrol. Earth Syst. Sci.*, *21*.
- Rutz, J. J., Shields, C. A., Lora, J. M., Payne, A. E., Guan, B., Ullrich, P., O'Brien, T., Leung, L. R., Ralph, F. M., Wehner, M., Brands, S., Collow, A., Goldenson, N., Gorodetskaya, I., Griffith, H., Kashinath, K., Kawzenuk, B., Krishnan, H., Kurlin, V., ... Viale, M. (2019). The Atmospheric River Tracking Method Intercomparison Project (ARTMIP): Quantifying Uncertainties in Atmospheric River Climatology. *Journal of Geophysical Research: Atmospheres*, *124*(24), 13777–13802. <https://doi.org/10.1029/2019JD030936>
- Rutz, J. J., Steenburgh, W. J., & Ralph, F. M. (2014). Climatological Characteristics of Atmospheric Rivers and Their Inland Penetration over the Western United States. *Monthly Weather Review*, *142*(2), 905–921. <https://doi.org/10.1175/MWR-D-13-00168.1>
- Schäfler, A., Craig, G., Wernli, H., Arbogast, P., Doyle, J. D., McTaggart-Cowan, R., Methven, J., Rivière, G., Ament, F., Boettcher, M., Bramberger, M., Cazenave, Q., Cotton, R., Crewell, S., Delanoë, J., Dörnbrack, A., Ehrlich, A., Ewald, F., Fix, A., ... Zinner, T. (2018). The North Atlantic Waveguide and Downstream Impact Experiment. *Bulletin of the American Meteorological Society*, *99*(8), 1607–1637. <https://doi.org/10.1175/BAMS-D-17-0003.1>
- Schäfler, A., Harvey, B., Methven, J., Doyle, J. D., Rahm, S., Reitebuch, O., Weiler, F., & Witschas, B. (2020). Observation of Jet Stream Winds during NAWDEX and Characterization of Systematic Meteorological Analysis Errors. *Monthly Weather Review*, *148*, 19.

- Shields, C. A., & Kiehl, J. T. (2016). Atmospheric river landfall-latitude changes in future climate simulations. *Geophysical Research Letters*, *43*(16), 8775–8782.
<https://doi.org/10.1002/2016GL070470>
- Shields, C. A., Rutz, J. J., Leung, L.-Y., Ralph, F. M., Wehner, M., Kawzenuk, B., Lora, J. M., McClenny, E., Osborne, T., Payne, A. E., Ullrich, P., Gershunov, A., Goldenson, N., Guan, B., Qian, Y., Ramos, A. M., Sarangi, C., Sellars, S., Gorodetskaya, I., ... Nguyen, P. (2018). Atmospheric River Tracking Method Intercomparison Project (ARTMIP): Project Goals and Experimental Design. *Geoscientific Model Development Discussions*, *January*, 1–55. <https://doi.org/10.5194/gmd-2017-295>
- Shields, C. A., Rutz, J. J., Leung, L.-Y., Ralph, F. M., Wehner, M., Kawzenuk, B., Lora, J. M., McClenny, E., Osborne, T., Payne, A. E., Ullrich, P., Gershunov, A., Goldenson, N., Guan, B., Qian, Y., Ramos, A. M., Sarangi, C., Sellars, S., Gorodetskaya, I., ... Nguyen, P. (2018). Atmospheric River Tracking Method Intercomparison Project (ARTMIP): Project goals and experimental design. *Geoscientific Model Development*, *11*(6), 2455–2474. <https://doi.org/10.5194/gmd-11-2455-2018>
- Sodemann, H., & Stohl, A. (2013). Moisture Origin and Meridional Transport in Atmospheric Rivers and Their Association with Multiple Cyclones*. *Monthly Weather Review*, *141*(8), 2850–2868.
<https://doi.org/10.1175/MWR-D-12-00256.1>
- Stephens, E., & Cloke, H. (2014). Improving flood forecasts for better flood preparedness in the UK (and beyond). *The Geographical Journal*, *180*(4), 310–316. <https://doi.org/10.1111/geoj.12103>
- Stohl, A., Forster, C., & Sodemann, H. (2008a). Remote sources of water vapor forming precipitation on the Norwegian west coast at 60N - A tale of hurricanes and an atmospheric river. *Journal of Geophysical Research: Atmospheres*, *113*(5). <https://doi.org/10.1029/2007JD009006>
- Stohl, A., Forster, C., & Sodemann, H. (2008b). Remote sources of water vapor forming precipitation on the Norwegian west coast at 60°N-a tale of hurricanes and an atmospheric river. *Journal of Geophysical Research: Atmospheres*, *113*(D5), n/a-n/a. <https://doi.org/10.1029/2007JD009006>
- Sumargo, E., McMillan, H., Weihs, R., Ellis, C. J., Wilson, A. M., & Ralph, F. M. (2021). A soil moisture monitoring network to assess controls on runoff generation during atmospheric river events. *Hydrological Processes*, *35*(1), e13998. <https://doi.org/10.1002/hyp.13998>

- Trigo, R. M., Varino, F., Ramos, A. M., Valente, M. A., ZÃazere, J. L., Vaquero, J. M., Gouveia, C. M., & Russo, A. (2014). The record precipitation and flood event in Iberia in December 1876: Description and synoptic analysis. *Frontiers in Earth Science*, 2. <https://doi.org/10.3389/feart.2014.00003>
- Tsuji, H., & Takayabu, Y. N. (2019). Precipitation Enhancement via the Interplay between Atmospheric Rivers and Cutoff Lows. *Monthly Weather Review*, 147(7), 2451–2466. <https://doi.org/10.1175/MWR-D-18-0358.1>
- UK Met Office. (2020). *Record breaking rainfall—Met Office*. <https://www.metoffice.gov.uk/about-us/press-office/news/weather-and-climate/2020/2020-winter-february-stats>
- Ulbrich, U., Pinto, J. G., Kupfer, H., Leckebusch, G. C., Spanghel, T., & Reyers, M. (2008). Changing Northern Hemisphere Storm Tracks in an Ensemble of IPCC Climate Change Simulations. *Journal of Climate*, 21(8), 1669–1679. <https://doi.org/10.1175/2007JCLI1992.1>
- Viale, M., & Nuñez, M. N. (2011). Climatology of Winter Orographic Precipitation over the Subtropical Central Andes and Associated Synoptic and Regional Characteristics. *Journal of Hydrometeorology*, 12(4), 481–507. <https://doi.org/10.1175/2010JHM1284.1>
- Waliser, D., & Guan, B. (2017). Extreme winds and precipitation during landfall of atmospheric rivers. *Nature Geoscience*, 10(3), 179–183. <https://doi.org/10.1038/ngeo2894>
- Warner, M. D., Mass, C. F., & Salathé, E. P. (2015). Changes in Winter Atmospheric Rivers along the North American West Coast in CMIP5 Climate Models. *Journal of Hydrometeorology*, 16(1), 118–128. <https://doi.org/10.1175/JHM-D-14-0080.1>
- Watts, G., Battarbee, R. W., Bloomfield, J. P., Crossman, J., Daccache, A., Durance, I., Elliott, J. A., Garner, G., Hannaford, J., Hannah, D. M., Hess, T., Jackson, C. R., Kay, A. L., Kernan, M., Knox, J., Mackay, J., Monteith, D. T., Ormerod, S. J., Rance, J., ... Wilby, R. L. (2015). Climate change and water in the UK – past changes and future prospects. *Progress in Physical Geography: Earth and Environment*, 39(1), 6–28. <https://doi.org/10.1177/0309133314542957>
- Zhou, Y., O'Brien, T. A., Ullrich, P. A., Collins, W. D., Patricola, C. M., & Rhoades, A. M. (2021). Uncertainties in Atmospheric River Lifecycles by Detection Algorithms: Climatology and

- Variability. *Journal of Geophysical Research: Atmospheres*, 126(8), e2020JD033711.
<https://doi.org/10.1029/2020JD033711>
- Zhu, Y., & Newell, R. E. (1994). Atmospheric rivers and bombs. *Geophysical Research Letters*, 21(18), 1999–2002. <https://doi.org/10.1029/94GL01710>
- Zhu, Y., & Newell, R. E. (1998a). A Proposed Algorithm for Moisture Fluxes from Atmospheric Rivers. *Monthly Weather Review*, 126, 725–735.
- Zhu, Y., & Newell, R. E. (1998b). A Proposed Algorithm for Moisture Fluxes from Atmospheric Rivers. *Monthly Weather Review*, 126, 11.
- Zsótér, E. (2006). Recent developments in extreme weather forecasting. *ECMWF, Newsletter Number 107*.
<https://doi.org/10.21957/KL9821HNC7>

Appendices

Appendix 1 Catchment descriptors for the study catchments (Flood Estimation Handbook, CEH; Ledingham et al., 2019)

Station Name	Size and Configuration				Altitude		Slope and Aspect					Permeability of underlying bedrock (%)									
	Catchment Area (km ²)	Longest Path LDP (km)	Mean Drainage Path Length (km)	SHAPE FACTOR, Sf (LDP/2)/sqr(Area)	Maximum Altitude (m)	Mean Altitude (m)	Mean Drainage Path Slope (DSPBAR)	Mean Aspect (ASPBAR)	Invariability in Aspect (0-1) (measure of directionality)	Flood Attenuation by Reservoirs and Lakes (FARL)	Average Annual Rainfall (SAAR) mm	BFIHOST (Base Flow Index)	SPRHOSR (Standard Percentage Runoff)	PROPWET	URBEXT	High	Moderate	Low	Very Low	Mixed	
79004	Scar Water at Capenoch	142.47	27.15	13.49	1.137	597.2	318.1	199.76	106.5	0.167	0.999	1730	0.446	42	0.66	0.0001	0	0	0	100	0
78003	Annan at Brydekirk	924.96	77.56	43.77	1.275	820	225.7	128.21	169.6	0.145	0.992	1446	0.486	39	0.62	0.0014	19.87	0.14	0	80.48	0
80001	Urr at Dalbeattie	196.94	37.85	20.38	1.348	423.3	155.1	81.17	169.7	0.131	0.969	1352	0.376	48.4	0.64	0.0004	0	0	0	100	0
81002	Cree at Newton Stewart	367	46.01	23.97	1.200	843	237.8	120.88	204	0.234	0.944	1712	0.342	50.8	0.69	0.0011	0	0	0	100	0
80003	White Laggan Burn at Loch Dee	5.71	4.22	2.03	0.883	657.6	440.5	252.37	2.9	0.367	0.996	2141	0.358	49.1	0.69	0	0	0	0	100	0
83006	Ayr at Mainholm	579.01	69.38	41.32	1.441	591.5	219.4	75.23	288.2	0.159	0.994	1221	0.33	46.1	0.62	0.0033	33.65	41.91	0	24.45	0

83013	Irvine at Glenfield	218				383.3	160.1	63.9			0.99	1222	0.35		0.59	0.0373	35.58	27.88	0	38.54	0
89003	Orchy at Glen Orchy	251.2				1082.3	365.6	252.3			0.89	2713	0.36		0.79	0.17	0	0	0	95.41	4.59
90003	Nevis at Claggan	69.2				1342.6	520.95	441.8			1	2913	0.43		0.81	0.17	0	0	0	92.97	7.03
93001	Carron at New Kelso	138.96	27.9	14.96	1.183	1052.7	356.4	297.66	185.6	0.02	0.884	2503	0.406	49.1	0.83	0.0001	0	0	0	100	0
12006	Gairn at Invergairn	145.91	34.12	16.67	1.412	1160.4	556.6	184.16	132.3	0.168	0.997	1036	0.452	42.7	0.64	0	0	0	0	100	0
12003	Dee at Polhollick	697.33	62.68	36.92	1.186	1308.9	621.2	224.44	94	0.035	0.99	1342	0.458	44.9	0.68	0.0001	0	0	0	94.84	5.16
12005	Muick at Invermuick	110.25	28.96	15.04	1.379	1149	589.8	192.23	8.5	0.146	0.961	1350	0.514	42.8	0.68	0.0001	0	0	0	100	0
12007	Dee at Mar Lodge	292.09	42	15.11	1.228	1308.9	682.7	240.3	117.1	0.088	0.99	1492	0.4	50.1	0.69	0.0001	0	0	0	98.04	1.96
94001	Ewe at Poolewe	441.14	47.39	25.92	1.128	1007.3	311.3	226.53	6.1	0.107	0.67	2345	0.365	50.1	0.83	0.0001	0	0	0	100	0
3003	Oykel at Easter Turnaig	331.92	31.02	16.61	0.851	1005.8	296.9	151.33	62.5	0.065	0.919	1962	0.359	53.6	0.81	0	0	0	0	99.99	0.01
4005	Meig at Glenmeanie	120.5				1052.7	462.7	289			0.92	2145	0.39		0.76	0	0	0	0	100	0
4006	Bran at Dosmucheran	116.1				913.5	330	164.6			0.81	2203	0.53		0.83	0	0	0	0	100	0

6008	Enrick at Mill of Tore	105.95	25.04	11.23	1.216	674.8	347.4	120.37	353.1	0.139	0.852	1349	0.43	43.6	0.7	0.0002	0	0	0	100	0
7001	Findhorn at Shenachie	415.87	50.98	25.63	1.249	935.3	559.9	141.77	22.9	0.106	0.992	1429	0.451	55.8	0.68	0	0	0	0	100	0
8013	Feshie at Feshie Bridge	231				1263.2	619.5	180.8			0.99	1286	0.48		0.7	0	0	0	0	100	0
95001	Inver at Little Assynt	137.5				1108.6	269.7	190.3			0.67	2208	0.4		0.77	0	0	0	0	87.01	12.99
96001	Halladale at Halladale	194.04	28.36	13.37	1.017	568.7	174.5	56.31	1.5	0.137	0.969	1055	0.298	55.6	0.69	0	0	0	0	100	0
96003	Strathy at Strathy Bridge	111.8				345.1	159.7	58.1			0.9	1090	0.29		0.6	0	0	8.94	0	91.06	0
96004	Strathmore at Allnabad	105				851.4	306.9	192.3			0.94	2455	0.35		0.85	0	0	0	0	100	0
85003	Falloch at Glen Falloch	80.3				1120	447.4	256.1			0.99	2847	0.38		0.78	0	0	0	0	99.95	0.05
16003	Ruchill Water at Cultybraggan	98.58	22.58	12.79	1.137	978.6	401	221.2	55.1	0.138	1	1940	0.428	44.5	0.59	0.0001	0	43.06	0	56.94	0
54005	Severn at Montford	2035.3	115.93	64.71	1.285	826.2	248.4	136.38	99	0.099	0.98	1145	0.472	38.4	0.5	0.0026	7.21	1.2	0	90.36	0
54008	Teme at Tenbury	1123.3	80.48	44	1.201	544.5	231.1	118.66	141.6	0.118	0.995	841	0.612	28.5	0.36	0.0062	0	0	0	77.75	22.25

55002	Wye at Belmont	1918.9	157.38	95.12	1.796	750	295.4	136.61	130	0.083	0.968	1223	0.473	39.7	0.49	0.0021	0	0	0	100	0
55003	Lugg at Lugwardine	879.6	85.74	48.93	1.445	659.7	190.2	96.87	125.6	0.141	0.982	814	0.587	33.8	0.35	0.0075	0	0	0	84.89	15.11
56001	Usk at Chainbridge	925	91.69	53.03	1.507	884.7	312.5	162.81	111	0.069	0.982	1368	0.596	29	0.56	0.0045	0	2.04	0	97.03	0.93
60001	Tywi at Ty Castell	1087.8				832.7		156.9			0.98	1535	0.48		0.59		0	0.83	0	99.17	0
60003	Taf at Clog-y- Fran	216.73	36.6	17.13	1.243	393	124.8	104.81	177.5	0.089	0.999	1420	0.553	34	0.46	0.0017	0	0	0	100	0
60006	Gwili at Glangwili	130.98	26.09	15.84	1.140	354.4	188.1	154.11	194.1	0.136	1	1603	0.536	35.1	0.52	0.0008	0	0	0	100	0
61001	Western Cleddau at Prendergast Mill	197.76	29.45	15.65	1.047	372.6	108.4	69.42	206.4	0.108	0.997	1276	0.56	32.6	0.44	0.0012	0	0.55	0	99.33	0.12
61002	Eastern Cleddau at Canaston Bridge	181.98	27.28	15.27	1.011	535.5	152.1	98.32	184.5	0.235	0.966	1436	0.536	35.3	0.44	0.0008	0	0	0	100	0
63001	Ystwyth at Pont Llolwyn	170.26	41	19.21	1.571	611.6	265.6	163.33	278.7	0.122	0.99	1456	0.488	39.2	0.63	0.0006	0	0	0	100	0
64002	Dysynni at Pont-y-Garth	75.2	18.54	9.64	1.069	890.3	313.1	329.55	206.6	0.203	0.952	2163	0.449	42.8	0.66	0.0002	0	0	0	100	0
65001	Glaslyn at Beddgelert	67.23	17.22	7.54	1.050	1078.4	339	323.2	208.8	0.072	0.909	2808	0.406	45.1	0.62	0.0003	0	0	0	100	0

65004	Gwyrfai at Bontnewydd	46.17	18.77	10.63	1.381	1067.3	294	218.18	267.8	0.286	0.868	2150	0.412	45.2	0.54	0.0009	0	0	0	100	0
65005	Erch at Pencaenewydd	19.47	11.94	6.77	1.353	551.4	177	99.06	179	0.5	0.991	1479	0.44	39.2	0.56	0	0	0	0	100	0
65006	Seiont at Peblig Mill	80.15	22.14	13.7	1.237	1063.1	320.9	268.29	301.8	0.244	0.854	2255	0.499	39.4	0.49	0.0051	0	0	0	100	0
66001	Clwyd at Pont-y- Cambwll	404.6	49.96	19.51	1.242	553.9	206.5	120.16	14.6	0.091	0.996	910	0.589	32.1	0.41	0.0036	20.19	18.72	0	61.09	0
66011	Conwy at Cwmlanerch	339.86	31.83	16.42	0.863	1050.6	341.6	173.11	19.9	0.01	0.98	2041	0.363	48.9	0.7	0.0005	0	0	0	100	0
102001	Cefni at Bodffordd	21.7				104.4	67.8	29			0.96	1061	0.45		0.45	0.0041	0	0	0	100	0
64001	Dyfi at Dyfi Bridge	464.56	39.92	20.06	0.926	903.4	281.2	276.17	222.21	0.071	0.995	1835	0.478	39.8	0.66	0.0004	0	0	0	100	0
62001	Teifi at Glan Teifi	897.27	102.55	45.9	1.712	591.9	209.2	112.35	285.7	0.103	0.995	1380	0.507	37	0.52	0.0017	0	0	0	100	0
71006	Ribble at Henthorn	448.05	70.15	33.48	1.657	691.4	237.4	90.24	197.7	0.096	0.999	1342	0.367	43.4	0.61	0.0074	0	96.5	0	3.48	0
72004	Lune at Caton	984.2	73.49	38.73	1.171	734.4	275.1	141.67	286.7	0.108	0.993	1522	0.404	43.7	0.64	0.0016	0	66.66	0	29.83	3.51
73012	Kent at Victoria Bridge	183				815.5	226.6	165.5			0.97	1787	0.5		0.71	0.0122	0	7.17	0	92.83	0

75003	Derwent at Ouse Bridge					945.4	307.7	247.4			0.79	2064	0.44		0.63	0.0072	0	0.99	0	99.01	0
75004	Cocker at Southwaite Bridge	116.78	27.37	14.08	1.266	853	300.6	296.54	310.2	0.129	0.832	1974	0.483	40.1	0.63	0.0001	0	0.05	0	99.95	0
75017	Ellen at Bullgill	102.25	29.84	14.93	1.475	650	164.5	80.63	321.1	0.311	0.984	1107	0.488	34.4	0.62	0.0037	1.98	56.06	0	16.64	25.32
76005	Eden at Temple Sowerby	618.58	60.86	29.65	1.223	796.6	283.1	101.55	322.5	0.105	1	1143	0.475	37	0.66	0.002	4.63	91.79	0	3.58	0
27006	Don at Sheffield Hadfields	365.29	50.59	23.4	1.323	543.4	261.7	108.69	73.4	0.286	0.891	1014	0.416	38.4	0.37	0.1078	0	43.38	0	0	56.62
27021	Don at Doncaster	1253.16	82.4	46.85	1.163	543.4	154	78.3	76.8	0.199	0.931	801	0.492	29.9	0.34	0.1181	2.26	12.98	0	0	84.75
27064	Went at Walden Stubbs	83.7				94.8	49.2	34.2			0.97	611	0.61		0.32	0.1197	18.45	0	0	0	81.55
27029	Calder at Elland	340.91	35.14	20.43	0.951	503.4	291.3	142.33	103.3	0.147	0.93	1257	0.455	38.5	0.57	0.0339	0	90.94	0	0	9.06
23006	South Tyne at Featherstone	323.09	35.48	19.58	0.986	891.9	429.8	125.7	12.3	0.198	0.995	1332	0.27	52.9	0.64	0.0008	0	100	0	0	0
45008	Otter at Fenny Bridges	110.2	26.31	12.52	1.253	302.2	179.5	94.58	181	0.098	0.996	1035	0.486	38.3	0.4	0.0089	0	46.04	0	0	53.96
45013	Tale at Fairmile	34.4				282.6	105.3	62.9			1	922	0.51		0.4	0.0786	36.12	31.92	0	0	31.96
46005	East Dart at Believer	22.29	13.27	6.22	1.405	601.6	458.3	96.98	144.6	0.256	1	2096	0.362	47.5	0.46	0	0	0	0	100	0

46014	Teign at Chudleigh	232.3				601.5	207.3	136.7		0.98	1228	0.57		0.46	0.032	0	2.29	0	96.92	0.79	
47001	Tamar at Gunnislake	920.07	71.05	39.43	1.171	580.3	155.1	88.17	220	0.031	0.994	1215	0.481	37	0.49	0.0034	0	0	0	100	0
47008	Thrushel at Tinhay	112.71	20.57	10.78	0.968	340.5	162.8	91.19	227.2	0.172	1	1144	0.422	39.1	0.5	0	0	0	0	100	0
47009	Tiddy at Tideford	37.37	15.77	8	1.289	283.5	109	123.5	151.7	0.199	1	1276	0.591	30.8	0.48	0.0073	0	0	0	100	0
47015	Tavy at Ludbrook					601.1	231.3	104.9			1	1555	0.55		0.48	0.0352	0	0	0	100	0
48004	Warleggan at Trengoffe	25.21	12.4	6.09	1.234	307.6	218.6	96.09	206.1	0.209	0.973	1445	0.5	35.7	0.45	0.0013	0	0	0	100	0
48005	Kenwyn at Truro	19.09	8.83	4.98	1.010	146.5	82.4	92.38	114.4	0.191	0.988	1100	0.601	32.6	0.42	0.0312	0	0	0	100	0
50001	Taw at UMBERLEIGH	832.32	61.23	34.61	1.061	811.4	181.8	106.94	219.9	0.071	0.997	1153	0.472	37.8	0.48	0.0007	0	2.77	0	97.23	0
50006	Mole at Woodleigh	327.64	32.27	19.15	0.891	490.5	210.1	127.29	216.3	0.171	0.999	1306	0.502	36.8	0.54	0.001	0	1.22	0	98.78	0
50007	Taw at Taw Bridge	72.13	27.71	12.97	1.631	603.3	233.8	99.09	15.8	0.215	0.989	1226	0.49	35	0.46	0.0011	0	8.59	0	91.41	0
50008	Lew at Gribbleford Bridge	71.1				286.4	172.4	81.5			1	1192	0.41		0.5	0.017	0	0	0	100	0

50009	Lew at Norley Bridge	20.2				277.6	172.65	77.2			1	1196	0.45		0.5	0.0127	0	0	0	100	0
51001	Doniford Stream at Swill Bridge	74.38	14.69	8.57	0.851	391.6	144.7	132.43	0.8	0.141	0.99	911	0.63	27.6	0.35	0.0077	9.62	27.54	0	40.89	21.83
51002	Horner Water at West Luccombe	20.49	12.03	6.31	1.328	516.8	340.6	216.92	23.9	0.287	0.978	1484	0.54	29.7	0.54	0	0.24	0	0	97.42	2.34
51003	Washford at Beggearn Huish	36.43	11.94	6.63	0.989	422.4	253.1	198.75	35.7	0.202	0.992	1153	0.586	31.5	0.38	0.0021	0	4.15	0	95.85	0
52003	Haleswater at Haleswater	93.55	19.06	9.43	0.985	391.8	108.8	87.52	158.8	0.296	0.99	851	0.622	30.6	0.35	0.0055	29.94	16.68	0	23.13	30.25
52005	Tone at Bishops Hull	203.63	39.93	17.7	1.399	573.4	43.8	99.88	68.2	0.178	0.979	964	0.562	32.9	0.36	0.0068	16.23	17.79	0	34.9	31.08
52016	Currypool Stream at Currypool Farm	15.72	8.93	4.65	1.126	382.6	181.1	136.25	63.1	0.457	1	934	0.586	29.2	0.35	0	0	0	0	54.89	45.11

Appendix 2 Percentages of Missing (M), Estimated (E), Suspect (S) and Unchecked (U) at each of the study catchments. Where some catchments appear twice, the raw data was supplied across multiple data files by the monitoring authority. Portions of missing data are highlighted by red text.

Catchment	Missing (M)	Estimated (E)	Suspect (S)	Unchecked (U)
120001	0.40	0.19	0.92	8.72
56001	1.21	0.24	2.19	12.72
60001	41.75	0.00	1.49	0.95
60003	1.74	6.52	0.00	0.97
60006	0.98	0.82	0.11	0.62
61001	0.01	2.02	0.00	0.78
61002	1.01	9.41	0.09	1.67
63001	0.62	8.39	0.03	0.56
64002	0.00	5.25	0.71	5.22
65001	0.68	0.14	7.37	2.96
65004	17.04	0.32	0.00	22.37
65005	0.29	0.01	0.00	23.90
65006	3.97	0.00	0.25	21.85
66001	9.35	0.36	0.04	16.57

66011	0.95	0.26	0.00	5.92
54005	75.23	0.01	0.00	0.00
54008	0.00	0.00	0.00	0.00
23006	1.66	0.00	1.18	0.04
55002	86.69	0.00	0.00	13.31
55003	86.96	0.00	0.00	13.04
71006	0.00	0.00	0.00	0.07
72004	0.00	0.00	0.00	0.36
73012	0.00	0.00	0.67	0.01
75003	0.00	0.00	0.00	0.52
75004	0.00	0.01	0.00	1.36
75017	0.00	0.00	0.07	0.18
76005	0.00	0.00	1.00	1.43
27006	0.00	0.00	0.00	13.61
27021	0.00	0.00	0.00	0.00
27064	0.00	0.31	0.22	0.00
27029	0.00	0.00	0.00	14.15

54005	0.02	3.26	0.00	11.77
54008	0.00	0.00	0.61	2.11
23006	0.46	1.94	5.49	0.41
55002	9.91	0.08	8.31	0.94
55003	9.97	3.81	2.89	2.92
71006	0.00	0.33	0.59	4.57
72004	0.00	4.91	2.10	4.34
73012	0.01	4.10	0.75	4.44
75003	0.00	4.25	0.78	1.76
75004	0.00	1.67	0.02	2.12
75017	0.00	0.41	0.60	2.25
76005	0.00	0.94	0.99	0.22
27006	0.00	0.00	0.28	0.23
27021	0.00	3.14	4.28	26.81
27064	0.00	1.53	0.17	0.42
27029	0.00	1.93	0.29	0.51
16003	0.00	0.25	0.97	0.30

3003	0.00	0.31	0.92	0.18
4005	0.00	0.37	1.14	0.20
4006	0.00	0.18	1.08	0.24
6008	0.00	0.00	0.28	0.13
7001	0.00	0.22	3.50	0.35
79004	0.00	3.87	0.05	0.27
80003	0.00	16.34	1.66	0.00
8013	0.00	0.29	8.34	0.25
85003	0.00	1.42	1.30	0.18
95001	0.00	0.06	0.29	0.19
96001	0.00	0.08	1.18	0.40
96003	0.00	0.02	1.86	0.94
96004	0.00	0.11	0.62	0.52
12003	0.00	N/A	N/A	N/A
12005	27.22	N/A	N/A	N/A
12006	27.24	N/A	N/A	N/A
12007	9.50	N/A	N/A	N/A

78003	22.29	N/A	N/A	N/A
80001	22.30	N/A	N/A	N/A
81002	0.00	N/A	N/A	N/A
83006	0.77	N/A	N/A	N/A
83013	58.18	N/A	N/A	N/A
89003	4.41	N/A	N/A	N/A
90003	9.65	N/A	N/A	N/A
93001	0.26	N/A	N/A	N/A
94001	0.00	N/A	N/A	N/A
51002	17.23	0.11	0.62	0.52
51002	0.00	0.11	0.62	0.52
51003	17.23	0.11	0.62	0.52
51003	0.00	0.11	0.62	0.52
51001	17.23	0.11	0.62	0.52
51001	0.00	0.11	0.62	0.52
52005	17.23	0.11	0.62	0.52
52005	0.00	0.11	0.62	0.52

52003	17.23	0.11	0.62	0.52
52003	0.00	0.11	0.62	0.52
52016	17.23	0.11	0.62	0.52
52016	0.00	0.11	0.62	0.52
50008	18.77	0.11	0.62	0.52
50008	0.00	0.11	0.62	0.52
50007	17.90	0.11	0.62	0.52
50007	0.00	0.11	0.62	0.52
50001	18.77	0.11	0.62	0.52
50001	0.00	0.11	0.62	0.52
50006	18.77	0.11	0.62	0.52
50006	0.00	0.11	0.62	0.52
48005	0.00	0.11	0.62	0.52
48004	1.72	0.11	0.62	0.52
47009	1.82	0.11	0.62	0.52
47008	1.76	0.11	0.62	0.52
47015	18.77	0.11	0.62	0.52

47015	0.00	0.11	0.62	0.52
47001	18.77	0.11	0.62	0.52
47001	0.00	0.11	0.62	0.52
50009	18.77	0.11	0.62	0.52
50009	0.00	0.11	0.62	0.52
46005	18.76	0.11	0.62	0.52
46005	0.00	0.11	0.62	0.52
46015	23.42	0.11	0.62	0.52
45013	1.62	0.11	0.62	0.52
45008	18.77	0.11	0.62	0.52
45008	0.00	0.11	0.62	0.52

Appendix 3 Distribution Results for the study catchments according to different duration AR catalogues. The catchments with no distribution results (either a preferential orientation or IVT Threshold) have been removed.

Catchment	9hr		12hr		15hr		18hr	
	% POT3 Floods Correlated to ARs	[Preferential Orientation] IVT Threshold	% POT3 Floods Correlated to ARs	[Preferential Orientation] IVT Threshold	% POT3 Floods Correlated to ARs	[Preferential Orientation] IVT Threshold	% POT3 Floods Correlated to ARs	[Preferential Orientation] IVT Threshold
54005	42	[240.9, 260.5] 420	34	[241.3, 260.9] 435	28	[239.2, 256.8] 470	24	[240.5, 255.4] 472
54008	30		25	[235.7, 256.8] 449	19	456	17	
55002	32	450	24	477	20	486	18	
55003	20	[240.2, 257.3] 428	15	[246.7, 258.6] 411	13		9	[247.9, 257.7] 451
56001	50	[229.2, 255.3] 538	40	[237.2, 256.0] 529	28	[238.0, 255.7] 538	23	[237.4, 254.6] 497
60001	41	[227.3, 251.8] 514	31	546	27	568	22	567

60003	38	578	30	598	24	588	21	[235.6, 256.9] 584
60006	42	571	31	581	20	571	17	[233.8, 251.8] 555
61001	27	[232.4, 254.1] 583	22	[235.7, 254.7] 572	17	[237.1, 253.2] 570	15	[236.8, 254.2] 584
61002	32	575	27	[234.6, 252.4] 595	21	[234.8, 255.4] 576	19	[235.1, 256.9] 570
63001	58	482	47	485	40	485	34	485
64002	45		35	449	30	450	27	
65001	53	[231.6, 250.5] 448	48	[233.4, 250.4] 429	35	[233.8, 250.9] 447	32	[233.9, 250.9] 452
65004	49	[226.8, 247.7] 483	38	[229.9, 248.9] 438	27	476	23	478
65006	54	[226.4, 248.9] 482	46	[227.5, 247.1] 483	33	479	28	484
66001	43	[232.6, 254.6] 414	38	[236.9, 256.5] 401	29	441	26	

66011	69	[236.3, 258.5] 436	56	[236.8, 258.5] 447	42	440	40	447
102001	33	[225.4, 250.3] 390	29		22	[231.8, 250.2] 411	21	
71006	63	[241.6, 265.6] 405	49	401	41	403	35	409
72004	65	[235.9, 258.8] 407	56	[238.4, 259.5] 412	46	408	41	411
73012	57	[233.2, 255.2] 397	42	[237.4, 258.1] 400	31	396	27	358
75003	46	[231.9, 245.7] 408	38	[234.6, 246.1] 442	32	[233.8, 247.4] 468	28	468
75004	54	[230.0, 250.9] 408	45	[233.6, 251.7] 402	32	[235.4, 253.7] 459	30	[235.7, 254.0] 480
75017	48	[232.7, 249.0] 416	42	[235.4, 257.0] 431.5	35	411	29	419

76005	53	[234.2, 253.7] 362		43	[236.6, 251.9] 376		32	[238.1, 253.4] 402		29	
27064	18		315	16		319	13		298	9	
27029	60	[242.3, 265.3] 410		49		404	40			34	
23006	49	[237.4, 257.8] 386		41			33			30	
79004	33		411	26		483	18		472	16	513
78003	47	[228.7, 248.8] 443		41	[230.1, 249.3] 458		29	[236.2, 249.1] 473		25	[237.0, 250.1] 438
80001	29	[222.3, 243.4] 408		24		467	17		467	14	476
81002	35		477	30		476	21		471	16	465
80003	28		423	24		432	19		431	18	430
83006	43		379	33		495	24		447	20	489
83013	27		447	21		544	15		444	10	
89003	55	[238.9, 263.3] 478		50		497	40	[244.2, 264.0] 506		32	[245.5, 264.5] 492

90003	49	[241.1, 259.3] 494	44	481	38	[243.6, 260.0] 499	27	[247.3, 260.7] 485
93001	55	[243.9, 264.1] 452	46	[244.3, 263.5] 488	42	[245.2, 263.5] 484	35	[244.7, 262.7] 475
12003	30	395	27	375	20	380	17	
12005	16	419	13	[225.7, 250.5] 414	9		6	
12007	34	393	31	390	23		17	
94001	51	485	44	459	40		33	
3003	43	[255.0, 273.4] 445	34		31	[254.0, 273.6] 267	28	
4005	49	[241.3, 258.1] 440	41	[242.6, 258.1] 414	35	[243.4, 258.2] 451	29	[243.8, 258.8] 458
4006	43	410	35		31		27	
6008	36	408	31		25		21	
7001	44	408	40		31		23	
95001	45	[248.0, 269.4] 445	38	[248.6, 267.9] 455	35	[248.7, 265.0] 469	31	[248.7, 263.8] 460

96004	45		38		33	[253.5, 267.6] 447		28	
85003	52	447	47	446	34		447	27	439
16003	33	[231.3, 251.4] 434	29	429	24		466	21	429
45008	14	546	10	549	7			5	
45013	13	544	8	553	8		553	6	
46005	36	[229.2, 252.6] 588	27	586	18		601	14	601
46014	21	542	14	509	13		537	9	556
47001	34	[244.5, 254.2] 585	27	[246.2, 259.0] 605	20	[247.3, 261.2] 599		15	[250.1, 262.8] 607
47008	31	[236.9, 251.8] 537	23	[245.2, 252.6] 566	16	[245.5, 253.6] 569		10	[248.3, 259.9] 553
47009	38	[235.9, 254.8] 592	28	[246.7, 260.8] 599	21	[247.9, 261.4] 602		16	[250.7, 262.5] 589
47015	35	[234.5, 252.6] 586	26	[238.3, 253.7] 580	18	[238.3, 254.2] 603		14	[238.3, 254.4] 585
48004	32	576	24	588	16		601	11	595

48005	19		592	13		628	10		640	8		628
50001	43	[249.1, 264.1] 570		33	[249.0, 266.8] 560		24	[250.1, 266.4] 576		20	[251.8, 272.3] 589	
50006	51	[247.1, 265.4] 566		41	[249.0, 265.8] 561		31	[249.6, 256.1] 573		26	[251.5, 268.6] 566	
50007	39	[237.0, 254.4] 544		28	[246.1, 258.0] 546		20	[247.4, 258.0] 556		15	[250.1, 262.0] 548	
50008	42	[236.2, 262.3] 535		29	[244.6, 260.6] 569		22	[246.2, 260.3] 591		17	[249.8, 261.7] 569	
50009	44	[235.2, 262.3] 540		32	[242.3, 263.7] 557		24	[242.6, 260.7] 552		21	[243.1, 261.7] 569	
51002	45	[242.0, 261.4] 535		36	[243.0, 262.5] 546		27	[242.6, 259.2] 540		23	[244.2, 262.7] 591	
51003	36	[235.9, 258.3] 538		26	[243.0, 261.1] 539		20	[242.6, 259.2] 540		17	[246.4, 262.9] 539	
52003	23	[241.1, 261.0] 534		17		527	11		523	9	[252.8, 262.9] 523	

52005	28	[233.0, 255.2] 545		21	536	14	536	10	
52016	24		531	18	518	11	523	8	530